Hellenic Mediterranean University

Inter-institutional Post Graduate Program on

“Nanotechnology for Energy Applications”



MASTER THESIS

Subject: Power Electronics design and integration towards efficient operation for monitoring of graphene-perovskite Solar farm

Supervisor : Prof. Emmanuel Kymakis (PhD Cambridge)

Advisor : PhD Candidate George Viskadouros

Postgraduate Student : Ioannis Kalogerakis

Registration Number : MTK10

HERAKLION CRETE 2021

Acknowledgments

I would like to warmly thank Prof. Emmanuel Kymakis who trusted me to complete this master thesis and undertook its supervision. As for the opportunity he gave me to study in the postgraduate program nanotechnology for energy applications and then to work as a researcher in the implementation of the solar farm, as well as for the valuable guidance and assistance he offered me during my master thesis.

Many acknowledgements to the Graphene Flagship for giving me this opportunity to work and to implementation this master thesis, in the margins of Graphene Core 2 project.

I would like to thank from the bottom of my heart Mr. Viskadouros Georgios who trusted me to complete this master thesis and also undertook its advisory. As well as for the support and valuable time he devoted to me to get here, as well as for the valuable guidance and help he offered me during the realization of my master thesis and the solar farm.

Finally, I want to express a huge thank you to my mother Krystalli Syntichaki and I dedicate this master thesis to her, for all this support, trust she has shown me all these years of my studies and for all those supplies she has offered me to make me a right and balanced person.

Abstract

The goal of the master thesis, is the design and construction of innovative full programmable power electronics device of IV-MPPT Charger Regulator, research new innovative algorithms towards efficient operation for monitoring of graphene-perovskite Solar farm and the realization of the Solar Farm. Research the behaviour of innovative Graphene Perovskite (GRAPES) photovoltaics technology and comparison of them with conventional technologies.

It will be done a small review, for the following chapters.

- In the first chapter there will be a introduction to the renewable energy sources, a historical review of photovoltaics and the need of MPPT devices.
- In the second chapter will be a theory of photovoltaics, the electrical characterization theory of them, the materials and the fabrication analysis that used to create the innovative GRAPES.
- In the third chapter is the fabrication of the innovative electronic device of IV-MPPT Charger Regulator and the complete analysis of it.
- In the fourth chapter analyzed all algorithms of the device and the literature review of MPPT algorithms.
- The fifth chapter is the user guide of IV-MPPT Charger Regulator.
- Finally in the sixth chapter is the experimental measurements of IV-MPPT Charger Regulator.

Table of contents

Acknowledgments 1
Abstract 2
Table of contents 3
1. Introduction 6
1.1 Renewable Energy Sources 8
1.1.1 Biomass 9
1.1.2 Hydropower 10
1.1.3 Tidal Energy 11
1.1.4 Geothermal Energy 12
1.1.5 Wind Energy 13
1.1.6 Solar Energy 14
1.2 Photovoltaics 15
1.2.1 History of Photovoltaics 15
1.3 Solar Irradiance and Maximum Power Point Tracking 17
2. Theory 19
2.1 Photovoltaic Effect 21
2.1.1 Photocurrent 21
2.2 Characteristic Curve Current (I) - Voltage (V) of Photovoltaic 22
2.2.1 Quantum Efficiency 23
2.3 Graphene 25
2.3.1 Fabrications methods 26
2.4 Perovskite 27
2.5 Molybdenum Disulfide (MoS_2) 29
2.6 Graphene Perovskite Photovoltaic Device Fabrication (GRAPES) 31
3. Fabrication of the Electronic Device of IV-MPPT Charger Regulator 33
3.1 Maximum Power Transfer Theorem 33
3.2 DC-DC Boost Converter 34
3.3 Hardware of Measurement System 37
3.3.1 Current Measurement 37
3.3.2 Voltage Measurement 39

3.3.3 Isolated Circuit for Current Measurement 40
3.3.4 Sources and Drivers Schematics 41
3.4 Power Losses of IV-MPPT Charger Regulator 43
3.4.1 Theoretical Approximation of DC-DC Boost Converter Power Losses 44
3.4.2 Practical Approximation of Measurement System Power Losses 50
3.4.3 Microcontroller Power Losses 51
3.4.4 Estimate Power Losses and Efficiency of the device 51
3.4.5 Material Costs for Device Fabrication 52
3.5 Construction Photos of the Device and its Description 53
4. Algorithms of IV-MPPT Charger Regulator 58
4.1 Explanation of IV Algorithms 58
4.1.1 Reverse Exhaustive Search (RES) 58
4.1.2 Forward Exhaustive Search (FES) 59
4.1.3 Reverse Forward Exhaustive Search (RFES) 59
4.1.4 Forward Reverse Exhaustive Search (FRES) 59
4.2 Explanation of MPPT Algorithms 60
4.2.1 Hill Climbing (HC) 60
4.2.2 Hill Climbing Perturb and Observe (HCPO) 62
4.2.3 Fractional Open Circuit Voltage (FOCV) 65
4.2.4 Fractional Short Circuit Current (FSCC) 68
4.2.5 Incremental Conductance (IC) 72
4.2.6 Maximum Power Quantumized Area Search (MPQAS1 and MPQAS2) 76
4.3 Explanation of PVBR Algorithms 84
4.3.1 Pmax Open Circuit Intervals (POCI) 84
4.3.2 Pmax Short Circuit Intervals (PSCI) 85
4.4 Literature Review of MPPT Algorithms 86
5. User Guide of IV-MPPT Charger Regulator 88
5.1 Instructions for connecting the machine 88
5.1.1 Step 1: Connection to the computer 89
5.1.2 Step 2: Connection of the metric system polarizations 90
5.1.3 Step 3: Output connection of the device to the battery 90

5.1.4 Step 4: Input connection of the device to the photovoltaic 91
5.1.5 Step 5: Disconnection of the machine 91
5.2 Instructions for using the PLX-DAQ-v2.11 datalogger 92
5.3 Instructions for using the Serial Monitor of Microcontroller 97
5.4 Features of IV - MPPT Charger Regulator 99
6. Experimental Measurements of IV-MPPT Charger Regulator 100
6.1 Solar Farm Realization 100
6.2 Current (I) - Voltage (V) Measurements and Experiments 105
6.2.1 Time Table of IV Algorithms at different Average Points 105
6.2.2 Hysteresis Effect and S-Shape IV Curves 107
6.2.3 Hysteresis at different IV Algorithms 108
6.2.4 Hysteresis at different Average Points 110
6.2.5 Hysteresis at different Photovoltaic Technologies 110
6.2.6 RFES and FRES Pauses Hysteresis Experiment 111
6.2.7 Electrical Characterization of different Photovoltaic Technologies 115
6.2.8 IV Curve Comparison and Collaboration with PV Blocks 121
6.3 Maximum Power Point Tracking (MPPT) Measurements and Experiments 123
6.3.1 FOCV and HCPO Algorithms Comparison at different PV Technologies also Comparison of Theoretical and Real Outdoor measurements 123
6.3.2 All MPPT Algorithms Comparison with a Commercial Device Algorithm at different PV Technologies in Clear Sky 128
6.3.3 All MPPT Algorithms Comparison with a Commercial Device Algorithm at GRAPES PV Technology in Cloudy Sky 136
6.4 Photovoltaics Behaviour Reading Algorithms Measurements and Experiments 140
6.4.1 Pmax Open Circuit Intervals Measurements 140
6.4.2 Pmax Short Circuit Intervals Measurements 140
Discussion - Conclusions - Future Development 142
Bibliography - References 143
Supporting Information - Annex 147

1. Introduction

You know that nowadays energy demand is extremely high and the most of this energy come from conventional energy sources such as oil, coal, natural gas or nuclear. But this energy sources have two major problems, first are finite sources and the second has environmental impacts (greenhouse effect, nuclear waste etc.).The mankind need energy sources that is renewable and environmental friendly, some of them is biomass, hydropower, tidal, geothermal, wind and solar.

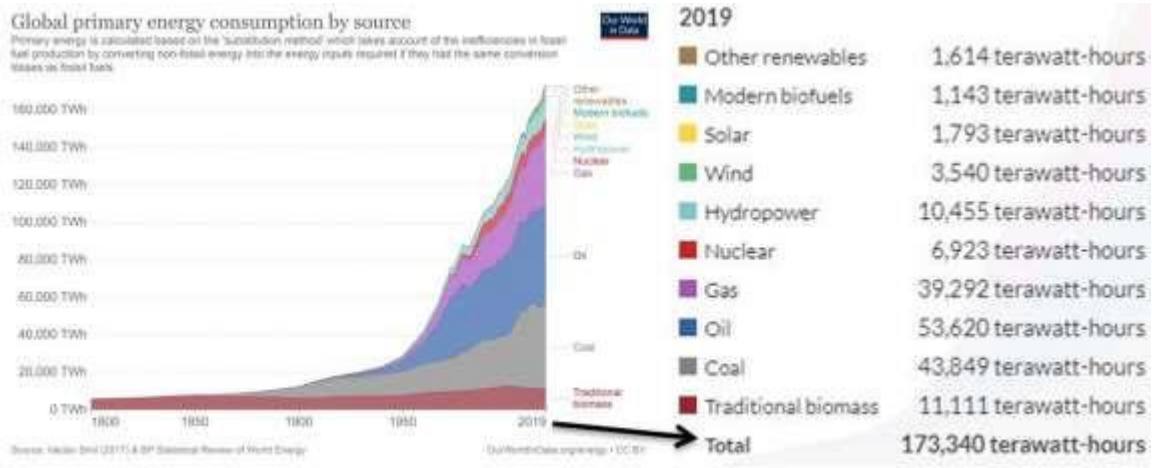


Image 1. Chart of global primary energy consumption, by source. **[1]**

As shown in the chart of Image 1. the renewable energy sources start to increase every year as result the decrease at carbon emissions that shown in Image 2. in grey dashed line.

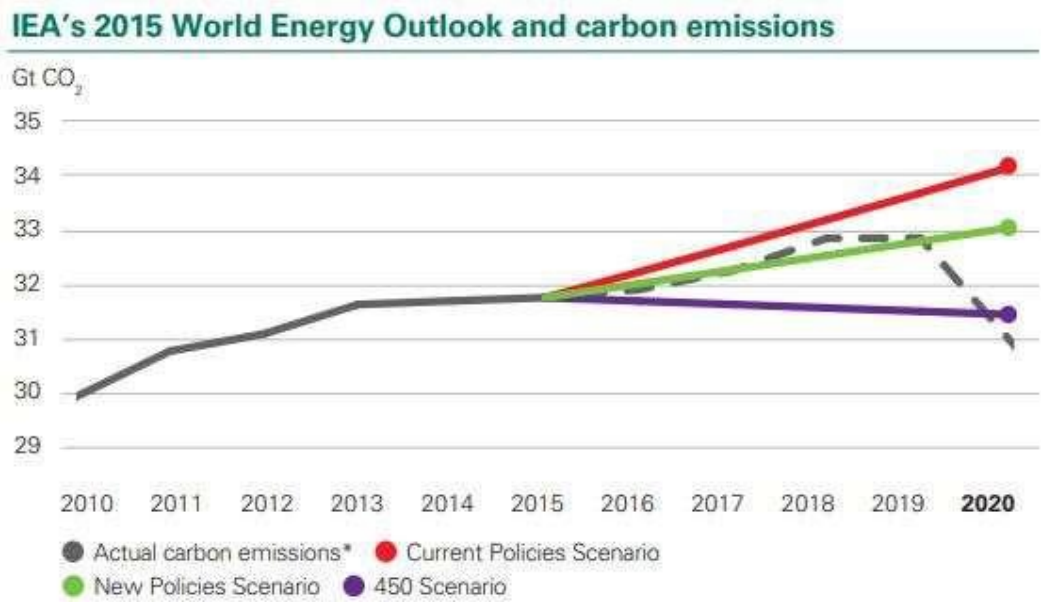


Image 2. IEA's 2015 World Energy Outlook and carbon emissions. **[2]**

In Image 2. is shown the chart of the International Energy Agency's World Energy Outlook (WEO) that published in November 2015, just before the Paris Conference of the Parties (COP), which are included three scenarios for carbon emissions based on different assumptions about the future setting of global energy policies:

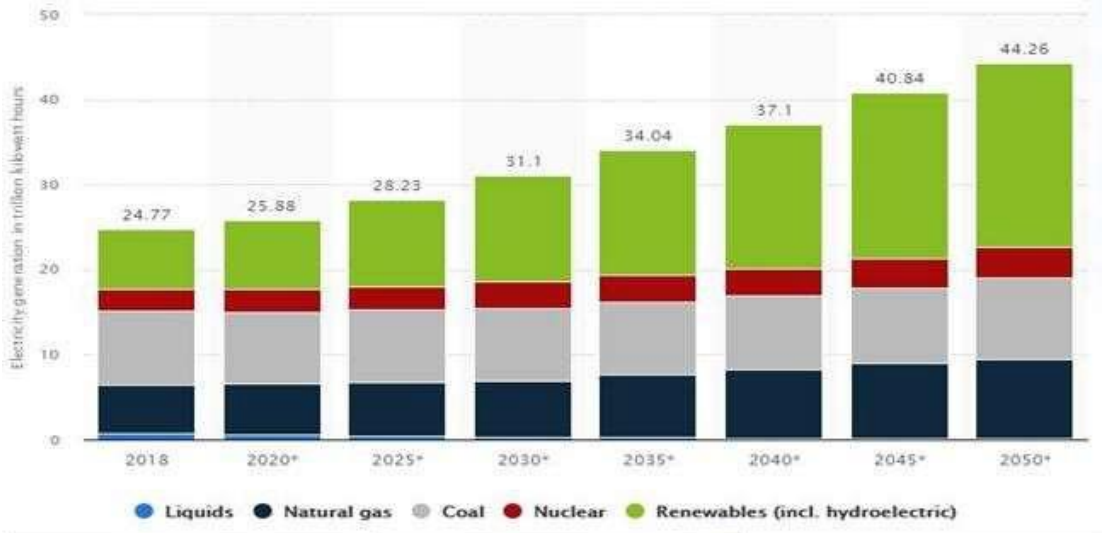
- A continuation of current policies (shown in red in the chart)
- The implementation of declared policy intentions (in green)
- And a set of policies consistent with limiting global temperature increases to 2˚C (in purple)

Undoubtedly, the most important element of the energy system needed to address the two aspects of the Paris Agreement:

- Respond to the threat of climate change
- Supporting sustainable development, is the need for rapid growth in renewable energy

Also, in the chart is shown in grey dashed line the actual carbon emissions. **[2]**

So the prediction of future growth of renewable energy sources is shown in Image 3.



2020*		2040*		2050*	
Liquids	0.63	Liquids	0.19	Liquids	0.17
Natural gas	5.91	Natural gas	8.11	Natural gas	9.25
Coal	8.5	Coal	8.6	Coal	9.6
Nuclear	2.71	Nuclear	3.28	Nuclear	3.58
Renewables (incl. hydroelectric)	8.13	Renewables (incl. hydroelectric)	16.92	Renewables (incl. hydroelectric)	21.66

Image 3. Projected electricity generation globally from 2018 to 2050, by source. **[3]**

As noticed the conventional sources are increasingly being replaced from renewable.

1.1 Renewable Energy Sources

Alternatively, to non-renewable energy sources that can't replenished from nature such as oil, coal, natural gas or nuclear, the renewable energy sources are natural resources which replenished day after day, the sun shines, wind blows, plants grow, rivers flow, ocean have waves and the inside of earth always is heat.

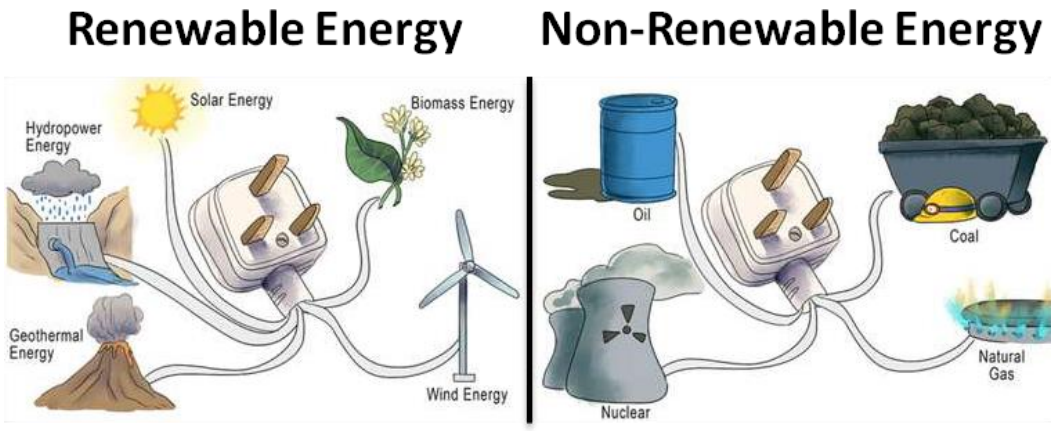


Image 4. Alternative renewable energy sources on left side and conventional at right **[4]**

The renewable energy is energy derived from sources that are naturally replenishing and the benefits are:

- Inexhaustible energy sources
- Contributes to independence from conventional energy sources
- Strengthen energy independence at national level
- Are environmentally and human friendly

the disadvantages are:

- They have low power and energy density
- Also show fluctuation in availability
- They characterized by a low utilization rate
- The installation cost is high

The major types of renewable energy sources are:

- Biomass
- Hydropower
- Tidal
- Geothermal
- Wind
- Solar

1.1.1 Biomass

The biomass is renewable organic materials that come from by products of recent living organisms and plants and can be converted into energy, namely biofuels through various processes, such as:

- Direct combustion to produce heat for buildings and is most common method to generate electricity in steam turbines
- Chemical conversion to create liquid fuels know as transesterification is used for converting vegetable oils, animal fats and greases into fatty acid methyl esters, which are used to produce biodiesel
- Thermochemical conversion such as gasification, hydrotreating and pyrolysis to produce gaseous, liquid and solid fuels respectively
- Biological conversion to create gaseous and liquid fuels know as fermentation to convert biomass into ethanol and anaerobic digestion to create renewable natural gas **[5]**

First generation biofuels are produced from crops

Second generation biofuels are produced from agricultural and forest residues

The benefits of biofuels are:

- Environmentally friendly
- New jobs position in biofuel production factories and in farms that grows plants for biofuels

The disadvantages are:

- Increased prices of products used to produce biofuels
- Possible worsening of hunger in developing countries due to rising food costs **[6]**



Image 5. Switchgrass fields and facilities in East Tennessee. | Photo courtesy of ORNL **[7]**

1.1.2 Hydropower

The hydropower is the power that produced from falling or fast running waters such as small or big rivers, water currents or water sources in water wheels as result the production of mechanical or electrical energy, this is achieved with a conversion of gravitational potential or kinetic energy of water source.

In a hydroelectric plants they create a dam with two height level the higher level and the lower one, they pumped water and store it at higher level, is artificial or natural places called it water tank or reservoir then the water is channeled into a downstream pipeline that acquires kinetic energy and rotates a watermills or hydro turbines, in the lower level of the dams the water is pumped again at the higher place for storage with help of other renewable energy sources such as wind turbines or photovoltaics.

Hydropower is a method of sustainable energy production.

The advantages of hydroelectrical plants are:

- Is a clean renewable energy source
- Can be immediately put into operation as soon as additional electricity is requested
- Through water reservoir and other needs can be met such as water supply, irrigation, wetland creation etc.

The disadvantages of hydroelectrical plants are:

- High cost of construction and repair of dams and equipment of electrical power stations, as well as long time until the completion of the project
- Severe environmental degradation in the reservoir area (population movement, degradation of areas, change in flora and fauna as well as the local climate)

International practice today focuses on the construction of small dams. **[6]**



Image 6. Three Gorges Dam, China is the world's largest hydro facility with generating capacity of 22500 megawatts (MW) **[8]**

1.1.3 Tidal Energy

Tidal energy produced by the surge of ocean waters during the rise and fall of tides this water intensity is a form of kinetic energy, also we can exploit the oscillation of the waves usually with the use of floats.

Some of tidal technologies are:

- Tidal barrages, fences, turbines, sea snakes, paddles, kites, wave floaters



Image 7. Wave Energy Conversion, SINN Power Setup R&D Facility Heraklion (2020) **[9]**

The advantages of tidal energy are:

- Is clean and renewable
- Also is predictable and reliable
- The equipment can last long
- Very effective at low speeds

The disadvantages of tidal energy are:

- Environmental impact especially tidal barrages which utilizes dams that means habitat destruction
- High construction and repair costs
- Scarcity of suitable locations
- Inconsistent, tides are not always constant, so it makes the power unreliable **[10]**

1.1.4 Geothermal Energy

Geothermal is the energy that produced from earth's subsurface in form of heat, produce steam and move turbines to generate electricity, or the heat can be used directly to heating water and then distributed to households to warm them (district heating) and distribute hot water in their faucet. Some forms of geothermal energy are:

- High enthalpy, heat of underground rocks and waters, Temperature > 150 ^{o}C
- Mid enthalpy, heat of underground rocks and waters, Temperature 90 ^{o}C to 150 ^{o}C
- Low enthalpy, heat of underground rocks and waters, Temperature 25 ^{o}C to 90 ^{o}C
- Shallow geothermal, heat of rocks in shallow depth and surface waters, Temperature < 25 ^{o}C **[6]**

The benefits of geothermal energy are:

- Environmentally friendly and has huge energy potential
- Sustainable, stable
- Heating and cooling
- Reliable energy source and doesn't have fluctuations

The drawbacks of geothermal energy are:

- Location restricted
- Environmental side effects, few gases naturally released from under earth's crust storage as result of digging
- Earthquakes due to alterations in the Earth’s structure because of digging
- High costs around $2 to $7 million for a plant with a 1-megawatt capacity
- Sustainability of geothermal energy fluid needs to be pumped back into the underground reservoirs faster than it is depleted **[11]**



Image 8. The Geysers Geothermal Complex 900 megawatts (MW) **[12]**

1.1.5 Wind Energy

The kinetic energy of the wind moves the blades of wind turbines, which are connected to electric generators and produce electricity.

The advantages of wind energy are:

- More distributed and decentralized energy production
- Clean energy, not greenhouse gas emissions in relation to conventional energy production methods
- Enhancing security of energy supply
- Is one of the most economical energy sources used today as the available source is abundant, the wind
- Does not hinder geographical and livestock activities as 99% of the land that hosts the wind farm is available for uses
- Modern wind turbines are very quiet, the volume level at 40 meters from the wind turbine is 50 to 60 decibels (db) , it corresponds to the intensity of a conversation

The disadvantages of wind energy are:

- Wind energy technology requires an initial investment higher than that of fossil fuel generators
- The wind is intermittent and does not always blow when electricity is required
- Suitable places for wind farms are often located in remote areas, away from cities where electricity is needed **[6]**
- High operational and maintenance costs about 10-15% of levelized cost per kWh produced of over the lifetime of the turbine in new turbines and increase to 20-35% by the end of the turbine's lifetime **[13]**



Image 9. Wind Farm Moni Toplou Sitia Crete installed 6.6 megawatts (MW) **[14]**

1.1.6 Solar Energy

Solar energy is characterized by the sum of different forms of energy that produced from the sun, such as light or light energy, heat or thermal energy, as well as various radiations or radiant energy.

Solar energy is utilized through various technologies that take advantage of both the heat and the electromagnetic waves of the sun. **[6]**

The technologies used to exploit solar energy are distinguished in:

- Thermal solar systems convert solar radiation into heat
- Passive solar and hybrid systems are the systems that with appropriate architectural designs and the use of appropriate building materials maximize the direct use of solar energy for heating, air conditioning or lighting
- Photovoltaic solar systems (PV) generate electricity directly from sunlight
- Concentrating solar power (CSP) systems use mirrors to concentrate the solar energy to produce steam for the use of traditional steam turbines or engines to generate electricity, the thermal energy concentrated in a CSP plant can be stored and used to produce electricity when it is needed, day or night **[15]**

The advantages of solar energy are:

- Solar energy is the cleanest renewable energy source
- The most abundant renewable energy source available
- Low cost

The disadvantages of solar energy are:

- Small amount of energy per unit area
- Problem of energy storage in large quantities



Image 10. Solar energy technologies, ***a)*** *Hellenic Mediterranean University Solar Farm, innovative Graphene Perovskites Photovoltaics,* ***b)*** *Solar water heater* **[17]**, ***c)*** *The world's largest concentrated solar farm at Morocco the Noor-Ouarzazate complex 580 MW* **[16]**

1.2 Photovoltaics

As shown above, the renewable energy sources are very clean, one-way solution to greenhouse effect and in reduction use of conventional energy sources. From all renewable sources solar energy are the best, because is the cleanest form of energy, mother of all renewable energy sources and is the most abundant energy source from all other.

From solar energy technologies the best are photovoltaics because they generate electricity directly from the sun, they have the lowest operational and maintenance cost from all other solar technologies and generally the lowest from all renewable sources also photovoltaics need little to no supervision, especially if they don't have mechanical parts like sun trackers and they are just static to one direction and inclination (not recommended for energy production).

1.2.1 History of Photovoltaics

The history of photovoltaics starts at **1839** Alexandre Edmond Becquerel discovers the photovoltaic effect (light - electricity conversion) the operating principle of solar cells, during experiments with metal electrodes and electrolytes.

In **1961** W. Shockley, H.J. Queisser publish a paper describing the efficiency limits of Solar Cells. J. Appl. Phys. 32 (1961) 510. This first calculation used the 6000K black body spectrum as an approximation to the solar spectrum, giving maximum efficiency 30% with energy bandgap in 1.1 eV **[18]**, the subsequent calculations have used to measured global solar spectra (AM1.5G) and included a back surface mirror to prevents emission from the rear side of the cell increases the maximum efficiency to 33.77% for a solar cell with a bandgap of 1.34 eV. **[19]**

At **1970** Establishment of large photovoltaic companies.

In **1985**, researchers of University of New South Wales in Australia have constructed a solar cell with more than 20 % efficiency

1992 Discovery of the photo-induced charge transfer in conjugated polymer – fullerene blends

In **1999**, researchers of University of New South Wales in Australia have constructed a solar cell with more than 24.5 % efficiency.

Around **2000** several governments install rules to subsidize PV (feed-in tariffs etc.) This leads to a real PV-boom especially in Europe.

In **2002** M. A. Green introduced the concept of 3rd Generation Photovoltaics. He classified various PV-technologies considering the efficiency potential and the overall costs.

In **2009** several companies established production capacities > 500 MW per year **[20]**

Today **2020-2021** we have the new concept of Graphene Perovskite solar cells and the tandems concept.

Generation of photovoltaics: **[20]**

- First generation is: Si considered cost and energy intensive (Czochralski process needs a lot of energy) but stable photovoltaics and are widely used by industry, use a lot of material but founded in abundance in nature (silicon makes up 27.7% of Earth's crust and it is the second most abundant element in the crust, being surpassed only by oxygen)
- Second Generation is: GaAs, CIGS, CdTe, thin film solar cells made from less material and can be used in portable applications
- Third Generation is: Emerging PVs like OPV and Perovskite solar cells made from less materials and has tunable bandgap and also can be used in wearable and portable applications, but is still in development
- Fourth Generation is: Quantum dot and Tandem concepts to overcome the Shockley - Queisser limit with theoretical new maximum Power Conversion Efficiency (PCE) at 47% as shown in NREL graph at Image 11. , but is still in development

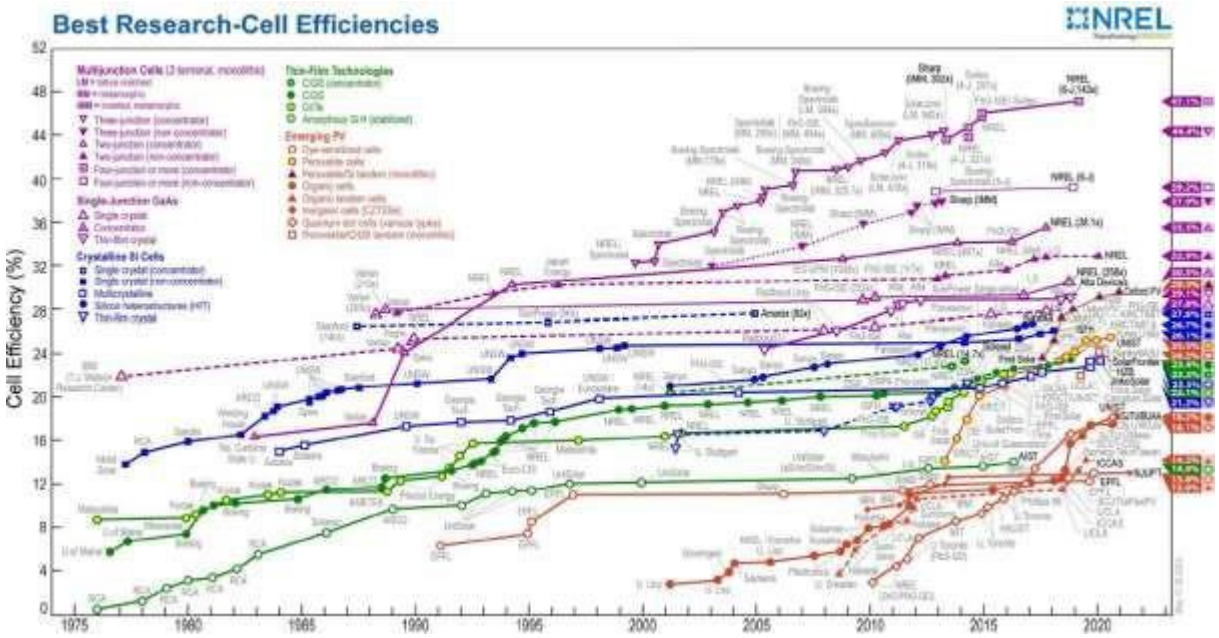


Image 11. NREL Graph for Photovoltaic Efficiencies over the passage of time **[21]**

1.3 Solar Irradiance and Maximum Power Point Tracking

As we know, the Earth rotate around itself and orbit around the Sun and consists of two hemispheres, the northern hemisphere and southern hemisphere.

The rotation of the Earth around its inclined axis (23.5^{o}) once every 24 hours that is one day, and the hemisphere of the Earth that faces the Sun during this rotation becomes day, while the other side becomes night, the rotation of the Earth around its axis causes the sequence of day and night.

The revolution of the Earth around the Sun is once every 365 days and 6 hours that is one year, this rotation of the Earth around the Sun causes the sequence of the four seasons the summer, spring, autumn and the winter. Also because of Earth tilt in its inclined axis 23.5^{o} we got seasonal changes like when one hemisphere has winter the other one has summer, same with autumn and spring, as shown at Image 12.

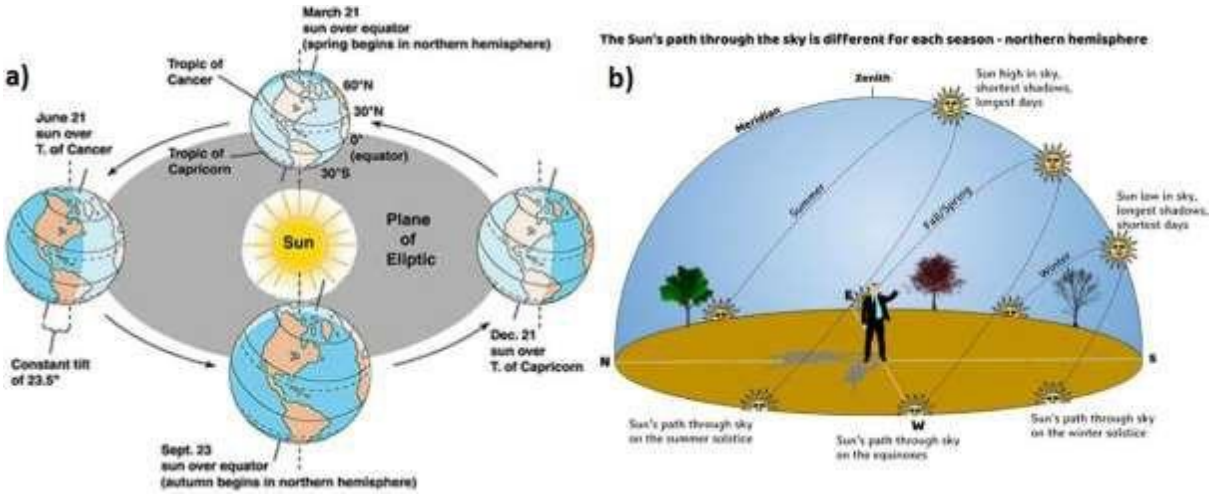


Image 12. ***a)*** *Earth positions at the different seasons of the year* **[22]** *,**b)** Sun's path through the sky in different seasons* **[23]**

With these information we can understand that solar irradiance isn't stable and changes all the time, at winter the distance of the Sun from the Earth are closer at 147,093,162 km called perihelion and the summer is further at 152,100,533 km called aphelion that means in winter we have more solar irradiation than summer. In calculation for optimization the position and inclination of photovoltaics we have to take this information into consideration too, so we can increase their efficiencies and avoiding the shading of fixed things like buildings or from other photovoltaics.

The internal resistances of photovoltaics are constantly changing with changes in radiation and temperature, as well as by other factors such as their degradation because of

aging, or humidity, or mechanical stress etc., as result when the photovoltaics they need to supply one load, they don't have the maximum power output not even when the solar irradiation is at peak, because the internal resistance of photovoltaics doesn't match the resistance of the load (we explain later in this master thesis the maximum power transfer theorem), so here take place the scenario of Maximum Power Point Tracking.

Maximum Power Point Tracker (MPPT) is the device that track the maximum power point in real time so we can have the maximum power conversion efficiency (PCE) of photovoltaics.

In device input connects the photovoltaics and its output with the load (battery or direct load etc), and running algorithms so it can recognize the changes of resistance in photovoltaics and adjusts its internal resistance to matching the photovoltaics internal resistance, so the power of its output is maximized and stabilized to supply the load (battery charging, direct load etc).

So with MPPT scenario either weather changes like cloudy, rainy day, or snow falling, changes in temperature, changes in irradiance, we can get in output the maximum power conversion efficiency (PCE) of photovoltaic at the specific time moment.

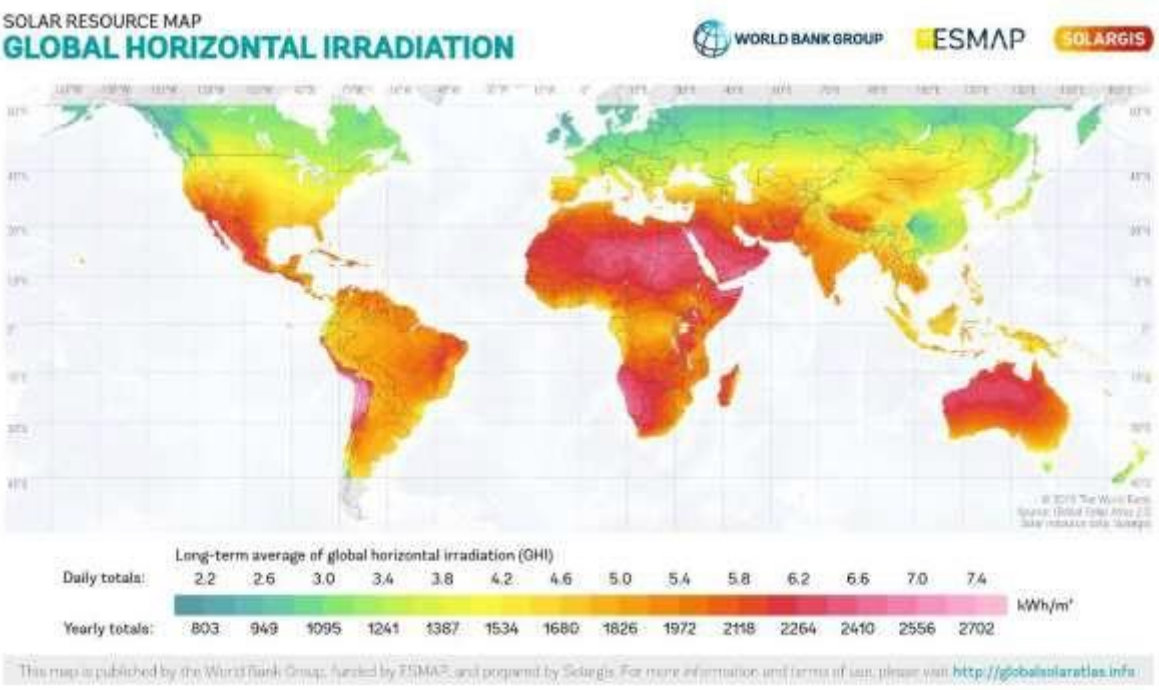


Image 13. Global Horizontal Irradiation (GHI) map **[24]**

As shown on GHI map Image 13., the irradiation varied from region to region.

2. Theory

The distinguish of materials depending on the total or partial fullness of the energy zone, classified into three categories:

- Conductors (metals), with zero energy bandgap (0 eV) , for example copper (Cu) , silver (Ag), gold (Au), electrons moves freely through the energy zones
- The insulators, with very high energy bandgap (>2.5 eV), for example diamond has 5.4 eV energy band gap, electrons can't move through the zones
- Semiconductors, the energy bandgap is small enough that one electron can move from the valence band to the conduction band under conditions like high temperature, electric field application, incident radiation in it

The Energy Bandgap (**Eg**) is the minimum energy required for excitation of an electron from the valence band to the conduction band, while creating a hole in it's place

If the energy bandgap is in units of electron volts (**eV**) and wavelength is on nanometers (**nm**) , then the maximum usable wavelength in a semiconductor with energy bandgap Eg (depends on the material) is: (Energy in one Photon is: $E = h \times v = \frac{hc}{\lambda}$, where Plank constant is: $h = 6.63 \times 10^{-34}\ J \times s$ and Speed of light $c = 3 \times 10^{8}\ m/s$)

$$\lambda_g(nm) = \frac{1240(eV \times nm)}{E_g(eV)}$$

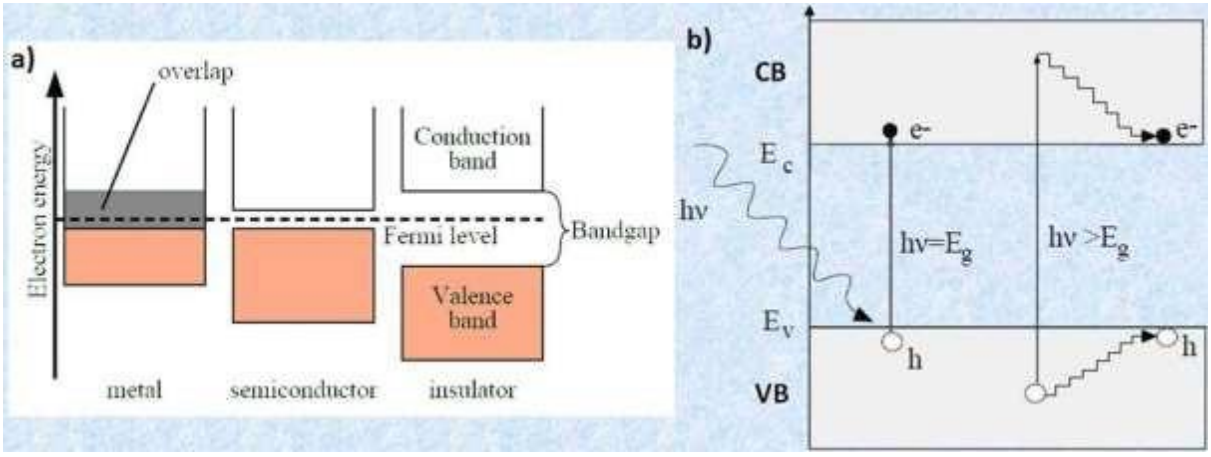
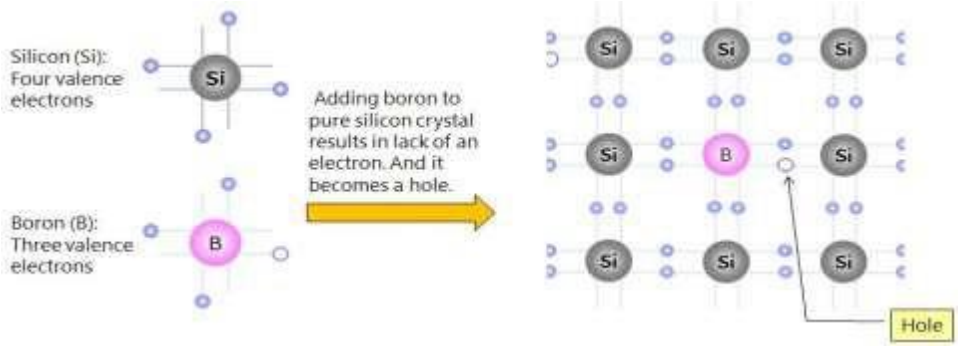


Image 14. ***a)*** *The energy band gap difference in a metal, a semiconductor and an insulator* **[25] ,** ***b)*** *Photon absorption from semiconductor material and energy bands Valence and Conduction* **[6]**

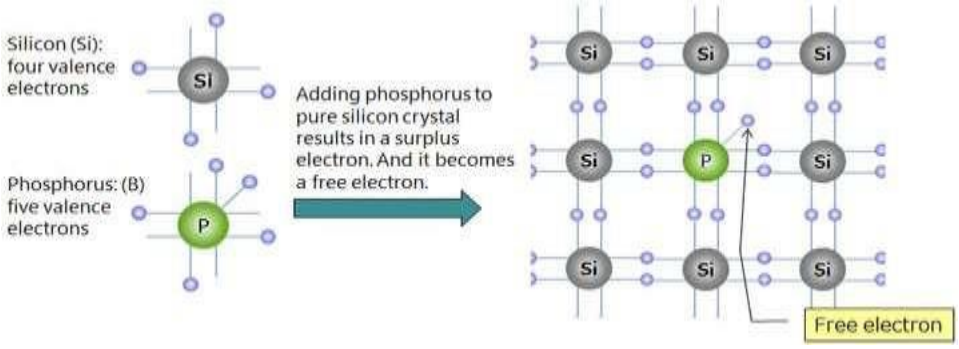
The semiconductors also classified into three categories:

- i: Intrinsic (pure) semiconductor undoped

- p: P-type semiconductor doped with majority carriers the holes **[26]**



- n: N-type semiconductors doped with majority carriers the electrons **[26]**



PN junction is called the contact surface between P-type and N-type semiconductor.

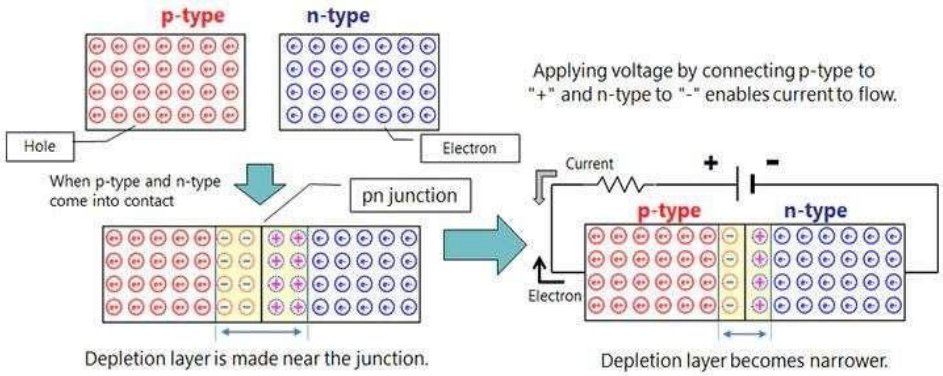


Image 15. PN junction **[26]**

As shown in the Image 15. the:

- Movement of electrons from the type N-type semiconductor to the P-type semiconductor
- Moving of holes from the P-type semiconductor to N-type semiconductor
- Mutual neutralization of the carriers and the creation of a depletion region on either side of the contact
- Potential barrier called the minimum potential V_0 to be applied externally to the diode to overcome the depletion region, the value of barrier potential lies between 0.3V – 0.7V depends on the type of material used **[6]**

2.1 Photovoltaic Effect

The photovoltaic effect is the generation of voltage and electric current in a material upon exposure to light. The result is:

- Photo creation of "free" carriers (photoconductivity)
- And creation of an internal electric field in the contact area of two semiconductors

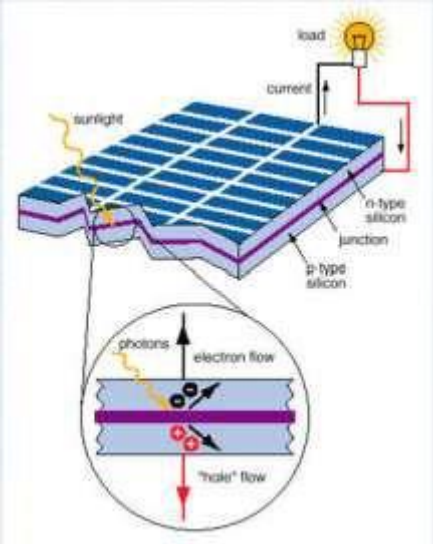


Image 16. Photovoltaic effect, PN junction exposure to sunlight **[6]**

2.1.1 Photocurrent

The absorbed photons produce mobile carriers (Photon ⟶ Electron + hole). The internal electric field pushes them to areas with similar loads, creating the current load stream.

The accumulated loads at the ends give the diode current, opposite of current load. Generating a photocurrent, when a photovoltaic cell receives an appropriate amount of radiation, it is excited and generates an electric current, the photocurrent density, will be proportional to the photons absorbed by the cell. **[6]**

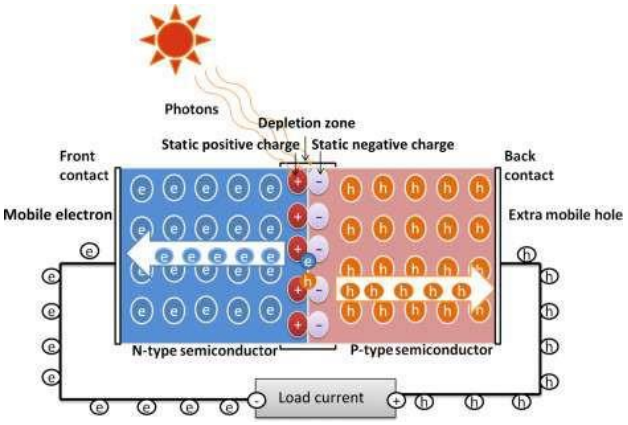


Image 17. Photocurrent generation and supply to the load **[27]**

2.2 Characteristic Curve Current (I) - Voltage (V) of Photovoltaic

The photovoltaic cells have a complex relationship between their operating environment and the maximum power they produce. The Fill Factor, abbreviated FF, is a parameter that characterizes the non-linear electrical behavior of the solar cell. The fill factor is defined as the ratio of the maximum power from the solar cell to the product of the open circuit voltage $\mathbf{V_{oc}}$ and the short circuit current $\mathbf{I_{sc}}$.

For each given set of operating conditions, the cells have a single operating point where the values of current (**I**) and voltage (**V**) of the cell result in maximum output power.

These values correspond to a specific load resistance, which is equal to $R = \frac{V}{I}$ as determined by Ohm's law. The power **P** is given as $P = V \times I$.

This is known as the Maximum Power Point (**MPP**) and corresponds to the "**knee**" of the curve.

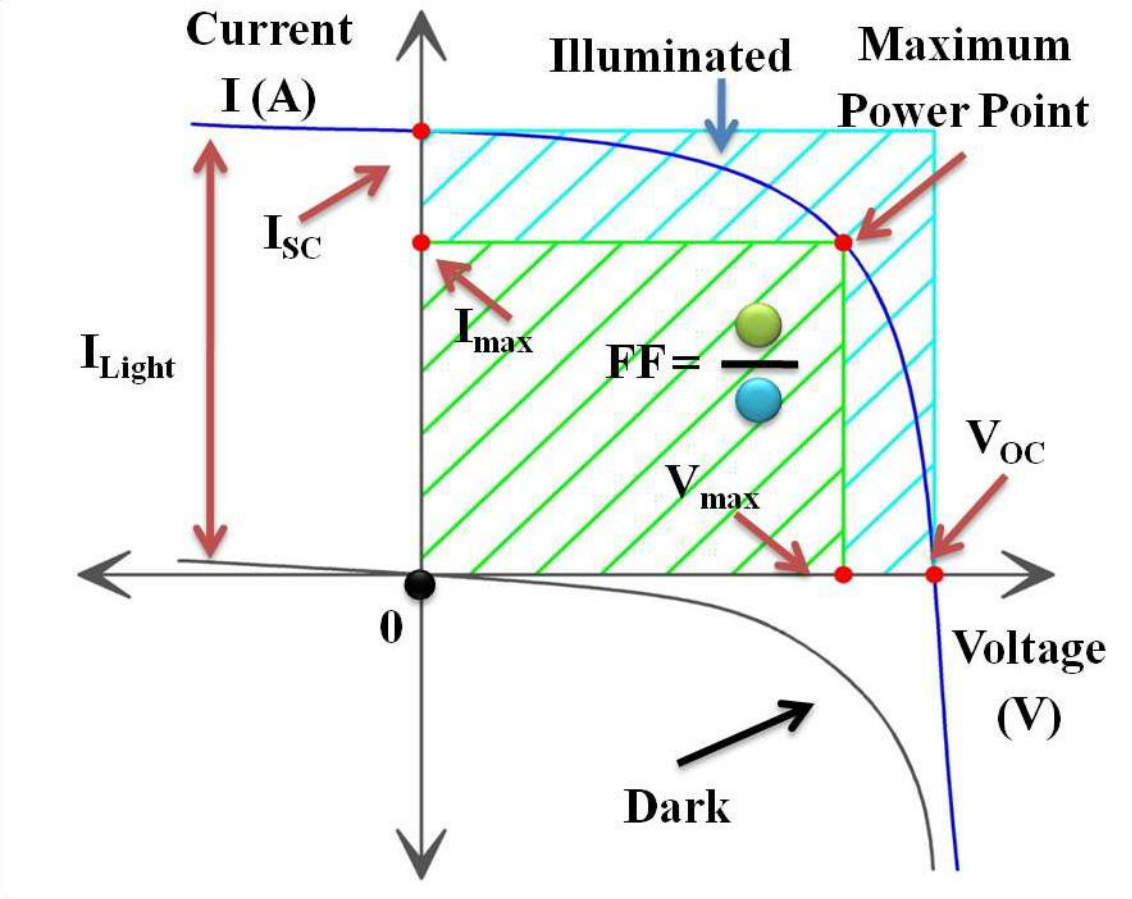


Image 18. Characteristic I - V Curve of Photovoltaic

Therefore the most basic parameters for the **<u>electrical characterization</u>** of a photovoltaic are:

- Open circuit voltage (**Voc**): The voltage at zero current

- Short circuit current (**Isc**): The current at zero voltage
- Power max or MPP (**Pmax**): The power at the "knee" of the I-V curve
- Current max (**Imax**): The current at Maximum Power Point
- Voltage max (**Vmax**): The voltage at Maximum Power Point
- Fill Factor (**FF**): the ratio of the maximum electrical power to the product of the short circuit current and the open circuit voltage of a photovoltaic cell: $FF = \frac{Imax \times Vmax}{Isc \times Voc}$
- Photovoltaic Efficiency (**n**): The ratio of the electric output power to the incoming power of the solar radiation incident on the surface of the frame.
  Photovoltaic efficiency calculation: $\boldsymbol{PCE}(\%) = \frac{FF \times Isc \times Voc}{G \times Area} = \frac{Imax \times Vmax}{Pin} = \frac{Pout}{Pin}$
  [where $Pin = G\,(\frac{W}{m^2}) \times Area(m^2)$]

2.2.1 Quantum Efficiency

Quantum efficiency is the ratio of the number of electricity carriers collected by a solar cell to the number of photons that fall on it for a given wavelength. It is given as a function of either wavelength or energy.

Quantum efficiency is classified into three categories:

- External quantum efficiency (**EQE**), which is the ratio of the number of current carriers collected by the solar cell to the number of specific energy photons that hit the cell from an external source. Includes optical loss effects such as transmission and reflection.

$$EQE(\%) = \frac{Number\ of\ collected\ electrons}{Number\ of\ incident\ photons}$$

- Internal quantum efficiency (**IQE**), which is the ratio of the number of current carriers collected by the solar cell to the number of photons of a specific energy that fall on it from an external source, but also absorbed by the cell. That is, it refers to the efficiency measured by the light left after its reflection and transmission.

$$IQE(\%) = \frac{Number\ of\ collected\ electrons}{Number\ of\ photons\ absorbed\ in\ active\ layer}$$

- Incident photon to current conversion efficiency (**IPCE**), which is the ratio of the number of current carriers through external circuit to the number of specific energy photons that hit the cell from an external source.

$$IPCE(\%) = \frac{Number\ of\ electrons\ through\ external\ circuit}{Number\ of\ incident\ photons}$$

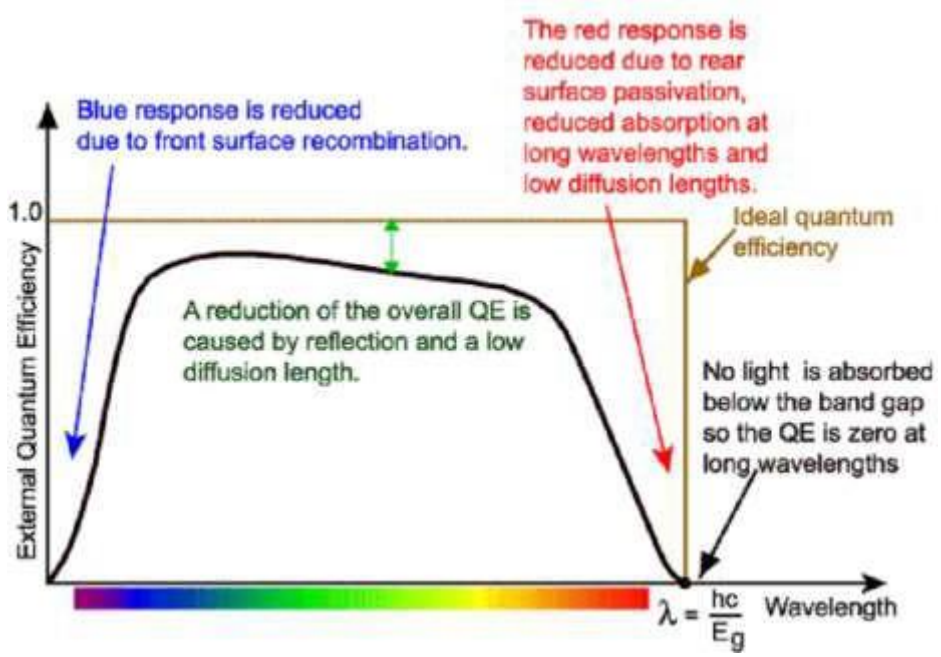


Image 19. Characteristic Curve of Quantum Efficiency **[28]**

The ideal quantum efficiency curve would have the form of square shape, however it decreases as a result of reconnections.

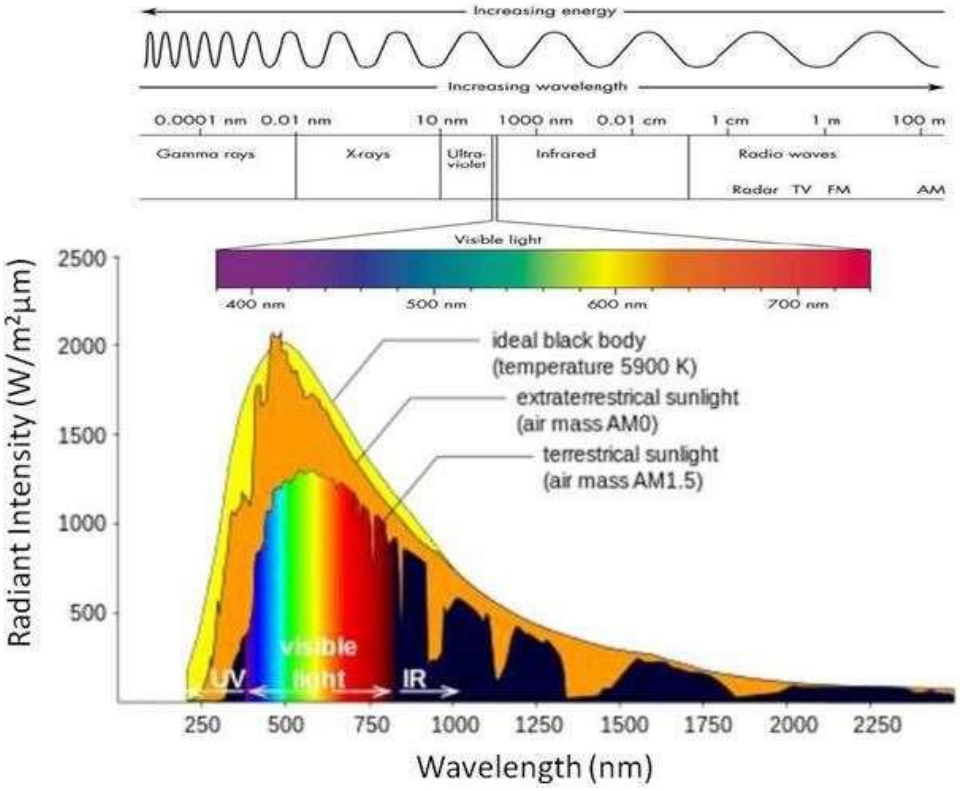


Image 20. The Electromagnetic Spectrum and Sunlight intensity on Earth **[28]**

2.3 Graphene

The composition and applications of graphene have revolutionized the scientific world and aroused worldwide interest.

A single layer of graphite is called graphene. Graphene is a 2D material, an allotropic form of carbon consisting of a single layer of sp^2 bound carbon atoms arranged in a hexagonal, honeycomb lattice. **[29]**

In 2004 Andre Geim and Konstantin Novoselov discovered graphene, they were able to isolate graphene sheets from raw graphite using the mechanical peeling method "Scotch Tape Exfoliation", this was achieved because graphene sheets are held together by weak Van der Waals forces and in 2010, they were awarded with the Nobel Prize in Physics. **[30]**

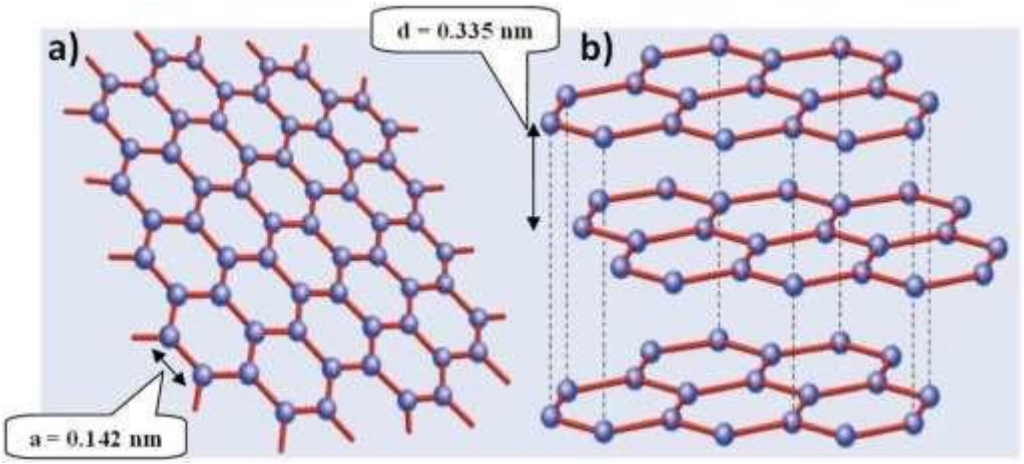


*Image 21. **a)** Graphene honeycomb lattice (2D), **b)** Graphite (3D)* **[30]**

As shown in Image 21. the neighbor atoms in graphene crystal lattice they have 0.142 nm atomic distance, the graphite layer by layer distance is 0.335 nm.

Graphene is a semiconductor with zero energy bandgap as shown at Image 22., conducts electricity better than any other known material at room temperature and is 98% transparent.

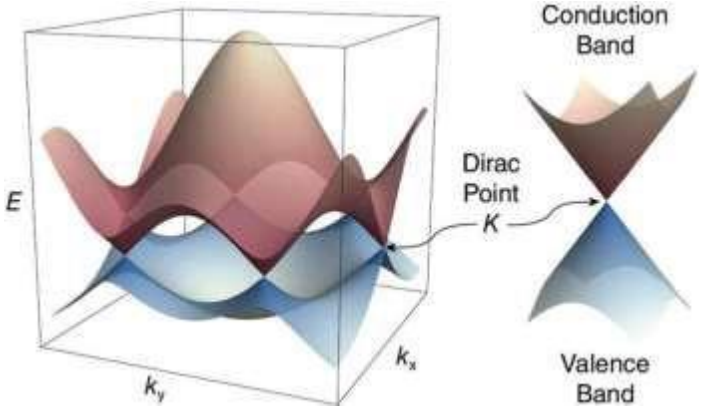


Image 22. Electronic band structure of Graphene and Dirac point **[31]**

With oxidation and reduction of Graphene we can have tunable energy bandgap.

Graphene oxide [Graphene Oxide (GO)] is an insulator that is not at all conductive but is soluble in organic solvents that allows it to be coated in films.

The purpose of reducing GO is to make the reduced graphene oxide [Reduced Graphene Oxide (rGO)], which has the mechanical properties of graphene (measure of elasticity Young ~1TPa, resistance before breaking 130 GPa, it's 200 times stronger than steel), is extremely conductive (adjustable energy gap) compared to GO which is insulating, as it remains and soluble in organic solvents making it an ideal material for many applications.

To achieve the reduction of GO to rGO there are mainly three methods, chemical (with hydrazine), thermal (~ 900 ^{o}C) and photochemical using laser, the bonds of the oxygen groups are broken and thus GO is reduced to rGO. **[28]**

2.3.1 Fabrications methods

The fabrication methods of graphene and other materials such us perovskite and molybdenum disulfide (MoS_2) are classified into two categories into Top down and Bottom up methods as shown at Image 23. , the known method "Scotch Tape Exfoliation"
is a top down method.

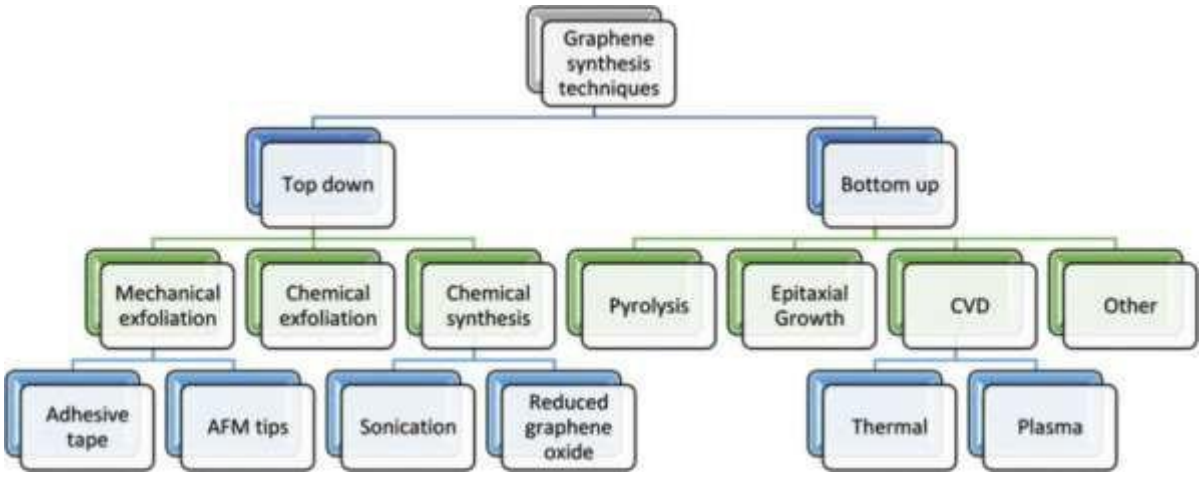


Image 23. Graphene fabrication methods **[32]**

Graphene synthesis techniques:

- In the top-down methods, bulk graphite material is always used, and it is exfoliated.
- In bottom-up methods graphene produced by molecular growth from small molecular carbon precursors with Chemical Vapor Deposition (CVD) or Epitaxial Growth on a

substrate, where controlled thickness (the number of layers) can be done using different substrate catalysts and growth parameters. **[33]**

In Graphene Perovskite solar cells (GRAPES), the graphene produced with Wet Jet Milling exfoliation (WJM) of graphite.

The WJM device uses a high-pressure jet stream to homogenize and exfoliate the sample, i.e. a multilayer material, in detail, a hydraulic mechanism and a piston provide the pressure to direct the solvent mixture [N-methyl-2-pyrrolidone (NMP)] and multilayer crystals in the processor, where the generation of shear forces promotes exfoliation of the sample.

The time during which the multilayer materials are subjected to exfoliation is less than one second. Immediately after the processor, the sample is cooled down by means of a chiller.

The WJM process can be repeated in cascade by adjusting the dimension of the nozzle (from 0.3 to 0.1 mm) in order to optimize the exfoliation process and to finely tune the morphology of the resulting flakes. **[34]**

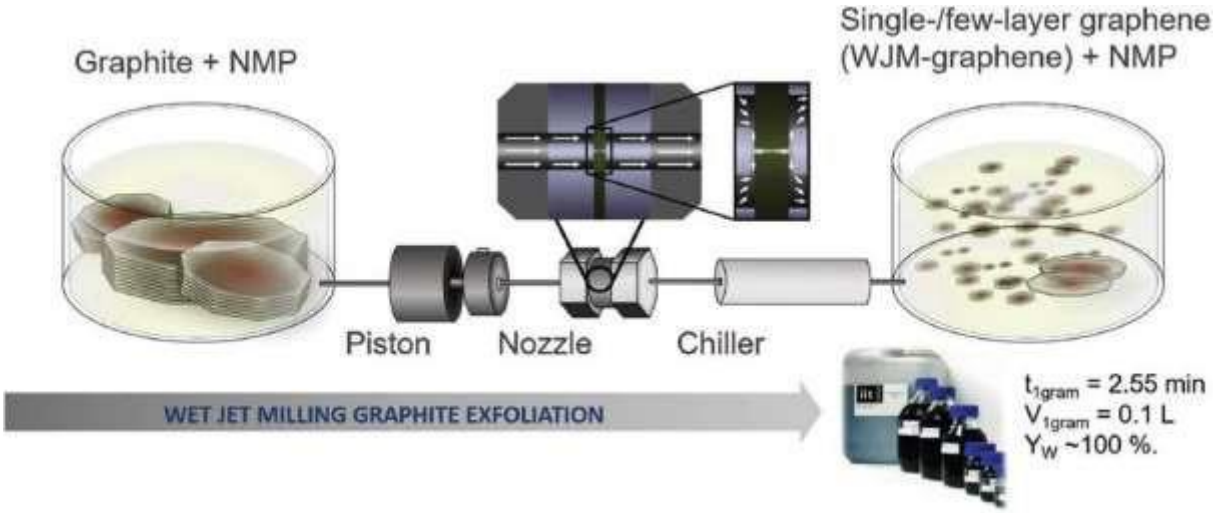


Image 24. Schematic illustration of the production of single-/few-layer graphene by WJM exfoliation of graphite

2.4 Perovskite

Perovskite called any material with a crystal structure similar to mineral perovskite. The mineral perovskite consists of calcium titanium oxide chemical formula $CaTiO_3$.

The mineral was first discovered in the Ural Mountains of Russia by Gustav Rose in 1839 and named after Russian mineralogist Lev Alekseyevich von Perovski (1792–1856).

- All perovskites have the structural formula ABX_3 (where typically, A= monovalent metal cation, B= divalent metal cation, X= halide anion or O^{2-} or S^{2-})

- Structure consists of a 3D network of corner sharing BX_6 octahedra
- The ideal perovskite has a cubic structure, as is seen in $CaTiO_3$

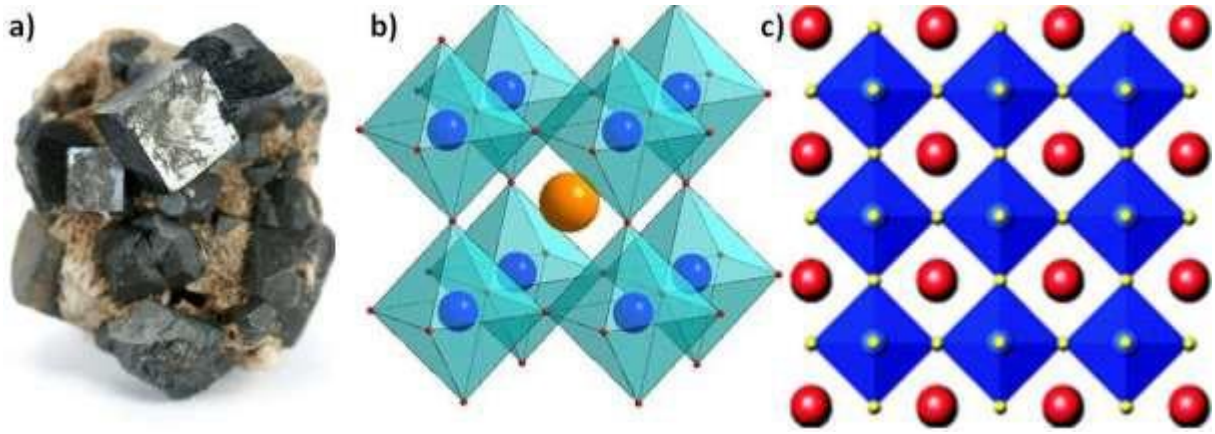
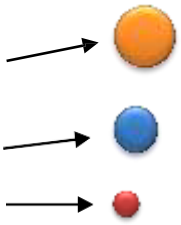


Image 25. ***a)*** *Mineral $CaTiO_3$ perovskite crystal* **[35]**, ***b)*** *3D Unit cell,* ***c)*** *Extended 3D structure* **[20]**

As shown at Image 25. at **b)** shape:

- A: large metal cations (2^+) (e.g. Ca)
- B: Small metal cations (4^+) (e.g. Ti)
- X: Anion (2^-) (e.g. O, usually O)



In 1926 Goldschmidt observed that if the A site cations were equal in size to the B site anions, so that they fit precisely into the 12 fold sites, then the length of the lines joining X-A-X is equal to ($2R_x$ +$2R_A$) or $\sqrt{2}$ times the edge of a cubic cell.

The Goldschmidt tolerance factor (t) is now used as a guide to predict the likelihood of a given combination of ions fitting into a 3D perovskite structure at a particular temperature and pressure. **[20]**

$$t = \frac{R_x + R_A}{\sqrt{2}(R_x + R_B)}$$

R_A is the radius of A cation, R_B is the radius of B cation and R_x is the radius of the anion.
In and ideal cubic structure t = 1. However lower symmetry structures do exist
$0.9 \leq t \leq 1$: Cubic, A and B ions have ideal size.
$0.71 \leq t \leq 0.91$: Orthorhombic / Rhombohedral / Hexagonal, A ions too small to fit into B ion interstices. **[20]**

Organic - inorganic perovskite semiconductors have recently revolutionized the field of solution processed photovoltaics.

These materials have enabled a rapid progression of solar cell efficiency from 4% to over 20 %, making this technology competitive with traditional silicon solar cells. **[20]**

Perovskite Photovoltaics advantages:

- Low materials and processing costs
- Tunable bandgap from 1.5 - 2.5 eV
- Good semiconductor properties, high absorption coefficient

Perovskite Photovoltaics disadvantages:

- Still in development for outdoor conditions
- Sun exposure degrade it
- Supply a load degrade it

The perovskite usually produced with chemical vapor deposition (CVD), a bottom up fabrication method. In GRAPES Photovoltaics, $MAPbI_3$ perovskite is used as active layer.

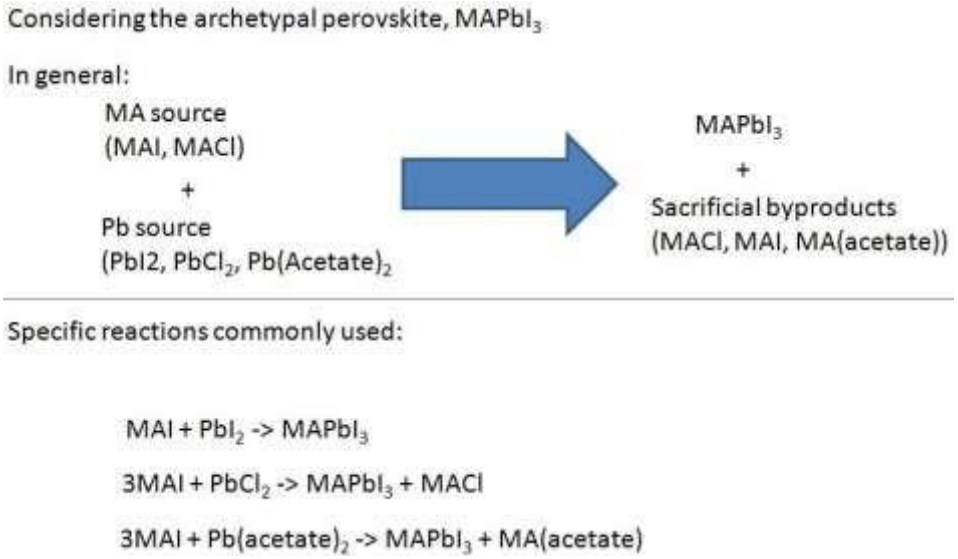


Image 26. How to form a $MAPbI_3$ perovskite **[20]**

2.5 Molybdenum Disulfide (MoS_2)

The molybdenum disulfide (MoS_2) is Transition Metal Dichalcogenide (TMD). TMD characterized the compounds that can be expressed by the formula $\mathbf{MX_2}$, where M are the transition metal atoms (Mo, W, etc.) and X are the atoms of chalcogenides (S, Se or Te). A layer of M atoms is between two layers of X atoms, like a sandwich.

They can be considered as a 2D strong X-M-X bond with a typical thickness of 0.6 nm to 0.7 nm, but the hold to other layers it happens with very weak Van der Waals forces.

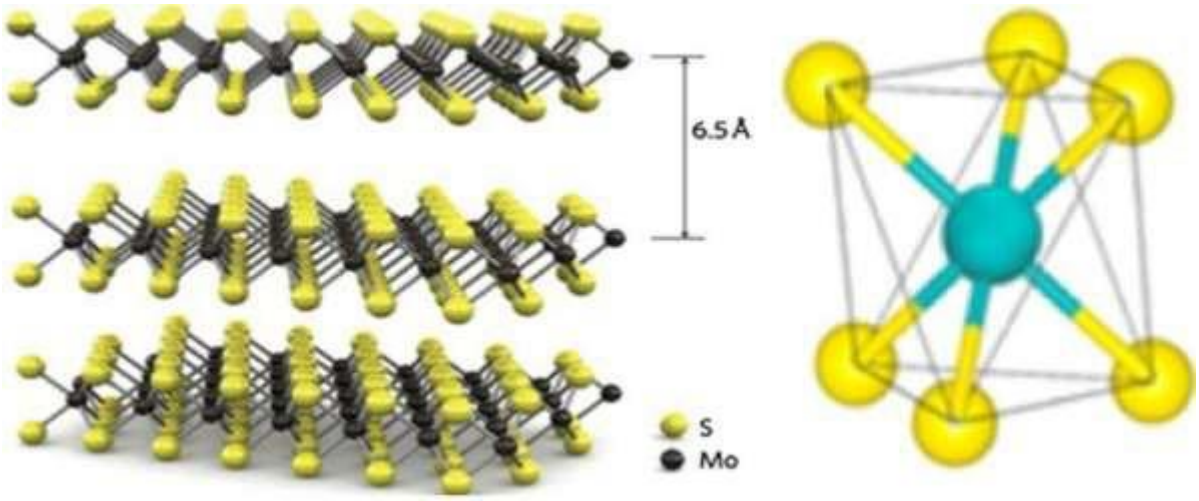


Image 27. 3D illustration of the structure of MoS2, single layers 0.65 nm thickness and a triangular prismatic and octahedral geometry **[36]**

The M and X atoms form a 2D hexagonal grid with the M atoms connected to 6 X atoms in a triangular prismatic and octahedral geometry

TMDs in bulk (3D) form are indirect energy bandgap semiconductors (Indirect bandgap), i.e. the maximum energy of the valence band is displayed at a different momentum value than the minimum energy at the bottom of the conduction band. While in the form of a single layer (2D Monolayer) they are direct energy bandgap semiconductors (Direct bandgap), the top of the valence band and the bottom of the conductivity band appear at the same momentum value (k), favoring the optoelectronic devices.

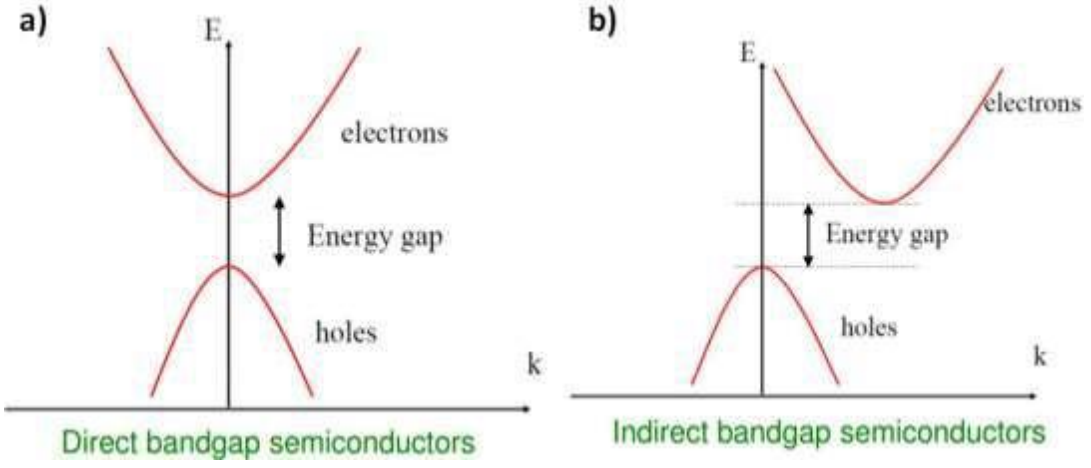


Image 28. ***a)*** *Direct energy bandgap semiconductors,* ***b)*** *Indirect energy bandgap semiconductors* **[37]**

The MoS_2 in its bulk form is a semiconductor with an indirect energy bandgap of ~ 1.2 eV, while in 2D ML it is a semiconductor with a direct energy bandgap of ~ 1.9 eV.

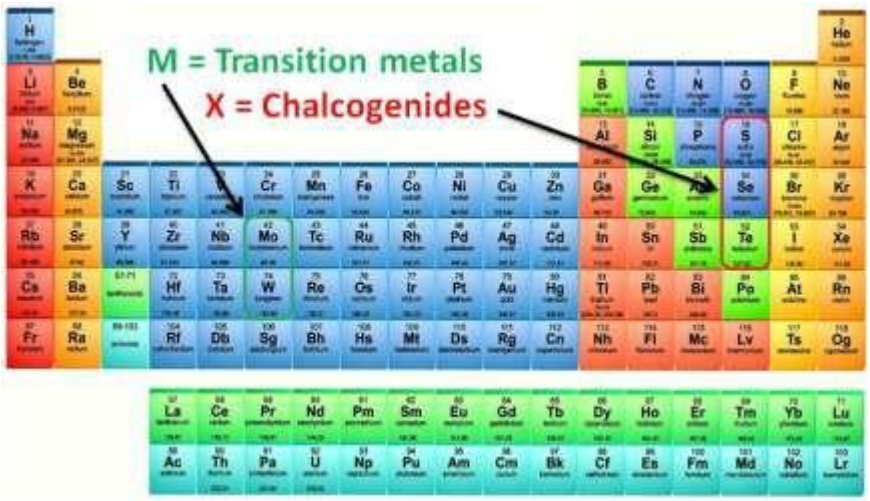


Image 29. Location of the TMDs in the Periodic Table

The MoS_2 usually produced with the same fabrication methods of the graphene. In GRAPES panels for MoS_2 fabrication, Liquid phase exfoliation used is a top down method.

2.6 Graphene Perovskite Photovoltaic Device Fabrication (GRAPES)

In fabrication of GRAPES photovoltaic devices (PVs) used 360 perovskite modules (PSM), each PSM has a substrate area of 11x11cm^2 and is composed by 9 in series connected perovskite solar cells (PSCs) with an active area 9.1cm^2 resulting in a total active area of 81.9 cm^2 deposited on 121 cm^2 substrate area.

The normal structure of graphene related materials (GRM) enabled cell stack selected as we can see in Image 30., in inverted structure hole transport layer is at the bottom (near the glass) and electron transport layer at the top. **[20]**

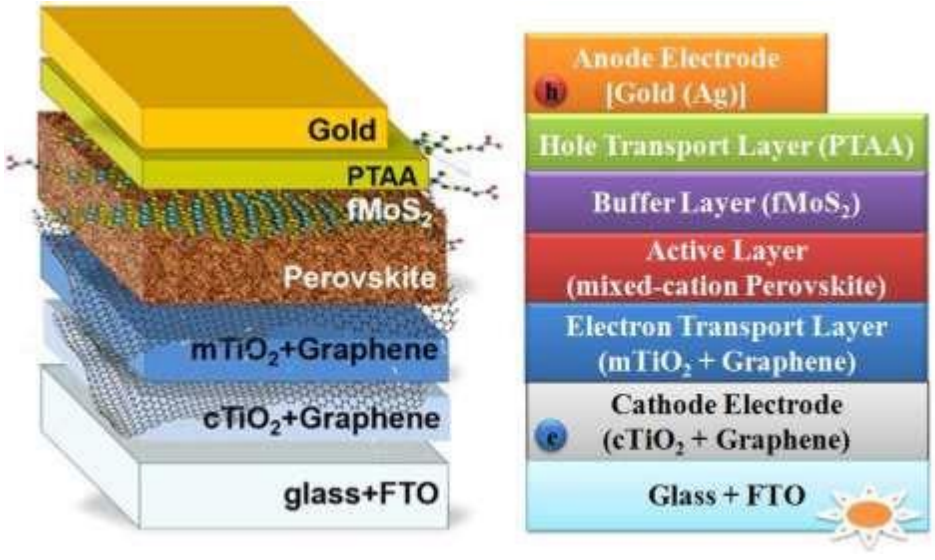


Image 30. GRAPES Photovoltaics normal structure

The graphene used in GRAPES PVs in form of flakes into the $mTiO_2$ ETL promote the crystallization of the perovskite wrapped within it, leading to an electron trap density of about one order of magnitude lower than one found in pristine ETL. Also used in $cTiO_2$ layer reduces the device dark current and improves the Fill Factor of the resulting perovskite solar cell (PSC).

The MoS_2 used in form of few layer flakes ($fMoS_2$) in the perovskite-HTL interface as buffer layer improves the hole transfer from the absorbing layer to the HTL, compared to reference devices without $fMoS_2$.

The use of graphene and $fMoS_2$ stabilizes the perovskite-ETL and perovskite-HTL interfaces respectively, under harsh testing conditions, such as prolonged illumination and thermal stress. The choice of PTAA as HTL was motivated by its intrinsic thermal stability at 85^{o}C, this temperatures requires during ISOS (**I**nternational **S**ummit on **O**rganic Photovoltaics **S**tability) stress test protocols and during conventional panel lamination processes.

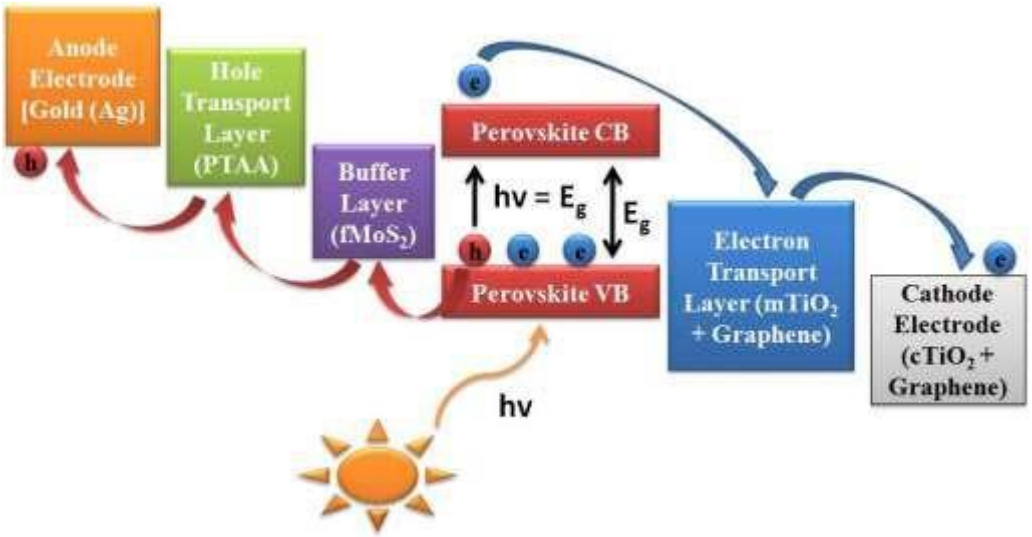


Image 31. GRAPES PVs Energy diagram

The incident radiation falls into GRAPES PVs as shown in energy diagram at Image 31., the photons absorbed by perovskite (Absorbing Layer) excites electrons from valence band to the conduction band, the excitation of electrons leaves a hole in valence band and now we have the generation of free mobile carriers electrons and holes. The electron transport layer collects the free electrons from absorbing layer and block the free holes, the collected electrons transferred to cathode electrode, respectively the buffer layer improves the hole transfer from the absorbing layer to the hole transport layer which in turn collects the holes and guide them to anode electrode, which with the cathode electrode we can use them to supply the electric loads, also the hole transport layer blocks the free electrons.

3. Fabrication of the Electronic Device of IV-MPPT Charger Regulator

The purpose of IV - MPPT Charger Regulator device is to run different IV, MPPT and Photovoltaics Behaviour Reading (PVBR) algorithms to study efficient the behavior of Graphene Perovskite (GPe) Photovoltaics and other technologies such as CdTe , Si , in real time outdoor. The device create curves IV, PV, PVBR, etc, also tracking the Maximum Power Point in real time, so the maximum power conversion efficiency (PCE) of photovoltaics achieved to charge batteries and study more extensively the photovoltaics because the device record the measurements, like energy yield (wh).

3.1 Maximum Power Transfer Theorem

The operational principle of the IV - MPPT Charger Regulator device is the maximum power transfer theorem.

The theorem of maximum power transfer states that the maximum power transferred from the source $\{V_{Thevenin}$, $R_{Thevenin}\}$ to the load $\{R_{Load}\}$ when the load resistance is equal to the Thevenin's equivalent resistance. **[38]**

- $\mathbf{R_{Load} = R_{Thevenin}}$

In our case the source are photovoltaics [GRAPES(G-Pe), CdTe, Si and more] and the load is **M**aximum **P**ower **P**oint **T**racker (**DC-DC Boost Converter**) or called **"IV - MPPT Charger Regulator"**, as we can see in the following diagram of Image 32.

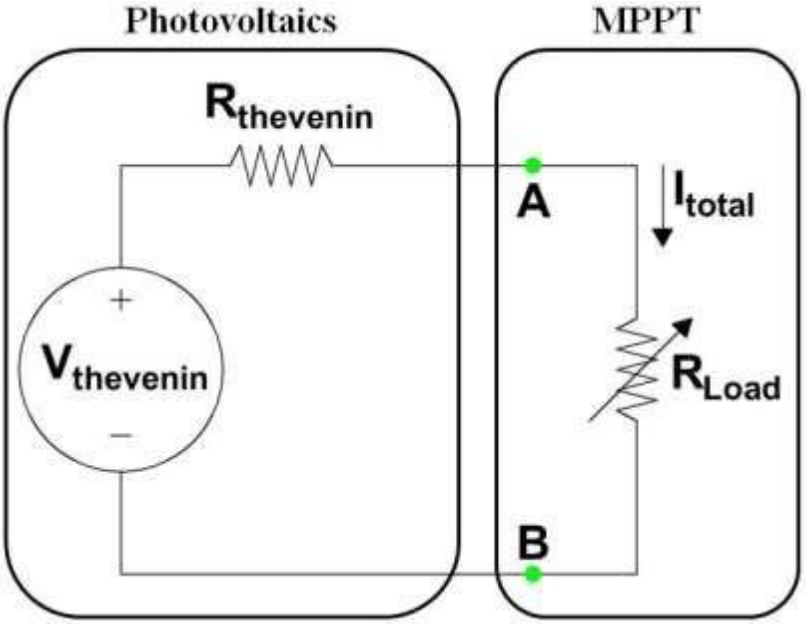


Image 32. Maximum Power Transfer Theorem Diagram

The purpose of MPPT device is to track the maximum power point in real time is to achieved the maximum power conversion efficiency (PCE) of photovoltaics.

The device can adjust the load (R_{Load}) so achieving to find the equivalent of internal photovoltaic resistance ($R_{Thevenin}$) in different weather, shading, inclination conditions, so the maximum power point achieved all the time.

The load adjustment become with help of microcontroller, with changes in Duty Cycle (**D**) of pulse width modulation signal (PWM) see Image 33. $\boldsymbol{D} = \frac{T_{on}}{T_{period}} = \frac{T_{on}}{T_{on}+T_{off}}$ **[39]**

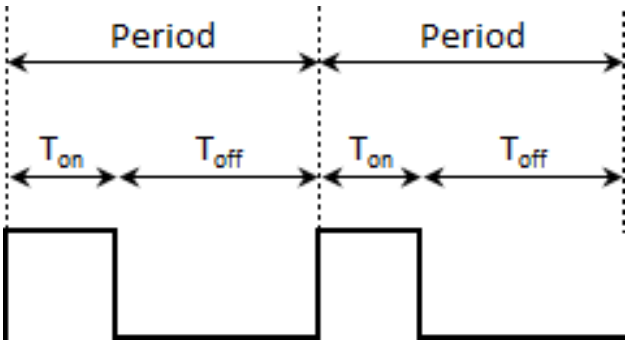


Image 33. PWM signal

3.2 DC-DC Boost Converter

The DC-DC Boost Converter is a device that step up the voltage while stepping down the current from its input to its output see Image 34., the output voltage is always higher than the input voltage.

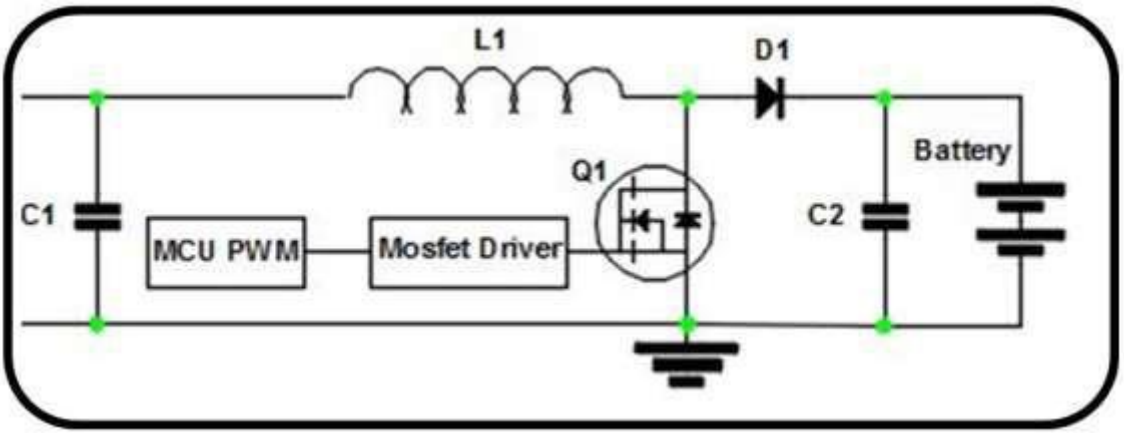


Image 34. DC-DC Boost Converter Device Schematic

The operational principle that drives the boost converter is the tendency of an inductor (**coil**) to resist changes in current by either increasing or decreasing the energy stored in the inductor magnetic field. **[41]**

With the use of PWM signal that drives the mosfet Q1, the DC-DC Boost Converter operates in two phases (states):

In the first phase the mosfet Q1 is ON and conducts like closed switch see Image 35., the input current flow in left loop (with red color), through inductor **L1**, then to mosfet **Q1** and last at capacitor **C1**, the energy start to stored into inductor L1 by generating a magnetic field in these phase. The polarity of the inductor at the left side is positive. **[40]**

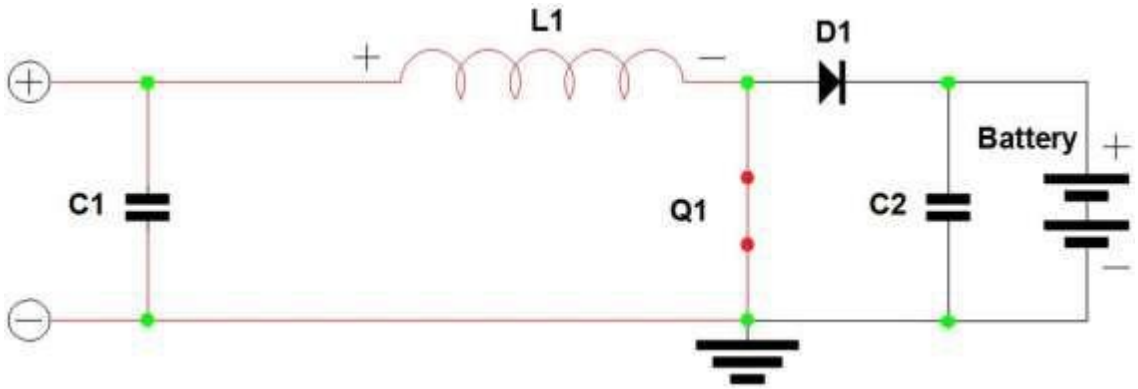


*Image 35. DC-DC Boost Converter mosfet Q1is **ON** phase (like closed switch)*

In the second phase the mosfet Q1 is OFF and doesn't conducts like open switch see Image 36., the current will be reduced as the impedance is higher, the previously stored magnetic field will be reduced in energy to maintain the current towards the load, thus the polarity will be reversed which mean the left side of the inductor will become negative. The result is the input and inductor **L1** are two sources in series causing a higher voltage to charge the capacitor **C2** through the diode **D1**. **[40]**

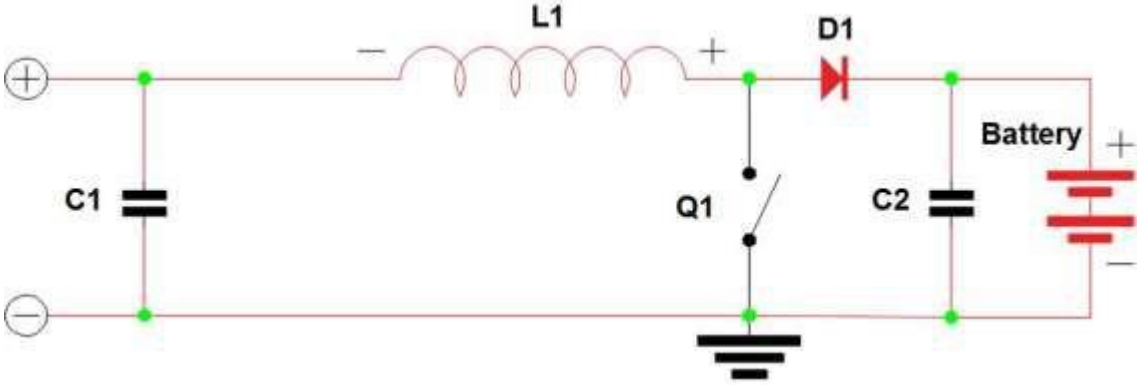


*Image 36. DC-DC Boost Converter mosfet Q1 is **OFF** phase (like open switch)*

In case the current in the coil is continuous it results: $\frac{vout}{v_{in}} = \frac{\cancel{I_{in}}}{I_{out}} = \frac{1}{1-D} => V_{out} = \frac{V_{in}}{1-D}$

and therefore in this case by controlling the pulse width (changes in D), it is possible to control the output voltage which will occur greater than the input. (By definition D < 1).

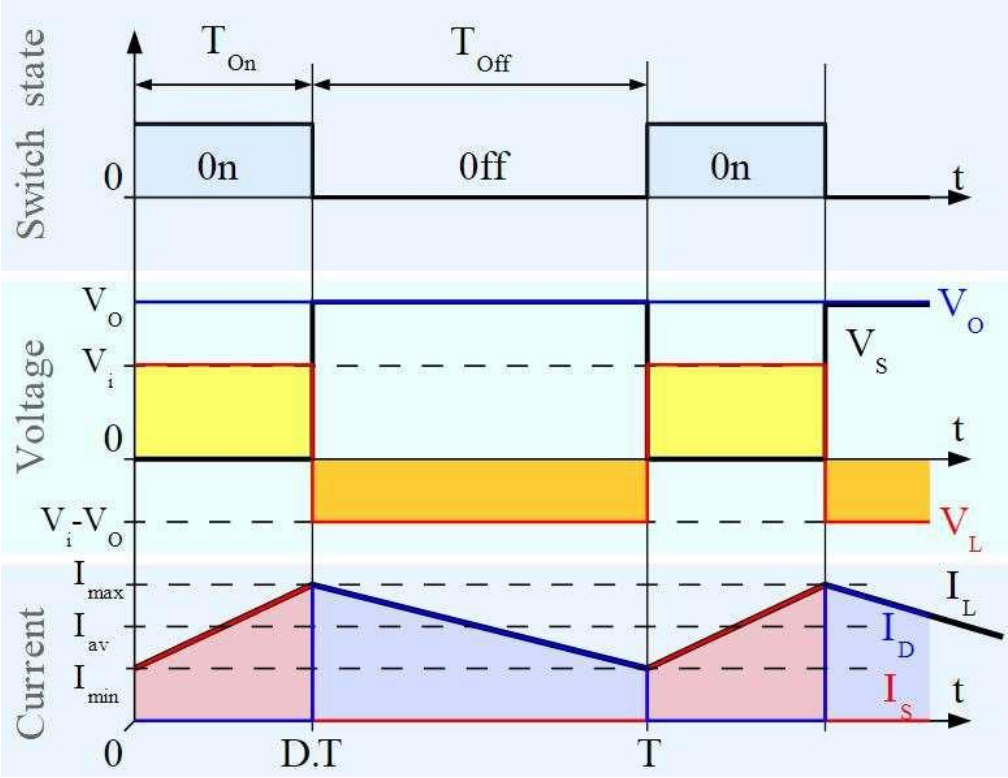


Image 37. Waveforms of inductor (coil) current and voltage in a DC-DC Boost Converter operating in continuous mode.**[41]**

The DC-DC Boost Converter topology selected because of the position of mosfet in the circuit, that can give these **two phases**, in the first phase with **mosfet ON** can have completely **short circuit**, so can collected, the Isc point in IV curve, and in the second phase with **mosfet OFF** can have completely **open circuit** if the voltage of photovoltaic is smaller or the same with the battery, because **D1** don't let the current flow if the voltage is smaller than battery's, must have the same voltage of battery plus the diode bias voltage to conduct with battery through **D1** to charge it, so can collected, the Voc point in IV curve.

The battery must always be plugged to converter before source it with photovoltaics. In the 0% duty cycle (mosfet always OFF) the battery give the starting voltage of open circuit it works like **dynamic load** in the system as shown above, when the duty cycle start to raise the voltage step up, so the current flow through **D1** and the converter starts to charge the battery, also when the charger and battery resistance become the same with photovoltaic (through the changes of duty cycle) the maximum power point achieved in IV curve, in the end if the duty cycle goes at 100% (mosfet always ON), achieving isolation from the battery as shown at Image 35. and in turn achieved short circuit with photovoltaic so this is short circuit current.

3.3 Hardware of Measurement System

The hardware of IV - MPPT Charger Regulator Measurement System designed that way as shown in following schematic diagram (Image 38.) motivated that the measurements are high voltages and common knowledge is that the conventional operation amplifiers (OPAM) voltage limits can't reach so high.

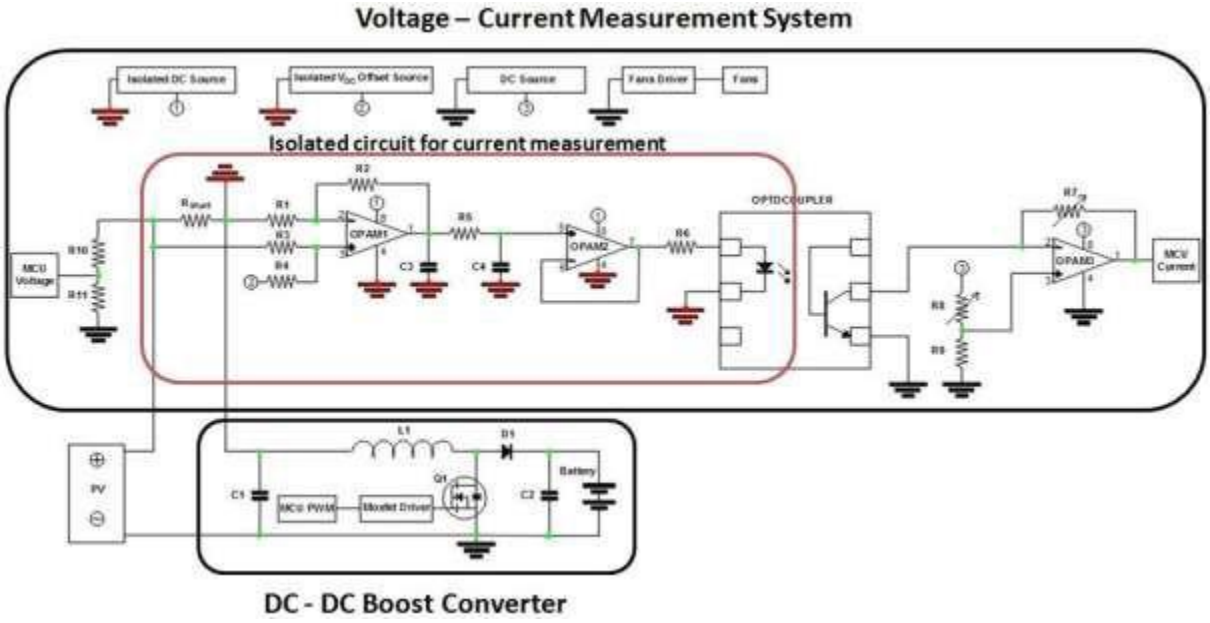


Image 38. IV - MPPT Charger Regulator Schematic Diagram

3.3.1 Current Measurement

As known from Ohm's law equation $I = \frac{V}{R}$ that can measure the current through the voltage drop across the two points of prototype resistance (**R_{shunt}**).

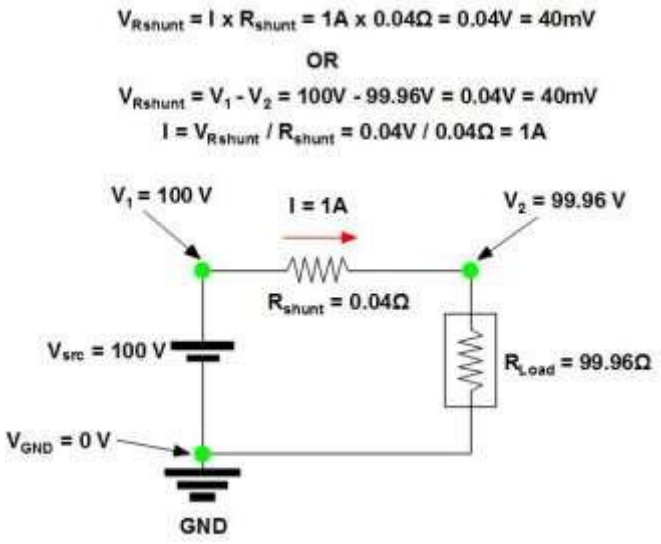


Image 39. Ohm's Law Example

So using this property of Ohm's Law in practical way, with one prototype resistance (extremely low resistance is used so don't have power loss in current measurement system) and measure the voltage drop across it and with Ohm's Law equation calculated the current.

Using the isolation circuit (Image 38.) for current measurement, because now don't have to measure high voltage like example (Image 39.) 100V or 99.96V and do the subtraction 100V - 99.96V = 0.04V , measure directly the voltage drop of prototype resistance (**R_{shunt}**) which is 0.04V (Image 40.) because putted the isolated ground at 99.96V and Kirchhoff's node method say that have new voltage reference as zero voltage and because used the isolation system all other device is unchanged. So now with conventional OPAM can measure this low voltage level for the current calculation measurement.

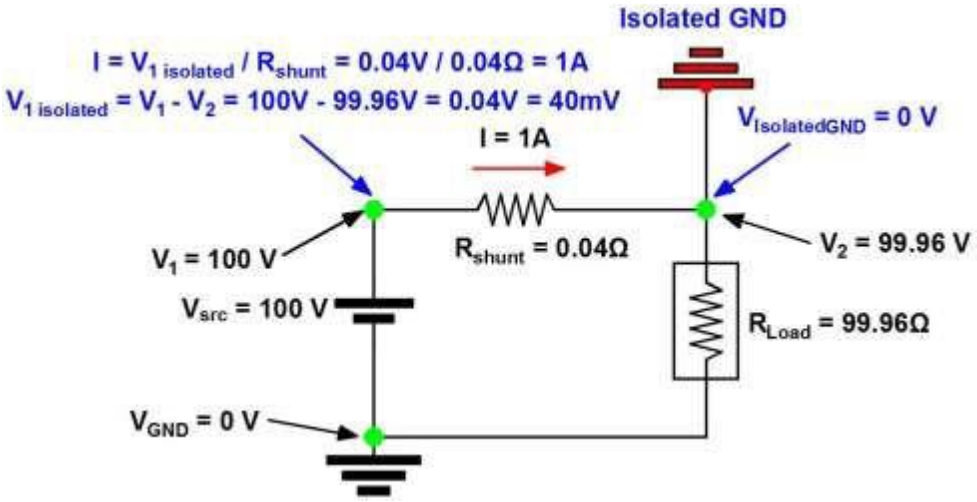


Image 40. Kirchhoff's node method , Isolation Voltage Example

For the isolation system is used an optocoupler, the led part of optocoupler is on isolation circuit and the transistor to boost converter system (Image 38.) that transfer the current measurement information to a microcontroller through a change of gain in non inverted amplifier.

Changes in current of isolation circuit change the optocoupler's Led illumination, then in turn changing the resistance of optocoupler's transistor so is used like resistance on non inverter amplifier see Image 41.

$$Amplifier\ Voltage\ Gain\ (Av) = (\frac{R7}{Roptocoupler's_transistor}) + 1$$

Voltage for current measurement that goes at MCU is:

$$V_{CURRENT} = Av \times ((\frac{R9}{(R9 + R8)}) \times DC\ Source_3)$$

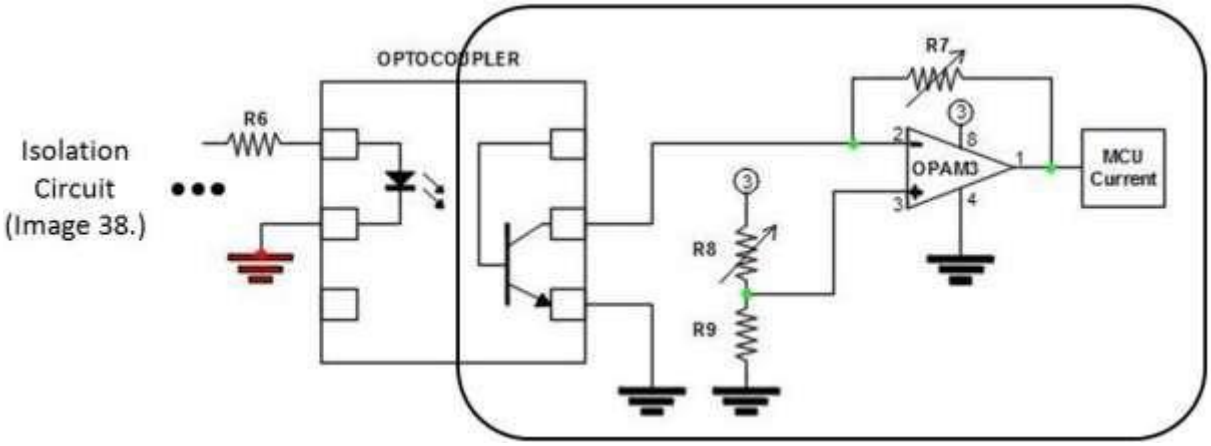


Image 41. Non Inverted Amplifier for Current Measurement

With that system (Image 41.) can be used different microcontroller technologies like ARM Cortex MSP432, STM32, or Arduino, because of configuration of the voltage level output.

3.3.2 Voltage Measurement

For voltage measurement is used a voltage divider circuit (Image 38.) so can divide the high voltage of photovoltaics to a voltage level of microcontroller, like the following example of voltage divider (Image 42.) (Extremely high resistances are used for extremely low current so don't have power loss in the voltage measurement system).

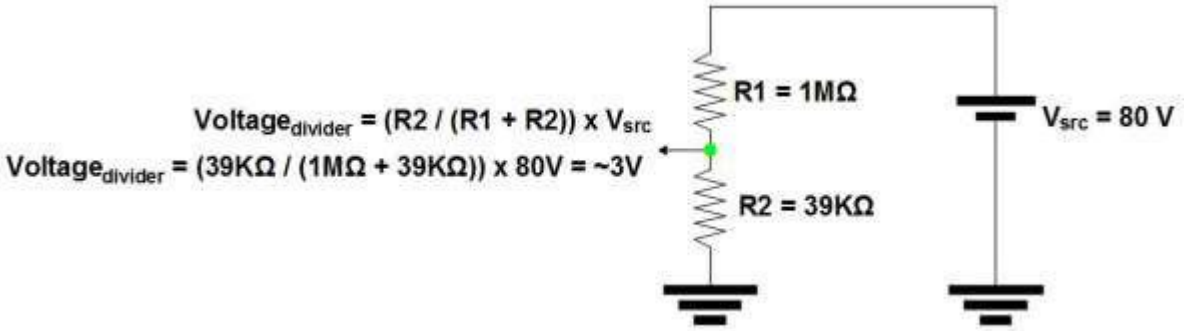


Image 42. Voltage Divider Example

3.3.3 Isolated Circuit for Current Measurement

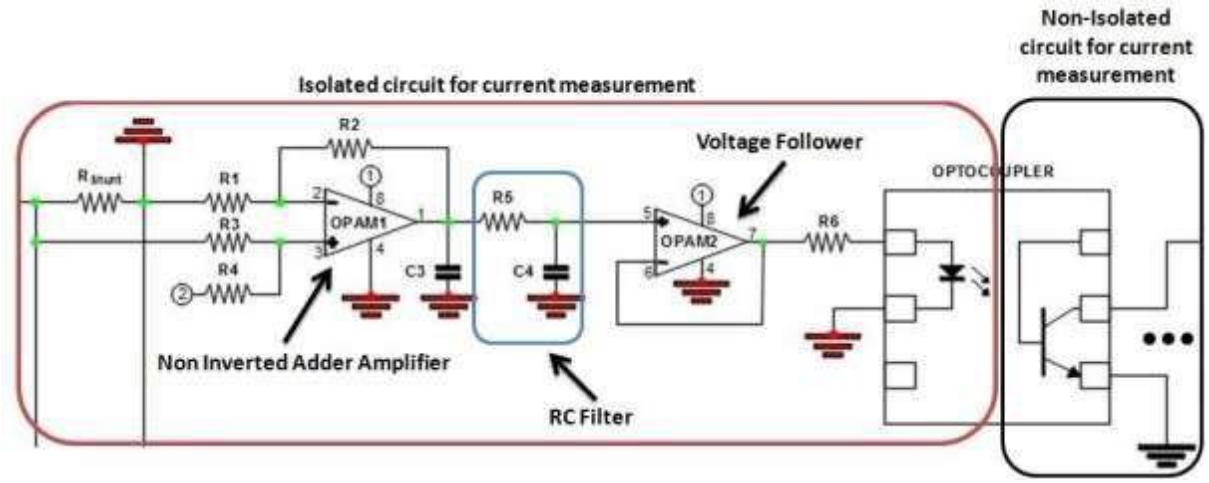


Image 43. Isolated Circuit for current measurement schematic diagram

After the current pass through the R_{shunt} and having the voltage drop as shown above in Image 40., it's used a non inverted adder amplifier and it's sum the voltage drop from R_{shunt} with the voltage from isolated voltage dc offset source and drive it into RC Filter to reduce any ripple from DC-DC Boost Converter, the filter allow frequencies up to 7.238 Hz.
The maths of this filter is (R5=1MΩ, C4=22nF):

$$F(Hz) = \frac{1}{2\times\pi\times R\times C} = \frac{1}{2\times 3.14\times 1M\Omega\times 22nF} = 7.238\ Hz$$

The non inverted adder amplifier with voltage dc offset source used so can have precise measurement, because with adding voltage from dc offset source, avoided the non linear region of operation amplifier material (LM6142) that it has ~ 3.8mV input voltage offset.

After the RC filter follows a voltage follower for signal amplification and the current pass through R6 resistance to drive the optocoupler's LED, must have in output of voltage follower 1.5V with open circuit so no current pass through R_{shunt} the R6 has the value of 150Ω so the maths for forward current that drive the optocoupler's 4n25 LED is:

$$I_F = \frac{1.5V}{150\Omega} = 0.01A = 10mA$$

so the relative current transfer ratio for 4n25 optocoupler at 25°C is 1 (linear) see the Image 44. from 4n25 datasheet.

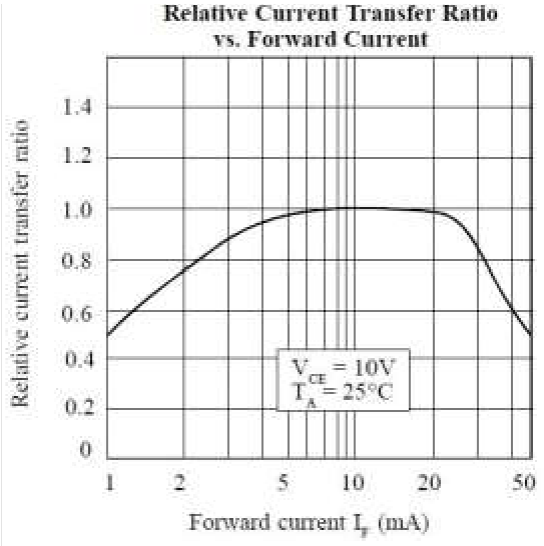


Image 44. Relative current transfer ratio to Forward current in 4n25 optocoupler

Any changes in current that pass through R_{shunt} change this 1.5V, every 1A have 40mV change with max at 3A, 120mV $[(1.5V + 0{,}12V) = 1.62V$ the new current $I_F = \frac{1.62V}{150\Omega} = 0{,}0108A = 10{,}8mA]$, this change the current that drives the optocoupler's LED so the non-isolated circuit of the optocoupler change respectively, this meaning the optocouplers transistor polarized and it's resistance become smaller that mean's changes in gains of the amplifier at Image 41. that shown above.

3.3.4 Sources and Drivers Schematics

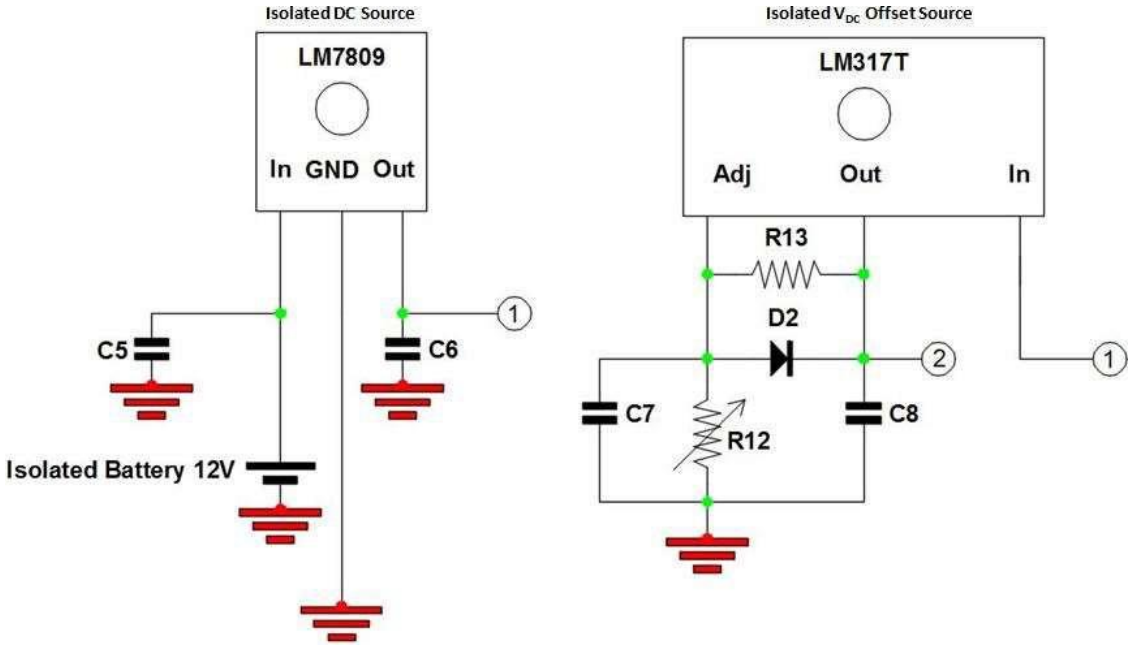


Image 45. Schematics of Isolated Sources

The Isolated Sources used as:

- 7809 used as Isolated DC Source that supply the isolation circuit generally
- LM317T used as Isolated V_{DC} Offset Source that supply the non inverted adder amplifier the 1.5V

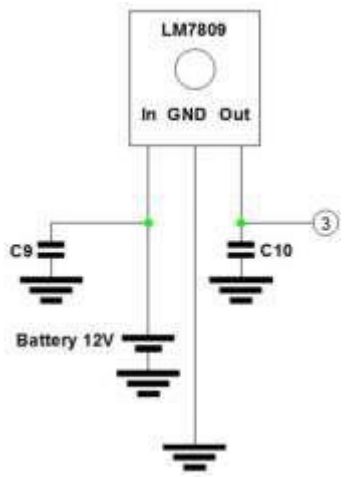


Image 46. Schematics of Non-Isolated DC Source

The Non-Isolated DC Sources used as:

- 7809 used as Non-Isolated DC Source that supply the Non-Inverted Amplifier for Current Measurement at Image 41.

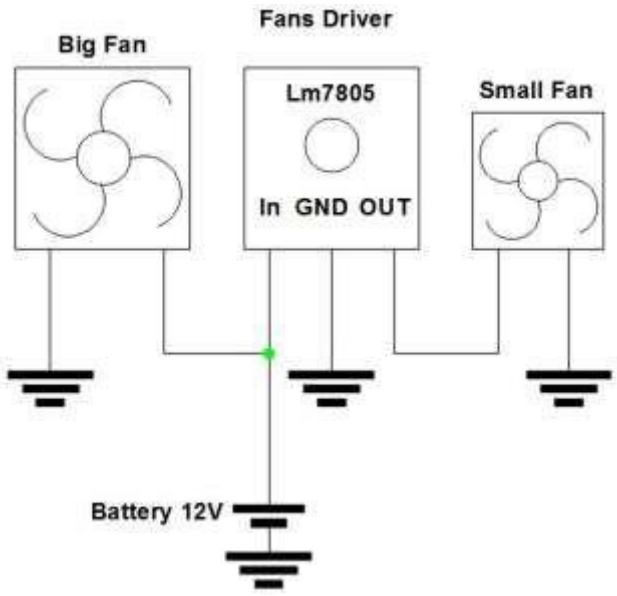


Image 47. Schematics of Fans Driver

As driver of the fans (big and small) used a 7805, the big fan supplied directly from 12V Source that also supply the 7805 too, the 7805 in his turn supply the small fan with 5V. The big fan used for cooling the whole system, the small one specifically for the R_{shunt}.

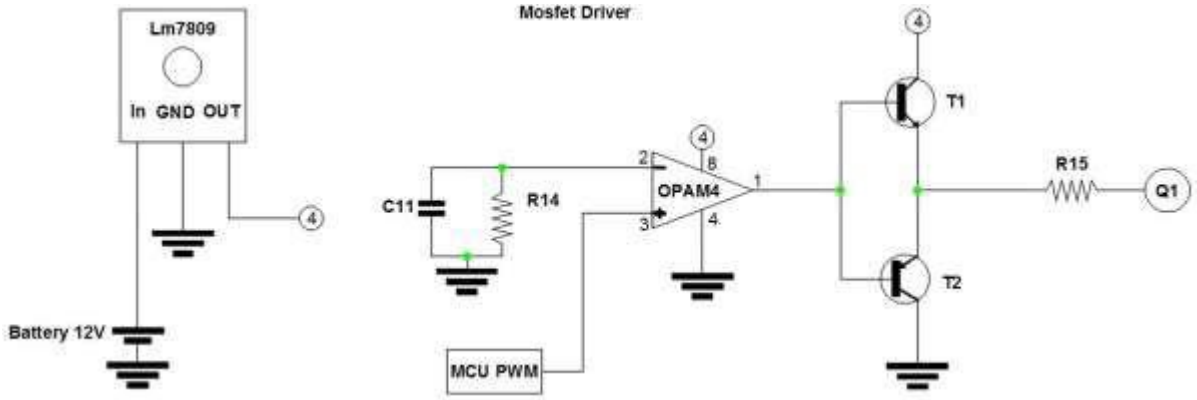


Image 48. Schematics of mosfet driver

The mosfet driver use:

- LM7809 for DC Source, to supply 9V the operation amplifier LM6142 and the two transistors T1[BC639 (NPN)] and T2[BC640(PNP)]
- OPAM4 is the LM6142 and works as comparator, the capacitor and the resistance ground the noise, so can achieved clear zero voltage so any change in (+) input give us full 9V at OPAM4 output, this change is the PWM signal from microcontroller. The PWM signal is 3926.25 Hz
- The T1 and T2 transistors are in push pull amplifier topology, to polarize the mosfet Q1 IRLB4030PBF and to discharge it's gate immediately so can produce the PWM signal, whole square like and not trapezoid shape

3.4 Power Losses of IV-MPPT Charger Regulator

The device of IV-MPPT Charger Regulator has power losses due to the following contributors:

- DC-DC Boost Converter
  - Inductor losses (2.8mH, 0.03Ω)
  - Mosfet losses (IRLB4030PBF)
    - Conduction losses
    - Turn on switching losses
    - Turn off switching losses
  - Diode losses (IXYS DSA50C100QB)
    - Voltage bias losses
    - Internal resistor losses
- Hardware of Measurement System

- Isolation system
  - Isolation Sources (LM7809, LM317T)
  - Voltage drop in Rshunt (0.04Ω)
  - Operation amplifiers
  - Optocoupler
- Non-Isolation system
  - Non-Isolation Sources (2 x LM7809, LM7805)
  - Operation amplifiers
  - Big Fan
  - Small Fan

❖ Microcontroller Power Losses

- Standby mode
- Pin for PWM Signal

3.4.1 Theoretical Approximation of DC-DC Boost Converter Power Losses

The DC-DC Boost Converter power losses theoretical approximation calculation done on CdTe #2 photovoltaic at $Solar\ Irradiance = 1023.398\ \frac{w}{m^2}$, (1 Sun) at maximum power point of Forward Exhaustive Search Scan IV (FES) at Duty Cycle (D) = 7.059%.

Electrical characteristics:

I_{sc} = 2.01A, V_{oc} = 51.46V, I_{max} = 1.653A , V_{max} = 37.72V, P_{max} = 62.35116W,

FF = 60.37%, CdTe #2 PCE = 8.462%.

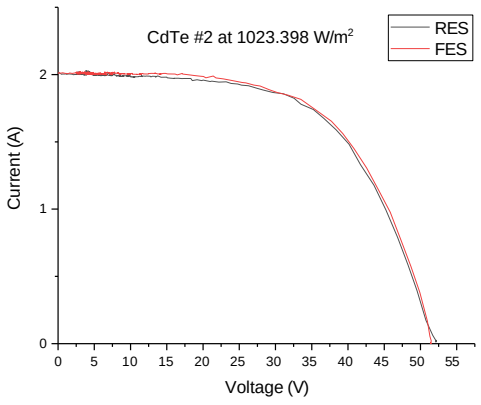


Image 49. Reverse and Forward IV of CdTe #2 Photovoltaic (25/08/2021)

Inductor power losses:

$$P_{Inductor} = I_{max}^2 \times R_L = 1.653A^2 \times 0.03\Omega = 0.08197227W$$

Mosfet power losses:

First need to find the $\mathbf{t_{on}}$ and $\mathbf{t_{off}}$ times as shown at the Images 50 and 51. to calculate the energy losses and then power losses. So this equations used.

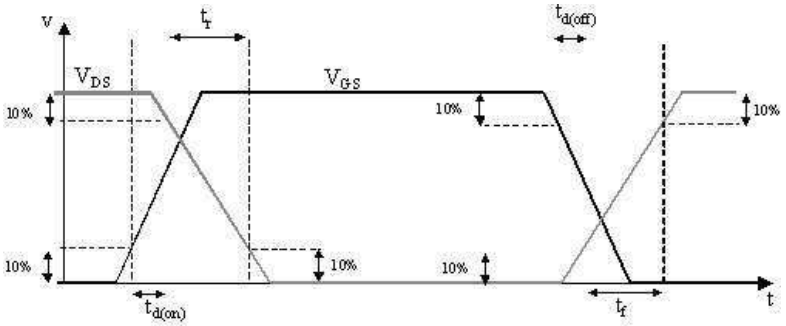


Image 50. Definition of Turn on and Turn off times **[42]**

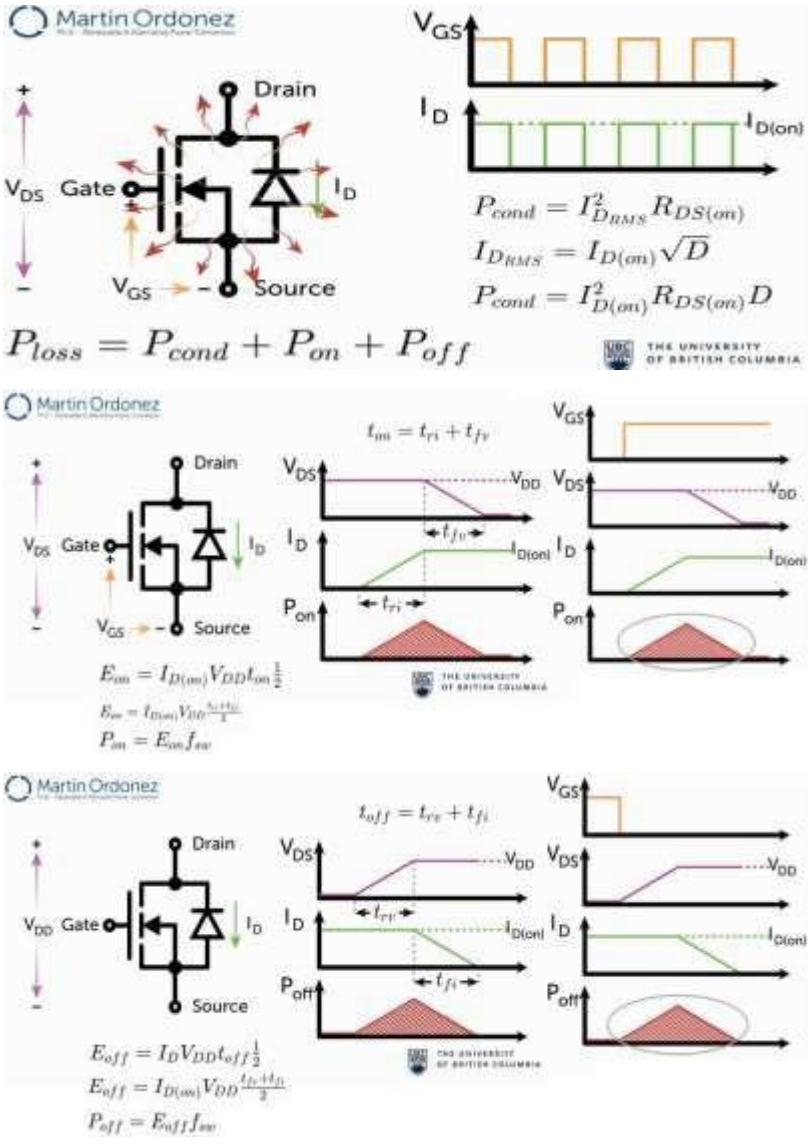


Image 51. Equations and graphs of mosfet power losses **[43]**

also for the search of $\mathbf{t_{on}}$ and $\mathbf{t_{off}}$, theory of capacitor needed, the time constant equation is: $t = R \times C$, and in Image 52. shown that at 5-time constants (t) a fully charged or discharged capacitor achieved.

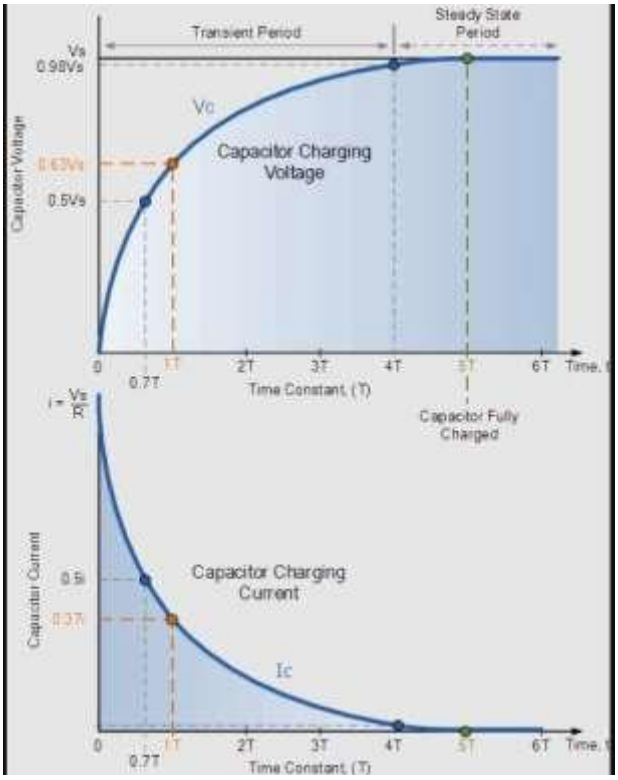


Image 52. Capacitor Charging-Discharging graph **[44]**

For the $\mathbf{t_{on}}$ and $\mathbf{t_{off}}$ calculations first go at mosfet's datasheet and extract the information that needed. (see the blue square at Image 53.)

Dynamic @ T_J = 25°C (unless otherwise specified)

Symbol	Parameter	Min.	Typ.	Max.	Units	Conditions
gfs	Forward Transconductance	320	—	—	S	V_{DS} = 25V, I_D = 110A
Q_g	Total Gate Charge	—	87	130	nC	I_D = 110A
Q_{gs}	Gate-to-Source Charge	—	27	—		V_{DS} = 50V
Q_{gd}	Gate-to-Drain ("Miller") Charge	—	45	—		V_{GS} = 4.5V ①
Q_{sync}	Total Gate Charge Sync. (Q_g - Q_{gd})	—	42	—		I_D = 110A, V_{DS} =0V, V_{GS} = 4.5V
$t_{d(on)}$	Turn-On Delay Time	—	74	—	ns	V_{DD} = 65V
t_r	Rise Time	—	330	—		I_D = 110A
$t_{d(off)}$	Turn-Off Delay Time	—	110	—		R_G = 2.7Ω
t_f	Fall Time	—	170	—		V_{GS} = 4.5V ①
C_{iss}	Input Capacitance	—	11360	—	pF	V_{GS} = 0V
C_{oss}	Output Capacitance	—	670	—		V_{DS} = 50V
C_{rss}	Reverse Transfer Capacitance	—	290	—		f = 1.0MHz
C_{oss} eff. (ER)	Effective Output Capacitance (Energy Related) ⑥	—	760	—		V_{GS} = 0V, V_{DS} = 0V to 80V ⑥
C_{oss} eff. (TR)	Effective Output Capacitance (Time Related) ⑦	—	1140	—		V_{GS} = 0V, V_{DS} = 0V to 80V ⑦

Image 53. Mosfet IRLB4030PBF time characteristics

For $\mathbf{t_{on}}$ calculation needed two times the Turn-On Delay Time [td(on)], as shown in the Image 50., first td(on) at 10% of V_{GS} is when the V_{DS} start to fall that means I_{DS} is at max

peak, then Rise Time (tr) follows at 90% of V_{DS} the V_{GS} is 100%, then the current flow through mosfet Drain and Source (DS), when the last td(on) 10% of V_{DS} need it to reach zero voltage that means closed switch and mosfet is full ON, the equation for t_{on} is:

$$t_{on} = td(on)x2 + tr$$

Needed the calculation of our times **t_{on}** and **t_{off}** from the datasheet because in datasheet used for time calculations external resistance R_G = 2.7Ω at gate of the mosfet, but have installed 10Ω, so extraction needed of the capacitor's values of the mosfet, to calculate the new **t_{on}** and **t_{off}** times where is:

$t_{d(on)} = 74ns$ from datasheet, in the new time, divide by five as shown at Image 52. to get the 1 time constant, so extraction of the capacitor value achieved: $\frac{t_{d(on)}}{5} = \frac{74ns}{5} = 14.8ns$,

the capacitor value is: $t = R_G \times C => C = \frac{t}{R_G} = \frac{14.8ns}{2.7\Omega} = 5{,}48nF$

the new time constant with our R_G = 10Ω is: $t = R_G \times C = 10\Omega \times 5{,}48nf = 54.81ns$

and the new time $t_{d(on)}$ at full charge is:$t_{d(on)} = t \times 5 = 54.81ns \times 5 = 274.05ns$

$tr = 330ns$ from datasheet, so: $\frac{tr}{5} = \frac{330ns}{5} = 66ns$

the capacitor value is: $t = R_G \times C => C = \frac{t}{R_G} = \frac{66ns}{2.7\Omega} = 24.44nF$

the new time constant with our R_G = 10Ω is: $t = R_G \times C = 10\Omega \times 24{,}44nf = 244.4ns$

and the new time tr at full charge is: $tr = t \times 5 = 244.4ns \times 5 = 1222ns$

So the **t_{on}** of our mosfet is: $\boldsymbol{t_{on}} = td(on)x2 + tr = 247.05ns \times 2 + 1222ns = \mathbf{1770.1}\boldsymbol{ns}$

For **t_{off}** calculation needed two times the Turn-Off Delay Time [td(off)], as shown in the Image 50., first td(off) at 90% (-10%) of V_{GS} is when the V_{DS} start to rise, the I_{DS} is at max peak, then the Fall Time (tf) follows at 10% (-90%) of V_{GS} the V_{DS} is at 90% and after one td(off) 10% we have 100% V_{DS} and the current I_{DS} stop flow through mosfet, that means opened switch and mosfet is full OFF, the equation for t_{off} is: $t_{off} = td(off)x2 + tf$

$t_{d(off)} = 110ns$ from datasheet, so: $\frac{t_{d(off)}}{5} = \frac{110ns}{5} = 22ns$

the capacitor value is: $t = R_G \times C => C = \frac{t}{R_G} = \frac{22ns}{2.7\Omega} = 8.148nF$

the new time constant with our R_G = 10Ω is: $t = R_G \times C = 10\Omega \times 8.148nf = 81.48ns$

and the new time $t_{d(off)}$ at full charge is: $t_{d(off)} = t \times 5 = 81.48ns \times 5 = 407.4ns$

$tf = 170ns$ from datasheet, so: $\frac{tr}{5} = \frac{170ns}{5} = 34ns$

the capacitor value is: $t = R_G \times C => C = \frac{t}{R_G} = \frac{34ns}{2.7\Omega} = 12.59nF$

the new time constant with our R_G = 10Ω is: $t = R_G \times C = 10\Omega \times 12.59nf = 125.9ns$
and the new time tf at full charge is: $tf = t \times 5 = 125.9ns \times 5 = 629.5ns$
So the $\mathbf{t_{off}}$ of our mosfet is: $\boldsymbol{t_{off}} = td(off)x2 + tf = 407.4ns \times 2 + 629.5 = \mathbf{1444.3ns}$

The total power loss at mosfet are switching losses which are Power on (P_{on}) and Power off (P_{off}) losses and power conduction losses (P_{cond}), see Image 54.

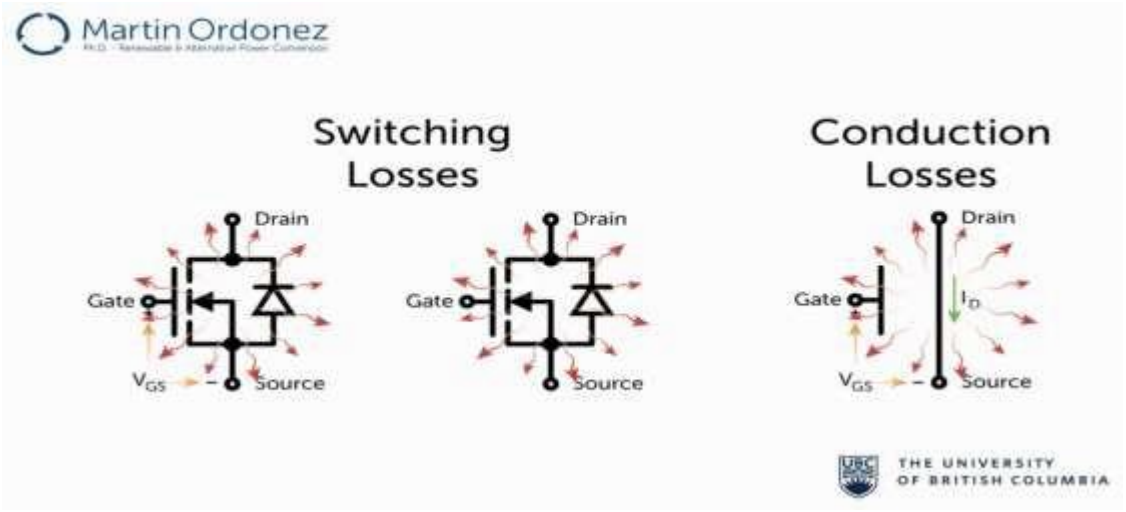


Image 54. Type of power losses at mosfet **[43]**

First to calculate the conduction losses needed the $R_{DS(ON)}$ value and extract it from mosfet datasheet see the blue square at Image 55., choose the value of 3.6mΩ because used the same V_{GS} for theoretical approximation of the new $\mathbf{t_{on}}$ and $\mathbf{t_{off}}$ times.

Static @ T_J = 25°C (unless otherwise specified)

Symbol	Parameter	Min.	Typ.	Max.	Units	Conditions
$V_{(BR)DSS}$	Drain-to-Source Breakdown Voltage	100	—	—	V	V_{GS} = 0V, I_D = 250µA
$\Delta V_{(BR)DSS}/\Delta T_J$	Breakdown Voltage Temp. Coefficient	—	0.10	—	V/°C	Reference to 25°C, I_D = 5mA ①
$R_{DS(on)}$	Static Drain-to-Source On-Resistance	—	3.4	4.3	mΩ	V_{GS} = 10V, I_D = 110A ③
		—	3.6	4.5		V_{GS} = 4.5V, I_D = 92A ③
$V_{GS(th)}$	Gate Threshold Voltage	1.0	—	2.5	V	V_{DS} = V_{GS}, I_D = 250µA
I_{DSS}	Drain-to-Source Leakage Current	—	—	20	µA	V_{DS} = 100V, V_{GS} = 0V
		—	—	250		V_{DS} = 100V, V_{GS} = 0V, T_J = 125°C
I_{GSS}	Gate-to-Source Forward Leakage	—	—	100	nA	V_{GS} = 16V
	Gate-to-Source Reverse Leakage	—	—	-100		V_{GS} = -16V
$R_{G(int)}$	Internal Gate Resistance	—	2.1	—	Ω	

Image 55. Mosfet IRLB4030PBF $R_{DS(ON)}$

So the power conduction losses calculation is:

$$P_{cond} = I_{max}^2 \times R_{DS(ON)} \times D = 1.653A^2 \times 0.036\Omega \times 0.07059 = 0.000694371W$$

Then continue with switching losses, with switching frequency (f_{sw}) of 3926.25 Hz from microcontroller's PWM signal, first calculation of the Power on losses done:

$$E_{on} = \frac{I_{max} \times V_{max} \times t_{on}}{2} = \frac{1.653A \times 37.72V \times (1770.1 \times 10^{-9})Sec}{2}$$

$$= 0.000055183894158\ Joules$$

$$P_{on} = E_{on} \times f_{sw} = 0.000055183894158\ Joules \times 3926.25\ Hz = 0.216665764W$$

Second calculation of Power off losses done:

$$E_{off} = \frac{I_{max} \times V_{max} \times t_{off}}{2} = \frac{1.653A \times 37.72V \times (1444.3 \times 10^{-9})Sec}{2}$$

$$= 0.000045026890194\ Joules$$

$$P_{off} = E_{off} \times f_{sw} = 0.000045026890194\ Joules \times 3926.25\ Hz = 0.176786828W$$

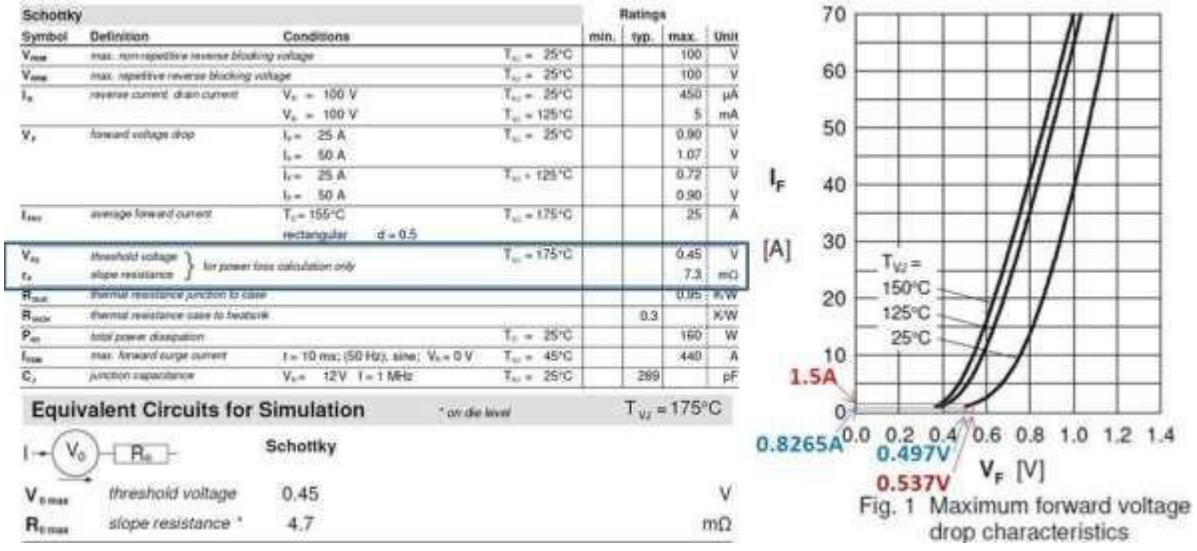
After the calculation of conduction and switching losses, calculated the total power mosfet losses P_{Mosfet} where is the sum of the conduction and switching losses:

$$P_{Mosfet} = P_{cond} + P_{on} + P_{off} = 0.000694371W + 0.216665764W + 0.176786828W$$

$$= 0.394146963W$$

So the total power mosfet losses is: $P_{Mosfet} = 0.394146963W$

Diode power losses follows, first extracted the needed information for calculations from Schottky Diode DSA50C100QB datasheet as shown at Image 56. and that is, the bias forward voltage V_{FW} = 0.45V and the slope resistance R_F = 7.3mΩ.



Schottky				Ratings			
Symbol	Definition	Conditions		min.	typ.	max.	Unit
V_{RSM}	max. non-repetitive reverse blocking voltage		T_{VJ} = 25°C			100	V
V_{RRM}	max. repetitive reverse blocking voltage		T_{VJ} = 25°C			100	V
I_R	reverse current, drain current	V_R = 100 V	T_{VJ} = 25°C			450	µA
		V_R = 100 V	T_{VJ} = 125°C			5	mA
V_F	forward voltage drop	I_F = 25 A	T_{VJ} = 25°C			0.90	V
		I_F = 50 A				1.07	V
		I_F = 25 A	T_{VJ} = 125°C			0.72	V
		I_F = 50 A				0.90	V
I_{FAV}	average forward current	T_C = 155°C	T_{VJ} = 175°C			25	A
		rectangular d = 0.5					
V_{F0}	threshold voltage } for power loss calculation only		T_{VJ} = 175°C			0.45	V
r_F	slope resistance }					7.3	mΩ
R_{thJC}	thermal resistance junction to case					0.95	K/W
R_{thCH}	thermal resistance case to heatsink				0.3		K/W
P_{tot}	total power dissipation		T_C = 25°C			160	W
I_{FSM}	max. forward surge current	t = 10 ms; (50 Hz), sine; V_R = 0 V	T_{VJ} = 45°C			440	A
C_J	junction capacitance	V_R = 12V f = 1 MHz	T_{VJ} = 25°C		289		pF

Equivalent Circuits for Simulation * on die level T_{VJ} = 175°C

Schottky

$V_{0\,max}$	threshold voltage	0.45	V
$R_{0\,max}$	slope resistance *	4.7	mΩ

Fig. 1 Maximum forward voltage drop characteristics

Image 56. Diode threshold voltage and slope resistance for power calculation

The DSA50C100QB Schottky diode has two diodes in same package in our device that diodes are connected parallel, so the current is split into two diodes, the maximum current of device is 3A, split in two with Kirchhoff's first law, the current that flow through each diode is 1.5A as shown with red arrow at Image 56., the blue arrow is the split of I_{max} = 1.653A that used for power loss calculation of the device with input the CdTe #2 Photovoltaic, for reasons of finding the real voltage drop.

The first power loss in diode is voltage bias losses (voltage drop) and the equation is:

$$P_{VFW} = V_{FW} \times I_{max} = 0.45V \times 1.653A = 0.74385W$$

The second power loss in diode is internal resistor (slope resistance) losses and the equation is: $P_{RF} = I_{max}^2 \times R_F = 1.653A^2 \times 0.0073\Omega = 0.019946586W$

So the total diode power losses is:

$$P_{Diode} = P_{VFW} + P_{RF} = 0.74385W + 0.019946586W = 0.763796586W$$

The total DC-DC Boost Converter power losses with input the CdTe #2 is:

$$P_{BCLOSS} = P_{Inductor} + P_{Mosfet} + P_{Diode}$$

$$P_{BCLOSS} = 0.08197227W + 0.394146963W + 0.763796586W = 1.239915818W$$

3.4.2 Practical Approximation of Measurement System Power Losses

The hardware power losses of measurement system was:

Isolation system measured with multimeter Mastech® MY-68 model, the current dissipation of the system at 12V supply from battery was ~0.035A so the power loss was: $P_{Isolation} = 12V \times 0.035A = 0.42W$, also the R_{shunt} is in isolation system and the power losses on it is: $P_{R_{shunt}} = I^2_{max} \times R_{shunt} = 1.653^2 \times 0.04\Omega = 0.10929636W$

The non isolation system measured directly from dc supply source measurement system UNI-T® model UTP3315TFL, the current dissipation of the system at 12V supply from DC source was ~0.33A so the power loss was: $P_{Non\ isolation} = 12V \times 0.33A = 3.96W$

So the practical approximation of hardware of measurement system total power losses is:

$$P_{hardware\ of\ measurement\ system} = P_{Isolation} + P_{R_{shunt}} + P_{Non\ isolation}$$

$$P_{hardware\ of\ measurement\ system} = 0.42W + 0.10929636W + 3.96W = 4.48929636W$$

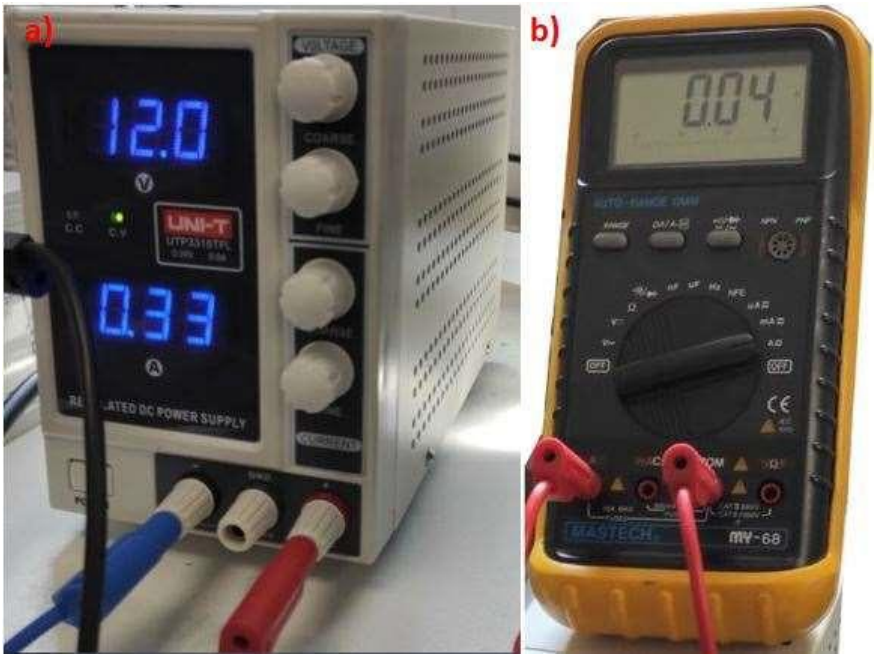


*Image 57.**a)** DC Source UNI-T® model UTP3315TFL, **b)** Multimeter Mastech® model MY-68*

3.4.3 Microcontroller Power Losses

The microcontroller which used is Atmel's® model Arduino Mega 2560, with current dissipation at standby mode $I_{standby}$ = 0.05254A at $V_{standby}$ = 5.15V **[45]**

Power losses in standby mode is:

$$P_{standby} = V_{standby} \times I_{standby} = 5.15V \times 0.05254A = 0.27W$$

Current dissipation in pin for PWM signal supply the mosfet driver is I_{PWM} = 0.02A at V_{PWM} = 5V **[46],**so the Power losses is:$P_{PWM\ Supply} = V_{PWM} \times I_{PWM} = 5V \times 0.02A = 0.1W$

Total MCU power losses is: $P_{MCU} = P_{standby} + P_{PWM\ Supply} = 0.27W + 0.1W = 0.37W$

3.4.4 Estimate Power Losses and Efficiency of the device

So the total power losses of IV-MPPT Charger Regulator with input the CdTe #2 is:

$$P_{IV-MPPT\ Charger\ Regulator} = P_{BCLOSS} + P_{hardware\ of\ measurement\ system} + P_{MCU}$$

$$P_{IV-MPPT\ Charger\ Regulator} = 1.239915818W + 4.48929636W + 0.37W$$

$$P_{IV-MPPT\ Charger\ Regulator} = 6.099212178W$$

Then the n(%) Efficiency of IV-MPPT Charger Regulator with input the CdTe #2 is:

$$n(\%) = \frac{P_{out}}{P_{in}} \times 100 = \frac{P_{in} - P_{IV-MPPT\ Charger\ Regulator}}{Pin} \times 100$$

$$n(\%) = \frac{62.35116\text{W} - 6.099212178W}{62.35116\text{W}} \times 100 = \frac{56.2519478W}{62.35116\text{W}} \times 100 = 90.22\%$$

3.4.5 Material Costs for Device Fabrication

The materials of fabrication of IV-MPPT Charger Regulator costs in euro:

Schematic Name	Materials Name	Values	Quantity	Price per piece (€)	Total Price (€)
Rshunt	WSHP2818R0400FEA	0.04Ω	1	1.41	1.41
R1,2,3,4,5,10	Resistors	1MΩ, 1% tolerance	6	0.231	1.386
R6	Resistors 2x75Ω in series	150Ω, 1% tolerance	2	0.171	0.342
R7,R8	Multiturn trimmer potentiometers	5KΩ, 1% tolerance	2	1.72	3.44
R9	Resistor 2x240Ω in series	480Ω, 1% tolerance	2	0.102	0.204
R11	Resistor	39KΩ, 1% tolerance	1	0.2	0.2
R12	Multiturn trimmer potentiometer	2KΩ, 1% tolerance	1	3.23	3.23
R13	Resistor	240Ω, 1% tolerance	1	0.2	0.2
R14	Resistor	1KΩ, 1% tolerance	1	0.2	0.2
R15	Resistor	10Ω, 1% tolerance	1	0.2	0.2
OPAM1,2 OPAM3 OPAM4	Operation Amplifier LM6142	Voltage Supply Range 1.8V to 24V, Current Supply Range 650μA per Amplifier	3	5.89	17.67
	LM6142 SMD PCB BASES x3		3	0.33	0.99
Isolated DC Source	Voltage Regulator LM7809	Output 9V , 1A	1	0.5	0.5
Isolated VDC Offset Source	Adjustable Regulator LM317T	Output 1.25V to 37V , 1.5A	1	0.24	0.24
DC Source	Linear Voltage Regulator LM7809	Output 9V , 1A	1	0.5	0.5
Fans Driver Source	Linear Voltage Regulator LM7805	Output 5V , 1A	1	0.35	0.35
Mosfet Driver Source	Linear Voltage Regulator LM7809	Output 9V , 1A	1	0.5	0.5
T1	Transistor BC639 (NPN)	V_{CE} 80V , I_C 1A	1	0.65	0.65
T2	Transistor BC640 (PNP)	V_{CE} 80V , I_C 1A	1	0.65	0.65
C1, C2 also C1,C2 small ones	Electrolytic Big Capacitors, Ceramic Capacitors the small one	1500μF, 100V and 100nF, 100V	2	12.31	24.62
C3,C4	MKT (Polyester) Capacitors	22nF, 63V	2	0.13	0.26
C5,9	MTK Capacitors	1 μF, 63V	2	0.13	0.26
C6,10	MTK Capacitors	220 nF, 63V	2	0.13	0.26
C7	Electrolytic Capacitors	10 μF, 63V	1	0.28	0.28
C8	MTK Capacitor	100 nF, 63V	1	0.13	0.13
C11	Electrolytic Capacitor	2.2 μF, 63V	1	0.28	0.28
Q1	Mosfet IRLB4030PBF	Max Voltage 100V, Max Current 180A	1	3.8	3.8
D1	IXYS DSA50C100QB	Shotkey diode	1	3.07	3.07
D2	IN4002	Si diode	1	0.1	0.1
L1	Inductor coil	2x2.8mH, 5A each inductor	1	9.93	9.93
Optocoupler	Vishay 4n25 Optocoupler	Linear at 10mA , Forward Voltage 1.5V	1	0.47	0.47
Big Fan	Fan	12V	1	2.4	2.4
Small Fan	Fan	5V	1	2.5	2.5
MCU	Atmel's® Arduino Mega 2560 Rev3	Microcontroler 5V, ~50mA Current Dissipation	1	29.61	29.61
	Plugs for connection		8	0.25	2
	Box of charger		1	10	10
	Aluminum heatsink x2 big		2	5.5	11
	Aluminum heatsink x4 small		4	1	4
	Consumables				
	Solder Wire		1	11.73	11.73
	Desolder Wire		1	1.21	1.21
	Copper Cables some meters		3	1.6	4.8
	Insulating tape		1	0.54	0.54
	Heat shrinkable tubes		1	1.5	1.5
Total Price of IV-MPPT Charger Regulator					157.612

Image 58. Table of materials and it's costs in euro (€)

As shown in Image 58. the total materials cost for fabrication of IV-MPPT Charger Regulator is almost 160€ (157.61€) .

3.5 Construction Photos of the Device and its Description

The device circuit of IV-MPPT Charger Regulator constructed on perforated boards, because needed big copper wires on DC-DC Boost Converter to avoid parasitic resistances.

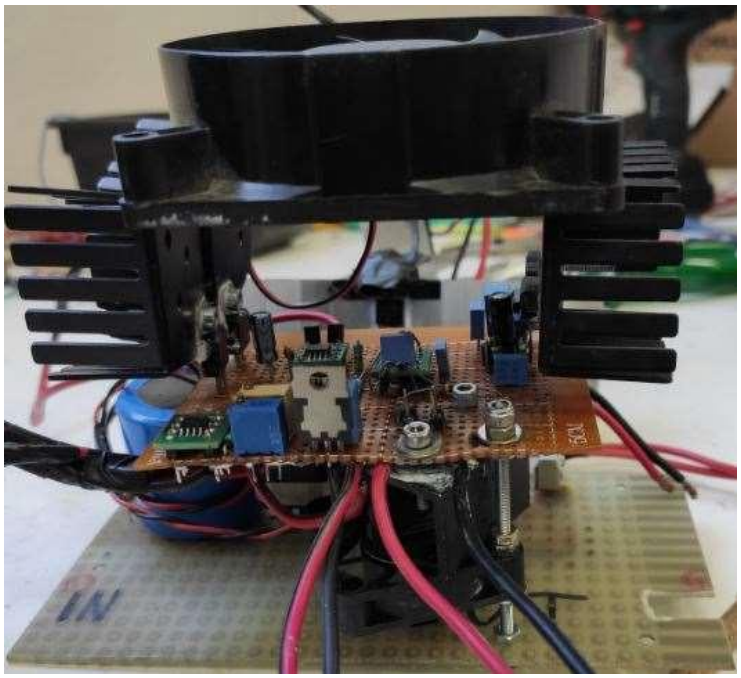


Image 59. Circuits of IV-MPPT Charger Regulator

When the circuit boards was ready it's connected with the aluminum heatsinks which contain on it, the mosfet and the diode of DC-DC Boost Converter.

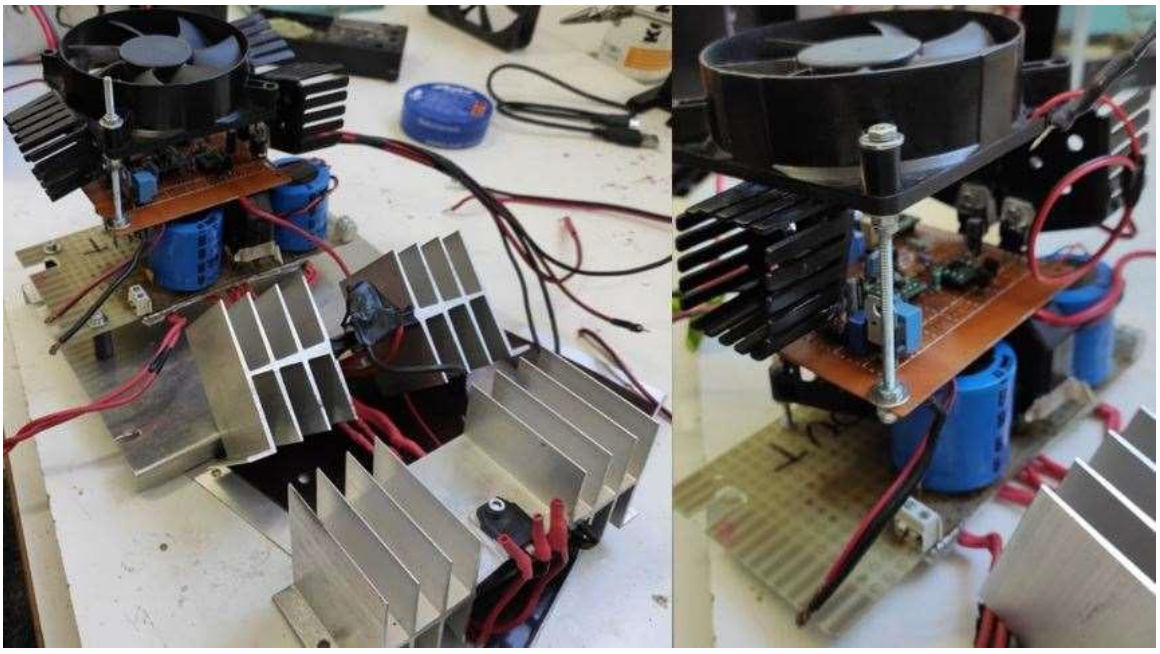


Image 60. Aluminum heatsinks with Mosfet and Diode connection to main circuit boards

In the Image 61. shown the position of each part of IV IV-MPPT Charger Regulator.

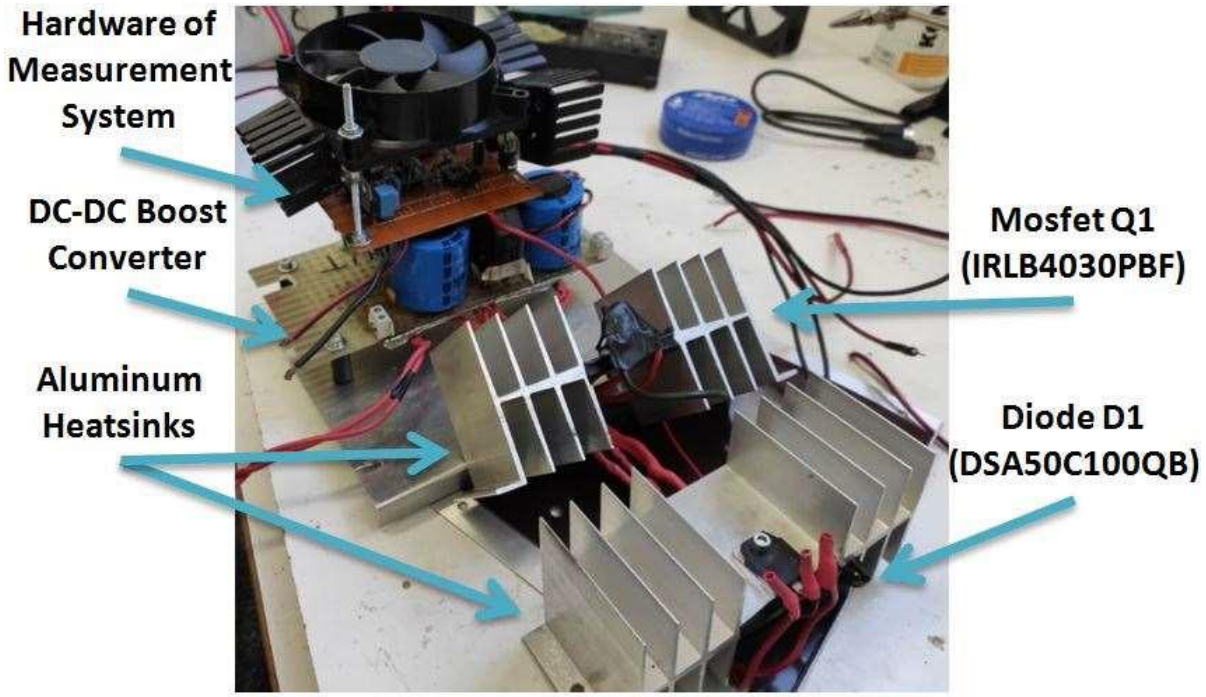


Image 61. Position of DC-DC Boost Converter and the Measurement System

Specifically shown the hardware of measurement system at Image 62. and position explanation of each material at Image 63.

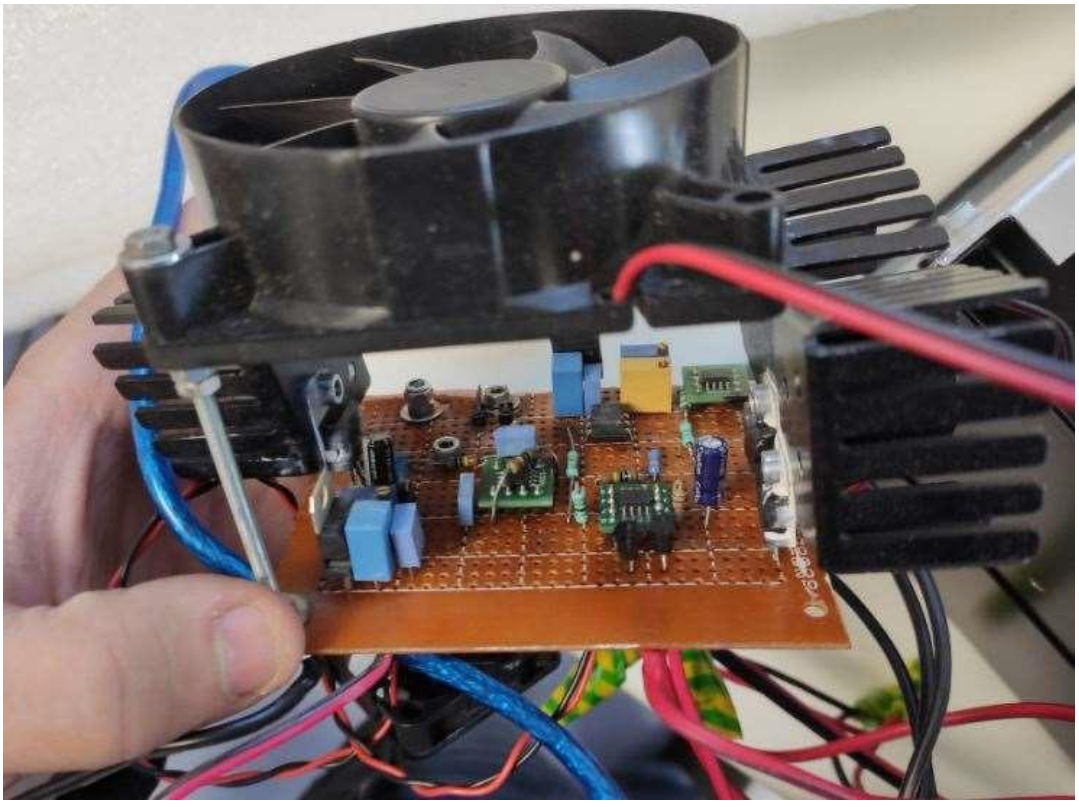


Image 62. Hardware of measurement system

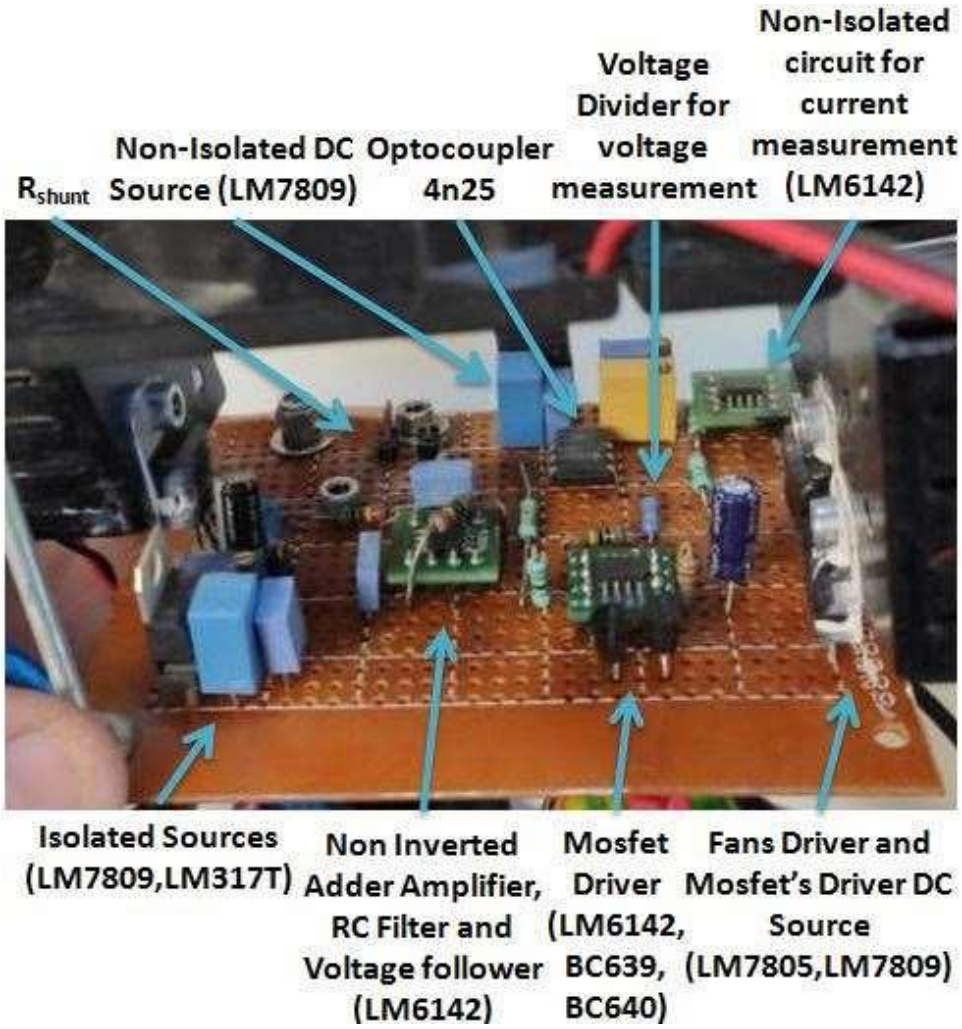


Image 63. Position of materials on hardware measurement system

Calibration of measurement system done, with Mastech® 8050 Bench Multimeters and Tektronix® TDS1012 Oscilloscope.

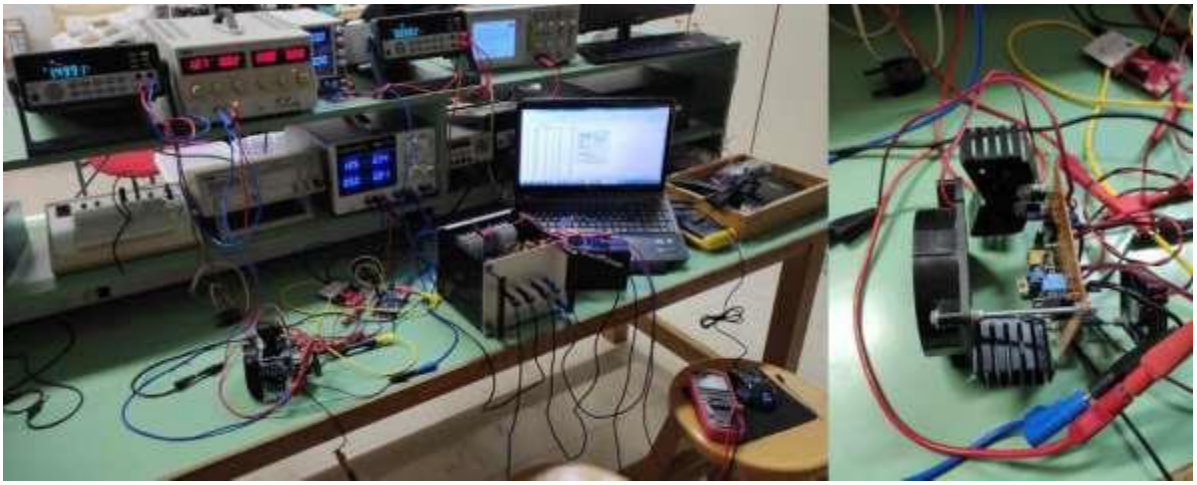


Image 64. Calibration of Measurement System

Afterwards, assembly all circuit boards and aluminum heatsinks into aluminum box, that first placed sockets for connections with input (PV), output (Battery), DC sources inputs for measurement system and usb input for microcontroller connection with the computer.



Image 65. a) Assembly before adding the microcontroller, b) Assembly finished

Then, having connection with PC to upload the software into IV-MPPT Charger Regulator microcontroller.



Image 66. Connection with computer for software upload

Innovative algorithms for IV,MPPT,PVBR were developed, the IV-MPPT Charger Regulator is completely programmable and anytime can be developed new algorithms and add it to it. Images follows with the rear and front view of the completed device.



Image 67. IV-MPPT Charger Regulator Device Complete

4. Algorithms of IV-MPPT Charger Regulator

The IV - MPPT Charger Regulator device is completely programmable and contain 13 algorithms classified as:

Four IV algorithms:

- Reverse Exhaustive Search (RES)
- Forward Exhaustive Search (FES)
- Reverse Forward Exhaustive Search (RFES)
- Forward Reverse Exhaustive Search (FRES)

Seven MPPT algorithms:

- Hill Climbing (HC)
- Hill Climbing Perturb and Observe (HCPO)
- Fractional Open Circuit Voltage (FOCV)
- Fractional Short Circuit Current (FSCC)
- Incremental Conductance (IC)
- Maximum Power Quantumized Area Search v1 (MPQAS1)
- Maximum Power Quantumized Area Search v2 (MPQAS2)

Two PVBR algorithms:

- Pmax Open Circuit Intervals (POCI)
- Pmax Short Circuit Intervals (PSCI)

4.1 Explanation of IV Algorithms

All IV algorithms take 256 points to create the IV Curve and each of 256 points is acquired from average of 200 points, so in total IV creation having
256 points x 200 points = 51200 points.

The RFES and FRES algorithms created to helps us to have better understanding in Hysteresis effect of GRAPES Photovoltaics and the right calculation of their PCE.

Also RFES and FRES are faster algorithms than solo RES or FES because immediately do the two scans.

4.1.1 Reverse Exhaustive Search (RES)

The RES IV Algorithm start scan from open circuit to short circuit. That means changing in Duty Cycle (D.C.) of Pulse Width Modulation (PWM) in microcontroller of

IV - MPPT Charger Regulator from 0 to 256 steps [0 steps (Duty Cycle 0%) is Open Circuit and 256 steps (Duty Cycle 100%) is Short Circuit, see Image 68.a. and 68.b. for Power - Voltage (PV) Curve respectively].

4.1.2 Forward Exhaustive Search (FES)

The FES IV Algorithm start scan from short circuit to open circuit. D.C. from 256 to 0 Steps.

4.1.3 Reverse Forward Exhaustive Search (RFES)

The RFES IV Algorithm start scan from open circuit to short circuit then immediately from short circuit to open circuit.

4.1.4 Forward Reverse Exhaustive Search (FRES)

The FRES IV Algorithm start scan from short circuit to open circuit then immediately from open circuit to short circuit.

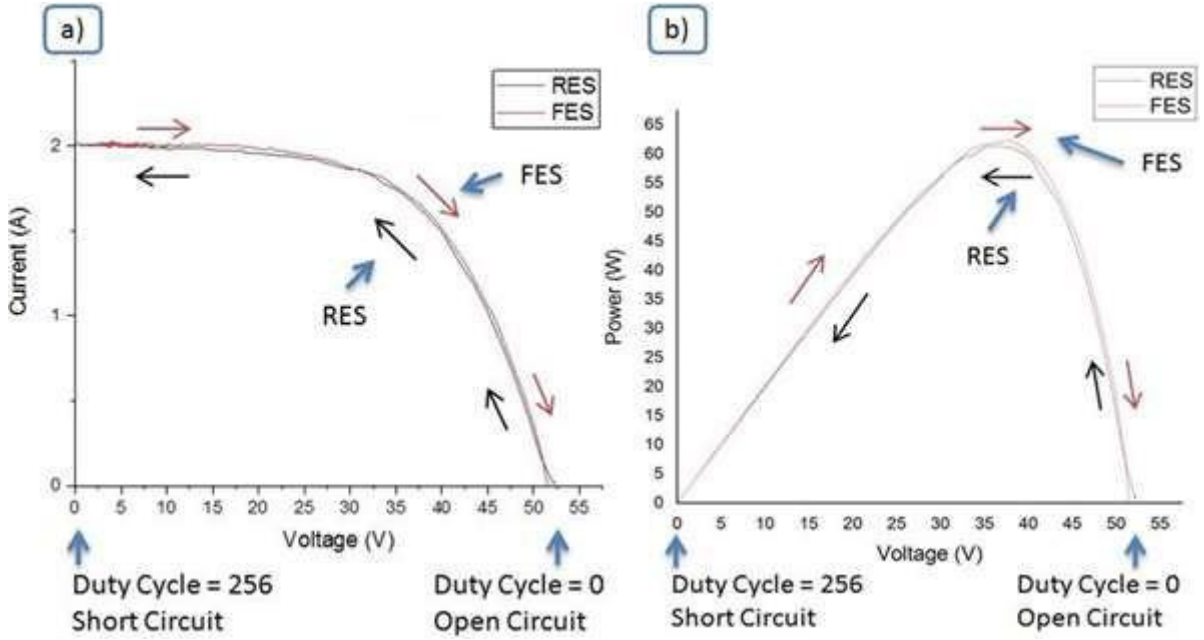


*Image 68. Scanning explanation of **a)** IV curves RES and FES, **b)** PV curves RES and FES*

4.2 Explanation of MPPT Algorithms

The MPPT algorithms measurements acquired live, each measurement is average of 200 points, all algorithms has 80% RES IV rescanning every ~10 minutes, and the change in steps is 3 steps out of 256 that means Duty Cycle change percentage is: $\frac{3}{256} \times 100 = 1.17\%$, 3 steps choosed so the HC, HCPO and IC algorithms doesn't easily trapped into local maximum.

4.2.1 Hill Climbing (HC)

In HC algorithm first scan from open circuit to 80% of IV Curve short circuit, and don't let the algorithm do short circuit in Photovoltaics (D.C. 0 to 80%) (Image 70.b. and 70.c.), extraction of the electrical characteristic like Voc, Vmax, Imax, Pmax, done, then start run at Pmax point and continuously scan and compare the new power measurement with the previous one, if the new scan measurement is higher than previous it increase the D.C. ,else if the new scan is lower than previous it decrease the D.C., changing D.C. steps up and down it can maintain the Pmax even with disturbances from changings in solar irradiance (clouds, or sun position at morning or afternoon, etc.) (Image 69.), also every **10 minutes and 34 seconds** repeats the scan from open circuit to 80% of IV short circuit to extract the new electrical characteristics (Image 70.), observed at Image 70.a. that we have slightly increase in power that means the algorithm has trapped in local maximum near the real maximum and the re- scanning find it.

- The advantages is that continuously scan so it can maintain the Pmax all the time.
- Also advantage is the simplicity of this algorithm creation.
- Disadvantages is that the algorithm can be trapped in local maximum when continuously scan for Pmax, that can be solved with increased steps in D.C.
- Also doesn't take into account the measure of voltage into the scanning process so it's slow down the finding of MPP, that can be solved with the improved algorithm Hill Climbing Perturb and Observe (HCPO) that it takes into account the voltage so it can know the direction of disturbance.
- The other disadvantage is that continuously changes in D.C. can mean power losses, also if the step is increased for trap escaping means extra power losses and lower resolution in finding Pmax.
- Also if the algorithm finds the MPP, never stays in the same Pmax it's perturbs back and forth around the MPP, that means extra power losses

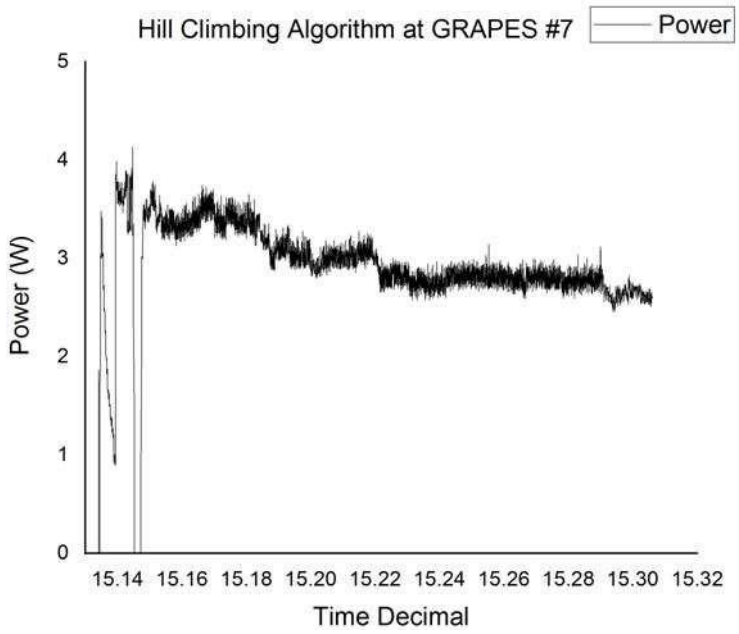


Image 69. HC Graph in GRAPES #7 (26/08/2021), Power - Time, it follows the sun fall

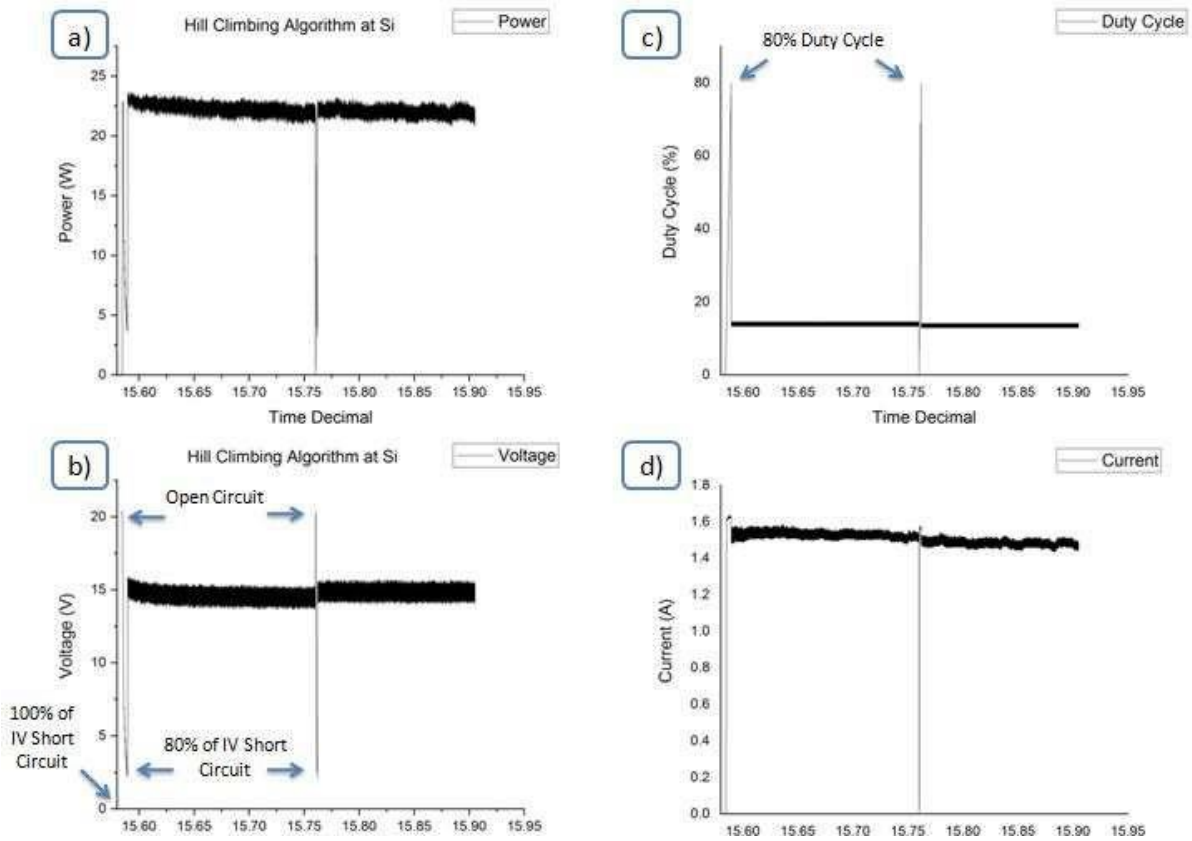


*Image 70. HC Graphs in Si (23/08/2021), **a)** Power - Time, **b)** Voltage - Time, **c)** Duty Cycle - Time, **d)** Current - Time*

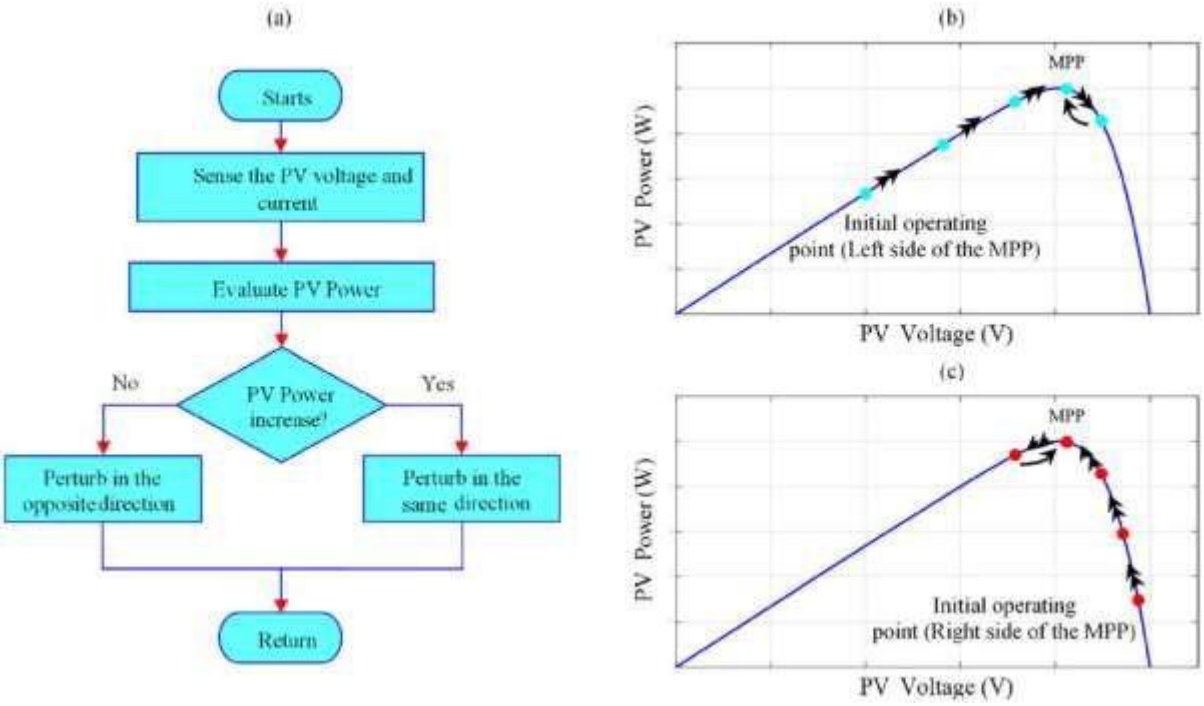


Image 71. ***a)*** *Hill Climbing Flow Chart* ***b)*** *and* ***c)*** *Power - Voltage characteristics of the PV operating points using the Hill Climbing algorithm* **[47]**

The Hill Climbing algorithm, of handmade device has initial operating point at the right side of the MPP, starts the scan from 0 duty cycle see Image 72.c.

4.2.2 Hill Climbing Perturb and Observe (HCPO)

The HCPO algorithm is the most widespread and commercial algorithm out there, the implementation of HCPO is inexpensive while being very robust and effective, also it's a simple algorithm.

In HCPO algorithm first scan from open circuit to 80% of IV Curve short circuit, and don't let the algorithm do short circuit in Photovoltaics (D.C. 0 to 80%) (Image 72.b. and 72.c.), extraction of the electrical characteristic like V_{oc}, V_{max}, I_{max}, P_{max}, done, then start run at P_{max} point, like HC and continuously scan and compare the new power measurement with the previous one:

- If the new scan measurement is a higher **(DP < 0)** than previous it's automatically check the voltage and compare it with the previous voltage if it's higher **(DV < 0)** it decrease the D.C., changing the D.C. steps, else if the voltage is lower **(DV > 0)** it increase the D.C. respectively
- Then if the new scan measurement is a lower **(DP > 0)** than previous it's automatically check the voltage again and compare it with the previous voltage if it's

higher **(DV < 0)** it increase the D.C., else if the voltage is lower **(DV > 0)** it decrease the D.C. respectively

The voltage and power combined, give the direction that moving and which side of MPP are:

- Increased power and voltage mean the direction is right ⟶ but in left side of MPP
- Increased power and decreased voltage mean the direction is left ⟵ but in the right side of MPP
- Decreased power and increased voltage mean the direction is right ⟶ and in right side of MPP
- Decreased power and voltage mean the direction is left ⟵ and in left side of MPP

The sign of $\frac{dP}{dV}$ where dP is the difference between power and dV is the difference between voltage of two succeeded point hill climbing involves a perturbation in the duty cycle of the DC-DC boost power converter.

It is observed from the flow chart (Image 73.) and from PV characteristic curve of the PV (Image 68.b. and 71.b, , 71.c.) that there are three main regions for operation:

- The first region is at the right side of MPP where the ratio between the power change over the voltage change $\frac{dP}{dV} < 0$ is negative
- The second region is at the left side of MPP where the ratio $\frac{dP}{dV} > 0$ is positive
- And the third region is at MPP exactly where the ration $\frac{dP}{dV} = 0$ is zero

so the HCPO algorithm changing the D.C. steps up and down depending on these three regions of operation it can maintain the Pmax and the voltage even with disturbances from changings in solar irradiance (clouds, or sun position at morning or afternoon, etc), also every **10 minutes and 34 seconds** repeats the scan from open circuit to 80% of IV short circuit to extract the new electrical characteristics (Image 72.),

- The advantages is that continuously scan so it can maintain the Pmax all the time.
- Also advantage is the simplicity of this algorithm creation and very good efficiency.
- Disadvantages is that the algorithm can be trapped in local maximum when continuously scan for Pmax and the Voltage, that can be solved with increased steps in D.C.
- The other disadvantage is that continuously changes in D.C. can mean power losses, also if the step is increased for trap escaping means extra power losses and lower resolution in finding Pmax.

- Also if the algorithm finds the MPP, never stays in the same Pmax it's perturbs back and forth around the MPP, that means extra power losses

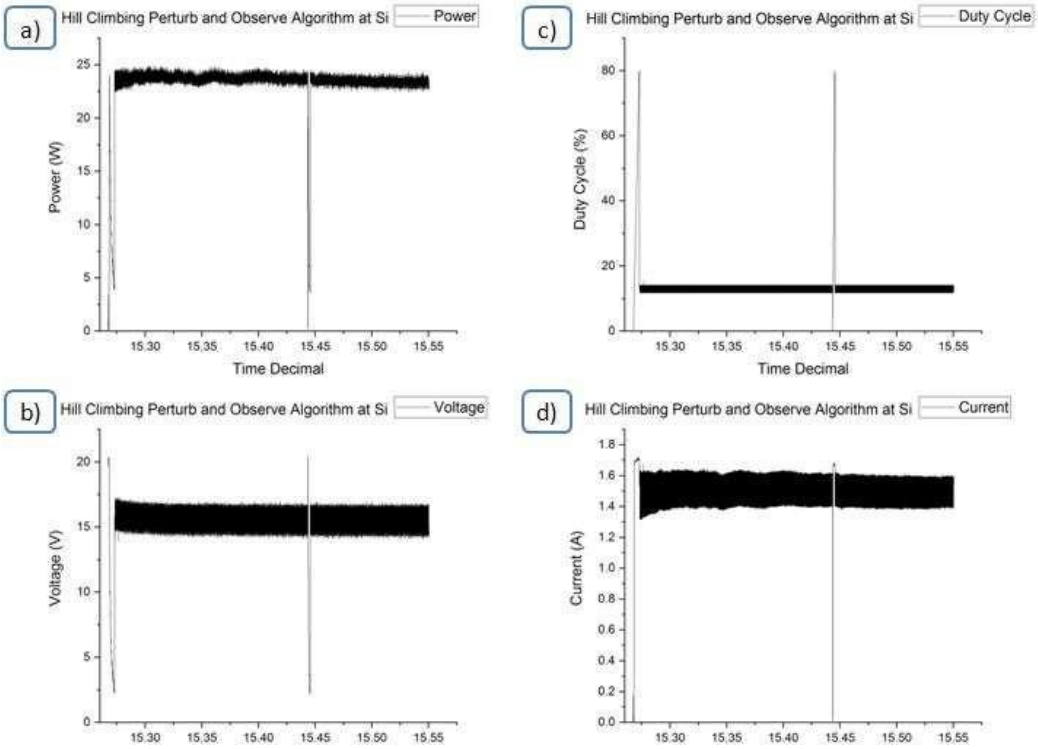


Image 72. HCPO Graphs in Si (23/08/2021), ***a)*** *Power - Time,* ***b)*** *Voltage - Time,* ***c)*** *Duty Cycle - Time,* ***d)*** *Current - Time*

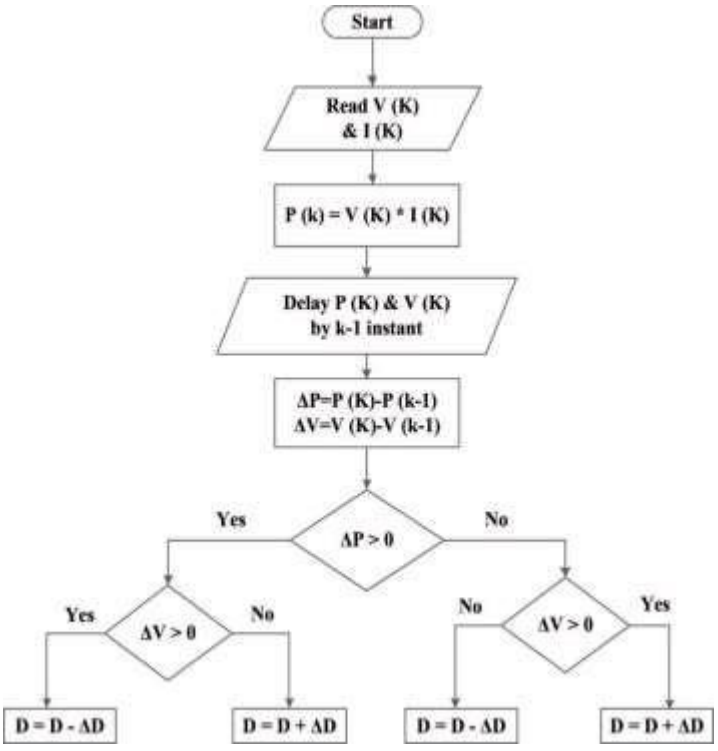


Image 73. Hill Climbing Perturb and Observe flow chart **[48]**

4.2.3 Fractional Open Circuit Voltage (FOCV)

The Voltage Open Circuit (V_{oc}) is crucial in GRAPES Photovoltaics as shown in Image 74., the V_{oc} is almost proportional to Solar Irradiance ($\frac{W}{m^2}$) for that reason, motivated and developed the Fractional Open Circuit Voltage (FOCV) MPPT algorithm.

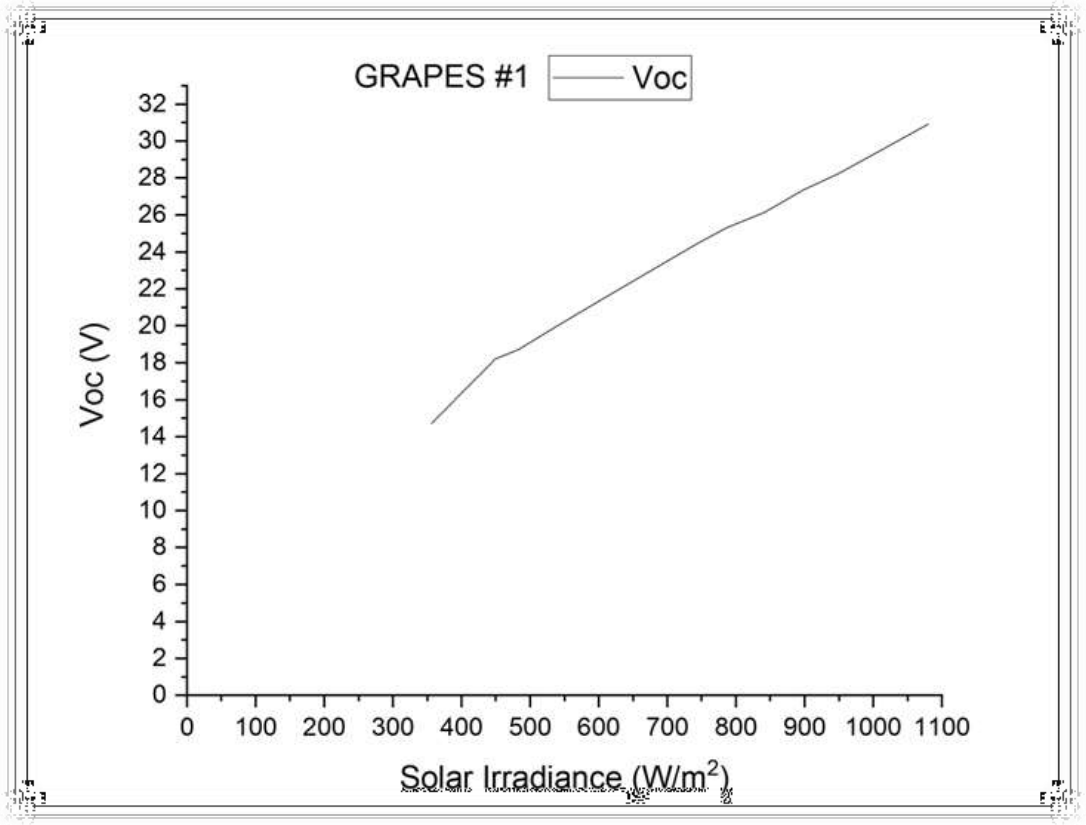


Image 74. GRAPES #1 Voc - IRR Curve

In FOCV algorithm first scan from open circuit to 80% of IV Curve short circuit, and don't let the algorithm do short circuit in Photovoltaics (D.C. 0 to 80%) (Image 75. and 76.c.), extraction of the electrical characteristic like V_{oc}, V_{max}, I_{max}, P_{max}, done, also calculate the $V_{\%} = \frac{Vmax}{Voc}$, obtain the Comparison Voltage (CV) CV = Vmax and

Duty Cycle at Comparison Voltage (DC_at_CV) , this process repeated every ~10 minutes, then setted the DC_at_CV in DC-DC Boost Converter, the converter stays constant at DC_at_CV for 2 minutes, after the 2 minutes pass the converter set DC to zero (Image 76.c.) to obtain the new Voc (Image 76.b.) and calculate the new Comparison Voltage

$CV = Voc \times V_{\%}$, first the converter it's set the DC_at_CV then changing the Duty Cycle until Photovoltaic Voltage is equal to Calculated Comparison Voltage (Image 76.b.) when the

converter finds the Voltage stays constant for 2 minutes and repeat the process, at 10 minutes and 28 seconds repeat the IV scan that shown in Image 75. and 76.c.

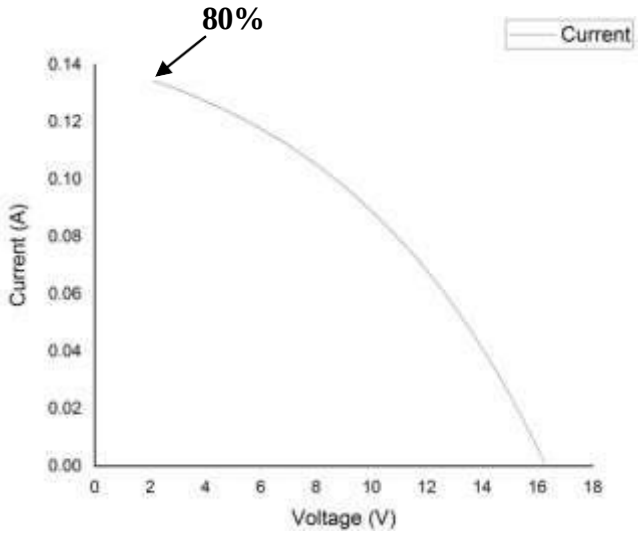


Image 75. First IV Scan 0 to 80% Duty Cycle of FOCV Algorithm in GPe Double Module, repeat every 10 minutes and 28 seconds

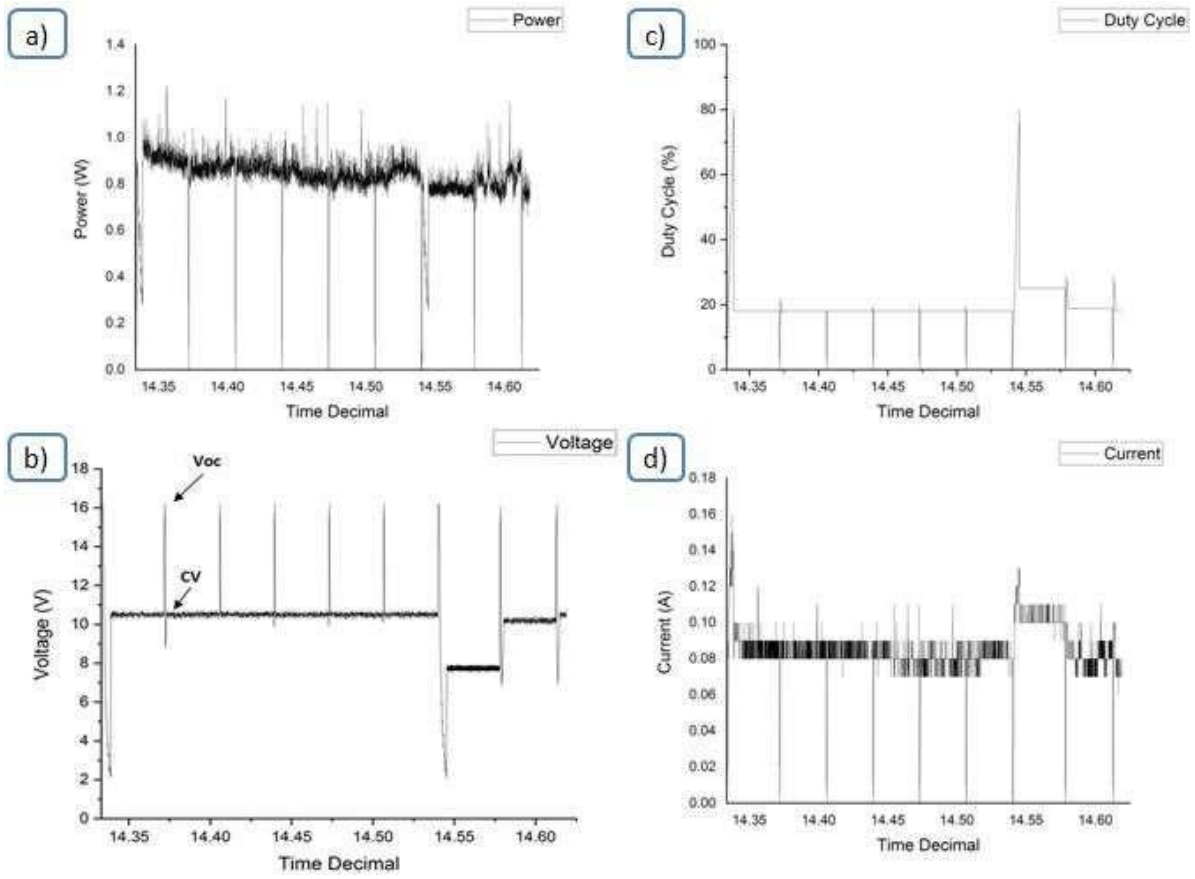


*Image 76. FOCV Graphs in GRAPES Double Module (13/06/2021), **a)** Power - Time, **b)** Voltage - Time, **c)** Duty Cycle - Time, **d)** Current - Time*

Follows the flow chart of FOCV algorithm for its better understanding see Image 77.

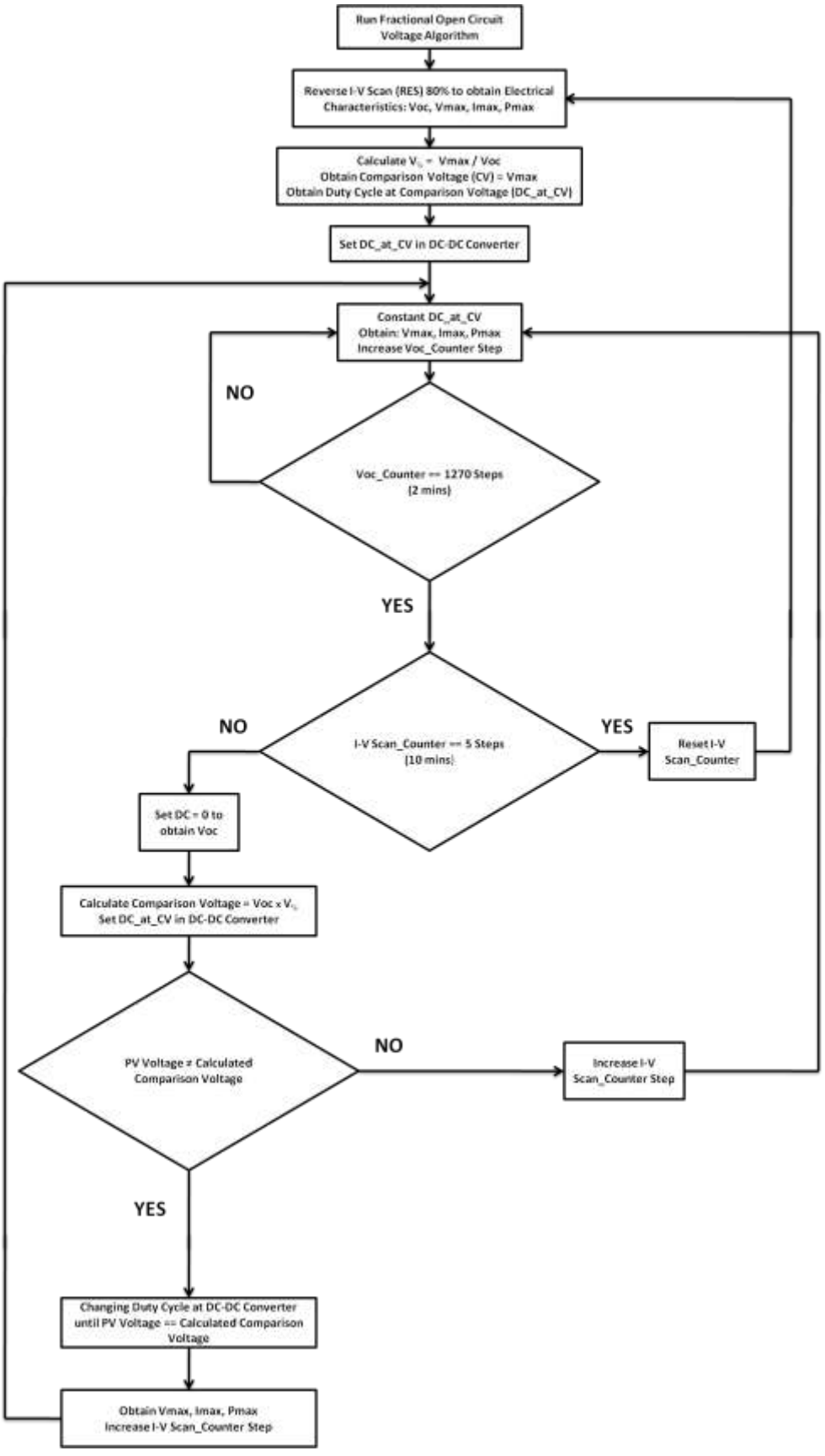


Image 77. Flow Chart of FOCV Algorithm

The advantages of the innovative FOCV algorithm are:

- It works very efficiently for GRAPES Photovoltaics because Voc is almost proportional to Solar Irradiance ($\frac{W}{m^2}$)
- It works periodically every 2 minutes so doesn't need high processing power from microcontroller
- And because works periodically does not strain the photovoltaics, the reason is that doesn't have changes in Duty Cycle

The disadvantages are:

- Because it work every 2 minutes in that interval any changes in solar irradiance can't be tracked that means losses in energy yield, that can be improved with lower intervals for example 1 minute
- An addition disadvantage is that the algorithm loses power when read the voltage at open circuit because the current doesn't flow then
- Also the classic FOCV changes the DC step by step until reach the new voltage that mean extra power losses until reach the needed voltage, thanks to the innovative change in this algorithm that goes immediately in DC at comparison voltage and search from there the comparison voltage the power losses reduced

4.2.4 Fractional Short Circuit Current (FSCC)

The Current Short Circuit (I_{oc}) in photovoltaics technologies (GRAPES, Si, CdTe etc) as shown in Image 78., is proportional to Solar Irradiance ($\frac{W}{m^2}$) , because known that the photocurrent density, is proportional to the photons absorbed by the photovoltaic, for that reason, motivated and developed the Fractional Short Circuit Current (FSCC) MPPT algorithm.

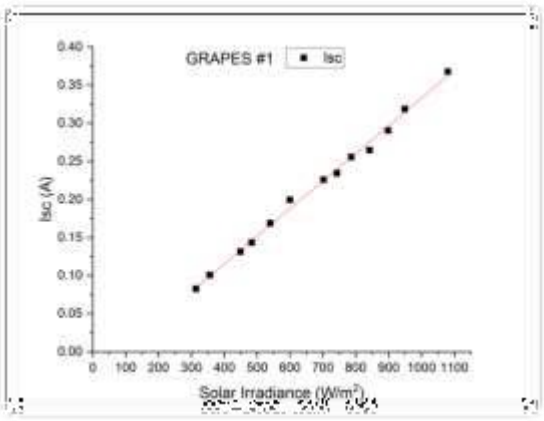


Image 78. GRAPES #1 Isc - IRR Curve

In FSCC algorithm first scan from open circuit to 100% of IV Curve short circuit, extraction of the electrical characteristic like V_{oc}, V_{max}, I_{sc}, I_{max}, P_{max}, done, also calculate the $C_{\%} = \frac{Imax}{Isc}$, obtain the Comparison Current (CC) CC = Imax and Duty Cycle at Comparison Current (DC_at_CC) , this process repeated every ~10 minutes, then setted the DC_at_CC in DC-DC Boost Converter, the converter stays constant at DC_at_CC for 2 minutes, after the 2 minutes pass the converter set DC to 100% (Image 80.c.) to obtain the new Isc (Image 80.d.) and calculate the new Comparison Current $CC = Isc \times C_{\%}$, first the converter it's set the DC_at_CC then changing the Duty Cycle until Photovoltaic Current is equal to Calculated Comparison Current (Image 80.d.) when the converter finds the Current stays constant for 2 minutes and repeat the process, at 10 minutes and 58 seconds repeat the IV scan that shown in Image 79. and 80.c.

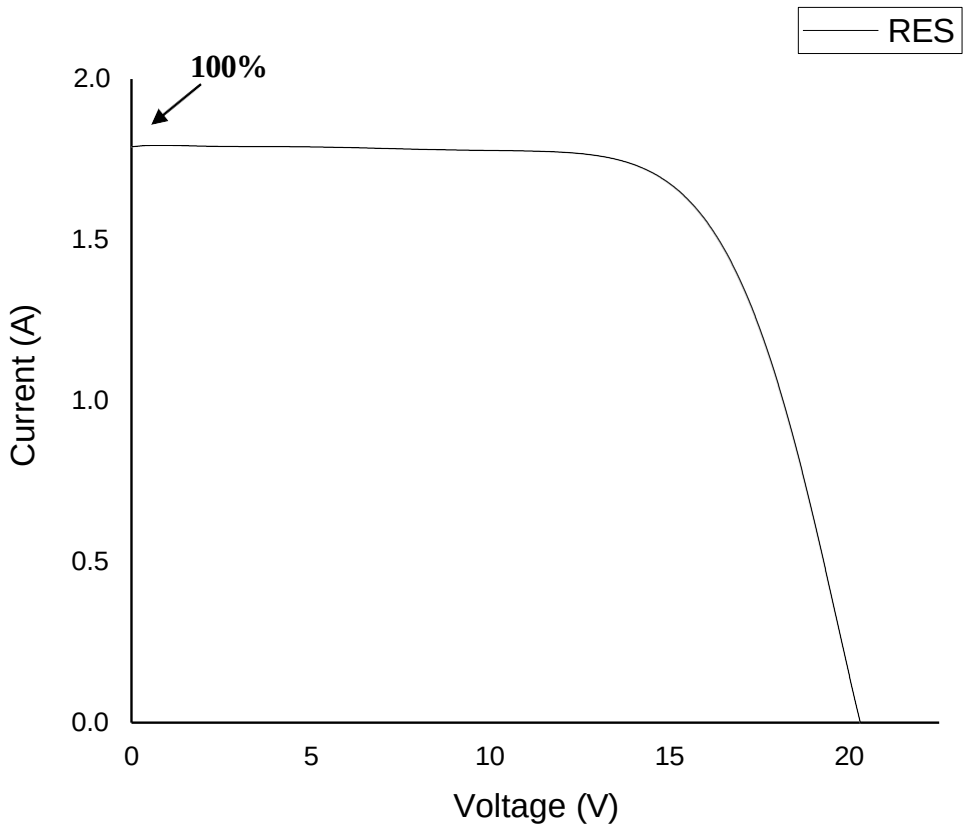


Image 79. First IV Scan 0 to 100% Duty Cycle of FSCC Algorithm in Si photovoltaic, repeat every 10 minutes and 58 seconds

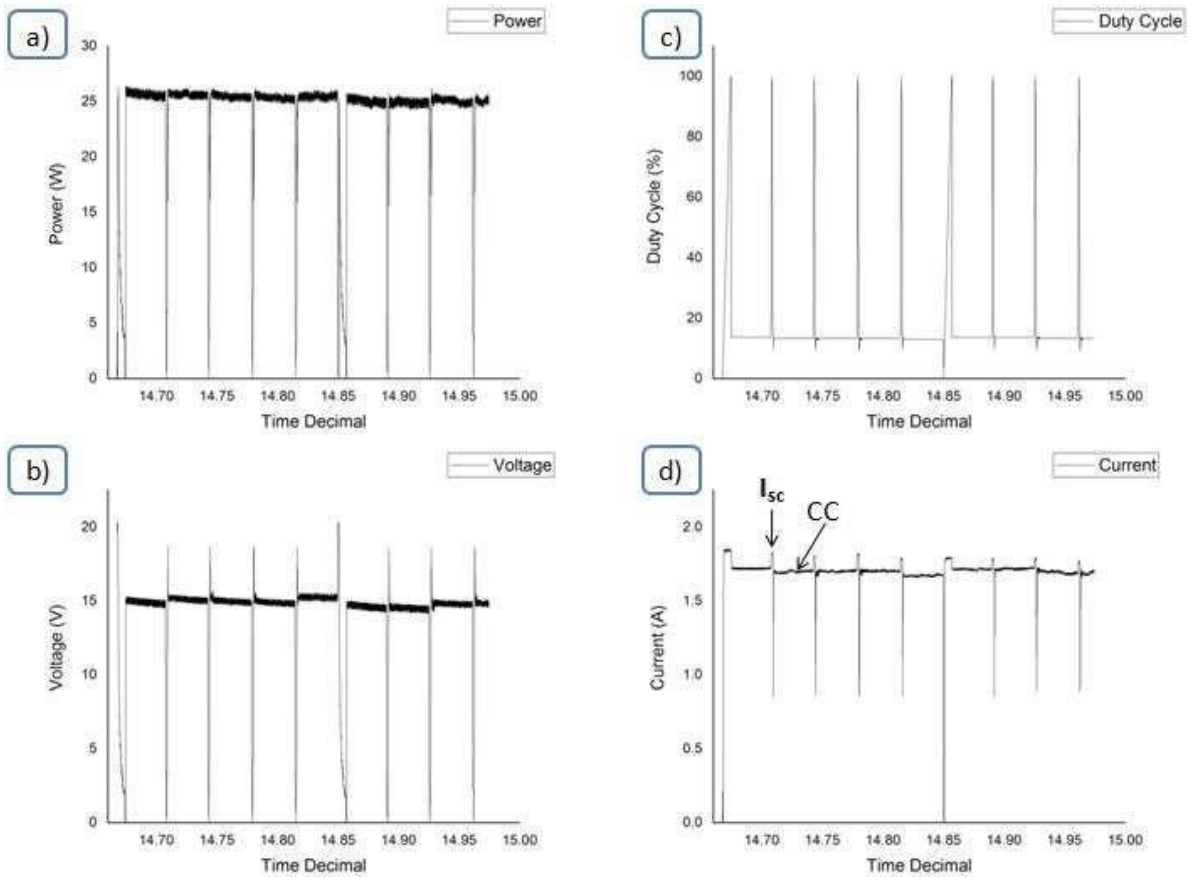


Image 80. FSCC Graphs in Si (23/08/2021), ***a)*** *Power - Time,* ***b)*** *Voltage - Time,* ***c)*** *Duty Cycle - Time,* ***d)*** *Current - Time*

Follows the flow chart of FSCC algorithm for its better understanding see Image 81.

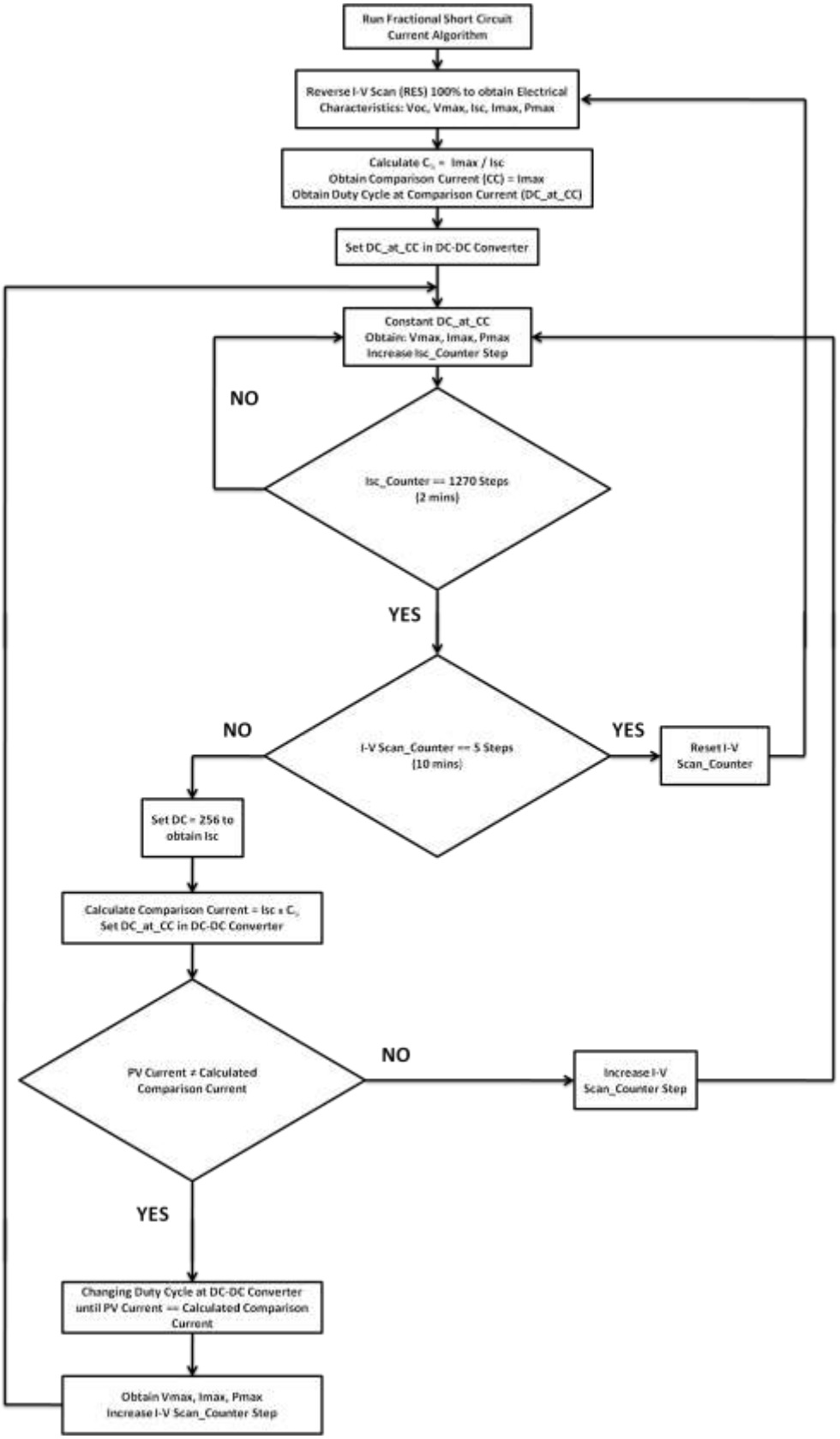


Image 81. Flow Chart of FSCC Algorithm

The advantages of the innovative FSCC algorithm are:

- It works efficiently for all photovoltaic technologies because Isc is proportional to Solar Irradiance ($\frac{W}{m^2}$)
- It works periodically every 2 minutes so doesn't need high processing power from microcontroller
- And because works periodically does not strain the photovoltaics, the reason is that doesn't have changes in Duty Cycle
- Also observed that FSCC algorithm is very stable in current changes as shown in the Image 80.d., in turn and with power 80.a.

The disadvantages are:

- Because it work every 2 minutes in that interval any changes in solar irradiance can't be tracked that means losses in energy yield, that can be improved with lower intervals for example 1 minute
- An addition disadvantage is that the algorithm loses power when read the current at short circuit because the voltage is zero
- Also the classic FSCC changes the DC step by step until reach the new current that mean extra power losses until reach the needed current, thanks to the innovative change in this algorithm that goes immediately in DC at comparison current and search from there the comparison current the power losses reduced
- In comparison with FOCV the FSCC algorithm short circuits the system isn't ideal state, because having big currents that means extra power losses at copper wires and big strain at all materials
- The Duty Cycle at DC-DC Boost Converter mustn't go up to 80% because the coil or the mosfet it can be destroyed if stays for big time at this state and FSCC algorithm goes at 100% for a little time
- Also short circuits can't be happened at big solar farms because it can be danger for whole facility that's why FOCV is preferable algorithm than FSCC

4.2.5 Incremental Conductance (IC)

The IC algorithm is the most popular and widely used algorithm. It overcomes the disadvantage of not staying at MPP that HCPO algorithm does. The implementation of IC is way more complex and difficult than HCPO, also is mathematical oriented algorithm, that means complex calculations which increases the hardware requirement and fabrication cost.

The theory behind IC algorithm is to determine the variation direction of the output terminal voltage of the photovoltaics by measuring and comparing the incremental conductance and the instantaneous conductance of photovoltaics. If the value of incremental conductance and the instantaneous conductance are equal, then it represents the operating point reaches the MPP maximum power point. **[49]**

In IC algorithm first scan from open circuit to 80% of IV Curve short circuit, and don't let the algorithm do short circuit in Photovoltaics (D.C. 0 to 80%) (Image 83.b. and 83.c.), extraction of the electrical characteristic like V_{oc}, V_{max}, I_{max}, P_{max}, done, then start running at P_{max} point, like HC, HCPO and continuously scan and compare the new power and the conductance measurements with the previous measurements. The basic idea of IC on a PV curve is shown at Image 82. The slope of the PV curve is zero at the MPP, increasing on the left side of the MPP and decreasing on the right side of the MPP.

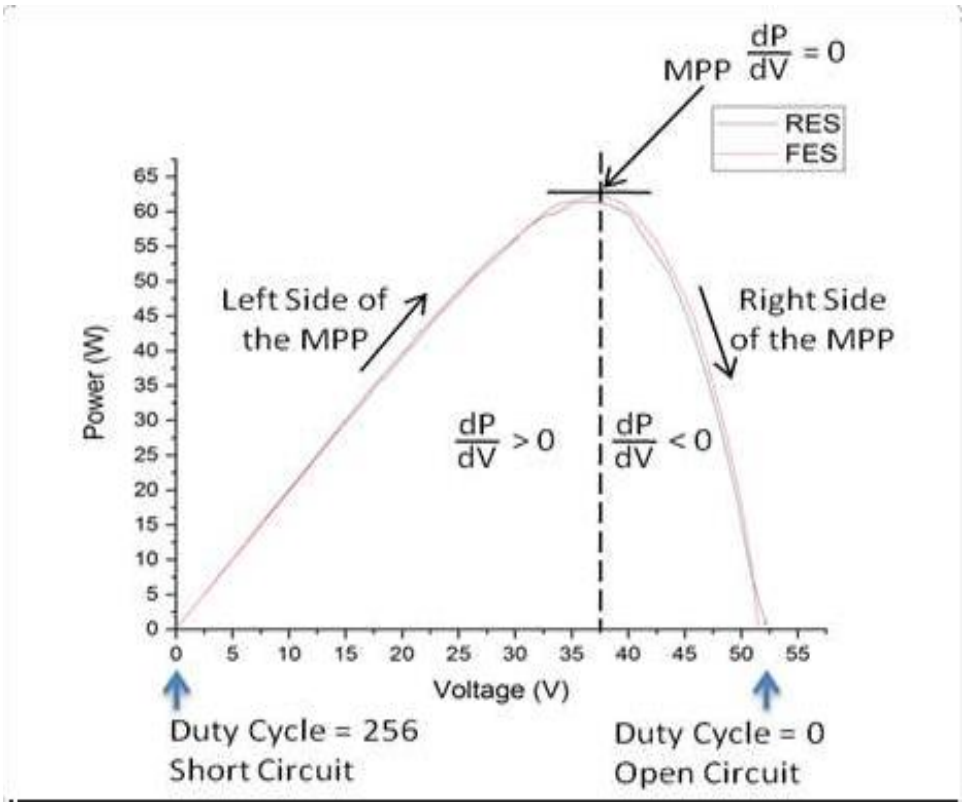


Image 82. Basic Idea of the Incremental Conductance Algorithm

So the mathematical equations of IC are:

- $\frac{dP}{dV} = 0\,, at\ MPP$
- $\frac{dP}{dV} > 0\,, Left\ Side\ of\ the\ MPP$
- $\frac{dP}{dV} < 0\,, Right\ Side\ of\ the\ MPP$

Since

$$\frac{dP}{dV} = \frac{d(IV)}{dV} = 1 + V\frac{dI}{dV} = 1 + V\frac{\Delta I}{\Delta V}$$

- $\frac{\Delta I}{\Delta V} = -\frac{I}{V}$, $at\ MPP$
- $\frac{\Delta I}{\Delta V} > -\frac{I}{V}$, $Left\ Side\ of\ the\ MPP$
- $\frac{\Delta I}{\Delta V} < -\frac{I}{V}$, $Right\ Side\ of\ the\ MPP$

so the IC algorithm changing the D.C. steps up and down depending on these mathematical equations and it can maintain the Pmax and the Conductance even with disturbances from changings in solar irradiance (clouds, or sun position at morning or afternoon, etc), also every **10 minutes and 34 seconds** repeats the scan from open circuit to 80% of IV short circuit to extract the new electrical characteristics (Image 83.),

The advantages of the IC algorithm are:

- That continuously scan so it can maintain the Pmax all the time.
- It has very good tracking efficiency, especially under rapidly changing of atmospheric conditions.
- Also if the algorithm finds the MPP, stays at it in contradiction of the HCPO that don't stay

Disadvantages of the IC algorithm are:

- That the algorithm can be trapped in local maximum when continuously scan for Pmax and the Conductance, but that can be solved with increased steps in D.C.
- The other disadvantage is that continuously changes in D.C. can mean power losses, also if the step is increased for trap escaping means extra power losses and lower resolution in finding Pmax.
- Also if the algorithm finds the MPP but has increased steps in D.C. and the atmospheric conditions slowly but continuously change, can't stay in the same Pmax and it's perturbs back and forth around the MPP such as HCPO, that means extra power losses, it can be solved with the addition of disturbance sensitivity check
- Another disadvantage is complexity of the algorithm that need complex calculations which increases the hardware requirement and fabrication cost respectively

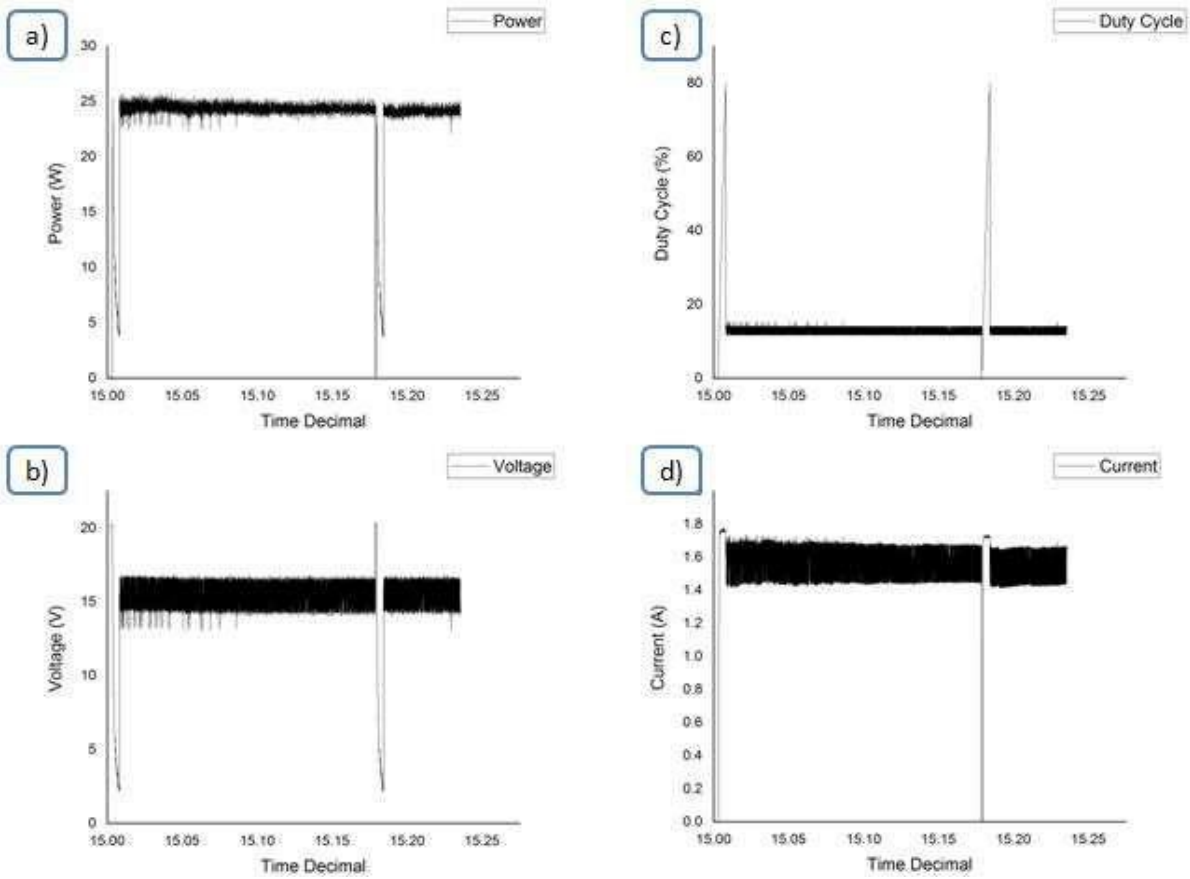


Image 83. IC Graphs in Si (23/08/2021), ***a)*** *Power - Time,* ***b)*** *Voltage - Time,* ***c)*** *Duty Cycle - Time,* ***d)*** *Current - Time*

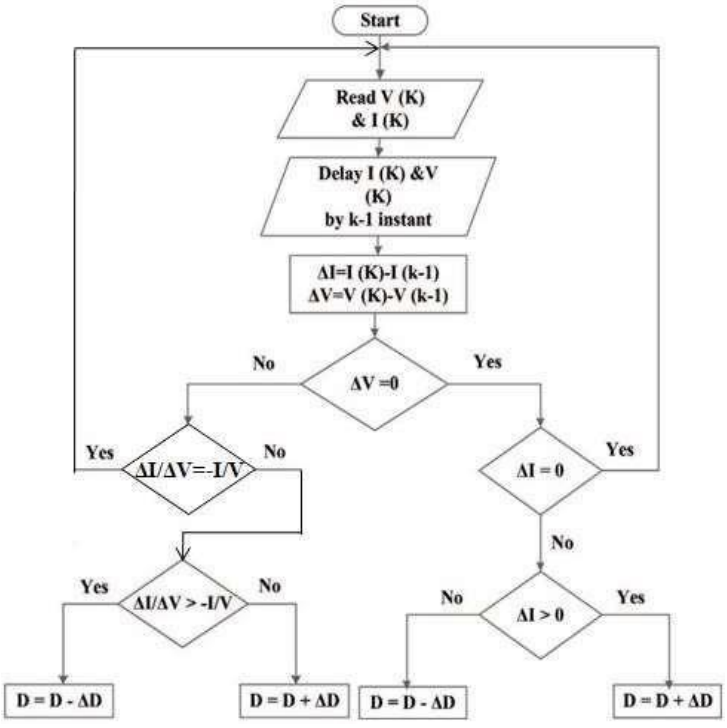


Image 84. Flow Chart of IC algorithm **[48]**

4.2.6 Maximum Power Quantumized Area Search (MPQAS1 and MPQAS2)

The innovative MPQAS algorithms version 1 and 2 are created so it can combine all the advantages of direct or online scanning (HC,HCPO,IC) and indirect or offline scanning (FOCV, FSCC) algorithms with less disadvantages of both types.

- Observed that in indirect type of algorithms, the ability to stop the microcontroller in constant duty cycle and every 2 minutes repeat the scanning has tremendous increased energy yield and less strain in photovoltaics, especially in clear sunshine days
- Also known that from direct algorithms, the constant scanning it can maintain the Pmax all the time

So needed the algorithm than can do both. The MPQAS v1 & v2 algorithms have the ability to recognize the pattern of the irradiance, so it can active or de-active the proper search, every time that need it depending on the conditions.

The MPQAS v1 and v2 it works in two states:

- First state is in unstable conditions with disturbances, such as weather (clouds, rain, snow etc), shading or inclination of photovoltaics
- Second state is in stable conditions without disturbances, such as a clear day with sunshine

In the MPQAS algorithm, before the two states take in place, it start with auto calibration of the algorithm first scan from open circuit to 80% of IV Curve short circuit, and don't let the algorithm do short circuit in Photovoltaics (D.C. 0 to 80%) (Image 90.b. and 90.c.), extraction of the electrical characteristic like V_{oc}, V_{max}, I_{max}, P_{max} , P_{max_check} and DP_Sensitivity_Limit, done, then start running at P_{max} point.

In more detail, every 10 minutes with IV Curve for electrical characteristics, also setted the algorithm trigger limits, so it can recognize the irradiance pattern, if is unstable irradiance (cloudy sky etc) or stable irradiance (clear sky etc), the upper power sensitivity limit and the lower power sensitivity limit, calculated with the following equations:

DP_Sensitivity_Limit_Percentage was set at algorithms codes (v1 and v2) at 5% of Pmax.

- $DP_Sensitivity_Limit = \frac{Pmax_Check \times \text{DP_Sensitivity_Limit_Percentage}}{100}$
- $Upper_Sensitivity_Limit = Pmax_Check + DP_Sensitivity_Limit$
- $Lower_Sensitivity_Limit = Pmax_Check - DP_Sensitivity_Limit$

So for example if having Pmax_Check (Pmax_Check is the previous Pmax in MPP searches and the first Pmax in every run of 80% IV RES curve, also it helps to set the trigger

limits) equal to 20W , the DP_Sensitivy_Limit, the Upper and Lower power sensitivity limits are:

$$DP_Sensitivity_Limit = \frac{Pmax_Check \times \text{DP_Sensitivity_Limit_Percentage}}{100} = \frac{20W \times 5}{100} = 1W$$

$$Upper_Sensitivity_Limit = Pmax_Check + DP_Sensitivity_Limit = 20W + 1W = 21W$$

$$Lower_Sensitivity_Limit = Pmax_Check - DP_Sensitivity_Limit = 20W - 1W = 19W$$

now the algorithm with all electrical characteristics and the power sensitivity limits calculated it can start.

The concept here is the recognition of the solar irradiance through the trigger limits, the algorithm after all the calculation shown above, starts at Pmax point (MPP) and keep it constant as FOCV and FSCC algorithm, so the microcontroller stop and works:

At the second state:

That means at stable conditions without disturbances (changes) in solar irradiance, periodically every one minute microcontroller start and work to refresh the MPP, for the maximum power point area track it is used in **version 1** (**MPQAS1**) the **Incremental Conductance** algorithm and in the **version 2** (**MPQAS2**) the **Hill Climbing Perturb and Observe** algorithm, for this search algorithms use the higher resolution possible for the microcontroller, the change in step of duty cycle is 1 step out of 256 that means Duty Cycle change percentage is $\frac{1}{256} \times 100 = 0.39\%$ and the reason is that the working at stable conditions, so don't have the risk of being trapped at a local maximum, so don't need to have more power losses from bigger steps such us 1.17% D.C. step. As known the disadvantage of HCPO and IC algorithms is if the algorithm finds the MPP, never stays in the same Pmax it's perturbs back and forth around the MPP, that means extra power losses, but in MPQAS the problem solved, because observed that the average change of duty cycles steps from back and forth around the MPP is exactly the same, so for the recognition if the solar irradiance is at stable state, this attribute used and if two duty cycle averages in row is the same, then can understand that are in stable conditions (clear sky), but to find exactly the MPP, it used from back and forth around MPP area the duty cycle steps to create starting and ending point for a local quantumized area RES IV curve, so having as starting point the less D.C. step -1 (stability step) and as the ending point the max D.C. step +1 (stability step) so scanning this local quantumized area IV RES curve with four points to get the exactly MPP D.C. and set the device at MPP and stop the microcontroller immediately again so doesn't need high processing power from microcontroller, the process repeat every 1 minute if no disturbances occurs.

Second State of MPQAS Algorithm

Time Decimal	Duty Cycle (%)	Voltage (V)	Current (A)	Power (W)	Step Change (%)	Duty Cycle Average (%)	Local IV Limits Calculation Duty Cycle + Step Change
12.3069	15.686	13.934	1.619	22.55	0	15.686	
12.3072	15.686	13.912	1.623	22.57	0	15.686	
12.3072	15.686	13.843	1.62	22.43	0	15.686	
12.3072	15.686	13.887	1.621	22.51	0	15.686	
12.3072	15.686	14.149	1.621	22.93	0	15.686	
12.3072	15.686	13.989	1.618	22.64	0	15.686	
12.3072	15.294	14.193	1.593	22.62	-0.392	15.49	14.902
12.3072	15.686	13.963	1.617	22.57	0.392	15.49	16.078
12.3075	14.902	14.624	1.554	22.72	-0.784	15.294	14.902 Lower Limit
12.3075	15.294	14.286	1.594	22.78	0.392	15.098	
12.3075	15.686	14.134	1.623	22.94	0.392	15.49	
12.3075	16.078	13.665	1.648	22.52	0.392	15.882	16.078 Upper Limit
12.3075	15.686	13.94	1.623	22.62	-0.392	15.882	The exact MPP was found
12.3075	15.686	14.202	1.62	23	0	15.686	
12.3075	15.686	13.97	1.616	22.58	0	15.686	
12.3078	15.686	13.796	1.62	22.35	0	15.686	
12.3078	15.686	13.912	1.622	22.57	0	15.686	

Perturbing back and forth around MPP, same Duty Cycle Averages 2 in row

Local RES IV Limits Calculation, starting and ending point for a local RES IV curve

Lower to Upper Limit Local Quantumized Area 4 point IV Scan

Exact MPP was found and D.C. set at it

Image 85. Measurements of Second Working State of MPQAS Algorithm at stable conditions without disturbances, at Si (30/07/2021)

If disturbances occur the algorithm proceed:

At the first working state:

In the first state the algorithm recognized that having disturbances of solar irradiance through the changes in photovoltaic power, if the distortion of power is out of the trigger limits for **ten times in row** the scanning process that shown above, automatically active and start to find the area of MPP (see Image 86), but because having unstable conditions (cloudy sky) the resolution changed into 3 steps, that means Duty Cycle change percentage is $\frac{3}{256} \times 100 = 1.17\%$ so don't have the risk of being trapped at a local maximum and find the MPP area, also when found the MPP area and is ready to do the local IV scan now added 3 steps, so having as starting point the less D.C. step -3 and as the ending point the max D.C. step +3, so scanning step by step this local quantumized area IV RES curve with ten points (quantumized in ten quantum points of 0.39% D.C. each one, 10 points x 0.39% = 3.9% of IV Curve) now than four (4 points x 0.39% = 1.56% of IV Curve) from the stable conditions to get the exactly MPP D.C. and set the device at MPP and stop the microcontroller if no more disturbances occurs, if the algorithm can't stabilized for about 5 minutes, automatically return to last refresh electrical characteristics and the power sensitivity limits that has been calculated and start from there.

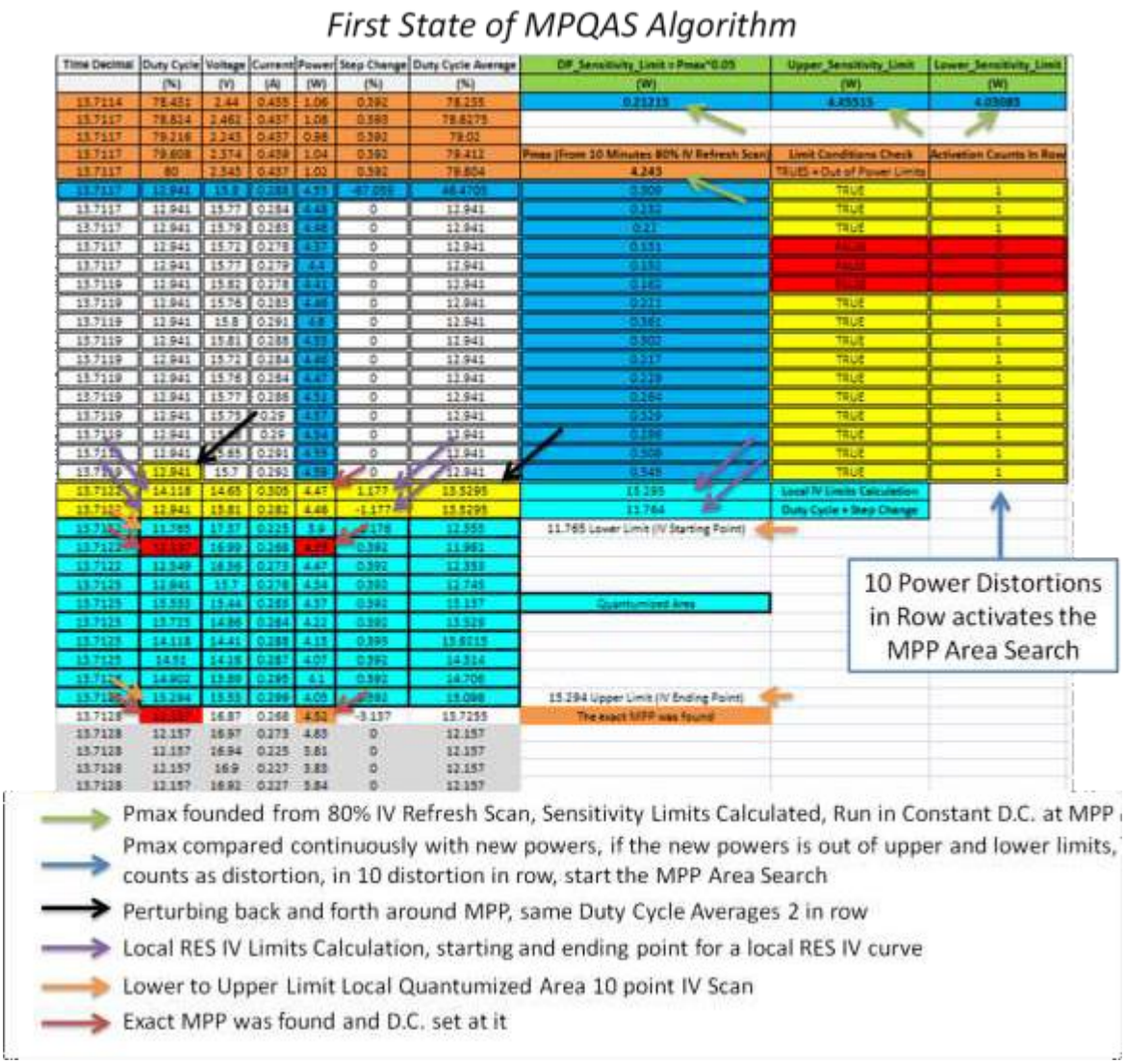


Image 86. Measurements of First Working State of MPQAS Algorithm at unstable conditions with disturbances, at GRAPES #7 (20/07/2021)

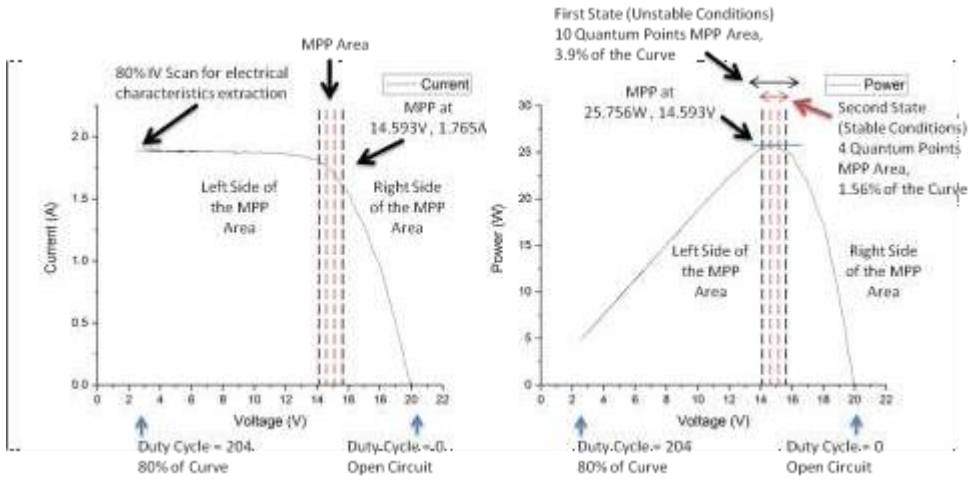
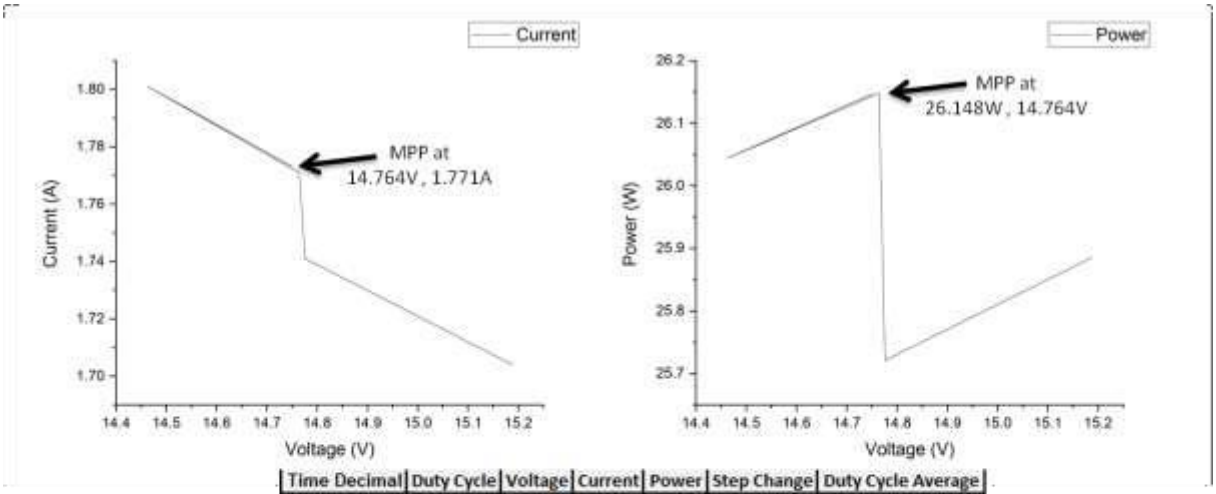


Image 87. MPP Quantumized Area Position of 10 and 4 points in IV and PV Curves, at Si



Time Decimal	Duty Cycle (%)	Voltage (V)	Current (A)	Power (W)	Step Change (%)	Duty Cycle Average (%)
13.4900	15.686	14.775	1.77	26.148	-0.392	15.882
13.4900	15.294	14.987	1.742	26.107	-0.392	15.49
13.4900	15.686	14.788	1.767	26.125	0.392	15.49
13.4903	14.902	15.189	1.704	25.886	-0.784	15.294
13.4903	15.294	14.776	1.741	25.721	0.392	15.098
13.4903	15.686	14.764	1.771	26.148	0.392	15.49
13.4903	16.078	14.463	1.801	26.044	0.392	15.882
13.4903	15.686	14.751	1.773	26.147	-0.392	15.882
13.4906	15.686	14.453	1.776	25.672	0	15.686

Image 88. Measurements of Local Quantumized Area 4 points IV Scan and 1.56% of IV and PV Curve, at Si (23/08/2021)

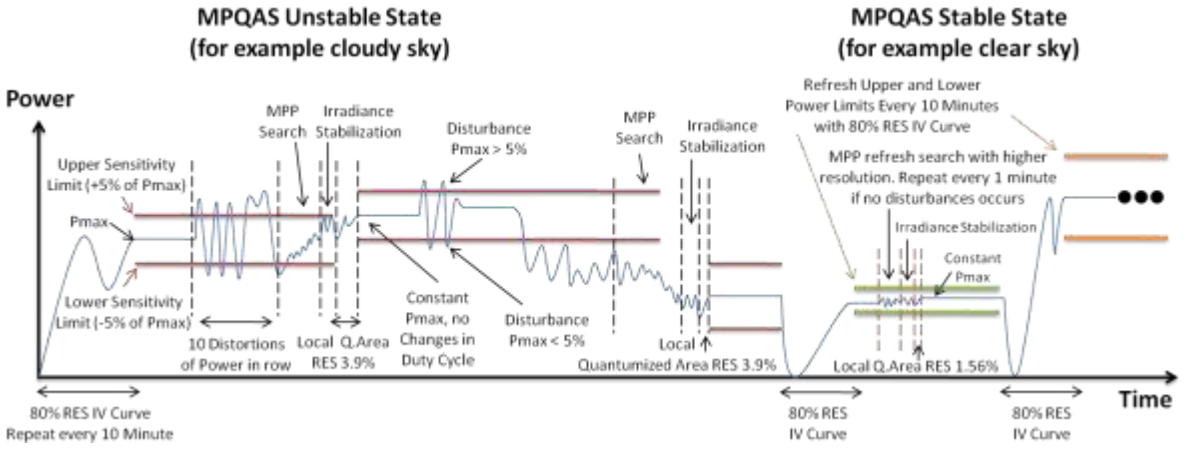


Image 89. MPQAS Algorithm Power - Time operation diagram at two working states, Unstable and Stable Conditions

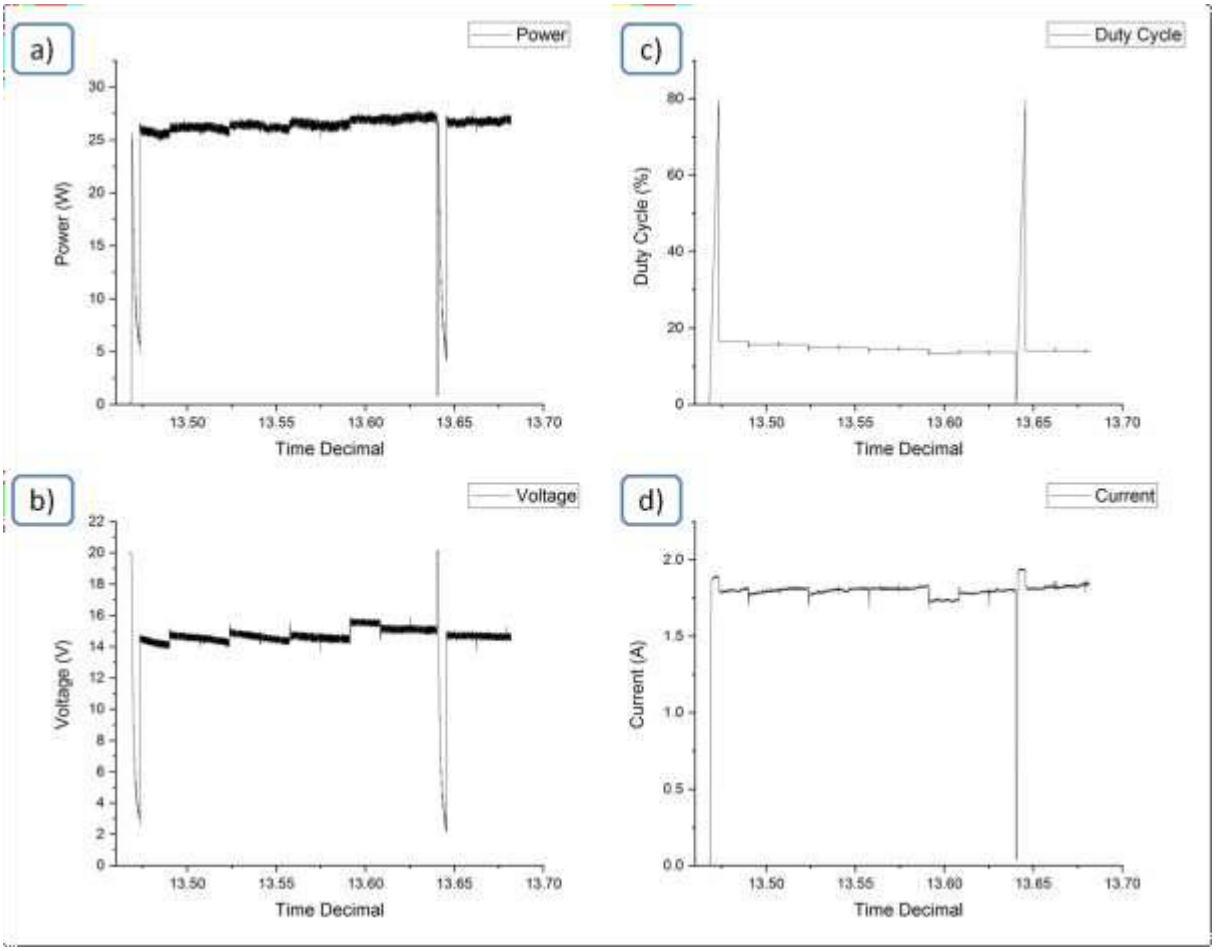


Image 90. MPQAS Graphs in Si (23/08/2021), ***a)*** *Power - Time,* ***b)*** *Voltage - Time,* ***c)*** *Duty Cycle - Time,* ***d)*** *Current - Time*

The advantages of the MPQAS v1 and v2 algorithms are:

- That can recognize irradiance pattern and choose if it's clear sky (Stable Conditions) to stay constant in D.C. of Pmax., so less power losses and does not strain the photovoltaics like FOCV and FSCC algorithms and repeat every one minute fast re-check the MPP Area (about one to two seconds) with maximum resolution so it can follow the sun changes in irradiance from morning to afternoon (Second Working State). Or if it cloudy sky (find 10 irradiance distortions in row, Unstable Conditions) that must activate the MPP scan with less resolution to avoid trapped in local maximum so it can maintain the Pmax all the time like IC and HCPO algorithms (First Working State), also if the algorithm finds the MPP and distortions of irradiance stop returns automatically at stable conditions to avoid more power losses
- It has very good tracking efficiency, especially under rapidly changing of atmospheric conditions especially the MPQAS1 because of use the IC Algorithm, MPQAS2 uses

HCPO Algorithm still very good tracking efficiency and sometimes faster MPP area recognition than MPQAS1 because of simplicity nature of HCPO

Disadvantages of the MPQAS v1 and v2 algorithms are:

- In first working state, at unstable conditions the change in lower resolution in D.C. so it can avoid trapped in local power maximum it can mean power losses, at least until it finds the MPP Area then the local quantumized area IV solve the problem of perturbing because stabilize the system and stop it at constant D.C. of exact Pmax, until it have again 10 distortions in row
- The system stability with 10 power distortion in row means, that have 10 power distortion losses ±5% that not recognized because of sensitivity limits
- Another disadvantage of MPQAS is complexity of the algorithm especially the MPQAS1 that use IC, means that need complex calculations which increases the hardware requirement and fabrication cost respectively

The two working states repeats continuously, also in MPQAS1 every **10 minutes and 20 seconds** and in MPQAS2 every **10 minutes and 22 seconds** repeats the scan from open circuit to 80% of IV short circuit to extract the new electrical characteristics and new sensitivity limits (Image 90.b. and 90.c.).

Follows the flow chart of MPQAS version 1 and version 2 algorithms.

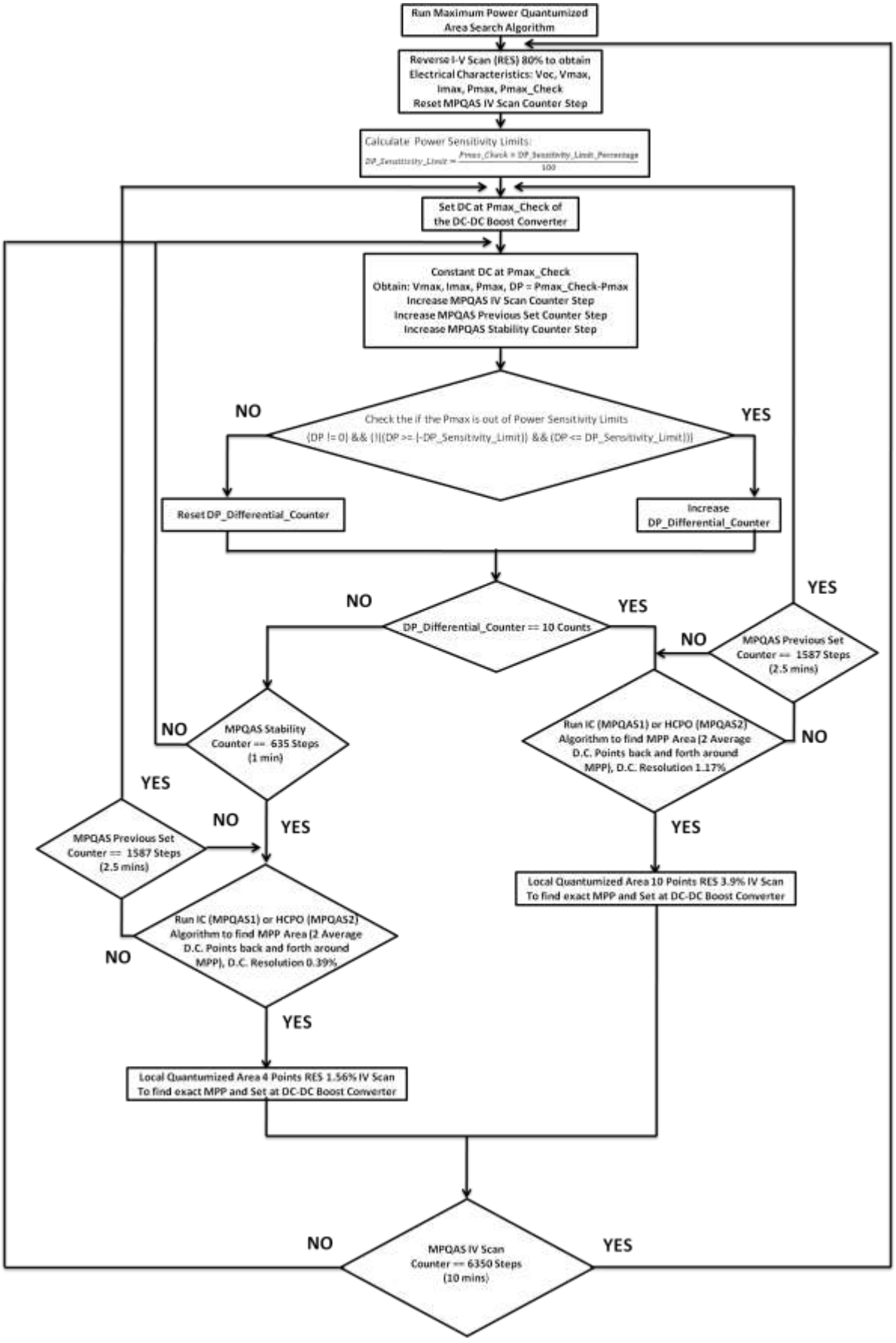


Image 91. Flow Chart of MPQAS Algorithm Version 1 and 2

4.3 Explanation of PVBR Algorithms

The PVBR algorithms measurements acquired live, in each measurement can setup the number of average points and the delay (seconds) of intervals, all algorithms has 100% RES IV rescanning every ~5 minutes, at IV scanning process the average points change automatically at 200 points and back at the selection average points when start to operate again. Due to the two disadvantages of GRAPES Photovoltaics, sun exposure degrade it and supply load degrade it, motivated to develop, two algorithms that can read these behaviours. For sun exposure behaviour developed the Pmax Open Circuit Intervals (POCI) and for supply load behaviour the Pmax Short Circuit Intervals (PSCI) algorithms.

4.3.1 Pmax Open Circuit Intervals (POCI)

In POCI algorithm first scan from open circuit to short circuit of IV Curve (RES) (see Image 92.c.), extract the electrical characteristic like Voc, Vmax, Isc, Imax, Pmax (see Image 92.), then start running at Pmax point for an instant (200 mS) then instantly go to Open Circuit for a given time (60 seconds for example see Image 92.) that selected in starting setup when this time pass, return to Pmax again, and repeat this Pmax to Open Circuit interval for 5 minutes, then can re-setup the algorithm with new delays or average points of Pmax measurement or stop the algorithm.

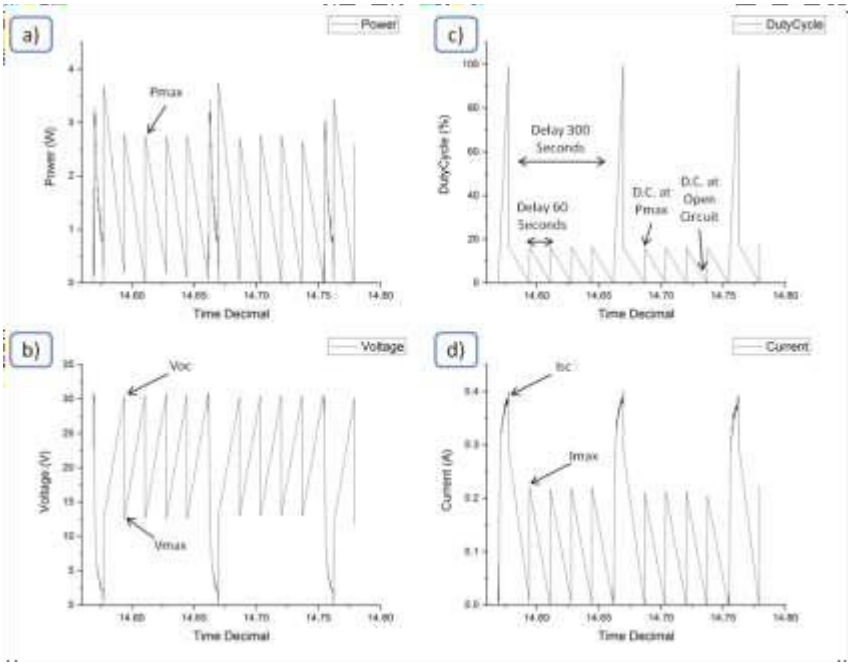


Image 92. POCI Graphs in GRAPES #8 (26/07/2021), Setup at 200 Average Points and 60 Seconds Open Circuit delay, ***a)*** *Power - Time,* ***b)*** *Voltage - Time,* ***c)*** *Duty Cycle - Time,* ***d)*** *Current - Time*

4.3.2 Pmax Short Circuit Intervals (PSCI)

In PSCI algorithm first scan from open circuit to short circuit of IV Curve (RES) (see Image 93.c.), extract the electrical characteristic like Voc, Vmax, Isc, Imax, Pmax (see Image 93.), then start running at Pmax point for an instant (200 mS) then instantly go to Short Circuit for a given time (60 seconds for example see Image 93.) that selected in starting setup when this time pass, return to Pmax again, and repeat this Pmax to Short Circuit interval for 5 minutes, then can re-setup the algorithm with new delays or average points of Pmax measurement or stop the algorithm.

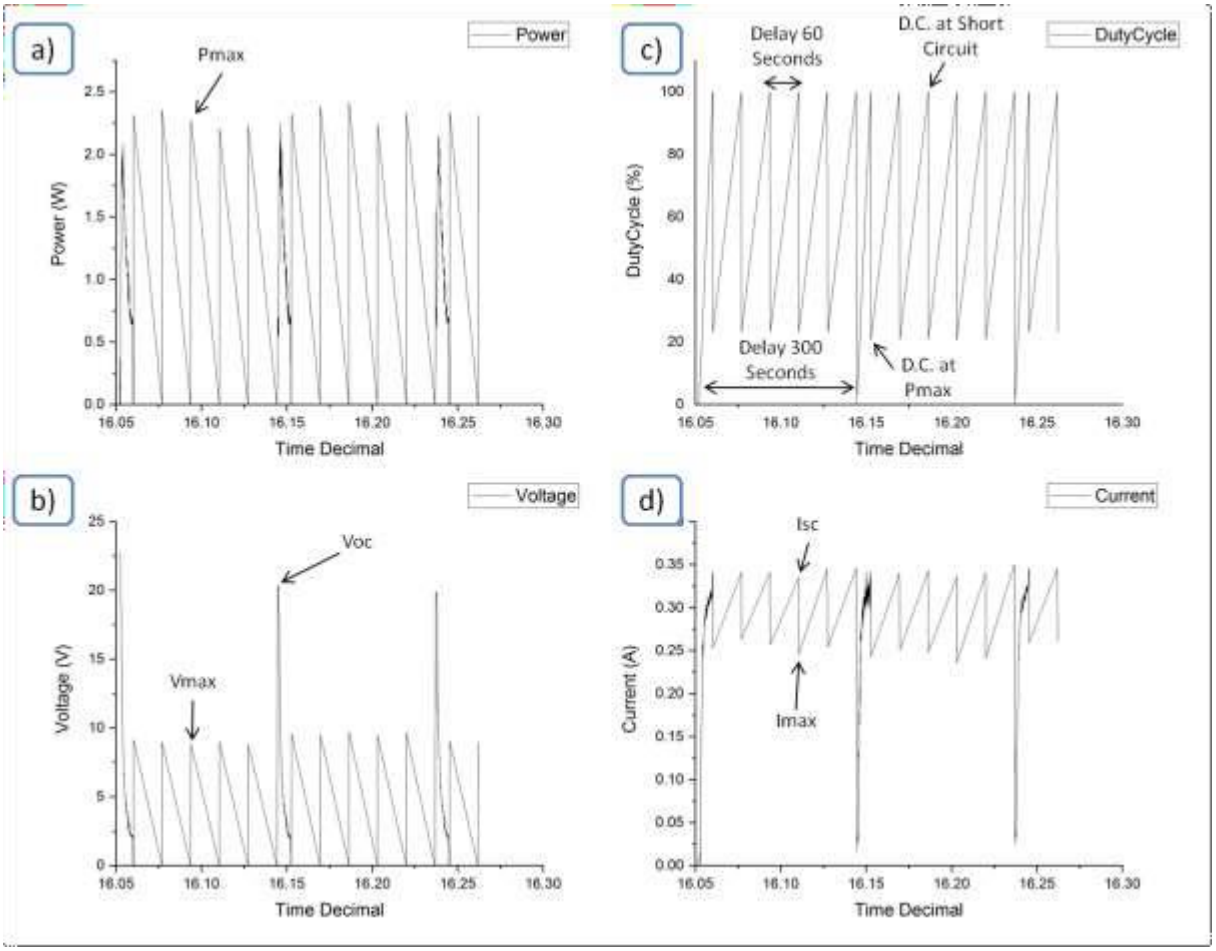


Image 93. PSCI Graphs in GRAPES #8 (26/07/2021), Setup at 200 Average Points and 60 Seconds Short Circuit delay, ***a)*** *Power - Time,* ***b)*** *Voltage - Time,* ***c)*** *Duty Cycle - Time,* ***d)*** *Current - Time*

As shown at Image 93. the PSCI algorithm is complete inverse than POCI see Image 92.

4.4 Literature Review of MPPT Algorithms

In literature review shown that the MPPT algorithms was classified into 3 major categories:

- Online
  - Hill Climbing Perturb and Observe (HCPO or P&O)
  - Incremental Conductance (IC or INC)
  - Slide Mode Control (SMC or just Slide Mode)
  - Parasitic Capacitance (PC)
  - Grey Wolf Optimizer (GWO)
- Offline
  - Fractional Open Circuit Voltage (FOCV or O.C. Voltage)
  - Fractional Short Circuit Current (FSCC or S.C. Current)
- Intelligent
  - Fuzzy Logic Control (Fuzzy)
  - Artificial Neural Network (ANN)
  - Particle Swarm Optimization (PSO)
  - Firefly (FA), Immune Firefly (IFA), Fast Convergence Firefly (FCFA)

MPPT Algorithms	Algorithm Complexity	Convergence Speed	Analog or Digital	PV array dependency	Tracking Accuracy	Hardware Implementation	Application
O.C Voltage	Low	Slow	Both	Yes	Low	Easy	Off Grid
S.C Current	Low	Slow	Both	Yes	Low	Easy	Off Grid
P&O	Low	Slow	Both	No	Medium	Easy	Both
INC	Medium	Fast	Digital	No	High	Moderate	Both
Fuzzy	Medium	Fast	Digital	Yes	Very High	Easy	Both
ANN	High	Fast	Digital	Yes	Very High	Difficult	Grid
PSO	High	Fast	Digital	No	Very High	Moderate	Both
Slide Mode	Medium	Fast	Digital	No	Medium	Difficult	Both

Image 94. Comparative characteristics of various MPPT algorithms **[49]**

MPPT techniques	Parameters		
	Convergence speed	Implementation complexity	Sensed parameters
P & O method	Varies	Low	Voltage
Inc Cond method	Varies	Medium	Voltage, current
Fractional V_{oc} method	Medium	Low	Voltage

Image 95. Comparative Study and Simulation of MPPT **[48]**

Reference	Reported MPPT efficiency (%)			
	Perturb-and-observe	Incremental conductance	Constant voltage	Parasitic capacitance
6	81·5	89·9		
5	85·0	88·0	73·0	
12			85·0	
14				99·8

Image 96. Summary of reported MPPT efficiencies for four algorithms **[50]**

Sky conditions	P&O		Inc		CV	
PV array	Days of data	η_{MPPT}	Days of data	η_{MPPT}	Days of data	η_{MPPT}
Clear	20	98·7	17	98·7	20	90·4
Partly cloudy	14	96·5	11	97·0	10	90·1
Cloudy	9	98·1	11	96·7	6	93·1
Overall	43	97·8	39	97·4	36	91·2
Simulator						
Overall	99·3		99·4		93·1	

Image 97. Overall MPP tracking efficiencies η(%) **[50]**

Sl. no.	MPPT methods	Simulation aspects			Hardware aspects			
		Tracking speed	Suitability under partial shading	Parameters tuning	Level of complexity	Efficiency	System cost	Convergence time
1	P&O	Low	NO	Not required	Low	Low	Low	Medium
2	Duty sweep	Low	Yes	Not Required	Medium	High	Medium	Medium
3	PSO	Medium	Yes	Required	Medium	High	Medium	Low
4	FA	Medium	Yes	Required	Medium	High	Medium	Low
5	FCFA	High	Yes	Not required	Medium	Very high	Medium	Very low

Image 98. Performance comparison of various MPPT Algorithms **[51]**

Observed that every MPPT algorithm is suit for different applications: **[49]**

- For example, for high end application like space satellites and orbital station, that needed to track the true MPP within a stipulated time period and no need of periodic tunning the HCPO and IC are the best choice (see Image 99.a.)
- In large scale photovoltaic farms, the best option is the hybrid (Both Online and Offline) MPPT algorithms (see Image 99.b.)
- At solar vehicles they require very fast convergence speed, the intelligent type of MPPT algorithms are the most appropriate choice (see Image 99.c.)
- Offline type algorithms will be sufficient for PV systems that used for street lighting since it doesn't require any more tight constraints and only easy and cheap implementation is required (see Image 99.d.)



Image 99. Different photovoltaic applications, ***a)*** *Nasa's©International Space Station* **[52]**, ***b)*** *Large Scale Photovoltaic Farm* **[53]**, ***c)*** *Toyota's© Prius Solar Car* **[54]**, ***d)*** *Street Lights* **[55]**

Also for every PV technology (GRAPES, CdTe, CIGS, Si etc), there is one MPPT algorithm that scale better than all others in this PV technology, for example in GRAPES is FOCV.

5. User Guide of IV-MPPT Charger Regulator

This is a guide for a proper use of IV-MPPT Charger Regulator, read it first before starting use the machine, to avoid damages on the machine, to the batteries or at photovoltaics and avoid to get harmed, from electricity or even starting a fire at facilities.

5.1 Instructions for connecting the machine

Steps:

1. First, we connect the IV - MPPT Charger Regulator to our computer
2. Secondly, we connect the polarizations of the metric system [12 Vdc (1) and (2)]
3. Then connect the output (BATTERY) of IV - MPPT Charger Regulator to the battery, the battery voltage must be the same or greater than the measurable Voc of the photovoltaic that we want to measure
4. Finally, we connect to the input (PV) of IV - MPPT Charger Regulator the photovoltaic to be measured
5. The steps are followed upside down from 4 to 1 for the correct disconnection of the system

5.1.1 Step 1: Connection to the computer

We connect the IV - MPPT Charger Regulator to the USB of our computer.



Image 100. IV - MPPT Charger Regulator USB port

5.1.2 Step 2: Connection of the metric system polarizations

The metric system of IV - MPPT Charger Regulator has 2 **isolated** polarizations, which want DC power supply 12V (**DC Source 12V**) separately each e.g. 2 power supplies or 2 batteries **NOT common GND (-) because it will be damaged.**

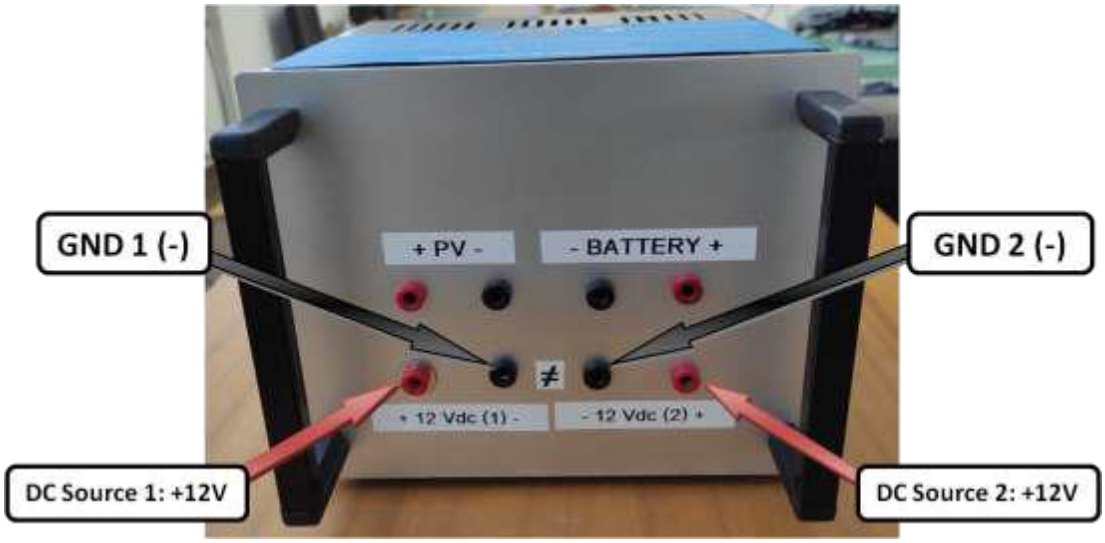


Image 101. Metric system connections

5.1.3 Step 3: Output connection of the device to the battery

Once the metric system is connected (Step 2), the next step is to connect the output of the IV - MPPT Charger Regulator to the desired battery (we never connect the battery inverse to the machine, because the machine will be damaged).

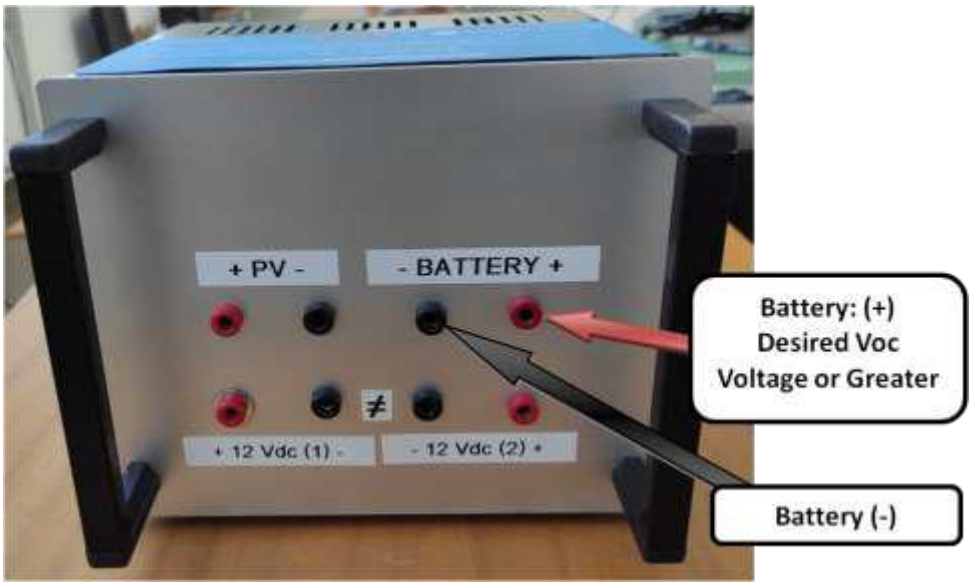


Image 102. Machine front and its output connection

5.1.4 Step 4: Input connection of the device to the photovoltaic

Then after connecting the output of the machine (Step 3), connect to its input, the photovoltaic to be measured.

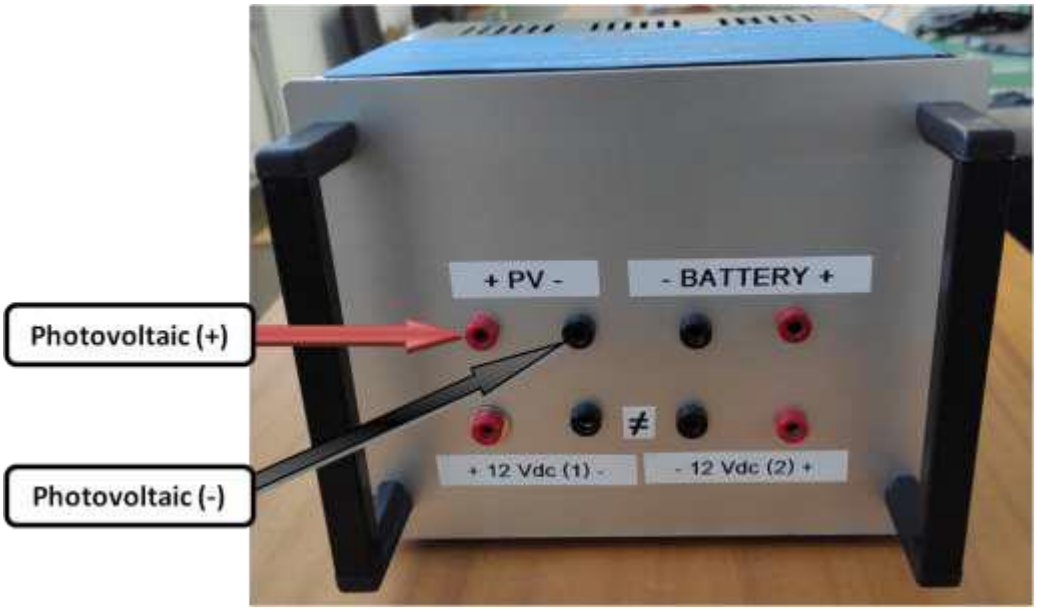


Image 103. Machine front and its input connection

5.1.5 Step 5: Disconnection of the machine

Finally, after taking the measurements and wanting to disconnect the machine, we follow the reverse connection procedure, go from step 4 to step 1, ie:

1. We first disconnect the photovoltaic from the input of the machine
2. Then remove the battery from the output of the machine
3. Then disconnect the polarizations of the metric system
4. Finally, since we have closed the datalogger PLX-DAQ-v2.11, we disconnect the IV - MPPT Charger Regulator from our computer by removing its USB from the computer port

   In the way above, the machine will be safely disconnect without the risk of damage.

5.2 Instructions for using the PLX-DAQ-v2.11 datalogger

For the record of electrical characteristics of the photovoltaic to be measured, we used the open source program that runs in Excel under the name PLX-DAQ-v2.11.

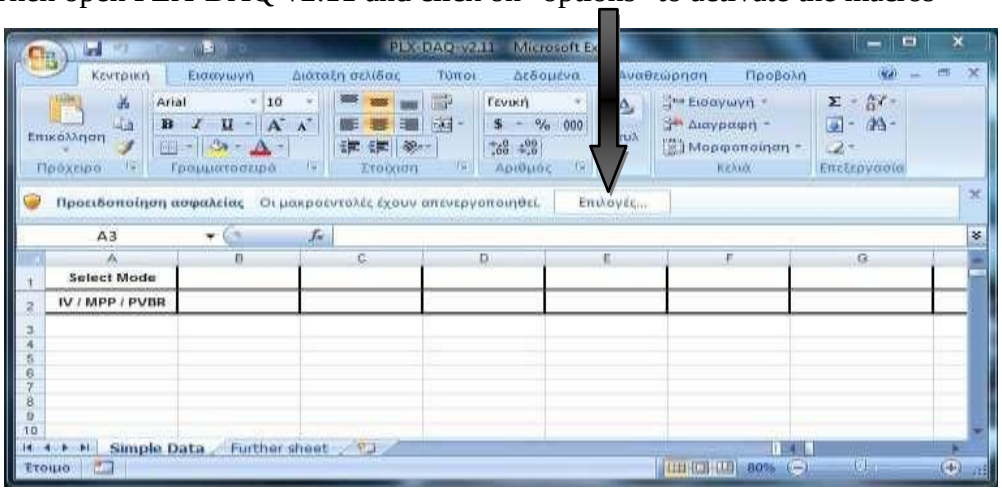
Steps:

- First the PLX-DAQ-v2.11 file must be in the same folder as the machine code

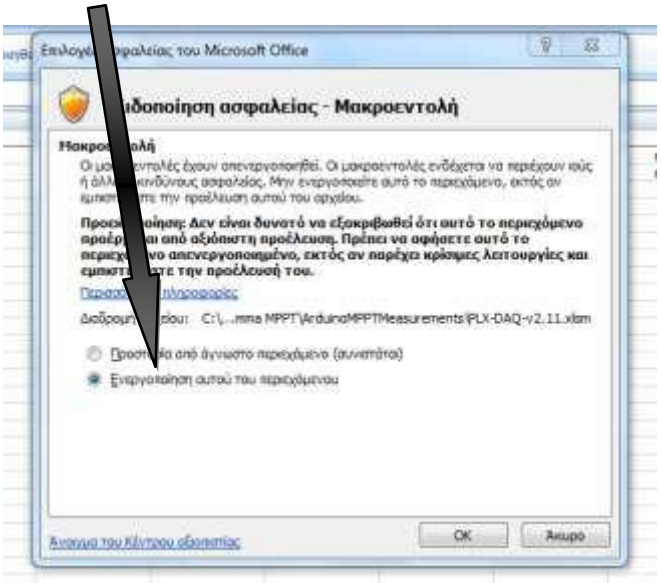


Image 104. Machine program file, together with the logger program

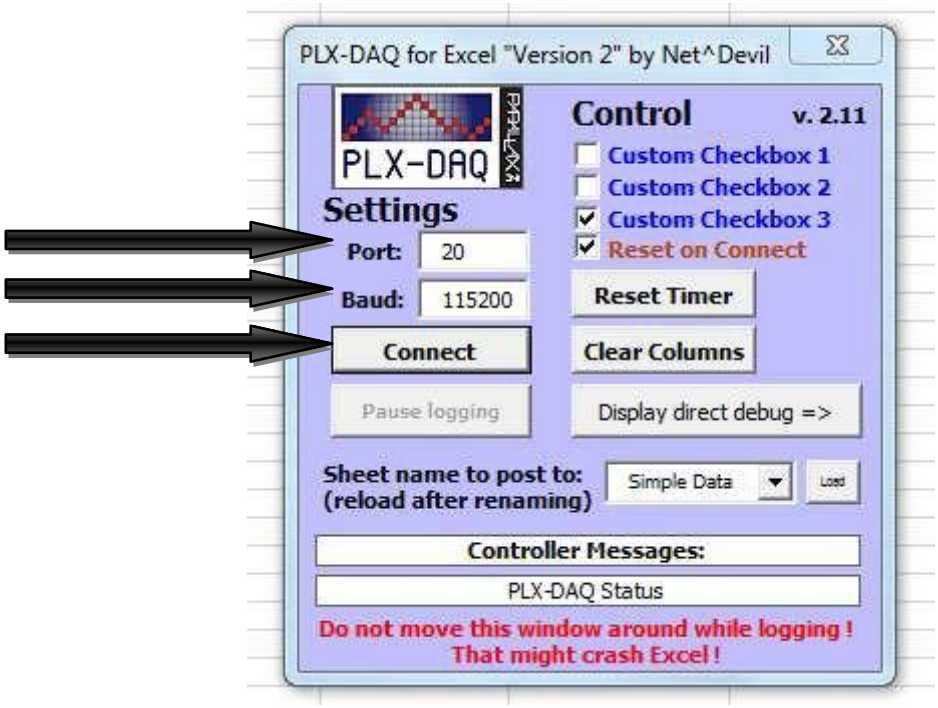
- Then open PLX-DAQ-v2.11 and click on "options" to activate the macros



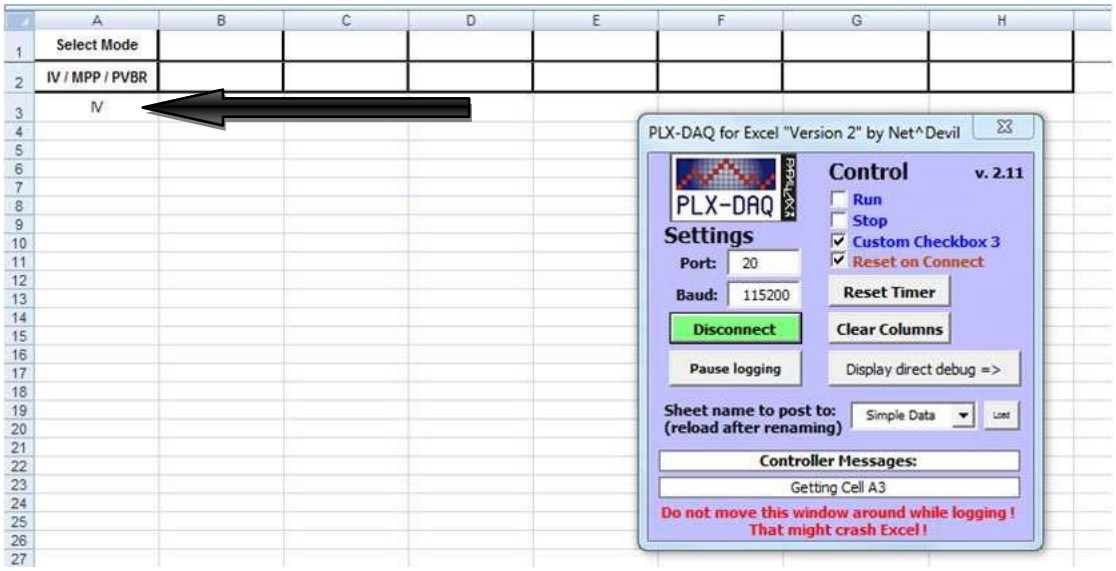
- Then select "enable this content"



- The program menu opens and we configure the port (Port) where the IV - MPPT Charger Regulator are located and the Baud Rate at 115200, then we press the Connect button



- If the connection is made correctly, the program waits for the Mode to be selected, in IV Mode, MPP Mode or PVBR Mode, writing in cell A3 of Excel **IV**, **MPP** or **PVBR** selects the corresponding Mode



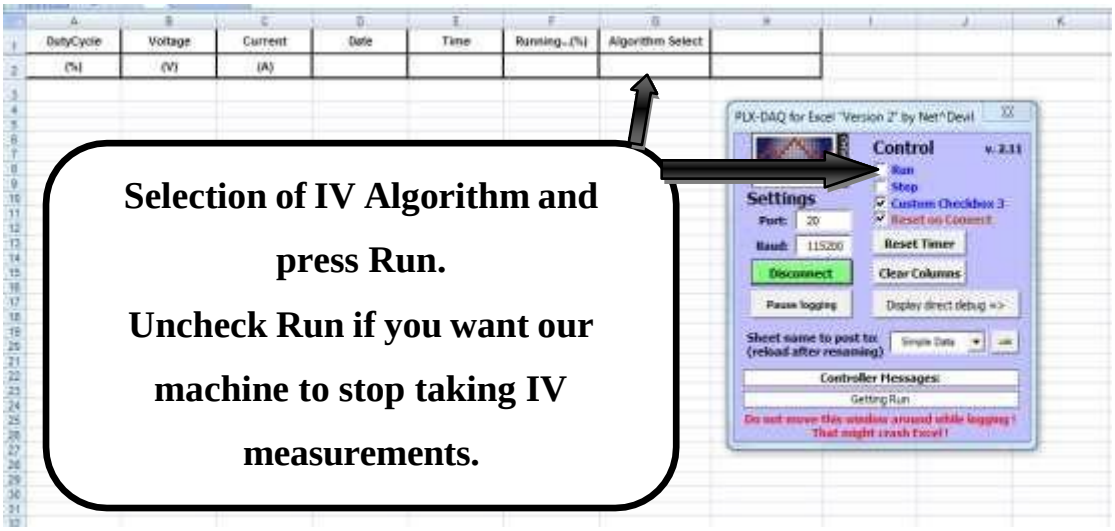


Image 105. IV Mode

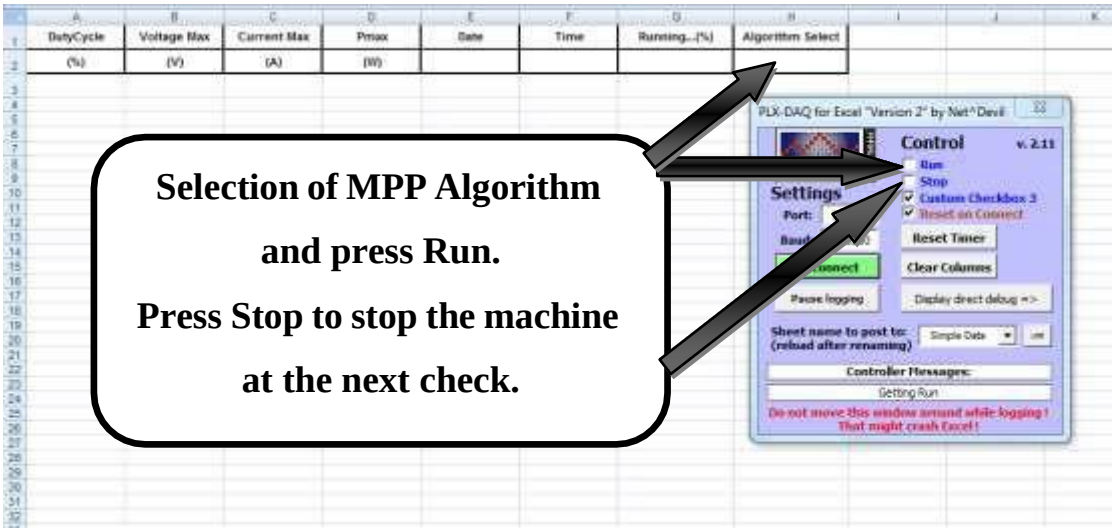


Image 106. MPP Mode

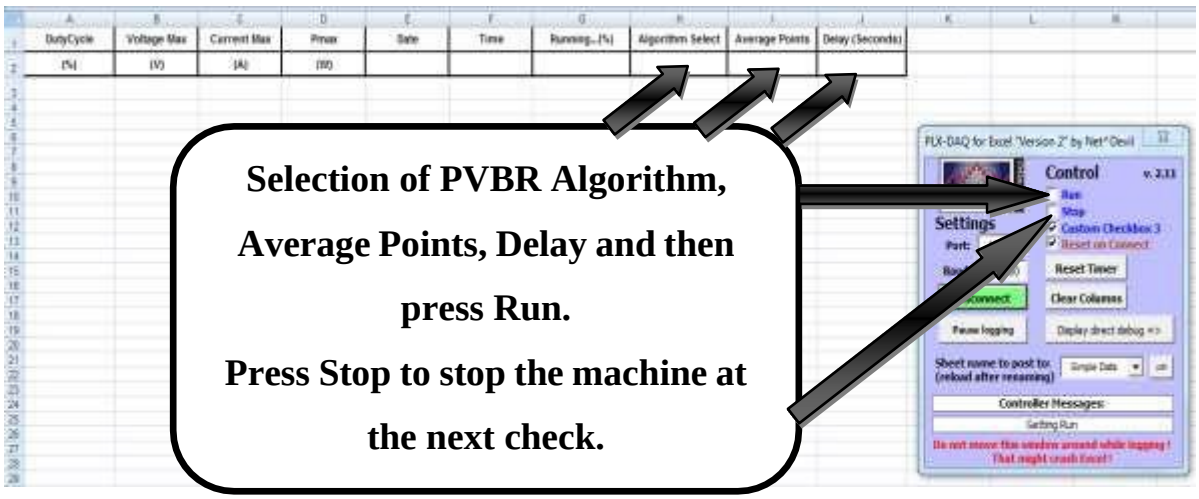


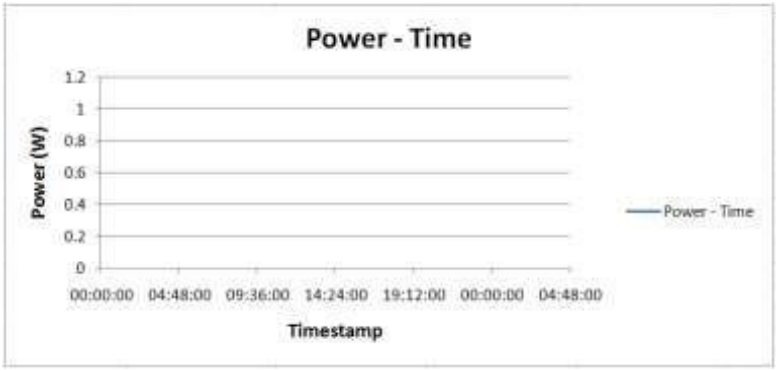
Image 107. PVBR Mode

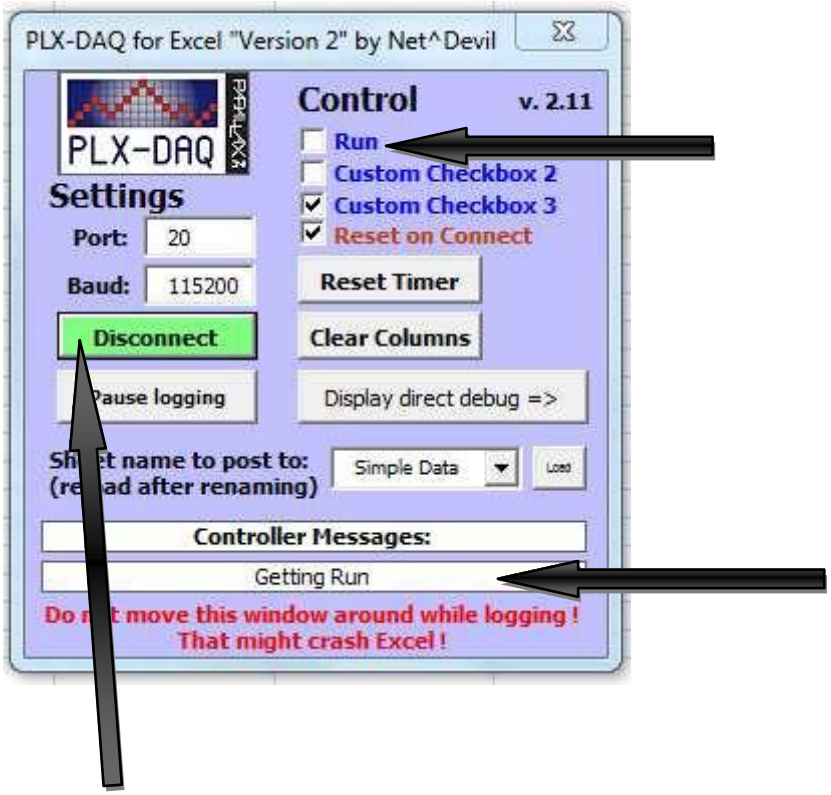
- By pressing Run in IV Mode, the corresponding algorithm is selected, which we have selected and starts recording in PLX-DAQ-v2.11 and informs at a rate of 100 how much it has completed, when it reaches 100% it starts to pass values in Excel, with the last one, automatically saves to a new file named 1 and for each subsequent file you save it names 2,3,4 ....



- Also for as long as Run is clicked the program keeps running and recording curves, when we uncheck it, it finishes the measurement it takes, it saves and waits until it will be pressed again, to select IV Mode again to start getting values again.

- Also in MPP Mode, Power - Time Graph live shown in real time, follows the Image of Power-Time Graph:





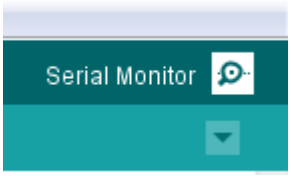
- Finally, press the Disconnect and close the log program and follow the process of disconnecting the machine as described in the instructions for connecting the machine in step 5.

5.3 Instructions for using the Serial Monitor of Microcontroller

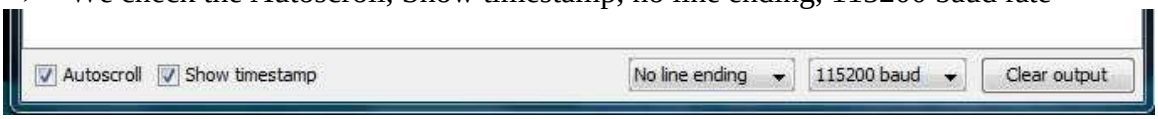
For MPPT algorithms record of electrical characteristics of the photovoltaic, we can use the Serial Monitor of our microcontroller.

Steps:

- First we open the Serial Monitor from this button



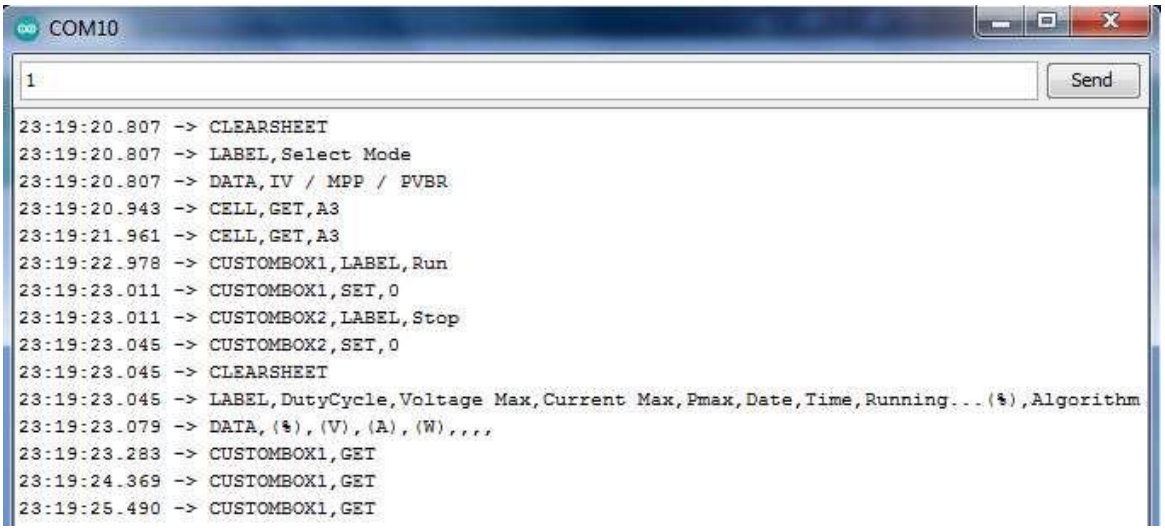
- We check the Autoscroll, Show timestamp, no line ending, 115200 baud rate



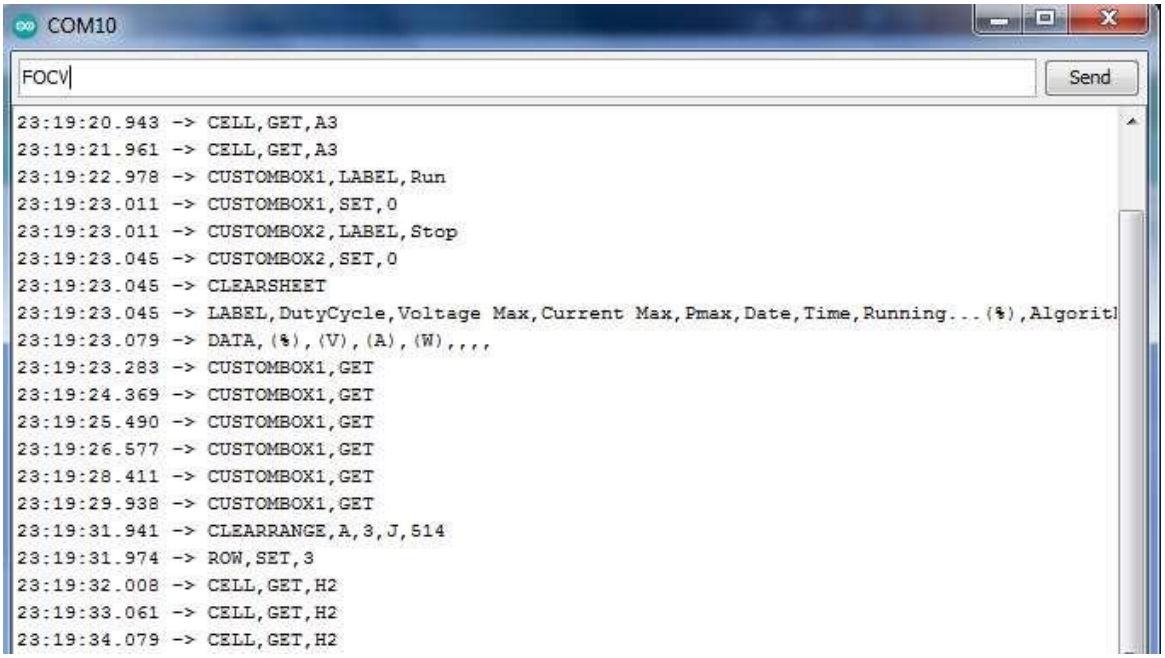
- Then write the "MPP" at Serial Port and send it (press Enter or Send)



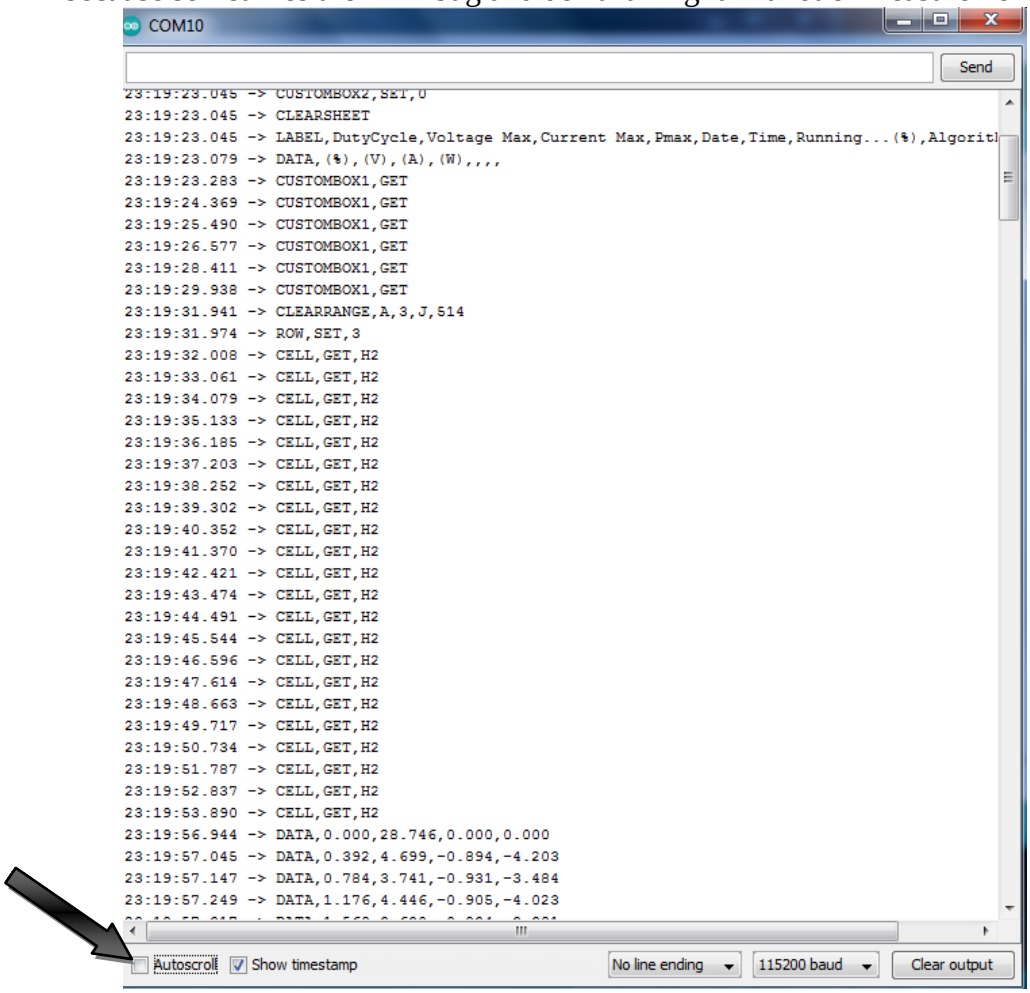
- When we see the message "CUSTOMBOX1,GET", we write "1" at Serial Port and send it maybe we need to send it 3 times, because in the code there is counter check of 3 TRUE to start the algorithm selection or in PLX-DAQ-v2.11 datalogger is the **RUN** box



- We continue with MPPT algorithm selection, when we see the message "CELL, GET, H2" we write the algorithm name and press Enter, for example FOCV



- Finally the algorithm start and run continuously without the choice of stopping it, the Serial Monitor choice is better for MPPT algorithms than PLX-DAQ-v2.11 datalogger because sometimes the PLX bug and don't run right in a lot of measurements



- In the end we can uncheck the Autoscroll and press CTRL+A to select all data then CTRL+C to copy it, then CTRL+V at a new excel file to paste it and save it

5.4 Features of IV - MPPT Charger Regulator

IV - MPPT Charger Regulator Characteristics	
Max Voltage	~60 V
Max Current	3 A
Sampling Time at 50 and 200 AVG Points	5 Seconds , 15 Seconds
Curve Points	255
Metric System - Voltage Bias	2 Separate Sources of 12 V
Metric System - Current Dissipation	~330 mA (Fans and Metric System) ~35 mA (Isolation Metric System)
IV Algorithms	Reverse Exhaustive Search (RES) Forward Exhaustive Search (FES) Reverse Forward Exhaustive Search (RFES) Forward Reverse Exhaustive Search (FRES)
MPPT Algorithms	Maximum Power Quantumized Area Search v1 (MPQAS1) Maximum Power Quantumized Area Search v2 (MPQAS2) Fractional Open Circuit Voltage (FOCV) Fractional Short Circuit Current (FSCC) Incremental Conductance (IC) Hill Climbing Perturb and Observe (HCPO) Hill Climbing (HC)
Photovoltaics Behaviour Reading Algorithms	Pmax Open Circuit Intervals (POCI) Pmax Short Circuit Intervals (PSCI)

6. Experimental Measurements of IV-MPPT Charger Regulator

The innovative Solar Farm facilities designed, so we can take IV, MPP, PVBR, etc. outdoor measurements for better understanding of different photovoltaic technologies and the certification of them. In this chapter we see the experimental measurements of IV-MPPT Charger Regulator and observations of them but first we'll see the realization of Solar Farm.

6.1 Solar Farm Realization

The Solar Farm consists of aluminum bases for photovoltaics at 30º which connected with 6mm^2 cables into devices, weather station CR1000X Campbell Scientific©, direct system MPPT inverter SMA Sunny Boy© which converts the direct current of the PV array to grid compliant alternating current, indirect system SMA inverter and grid charger Sunny Island© that connects with batteries and with Sunny boy, also Victron Energy Phoenix inverter and MPPT blue solar 100 | 30 charger©, and more devices for IV curves like PVBlocks, HT IV analyzer, Keysight B290ZA, Keysight for Nyquist curves etc., all devices have connection to internet through wifi and ethernet. Also has the **handmade** IV-MPPT Charger Regulator. It follows Top View of Solar Farm facilities and Monolinear Diagrams of devices connections.

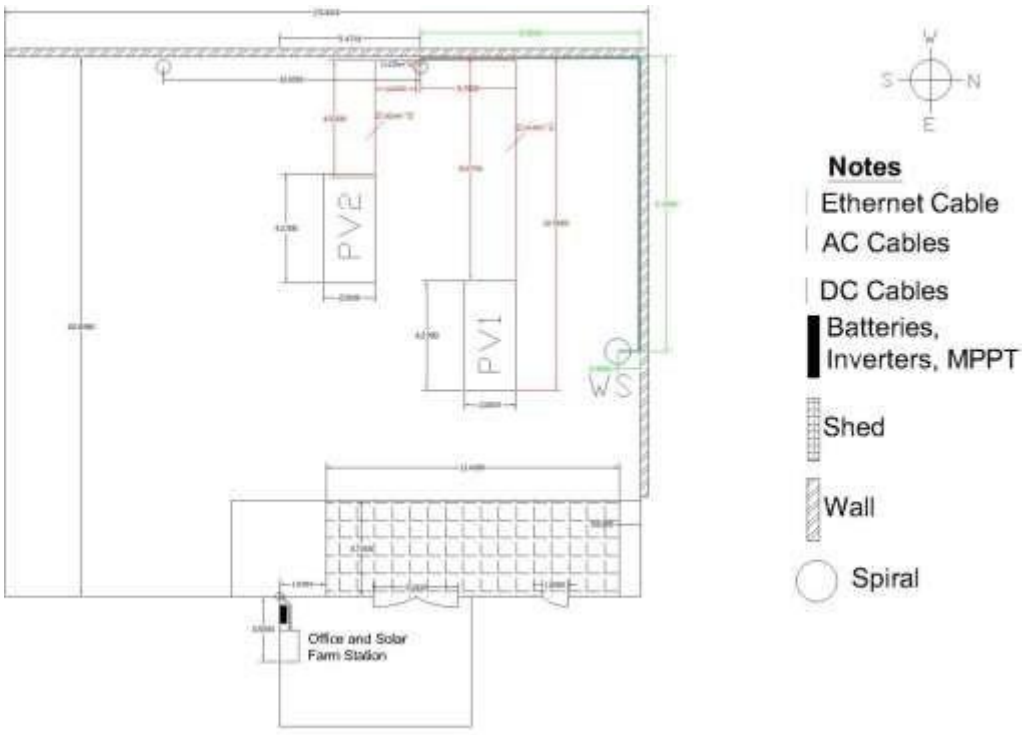


Image 108. Solar Farm Top View

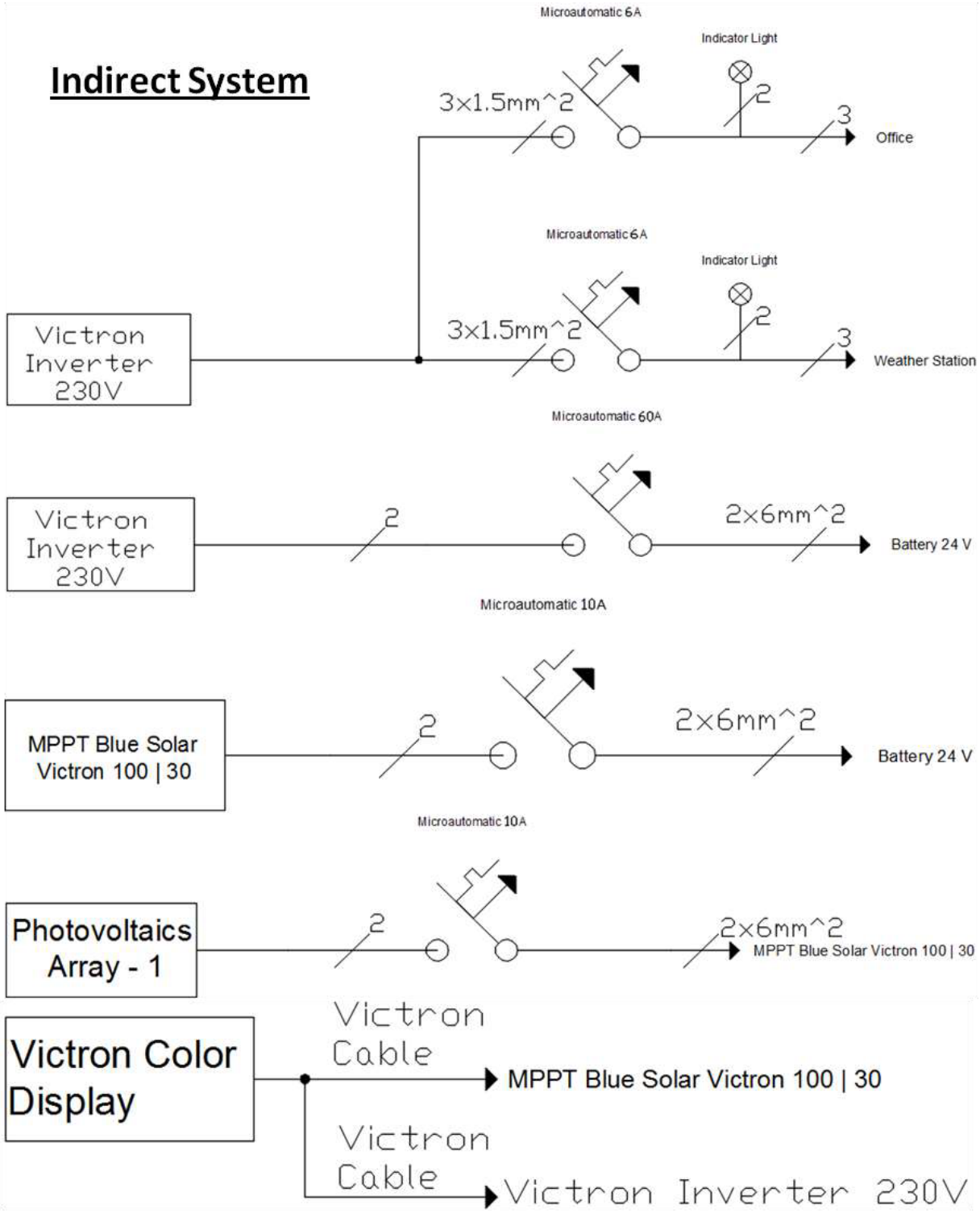


Image 109. Monolinear Diagram of Indirect System

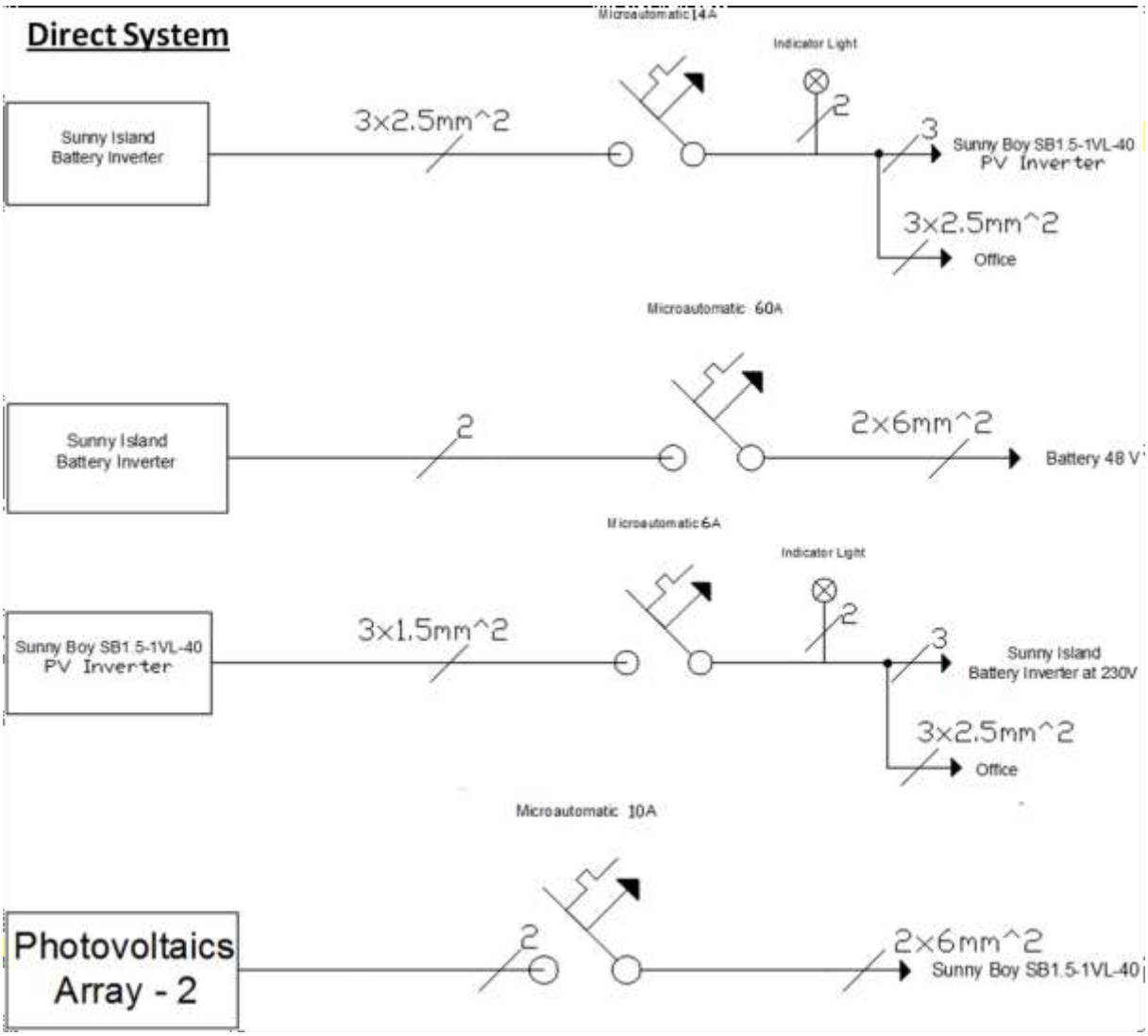


Image 110. Monolinear Diagram of Direct System

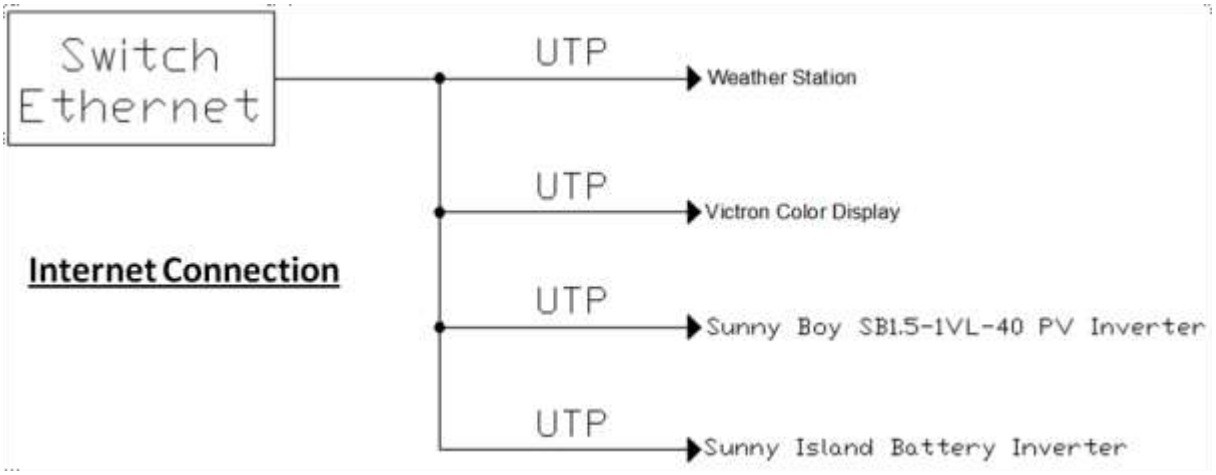


Image 111. Monolinear Diagram of Internet Connection

It follows photos of aluminum bases and its materials.



Image 112. Materials of aluminum bases

At Image 112. shown from left to right, aluminum bars to create verticals triangles and horizontal connections, clips for edges and middle points to keep photovoltaics stable on the bases and the bases for screws that we can change the width of borders, see Image 113. the aluminum bases completed. At Image 114. we see the GRAPES at Landscape setup.



Image 113. Aluminum Bases with 30º inclination, also cement at base to keep them stable



Image 114. Solar Farm with different photovoltaic technologies, GRAPES at Right



Image 115. Commercial Devices of Solar Farm, ***a)*** *Keysight B290ZA©,* ***b)*** *Victron Energy Phoenix Inverter©,* ***c)*** *SMA Sunny Island©,* ***d)*** *Sunlight Batteries©,* ***e)*** *SMA Sunny Boy©,* ***f)*** *HT IV Analyzer©,* ***g)*** *PVBlocks©,* ***h)*** *Victron Energy Blue Solar Charger©,* ***i)*** *CR1000X Campbell Scientific©*

In experiments design, for the measurements used as input of IV-MPPT Charger Regulator, the different technologies of photovoltaics and the batteries as output of the device,

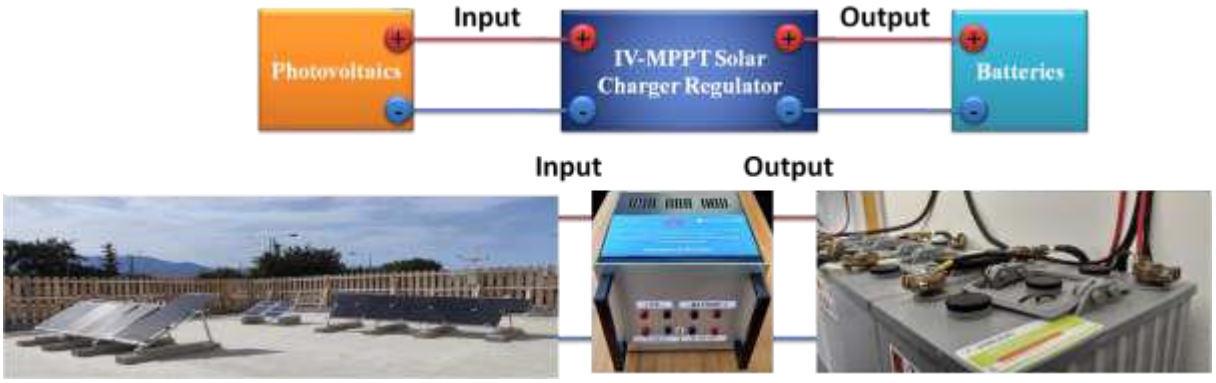


Image 116.General experimental setup for measurements

also the weather station used for weather data such as solar irradiance (Pyranometer), ambient temperature, panel temperature (Thermocouples), humidity, atmospheric pressure, wind speed and wind direction. The other commercial devices also used for comparison and collaboration with handmade device.

6.2 Current (I) - Voltage (V) Measurements and Experiments

The IV-MPPT Charger Regulator can run four IV algorithms as shown at chapter 4. the RES, FES, RFES, FRES, first we'll see a timetable of algorithms and IV Curves for time check on different Average Points and why choosed to calibrate our machine at 200 Average Points. Also we'll see the Hysteresis effect at GRAPES photovoltaics.

6.2.1 Time Table of IV Algorithms at different Average Points

Average Points	Reverse Exhaustive Search (RES)	Forward Exhaustive Search (FES)	Reverse Forward Exhaustive Search (RFES)	Forward Reverse Exhaustive Search (FRES)
	Time (Seconds)	Time (Seconds)	Time (Seconds)	Time (Seconds)
10	2.6	2.65	5.22	5.27
50	5.23	5.33	10.01	10.11
100	8.48	8.65	16.8	16.96
150	11.61	11.84	23.29	23.52
200	14.91	15.20	29.86	30.15
250	18.16	18.51	36.22	36.57
300	21.22	21.63	42.74	43.16
1000	67.17	68.48	134.63	135.94
5000	335	335.29	670	670.29
RES and FES: Accepting Rows at Excel and Autosave Time (Seconds)		7.69	RFES and FRES: Accepting Rows at Excel and Autosave Time (Seconds)	16

Follows Solo RES IV Curves and RFES IV Curves on different average points at GRAPES#9

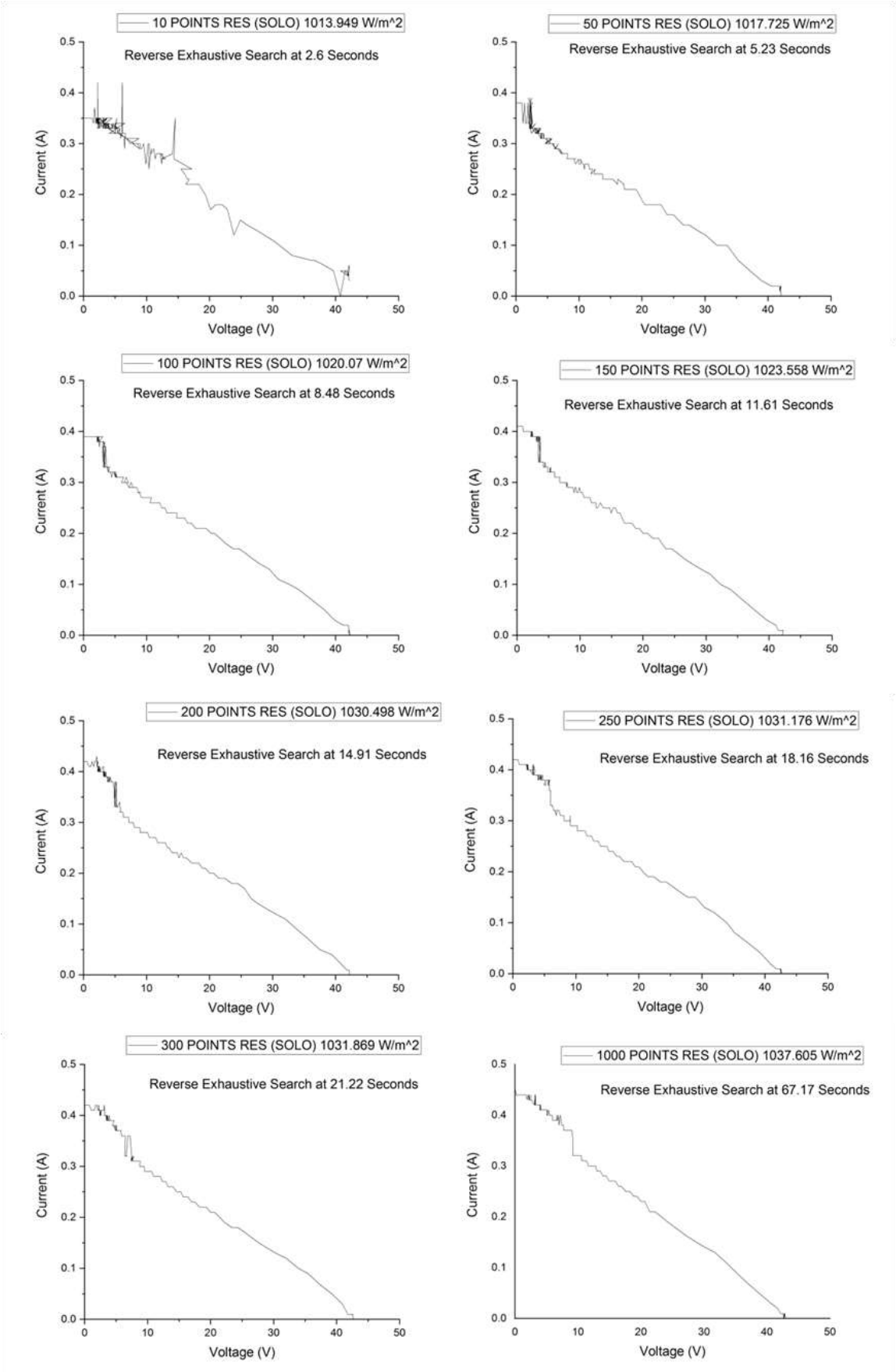


Image 117. Solo RES IV Curves in different Average Points, at GRAPES #9 (07/06/2021)

6.2.2 Hysteresis Effect and S-Shape IV Curves

As shown at Image 117. and 118. as the average point raise the better the curve but the sampling time raise too, in real time conditions needed to take the IV curve as fast as possible because having distortions from the environment, the measurement may be is wrong.

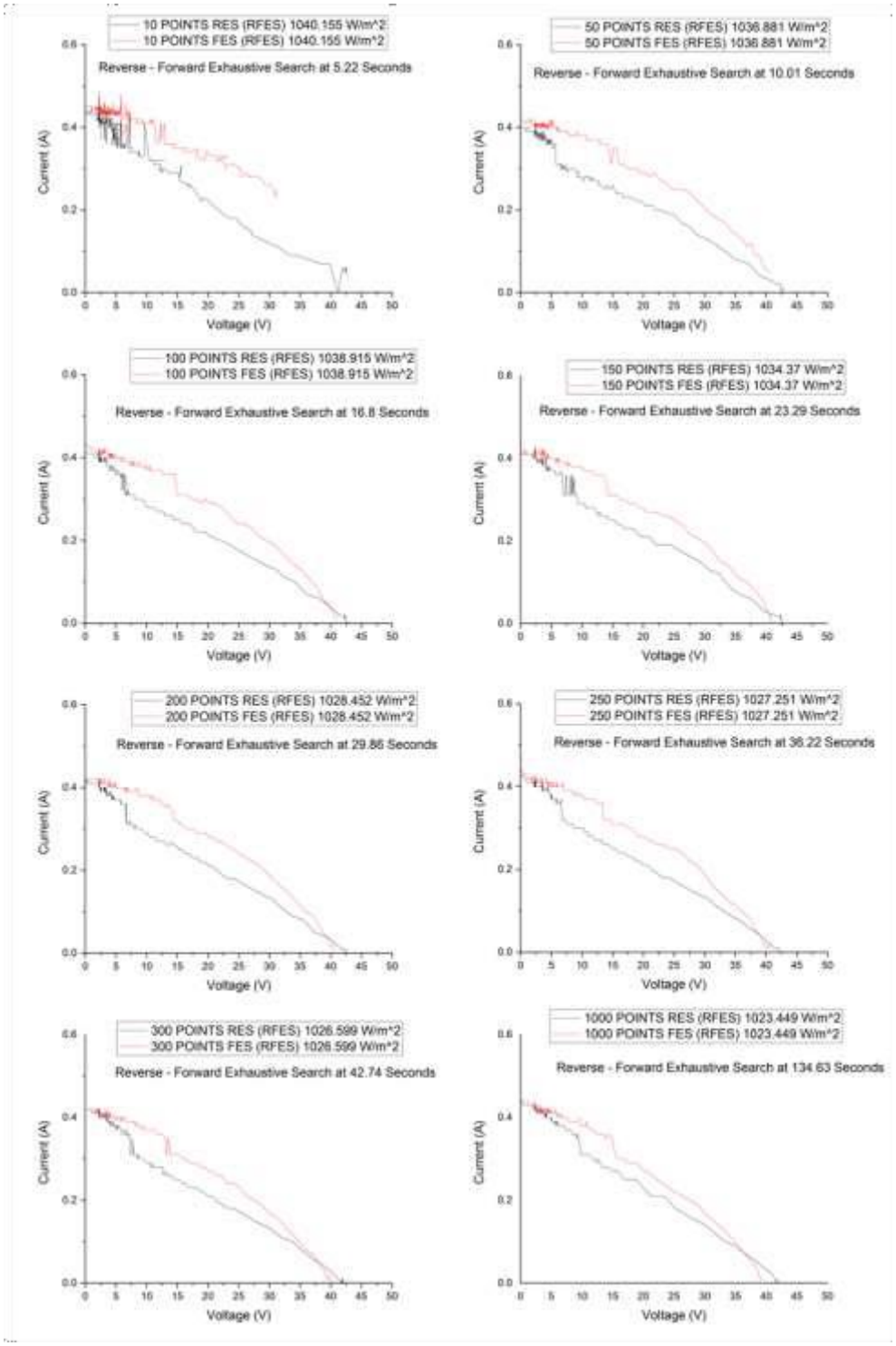


Image 118. S-Shape Check, RFES IV Curves in different Average Points, at GRAPES #9

Since the hysteresis effect is very common in fast IV scans on emerging PV devices particularly on perovskites **[57]**, the GRAPES IV Curves must be slow as possible so the internal ions manage to stabilize, the internal electronic ionic effects produces hysteresis in the Current Voltage curves (regular hysteresis is capacitive, and inverted hysteresis is inductive). and a dependence of the temporal response on the conditions of the previous stimulus applied to the photovoltaics**[56]**. Observed at Image 118. that the measurement at **200 average point**s has enough time to take a right curves with stabilization of S-Shape of Hysteresis effect and small sampling time ~15 seconds per curve (see Image 117. solo curve time at 200 average point) to be able to avoid the most weather distortions.

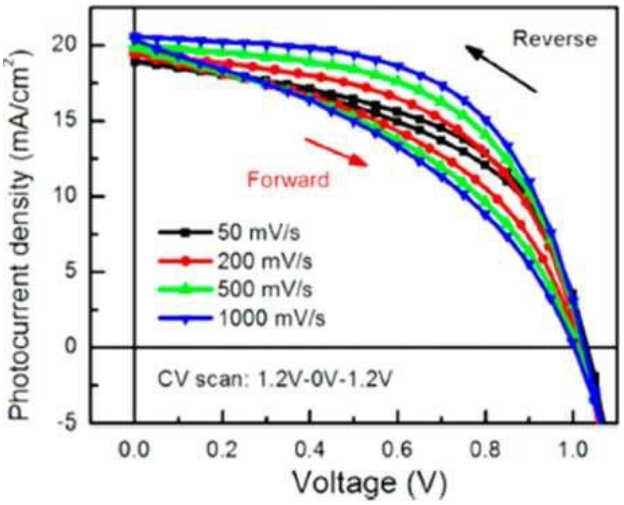


Image 119. J−V response for PSCs with different CV scan rates, Copyright 2015 American Chemical Society© **[56]**

As shown in Image 119. the faster the scan rate the bigger the hysteresis effect, in our case the scan rate is the average points that slow down the scan process.

6.2.3 Hysteresis at different IV Algorithms

After choosed, the 200 average points, must do a comparison to four IV algorithms for hysteresis effect on GRAPES photovoltaics. Hysteresis is the deviation of Pmax at the two IV Curves RES and FES.

The calculation of hysteresis become with the following equations:

- If the Pmax at RES scan is bigger: $Hysteresis(\%) = \frac{Pmax_{RES} - Pmax_{FES}}{Pmax_{RES}} \times 100$
- If the Pmax at FES scan is bigger: $Hysteresis(\%) = \frac{Pmax_{FES} - Pmax_{RES}}{Pmax_{FES}} \times 100$

It follows hysteresis histograms of the four different IV algorithms, solo RES and solo FES used for the calculation SOLO, then RFES and FRES algorithms.

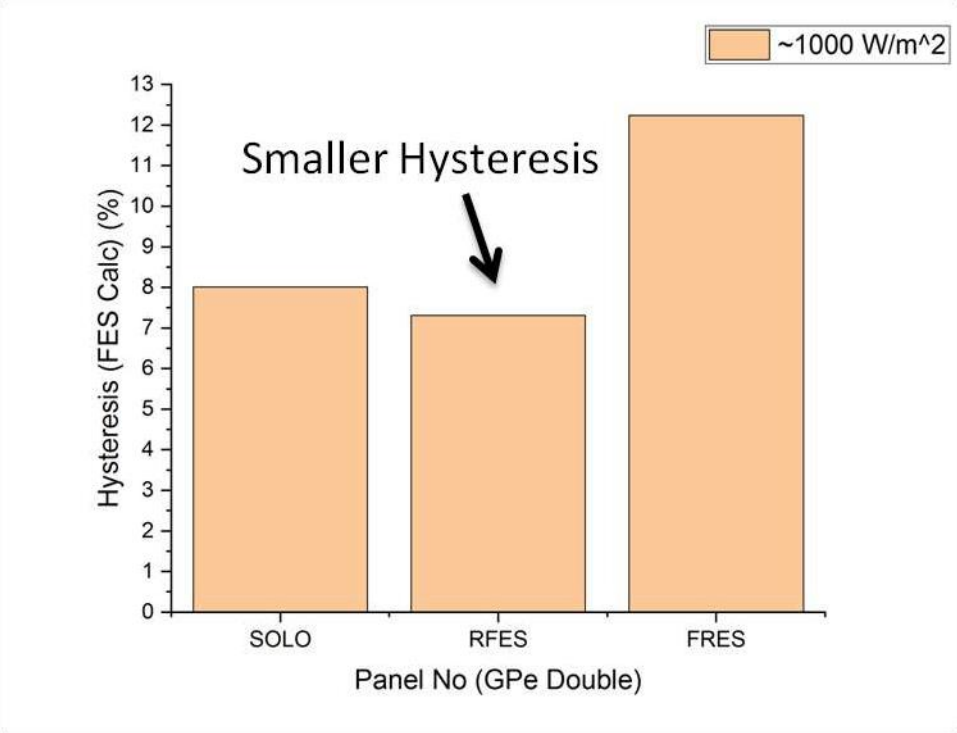


Image 120. Hysteresis Histogram at the different IV Algorithms, Pmax at FES is bigger, GRAPES Double Module (09/06/2021)

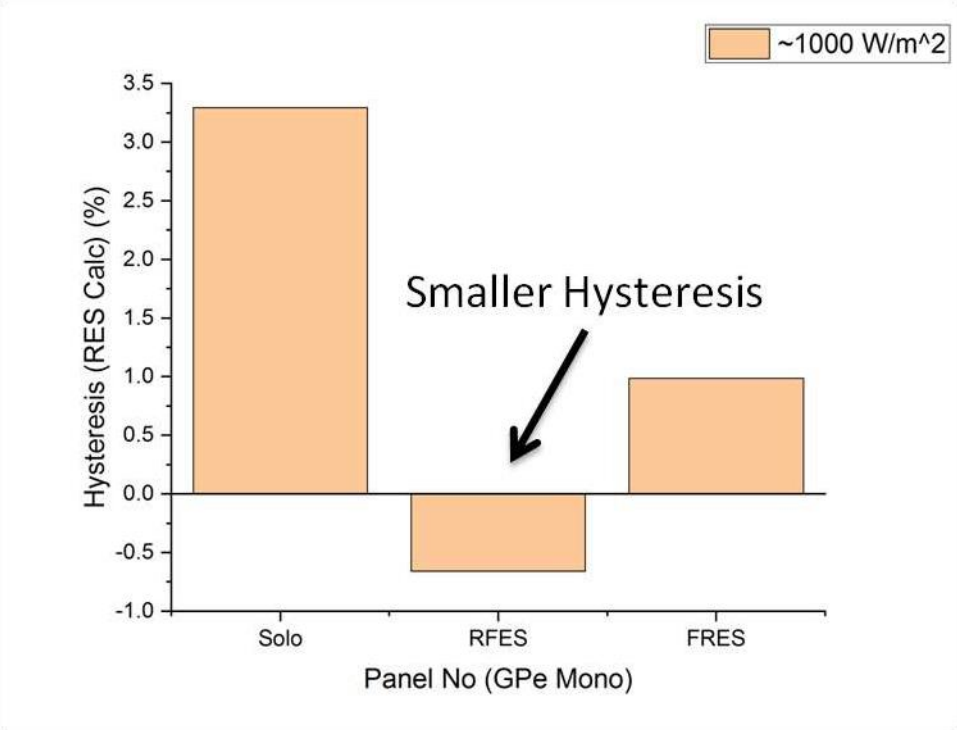


Image 121. Hysteresis Histogram at the different IV Algorithms, Pmax at RES is bigger except the RFES is Pmax at FES is bigger,but the calculation become with the same equation at all algorithms used Pmax at RES bigger equation, GRAPES Mono Module (09/06/2021)

From Images 120. and 121., observed that RFES algorithm for GRAPES Photovoltaic has the less hysteresis effect than the SOLO and FRES. Also known from chapter 4. that the RFES algorithm is less stressful in photovoltaics because do short circuit to the photovoltaics only once time in contradiction to FRES that do two times short circuit (one at start to begin the algorithm from short circuit to open circuit and then finish on short circuit). Also observed that at GRAPES photovoltaics numbers 1-9 FES scan always have the bigger Pmax and that's happened because it start at short circuit and the electrons accumulate in the interlayers, of the photovoltaics, behaviour like charging a capacitor , then when released the photovoltaic having more electron flow at circuit, that means more current and respectively more power output.

6.2.4 Hysteresis at different Average Points

At Image 119. shown that the faster the scan rate the bigger the hysteresis effect, in Image 122., observed the same thing at 10 average points (Faster Scan) having the bigger Hysteresis at 33.64% and at 5000 points (Slower Scan) only 5.2%.

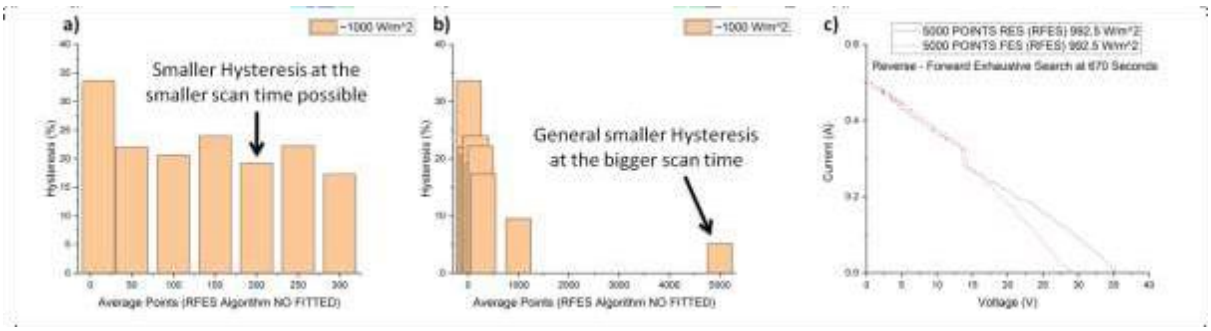


Image 122. Hysteresis at different average points, ***a)*** *Average Points from 10 to 300,* ***b)*** *Average Points from 10 to 5000* ***c)*** *S-Shape Check, RFES IV Curve at 5000 Average Points, at GRAPES#7 (17/06/2021)*

Observed at Image 122.a. that the Hysteresis at 200 average points is smaller, at the smaller scan time possible, the percentage is 19.22% at 29.86 seconds RFES scan (see time table chapter 6.2.1). So this is another reason to set the IV-MPPT Charger regulator at 200 average point.

6.2.5 Hysteresis at different Photovoltaic Technologies

Every photovoltaic technologies have or not their own hysteresis effect because is depended on fabrication materials they used.

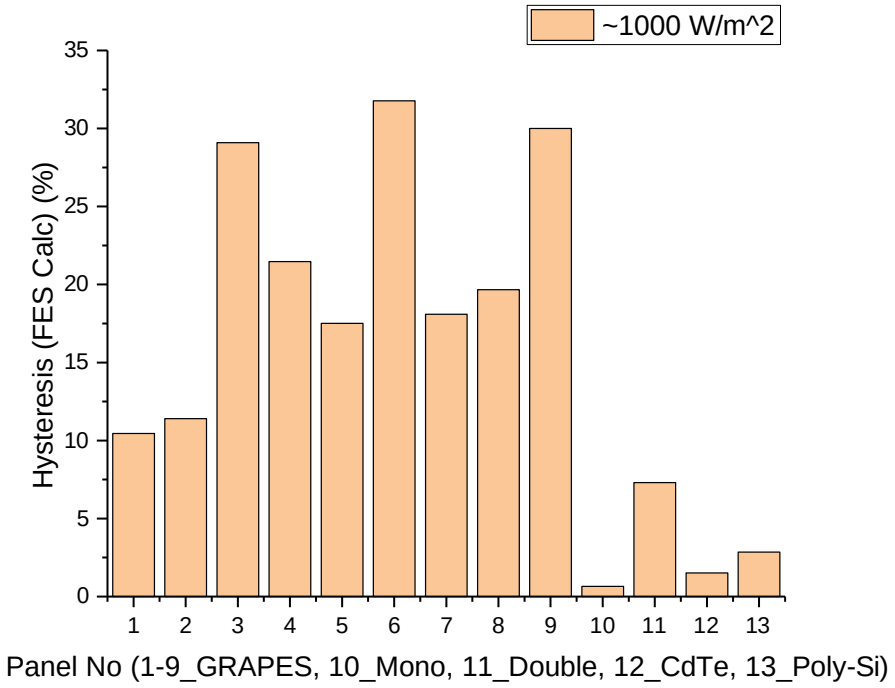


Image 123. Hysteresis at different photovoltaic technologies

As shown at Image 123. the GRAPES technologies has bigger hysteresis in comparison to CdTe and Polycrystalline Si that have almost zero hysteresis, this happened due to degraded perovskite material that is unstable and has dielectric behaviour, also observed that the mono module is the only one at GRAPES technologies that has almost zero hysteresis, maybe this happened because all other GRAPES has more modules connected in series and parallel connections. The mono module and double module GRAPES are less degraded than all other GRAPES and as observed, the hysteresis is less than all other GRAPES photovoltaics. So hysteresis maybe is measure of degradation of GRAPES.

6.2.6 RFES and FRES Pauses Hysteresis Experiment

Like PVBR Algorithms (Sun exposure degradation and Supply load degradation), wanted to test the behaviour of GRAPES photovoltaics at different Pauses at short circuit and open circuit to observe changes in hysteresis. Used RFES and FRES algorithms. For short circuit used RFES algorithm in different delays, it start scan from open circuit to short circuit pauses at short circuit for different delays then scan back to open circuit. For open circuit used FRES algorithm in different delays, it start from short circuit to open circuit pauses at open circuit for diffent delays then scan back to short circuit. It follows IV S-Shape RFES and FRES Curves.

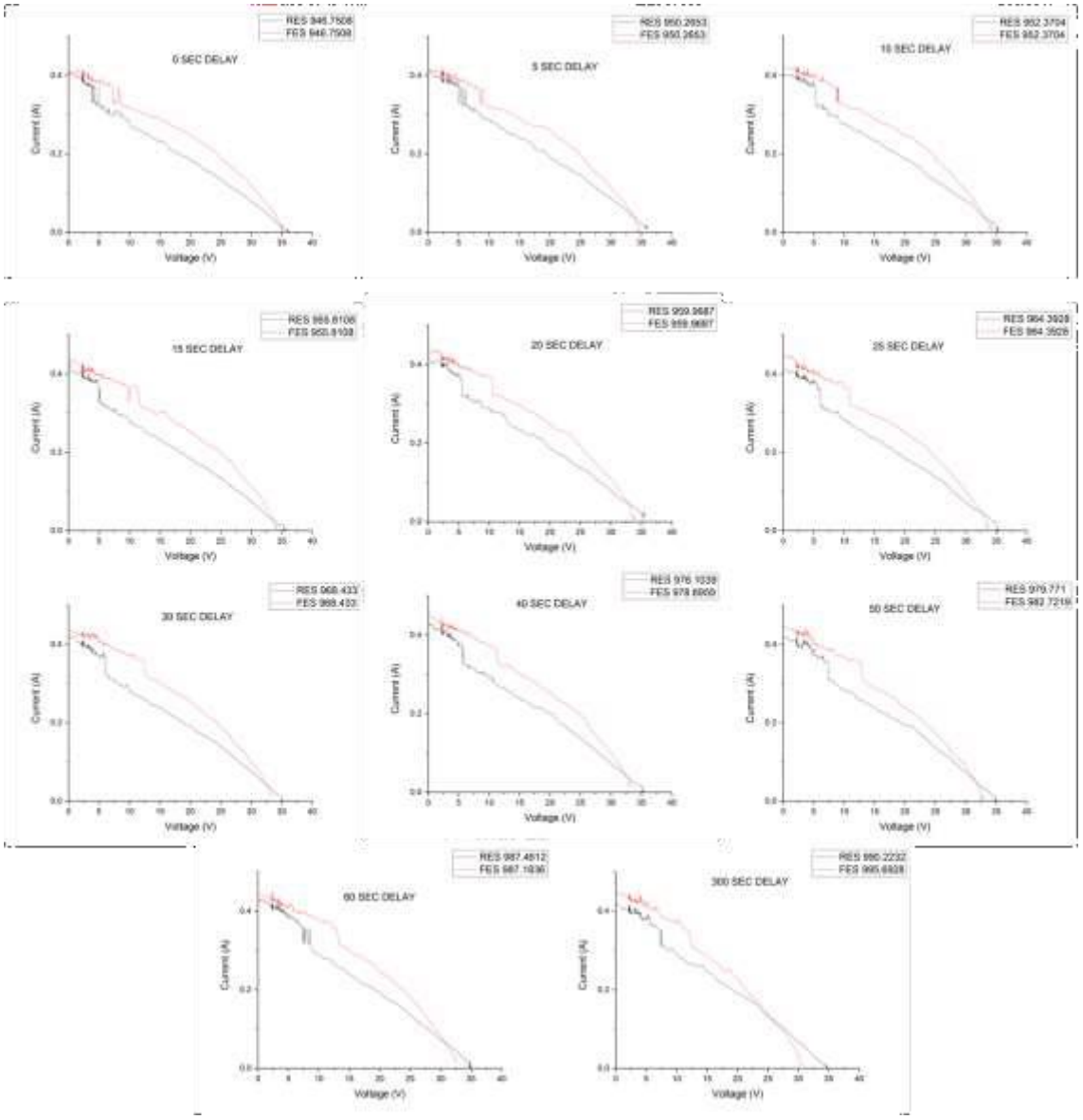


Image 124. IV S-Shape Curves RFES Algorithm at different delay pause times at Short Circuit, GRAPES#8 (12/07/2021)

At Image 124. observed that with raise at short circuit (S.C.) pauses, have raised current and decreased voltage at FES scan, that means change in the resistance of the photovoltaic, it decreased too from Ohm's law $R = \frac{V}{I}$, proved here that supply load and sun exposure degrade the shunt resistance of the photovoltaic because observed that voltage at open circuit is decreased (see the changes of shunt resistance at **[58]** and series resistance at **[59]**). Shunt resistance R_{SH} accounts for current leakage as a result of trap states, pinholes and edge effects. In ideal case R_{SH} should be infinite**[20]**. Series resistance R_s accounts for bulk and interface resistances of each layer of the cell and contacts. It can be calculated by the slope of the J-V curve around V_{oc} and under ideal circumstances should be zero **[20]**.

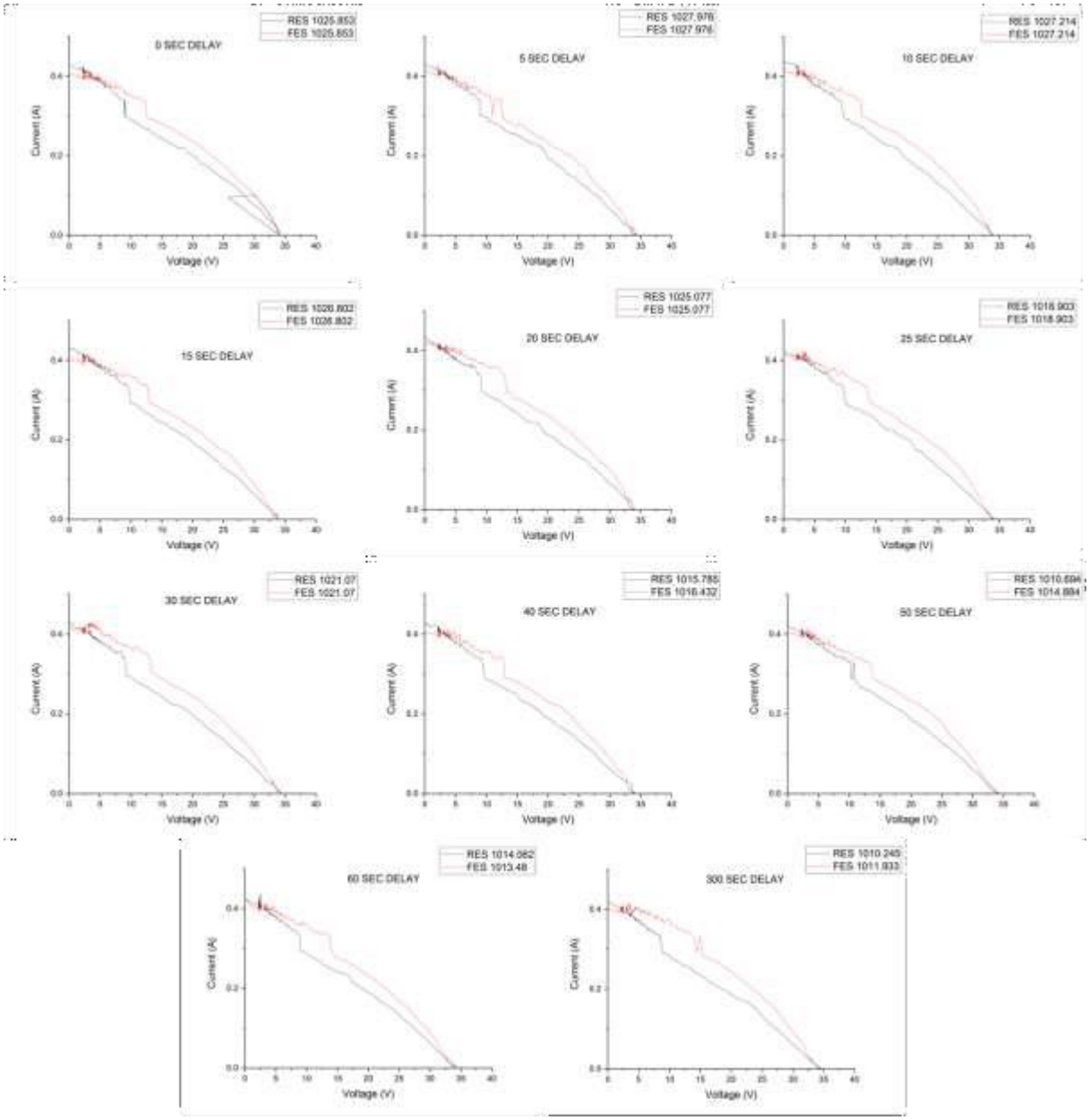


Image 125. IV S-Shape Curves FRES Algorithm at different delay pause times at Open Circuit, GRAPES#8 (12/07/2021)

At Image 125. observed that with raise at open circuit (O.C.) pauses, have slightly raised current and same voltage at RES scan, that means the rest time let photovoltaic regenerate slightly, but if compared to the RES curve from image 124. at 300 sec delay (First measurement without delay) which the solar irradiance is 990 W/m^2 (12:35) and the FES from Image 125. at 300 sec delay (First measurement without delay) with solar irradiance 1011 W/m^2 (14:12), will shown that the exposure at sun degrade the current of the photovoltaic, at 990 W/m^2 and 51.72 ºC, having bigger current that 1011 W/m^2 and 50.34 ºC that proves the degradation of the photovoltaic.

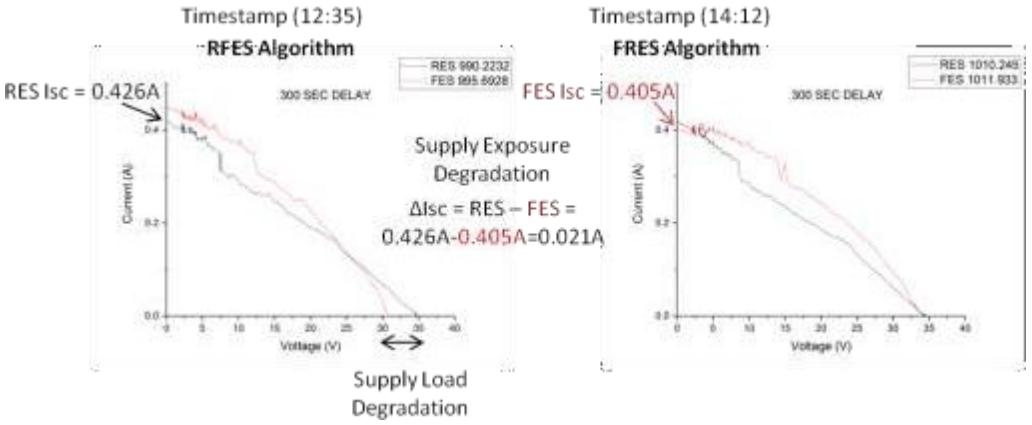


Image 126. Short Circuit Current comparison of the starting curves, RES at RFES and FES at FRES, at ~1000 W/m^2, with 97 minutes apart from each other and colder for 1.38^{o}C

It follow graphs for hysteresis change based on IV S-Shape Curves from Image 124. and 125.

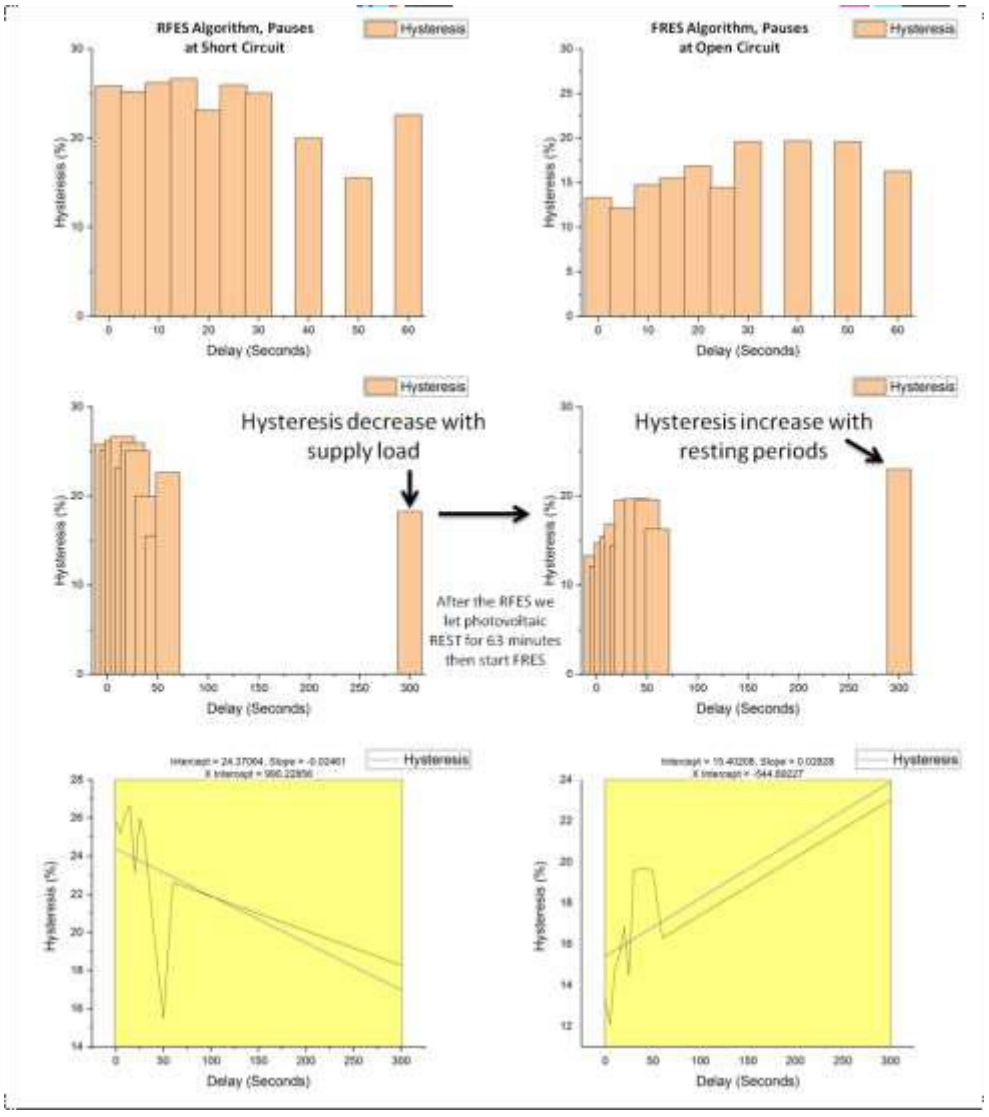


Image 127. Hysteresis changes with pauses at S.C. and O.C.

RFES Algorithm, Pauses at Short Circuit

Pmax RES (W)	Pmax FES (W)	Hysteresis FES (%)	Hysteresis RES (%)	Timestamp Date - Time	Solar Irradiance (W/m²)	Patm mb	RH_Avg (%)	WS (m/s)	WD deg	Tair_Avg (°C)	Temp_TC_1 (°C)	Panel No GPe	Delay (Seconds)
3.718786	5.01312	25.81893112	-34.80528323	12/7/21 12:04	946.7508	1003.449	43.294	3.567265	332.8577	29.881	50.23577	8	0
3.93519	5.260464	25.19310084	-33.67750985	12/7/21 12:06	950.2853	1003.454	42.853	3.652855	327.6266	29.98	50.27841	8	5
3.787088	5.1336	26.22939068	-35.55510962	12/7/21 12:08	952.3704	1003.427	42.729	3.766402	336.2512	29.91	49.95913	8	10
3.720504	5.072494	26.65335829	-36.33889387	12/7/21 12:11	955.8108	1003.482	42.871	4.239147	320.7619	29.795	49.22883	8	15
3.963848	5.157098	23.13805167	-30.10338945	12/7/21 12:14	959.9687	1003.415	43.109	3.648576	35.44362	29.825	49.37024	8	20
3.73681	5.046048	25.94578012	-35.03619397	12/7/21 12:17	964.3928	1003.359	42.853	3.150036	20.584	29.854	50.05965	8	25
3.83538	5.118204	25.06394821	-33.44713806	12/7/21 12:20	968.433	1003.42	43.472	2.728483	355.8818	30.167	52.22691	8	30
4.068108	5.081884	19.98031426	-24.9912486	12/7/21 12:24	976.1039	1003.383	45.23	1.709919	44.9121	30.153	53.10353	8	40
				12/7/21 12:25	978.8959	1003.412	43.892	2.908222	327.8045	30.308	52.78794	8	
4.05061	4.794192	15.51005884	-18.3572844	12/7/21 12:27	979.77	1003.414	43.527	3.18211	332.5268	30.159	51.27501	8	50
				12/7/21 12:28	982.7219	1003.415	43.965	2.184987	312.399	30.159	52.68576	8	
3.876795	5.00942	22.60990294	-29.21548889	12/7/21 12:31	987.4613	1003.359	42.049	2.7698	9.991325	30.209	51.67085	8	60
				12/7/21 12:32	987.1838	1003.411	43.228	3.665698	339.0939	30.068	52.31275	8	
3.85309	4.714668	18.27505139	-22.36185941	12/7/21 12:35	990.2232	1003.442	44.681	2.565862	8.899843	30.223	51.71419	8	300
				12/7/21 12:40	995.6928	1003.434	45.217	2.916781	19.97581	30.022	53.04912	8	

FRES Algorithm, Pauses at Open Circuit

Pmax RES (W)	Pmax FES (W)	Hysteresis FES (%)	Hysteresis RES (%)	Timestamp Date - Time	Solar Irradiance (W/m²)	Patm mb	RH_Avg (%)	WS (m/s)	WD deg	Tair_Avg (°C)	Temp_TC_1 (°C)	Panel No GPe	Delay (Seconds)
4.118952	4.75136	13.31004178	-15.35361422	12/7/21 13:45	1025.853	1003.406	44.132	3.048887	354.2544	30.351	52.67034	8	0
4.185264	4.761672	12.1051597	-13.77232117	12/7/21 13:48	1027.976	1003.328	43.096	4.187795	273.5557	30.607	52.34144	8	5
4.067484	4.770558	14.73777281	-17.28523087	12/7/21 13:50	1027.214	1003.391	43.274	3.27198	326.259	30.69	52.9369	8	10
3.957525	4.682424	15.48127636	-18.31697841	12/7/21 13:52	1026.802	1003.298	42.981	2.58726	351.6082	30.874	53.67954	8	15
3.971134	4.778174	16.84695742	-20.26018158	12/7/21 13:54	1025.077	1003.341	42.207	2.531626	301.251	31.16	53.4403	8	20
4.082684	4.772678	14.4570947	-16.90840179	12/7/21 13:57	1018.901	1003.351	40.838	2.782719	7.615934	31.001	53.9367	8	25
4.00114	4.976595	19.60085155	-24.37942686	12/7/21 14:00	1021.07	1003.255	40.422	2.574421	79.93717	31.513	53.794	8	30
3.867516	4.8147	19.6717122	-24.49075841	12/7/21 14:03	1016.432	1003.296	42.053	3.455998	292.5764	31.074	53.66513	8	40
				12/7/21 14:04	1015.785	1003.299	41.559	2.904378	6.42744	31.315	53.89648	8	
3.868268	4.811356	19.59962222	-24.37752503	12/7/21 14:06	1014.884	1003.383	40.524	3.898918	316.4258	31.259	53.66155	8	50
				12/7/21 14:07	1010.694	1003.322	41.496	4.102202	303.8809	30.917	55.167	8	
3.895122	4.653155	16.29073177	-19.46108492	12/7/21 14:09	1011.48	1003.359	43.294	3.888228	333.3161	30.532	52.86019	8	60
				12/7/21 14:10	1014.062	1003.336	42.235	3.818619	350.9184	30.807	52.33461	8	
3.807564	4.945802	23.01422499	-29.89412653	12/7/21 14:12	1011.933	1003.373	42.29	3.142595	30.33714	30.508	52.56427	8	300
				12/7/21 14:17	1010.249	1003.328	41.791	3.693375	334.7573	30.818	51.89405	8	

Image 128. Hysteresis Calculation Tables of RFES and FRES Algorithm Pauses Experiment

6.2.7 Electrical Characterization of different Photovoltaic Technologies

For electrical characterization of the GRAPES photovoltaics, light soaked it first about 45 minutes to 1 hour, upon exceeding a threshold of continuous light exposure the performance gradually decreases for most GRAPES panels this is about 45 minutes to 1 hour (see Image 129.), for continuous illumination at 1000 W/m^2 s, due to the formation of light activated meta stable trap states associated to spatially localized small polarons deep within the band gap, while contribution from intrinsic defects, ion migration, or ferroelectric domains cannot be excluded **[60]**.

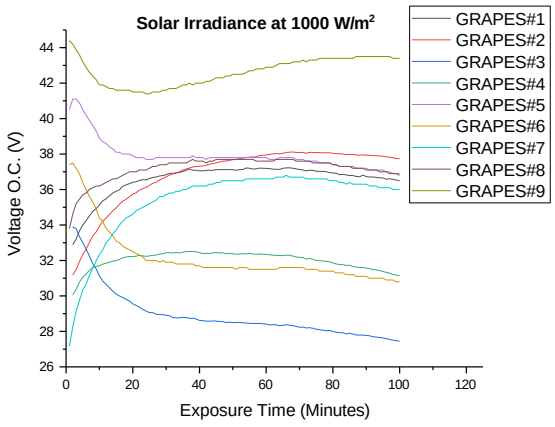


Image 129. Light Soaking of GRAPES Photovoltaics (27/08/2021)

Also for all different technologies photovoltaics, have been made two tables of electrical characterization, for FES and RES Scans respectively. For the measurements used the RFES algorithm with 200 average points at ~1000 W/m^{2}on IV-MPPT Charger Regulator. Following the IV and PV Curves for all different technologies photovoltaics and for better comprehension of GRAPES IV and PV Curves measurements, fitted it with polynomial fit order 2, that's why some measurements observed (at Mono Module), that Imax is bigger than Isc that isn't real of course, but for the comparison needs, used same fit at all GRAPES.

Reverse Exhaustive Search Scan

Voc	Isc	Vmax	Imax	Pmax	FF	Pin	PCE	Timestamp	Solar Irradiance	Patm	RH_Avg	WS	WD	Tair_Avg	Panel Temperature	Panel No
(V)	(A)	(V)	(A)	(W)	(%)	(W)	(%)	dom time	(W/m^2)	mb	(%)	(m/s)	deg	(°C)	(°C)	PV Technologies
10.880	0.429	15.280	0.398	5.176	23.899	326.558	0.970	17/6/21 13:03	1020.495	1010.987	61.919	1.419	270.656	25.265	57.972	GRAPES#1
34.570	0.407	17.409	0.397	5.420	24.340	326.557	1.040	17/6/21 13:43	1019.802	1010.990	59.470	2.065	326.592	25.074	56.521	GRAPES#2
24.720	0.261	12.298	0.130	1.594	24.564	328.647	0.480	17/6/21 13:33	1027.023	1010.989	60.106	2.155	7.028	25.104	56.718	GRAPES#3
28.590	0.351	13.222	0.184	2.134	21.503	325.335	0.661	17/6/21 13:46	1016.671	1010.947	61.887	1.808	78.627	24.874	57.213	GRAPES#4
38.400	0.505	15.129	0.259	4.938	26.994	327.051	1.516	17/6/21 13:37	1022.034	1010.996	60.802	1.770	334.341	25.394	58.190	GRAPES#5
29.120	0.469	14.079	0.225	3.164	23.170	326.085	0.970	17/6/21 13:45	1019.017	1010.964	61.118	2.022	290.016	25.029	56.843	GRAPES#6
38.330	0.487	16.809	0.254	4.357	23.358	327.604	1.330	17/6/21 13:41	1023.784	1011.003	58.638	1.988	6.473	25.315	57.179	GRAPES#7
35.970	0.471	16.291	0.228	4.178	24.650	327.363	1.275	17/6/21 13:39	1023.633	1010.982	60.816	2.072	320.769	25.357	56.737	GRAPES#8
44.010	0.491	22.277	0.215	4.792	23.570	327.494	1.464	17/6/21 13:31	1023.231	1010.992	62.551	1.522	6.145	24.917	56.159	GRAPES#9
9.120	0.149	5.598	0.118	0.660	48.694	16.376	6.489	1/6/21 14:45	969.000	1006.000	64.770	2.771	125.700	23.000	50.730	GRAPES Mono Module
16.950	0.148	10.348	0.099	1.000	39.706	32.209	4.869	2/6/21 12:43	1019.007	1011.219	63.418	2.138	5.017	22.979	64.713	GRAPES Double Module
52.159	2.010	39.693	1.675	61.408	58.527	758.847	8.394	25/8/21 13:26	1023.398	1005.107	61.380	1.894	2.330	28.252	52.424	CdTe
19.995	1.878	14.693	1.773	24.651	69.135	256.761	10.143	24/8/21 13:31	998.215	1003.837	65.711	1.482	301.647	27.696	51.495	Polycrystalline Si

Forward Exhaustive Search Scan

Voc	Isc	Vmax	Imax	Pmax	FF	Pin	PCE	Timestamp	Solar Irradiance	Patm	RH_Avg	WS	WD	Tair_Avg	Panel Temperature	Panel No
(V)	(A)	(V)	(A)	(W)	(%)	(W)	(%)	dom time	(W/m^2)	mb	(%)	(m/s)	deg	(°C)	(°C)	PV Technologies
20.220	0.427	14.518	0.264	3.547	61.049	326.558	1.088	17/6/21 13:35	1020.495	1010.987	61.919	1.419	270.656	25.265	57.972	GRAPES#1
30.210	0.409	16.802	0.253	3.891	61.224	326.557	1.183	17/6/21 13:43	1019.802	1010.990	59.470	2.065	326.592	25.074	56.521	GRAPES#2
25.420	0.257	14.555	0.154	2.248	34.417	328.647	0.684	17/6/21 13:33	1027.023	1010.989	60.106	2.155	7.028	25.104	56.718	GRAPES#3
27.670	0.342	14.848	0.185	2.746	27.098	325.335	0.844	17/6/21 13:46	1016.671	1010.947	61.887	1.808	78.627	24.874	57.213	GRAPES#4
35.300	0.488	19.964	0.301	6.011	34.907	327.051	1.838	17/6/21 13:37	1022.034	1010.996	60.802	1.770	334.341	25.394	58.190	GRAPES#5
31.380	0.449	17.569	0.365	6.418	62.966	326.085	1.422	17/6/21 13:45	1019.017	1010.964	61.118	2.022	290.016	25.029	56.843	GRAPES#6
34.090	0.477	18.917	0.281	5.320	32.798	327.604	1.624	17/6/21 13:41	1023.784	1011.003	58.638	1.988	6.473	25.315	57.179	GRAPES#7
33.730	0.450	19.043	0.273	5.201	34.258	327.363	1.588	17/6/21 13:39	1023.633	1010.982	60.816	2.072	320.769	25.357	56.737	GRAPES#8
42.480	0.443	24.289	0.282	6.846	36.404	327.494	2.091	17/6/21 13:31	1023.231	1010.992	62.551	1.522	6.145	24.917	56.159	GRAPES#9
8.940	0.151	5.530	0.128	0.885	49.381	16.376	6.531	1/6/21 14:45	969.000	1006.000	64.770	2.771	125.700	23.000	50.730	GRAPES Mono Module
16.880	0.142	10.478	0.103	1.078	44.924	32.209	5.037	2/6/21 12:43	1019.007	1011.219	63.418	2.138	5.017	22.979	64.713	GRAPES Double Module
51.461	2.007	37.720	1.653	62.353	60.170	758.847	8.462	25/8/21 13:26	1023.398	1005.107	61.380	1.894	2.330	28.252	52.424	CdTe
20.906	1.889	15.403	1.761	26.815	71.068	256.761	10.442	24/8/21 13:31	998.215	1003.837	65.711	1.482	301.647	27.696	51.495	Polycrystalline Si

Image 130. Electrical Characterization tables for different PV technologies

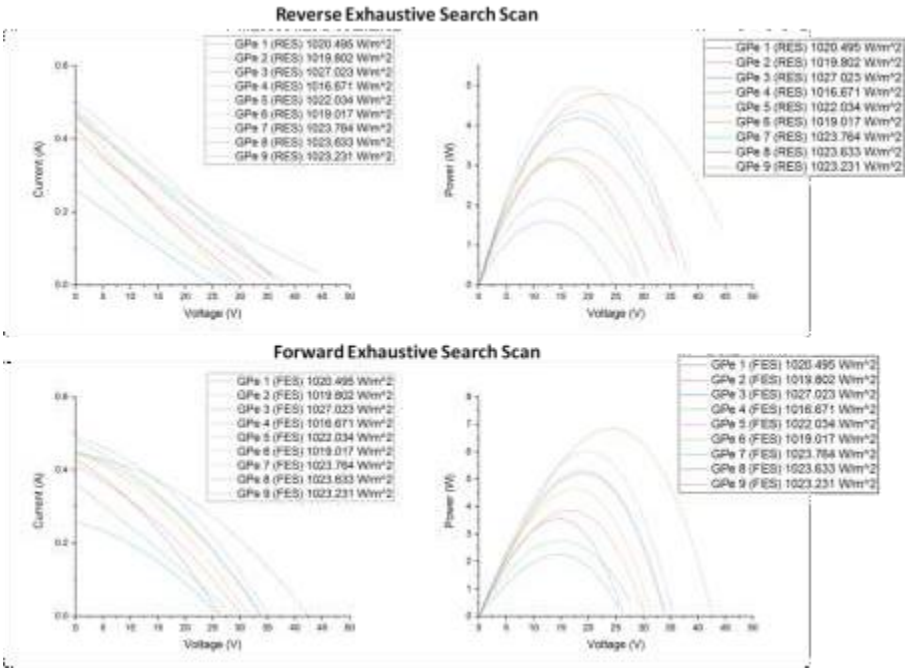


Image 131. GRAPES#1 to #9, IV and PV Curves

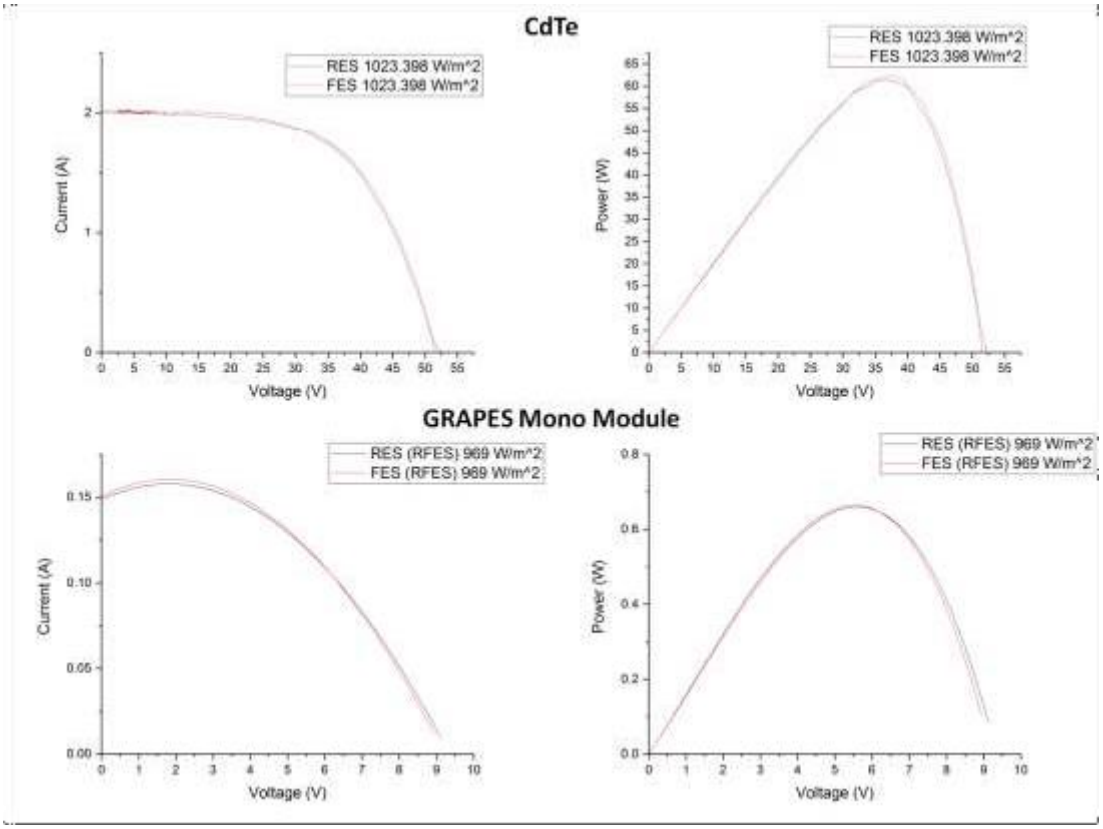


Image 132. CdTe, GRAPES Mono Module, IV and PV Curves

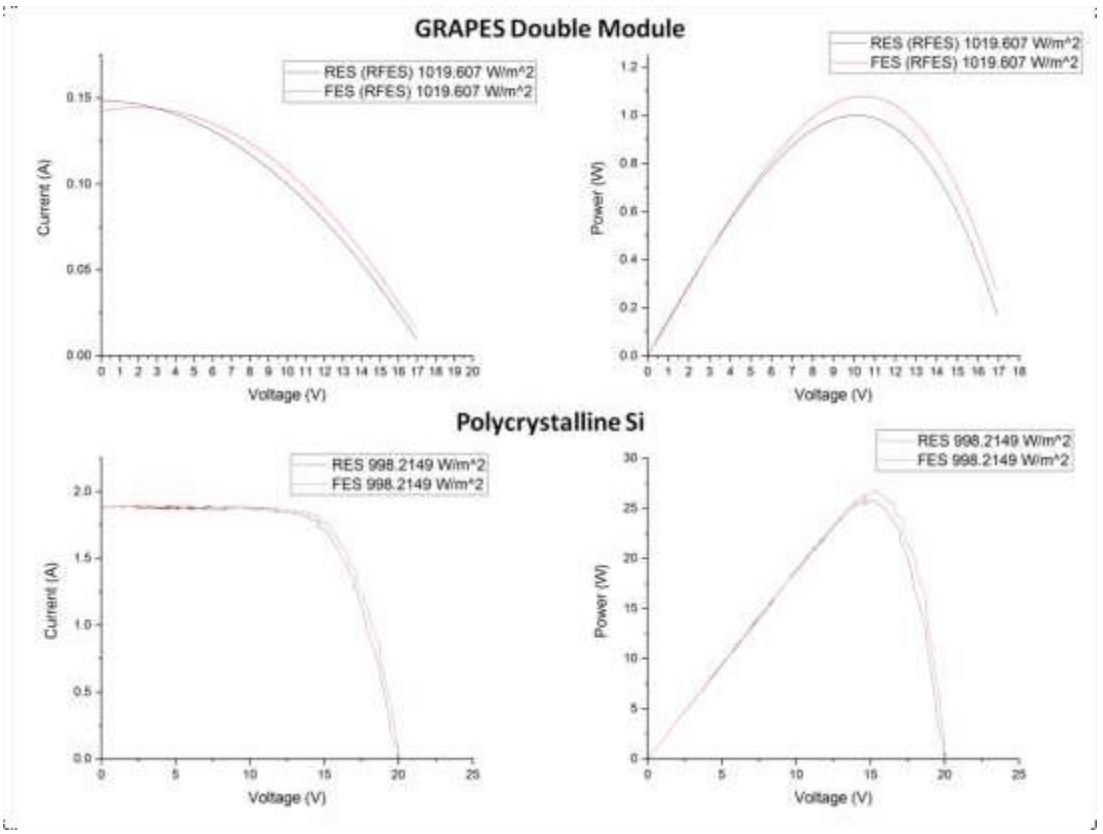


Image 133. GRAPES Double Module, Polycrystalline Si, IV and PV Curves

The experiment of electrical characterization continuous, now at different irradiations in different photovoltaic technologies. Also used and different algorithms, for the CdTe used solo RES and FES, FRES at GRAPES#1 and #3 and RFES for Si.

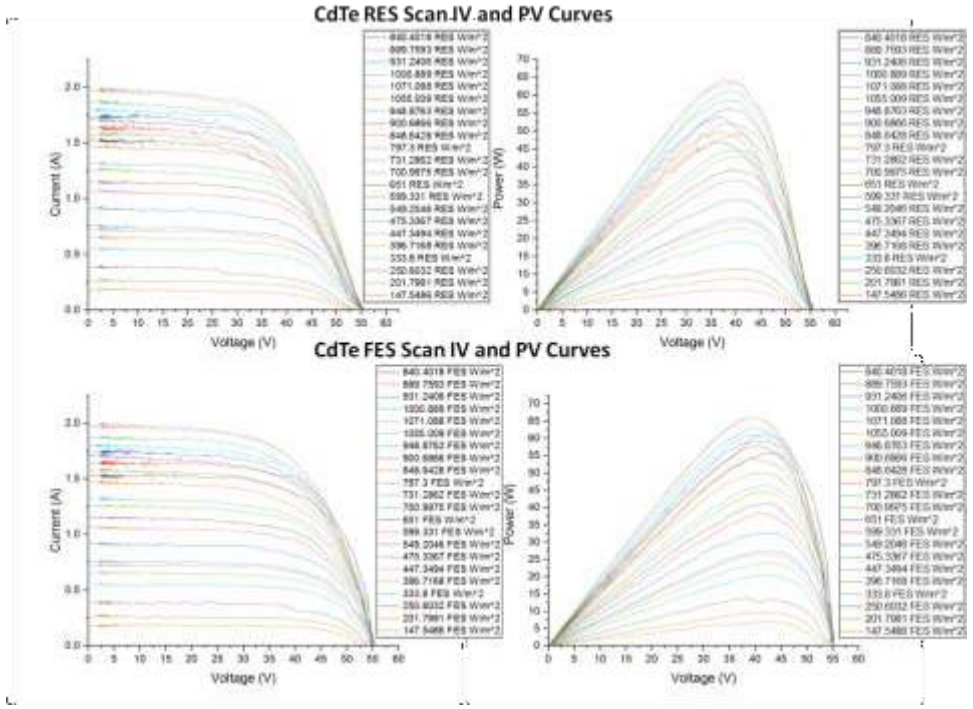


Image 134. CdTe IV and PV Curves at different irradiations

At CdTe observed that current is proportional to solar irradiation but not the voltage.

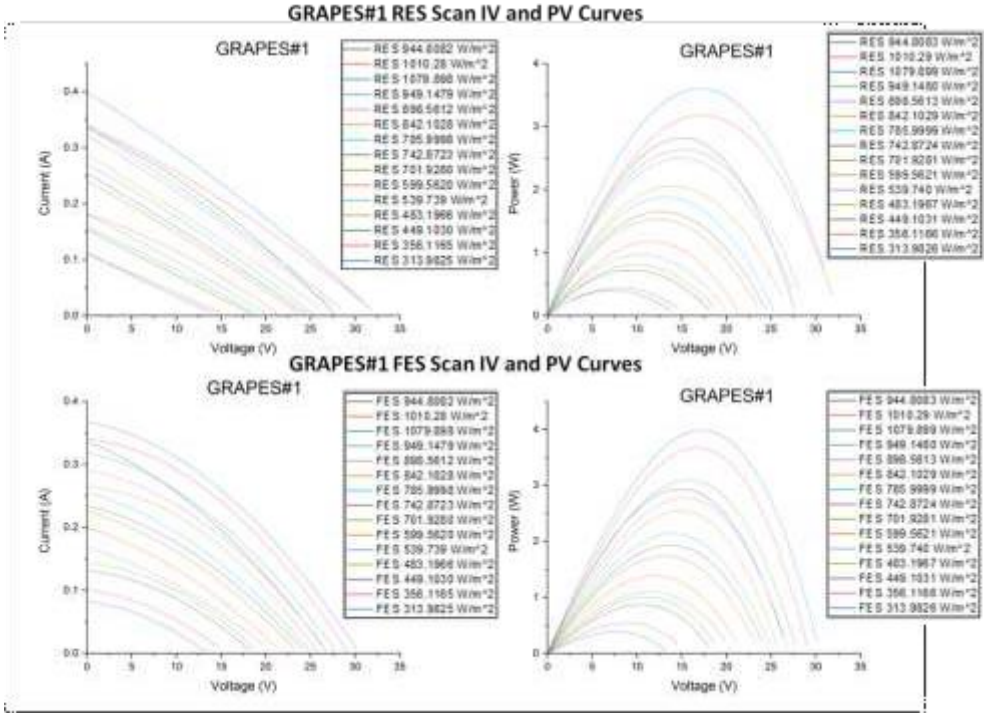


Image 135. GRAPES#1 IV and PV Curves at different irradiations

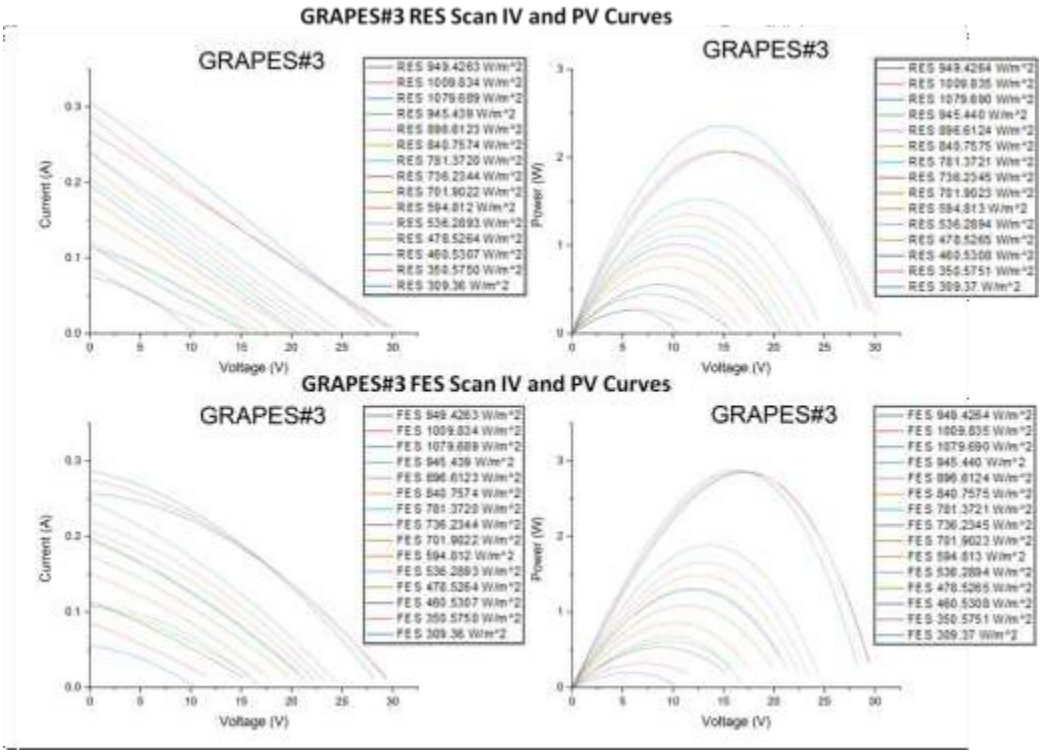


Image 136. GRAPES#3 IV and PV Curves at different irradiations

At GRAPES#1 and #3 also observed that the #3 Power degradation is faster than #1. In both photovoltaics, the current is proportional to solar irradiation and the voltage is almost proportional.

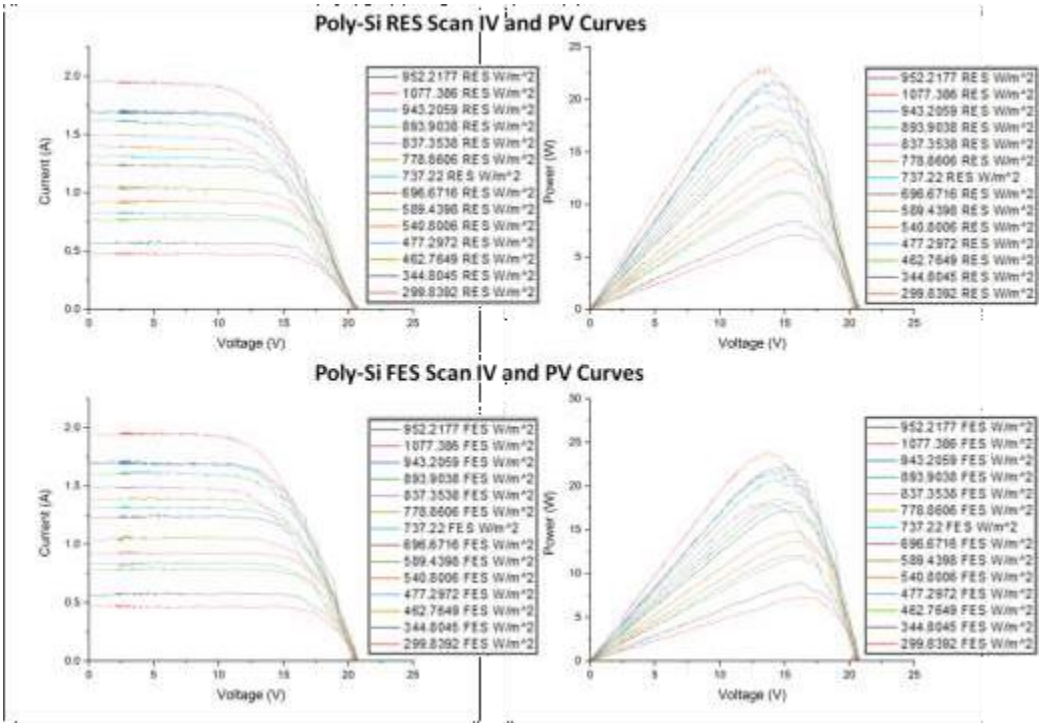


Image 137. Polycrystalline Si IV and PV Curves at different irradiations

In the Si photovoltaic known that the current is proportional to solar irradiation and the voltage is logarithmic, not proportional to it.

It follows a monthly experiment on GRAPES#3, of resting and using periods, to check, the exposure at the sun and supply load, degradation, at utilize period and the regeneration of the panel at resting periods.

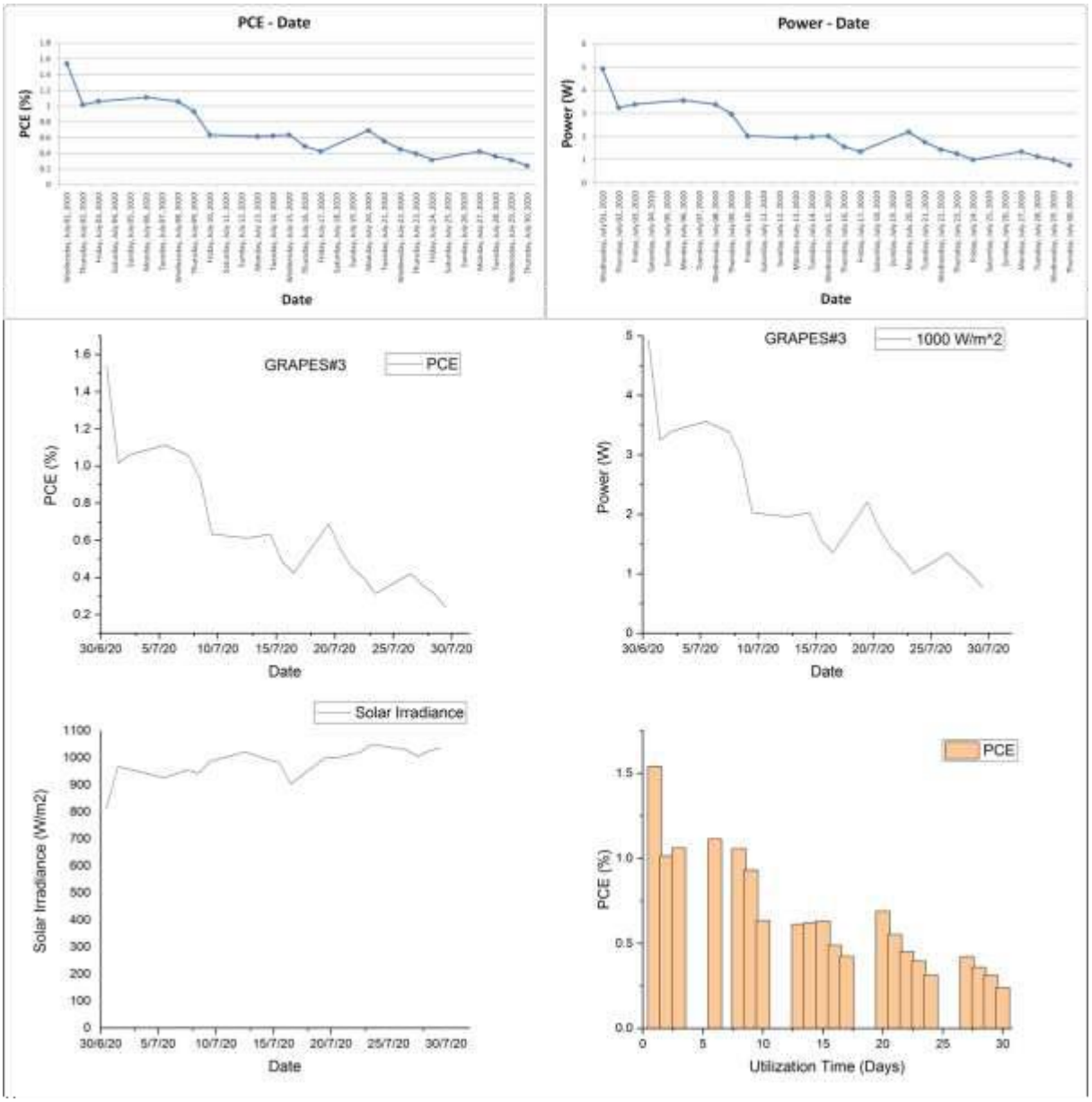


Image 138. Monthly Degradation and Regeneration of the GRAPES#3

Clearly observed that, when using (exposure at the sun and supply a load) the panel, it lose gradually PCE day after day and it lose power in turn. Also after of 2 or 3 days resting period observed that some PCE regenerate but never bigger than the first use PCE (see Image 138). Further at Image 139. shown the degradation and regeneration mechanisms.

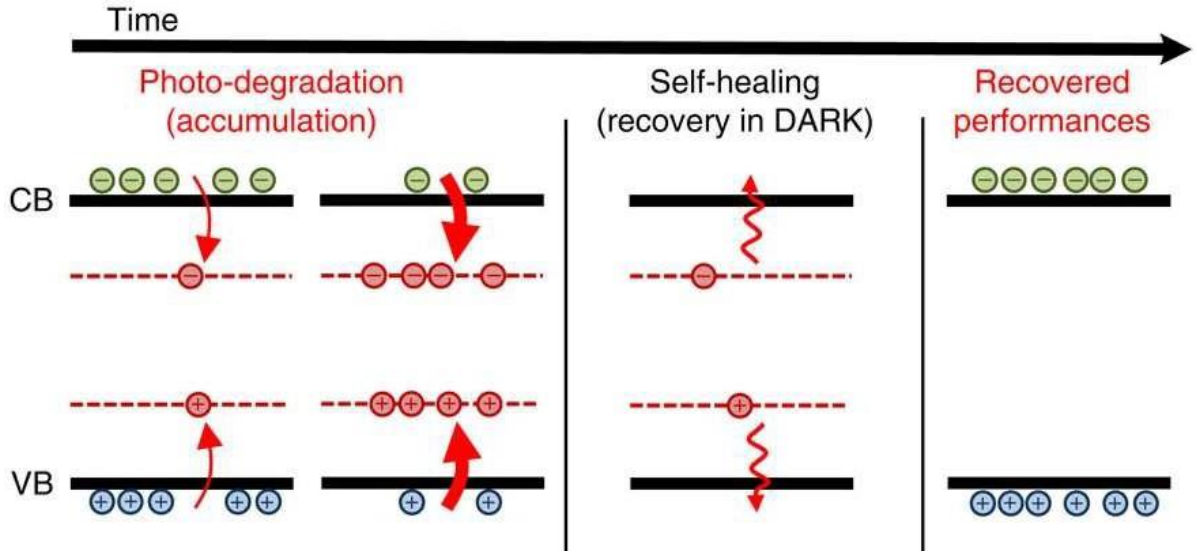


Image 139.Schematics of photocurrent degradation and regeneration mechanism **[60]**

Based on perovskite layer structure, sketch of progression the VB and CB for three states:

- During photo degradation and accumulation
- During recovery in dark
- Under illumination after self-healing (regeneration)

The red dotted lines refer to light activated meta stable trap states that relax in dark returning the device to its steady state. The arrows shows how the photogenerated carriers can populate those light activated trap states under light or relax in dark over time **[60]**.

6.2.8 IV Curve Comparison and Collaboration with PV Blocks

For extra check of the correct operation of the handmade IV-MPPT Charger regulator, also used the commercial electronic load device with name PV Blocks, that can create IV Curves, it uses the Forward Scan algorithm (FES).

So taken one IV Curve from each machine and compare it (see Image 140.). Furthermore, collaboration of the two devices achieved and take additionally extra IV curves to observe once more the sun exposure and supply load degradation (see Image 141.b.), as well as the almost proportionality of GRAPES Voltage (see Image 141.a.).

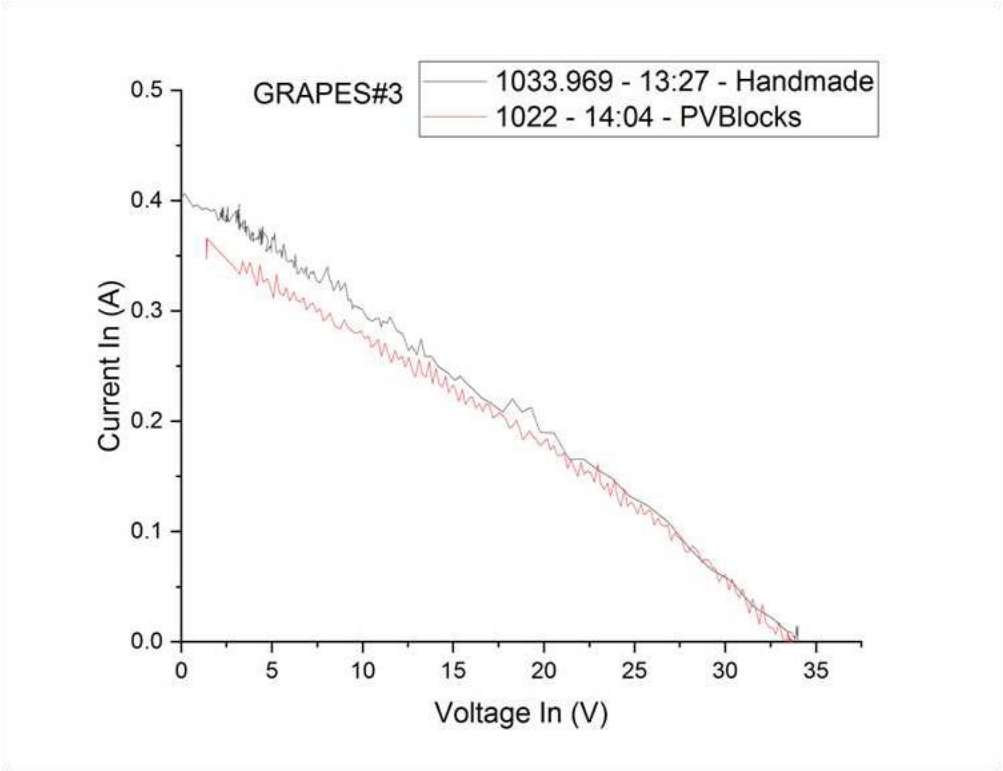
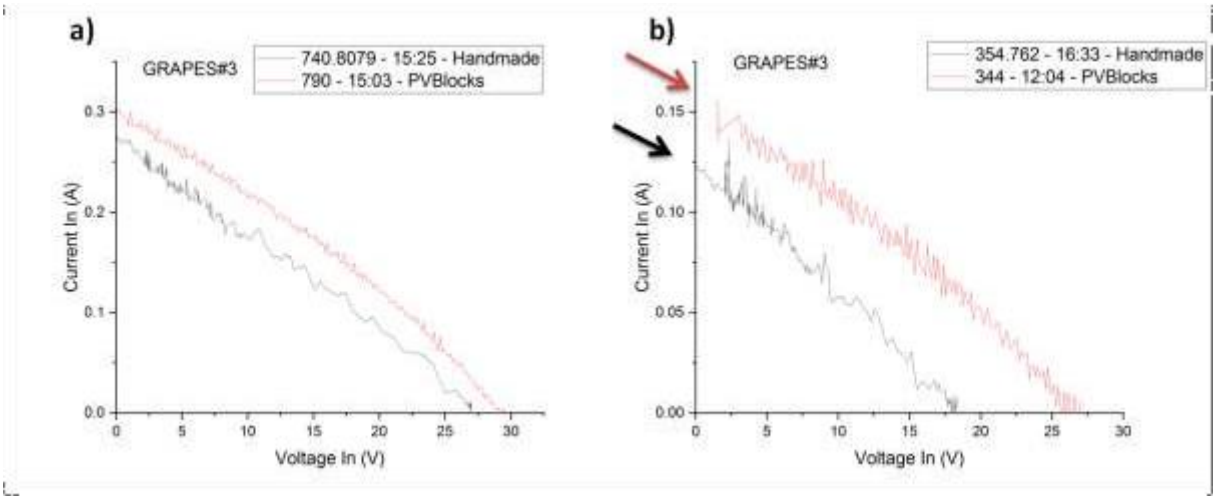


Image 140. Comparison of the IV Curves of the two devices

As shown in Image 140. the two devices take the same measurement, on the same panel with only a slightly difference in short circuit current for some mA and that's because of ~11W/m^2 difference of the irradiance and known that the current on the photovoltaics is



proportional to solar irradiance, additionally at GRAPES and the voltage is almost proportional to solar irradiance.

Image 141. IV Curves of the two devices collaboration, ***a)*** *different irradiation to observe the current and voltage proportionality of GRAPES photovoltaics,* ***b)*** *same irradiation four and a half hours from each other to observe the degradation from sun exposure and supply a load*

6.3 Maximum Power Point Tracking (MPPT) Measurements and Experiments

In this chapter IV-MPPT Charger Regulator MPPT algorithms used for Energy Yield knowledge of GRAPES technology, three experiments follows Comparison of FOCV and HCPO algorithms, clear and cloudy sky days, all algorithms measurements. Then for the first two experiments also used CdTe and Polycrystalline for comparison reasons.

6.3.1 FOCV and HCPO Algorithms Comparison at different PV Technologies also Comparison of Theoretical and Real Outdoor measurements

First extracted electrical characteristics of GRAPES#2 for each algorithm (FOCV and HCPO), from RES and FES algorithms, and with weather data from weather station of solar farm, used for creation of theoretical MPPT measurements to compare it with the real MPPT measurements, for extraction of the real IV - PV Curves of GRAPES Photovoltaics for FOCV algorithm, also used the most commercial algorithm HCPO for comparison with FOCV algorithm. Each measurement for this experiment was 15 minutes.

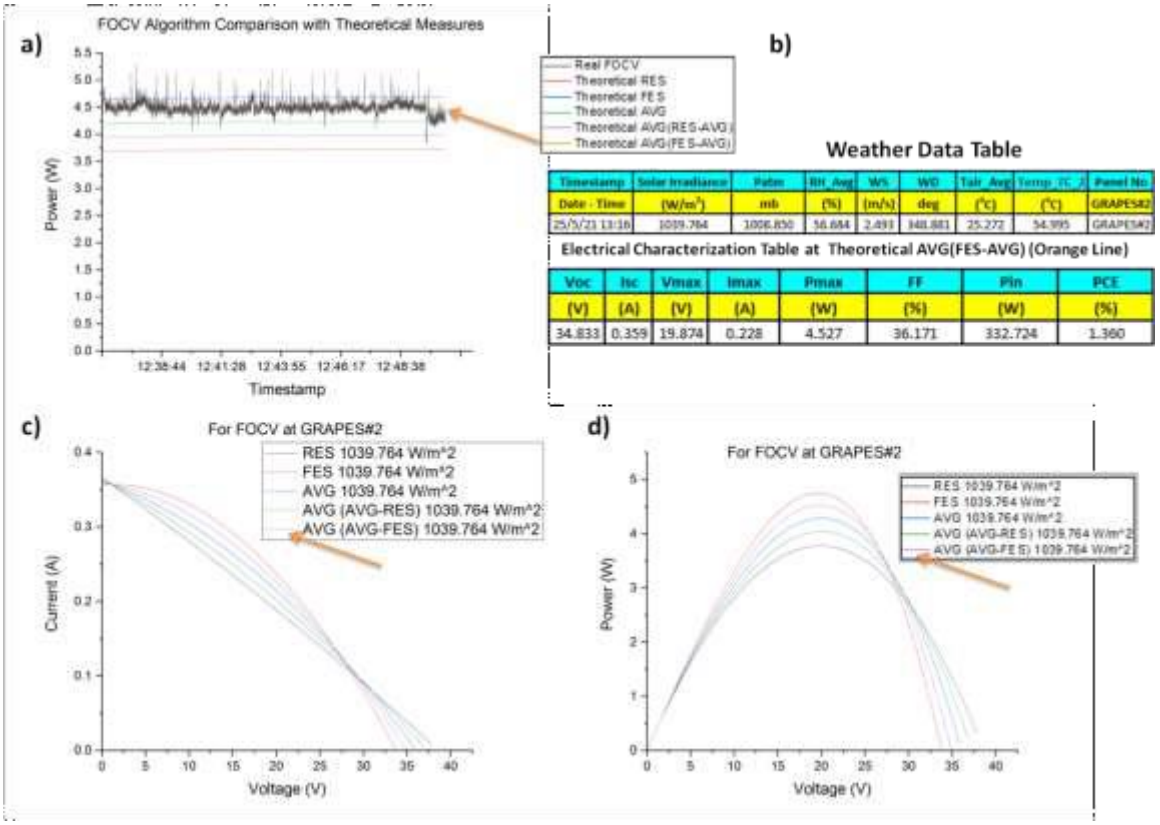


*Image 142. FOCV algorithm real time measurements comparison with theoretical measurements, **a)** Power - Time graph, **b)** Tables of Weather data and E.C., **c)** IV Curves real time and theoretical, **d)** PV Curves real time and theoretical, at GRAPES#2 (25/05/2021)*

Observed from Image 142.a. that the real Pmax of FOCV algorithm at GRAPES is equal to Average of theoretical FES with theoretical Average of RES and FES see Orange Line of Image 142.a., $Average(FES\ and\ (Average(RES\ and\ FES))$. Images 142.c. and 142.d. are IV-PV Curves respectively that created from real RES and FES then in turn the calculation of theoretical averages with these characteristics and with weather data created the theoretical Pmax - Time graphs of Image 142.a., also from these curves and weather datas, extracted the electrical characteristics table of Image 142.b. Follows HCPO algorithm for comparison with FOCV at same photovoltaic.

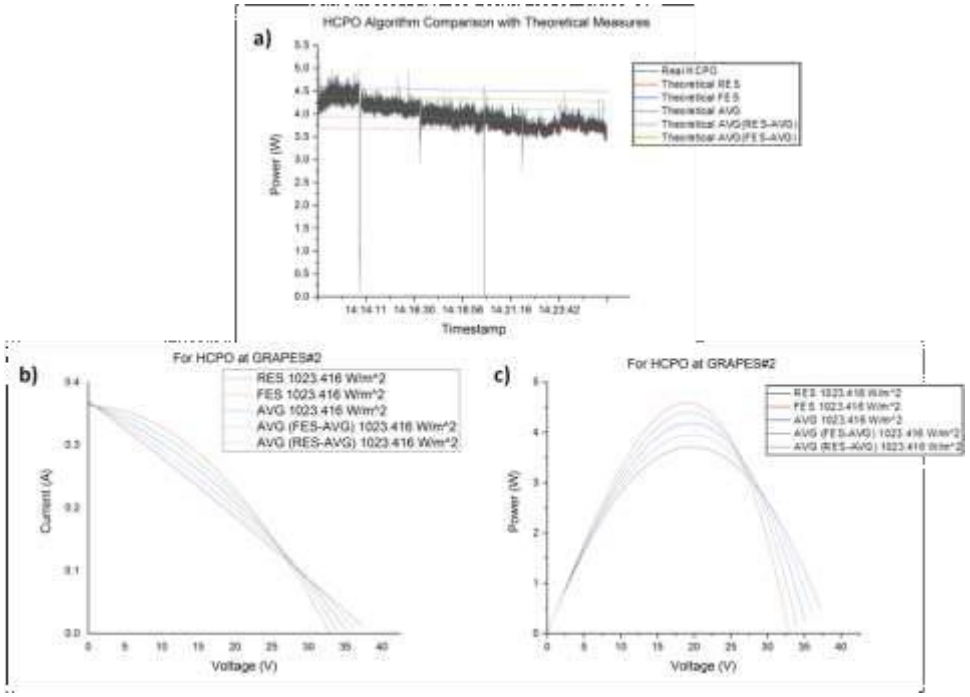


Image 143. HCPO algorithm real time measurements comparison with theoretical measurements, ***a)*** *Power - Time graph,* ***b)*** *IV Curves real time and theoretical,* ***c)*** *PV Curves real time and theoretical, at GRAPES#2 (25/05/2021)*

Comparison of FOCV and HCPO algorithms at GRAPES#2 (25/05/2021)	
E.Y. from the Sun for FOCV (Wh/m^2)	255.8
FOCV Energy Yield (Wh/m^2)	1.938
Total GRAPES#2_FOCV Efficiency n(%)	0.758
E.Y. from the Sun for HCPO (Wh/m^2)	252.15
HCPO Energy Yield (Wh/m^2)	1.712
Total GRAPES#2_HCPO Efficiency n(%)	0.679
Comparison Efficiency n(%) FOCV > HCPO	10.42

Observed that FOCV algorithm has better energy yield than HCPO at GRAPES#2 for 10.42%.

With the same calculations follows Power - Time graphs and comparison tables of FOCV and HCPO algorithms on GRAPES mono, double modules also and CdTe and Polycrystalline-Si.

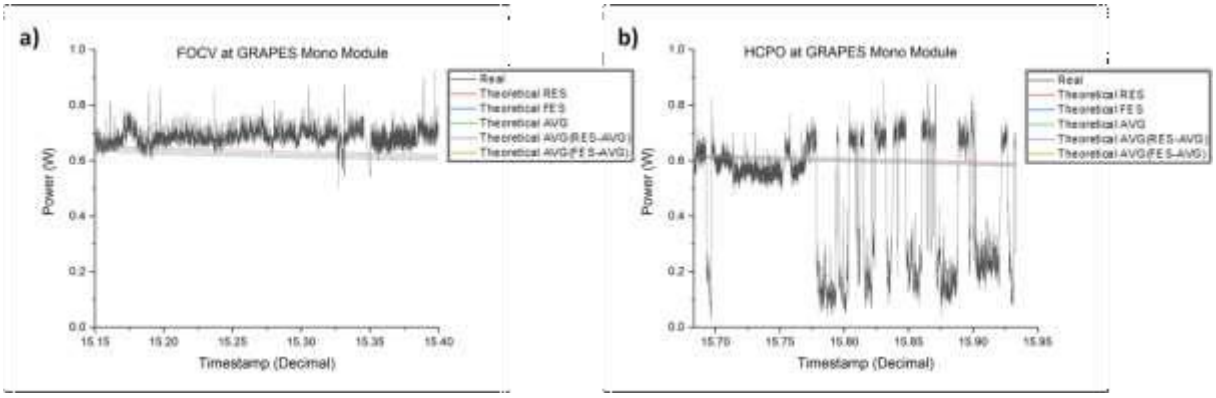


*Image 144. Power - Time Graphs **a)** FOCV Algorithm, **b)** HCPO Algorithm, at GRAPES Mono Module (01/06/2021)*

Comparison of FOCV and HCPO algorithms at GRAPES Mono Module (01/06/2021)	
E.Y. from the Sun for FOCV (Wh/m^2)	229.65
FOCV Energy Yield (Wh/m^2)	10.178
Total GRAPES Mono_FOCV n(%)	4.432
E.Y. from the Sun for HCPO (Wh/m^2)	210.48
HCPO Energy Yield (Wh/m^2)	6.686
Total GRAPES Mono_HCPO n(%)	3.177
Comparison n(%) FOCV > HCPO	28.32

Observed that FOCV algorithm has better energy yield than HCPO at GRAPES Mono Module for 28.32%.

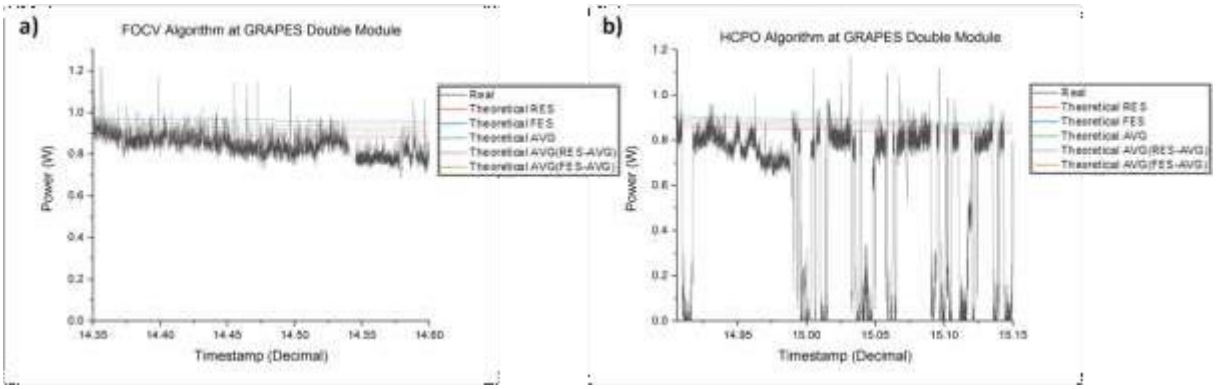


*Image 145. Power - Time Graphs **a)** FOCV Algorithm, **b)** HCPO Algorithm, at GRAPES Double Module (04/06/2021)*

Comparison of FOCV and HCPO algorithms at GRAPES Double Module (04/06/2021)	
E.Y. from the Sun for FOCV (Wh/m^2)	248.85
FOCV Energy Yield (Wh/m^2)	6.648
Total GRAPES Double_FOCV n(%)	2.671
E.Y. from the Sun for HCPO (Wh/m^2)	234.7
HCPO Energy Yield (Wh/m^2)	4.463
Total GRAPES Double_HCPO n(%)	1.902
Comparison n(%) FOCV > HCPO	28.8

Observed that FOCV algorithm has better energy yield than HCPO at GRAPES Double Module for 28.8%.

FOCV Algorithm is better than HCPO overall at all GRAPES technology photovoltaics.

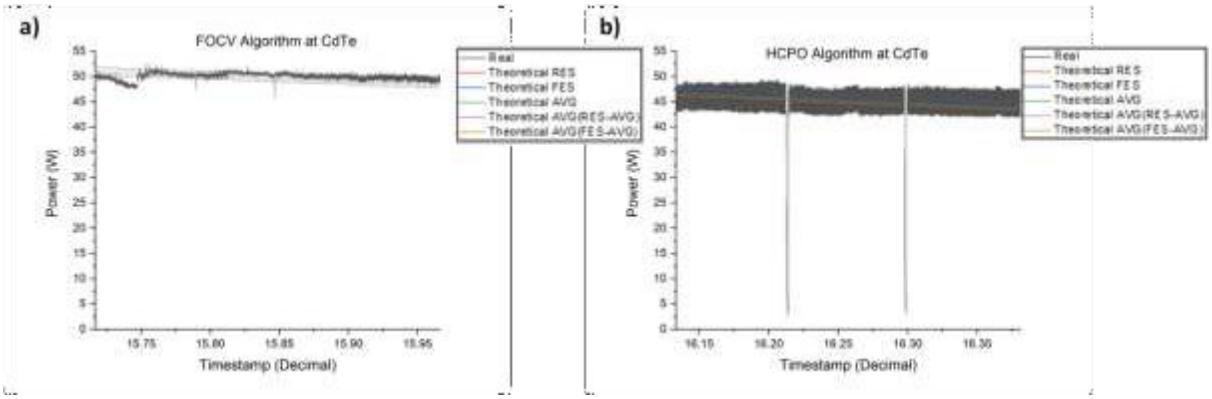


*Image 146. Power - Time Graphs **a)** FOCV Algorithm, **b)** HCPO Algorithm, at CdTe (25/05/2021)*

Comparison of FOCV and HCPO algorithms at CdTe (25/05/2021)	
E.Y. from the Sun for FOCV (Wh/m^2)	204.19
FOCV Energy Yield (Wh/m^2)	17.376
Total CdTe_FOCV n(%)	8.51
E.Y. from the Sun for HCPO (Wh/m^2)	185.455
HCPO Energy Yield (Wh/m^2)	15.556
Total CdTe_HCPO n(%)	8.388
Comparison n(%) FOCV > HCPO	1.433

Observed that FOCV algorithm has slightly better energy yield even in thin film technology of CdTe than HCPO for 1.433%.

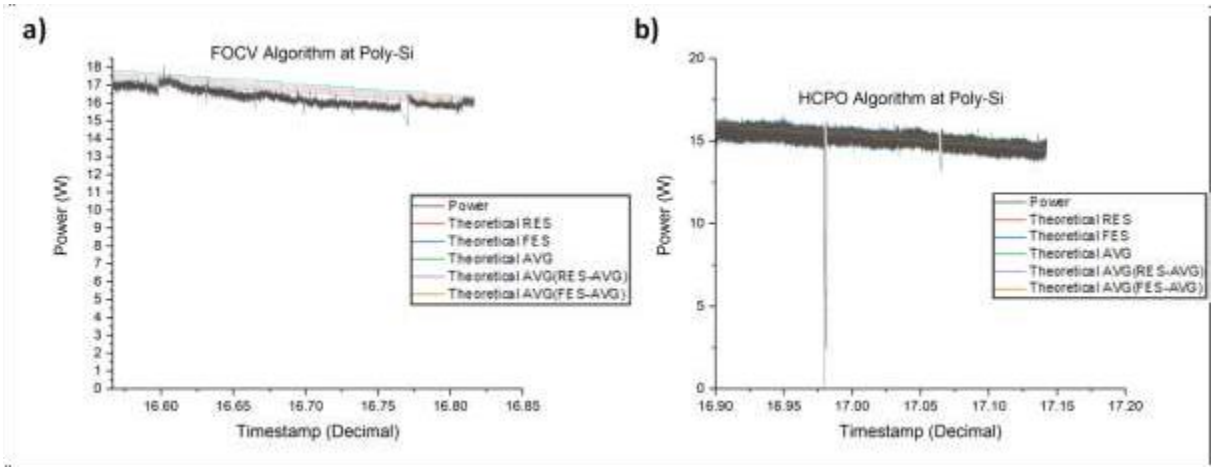


*Image 147. Power - Time Graphs **a)** FOCV Algorithm, **b)** HCPO Algorithm, at Poly-Si (25/05/2021)*

Comparison of FOCV and HCPO algorithms at Polycrystalline Si (25/05/2021)	
E.Y. from the Sun for FOCV (Wh/m^2)	163.535
FOCV Energy Yield (Wh/m^2)	15.88
Total Poly-Si_FOCV n(%)	9.71
E.Y. from the Sun for HCPO (Wh/m^2)	145.168
HCPO Energy Yield (Wh/m^2)	14.52
Total Poly-Si_HCPO n(%)	10
Comparison n(%) HCPO > FOCV	2.94

Observed that HCPO algorithm has slightly better energy yield in Polycrystalline Si than FOCV for 2.94%.

6.3.2 All MPPT Algorithms Comparison with a Commercial Device Algorithm at different PV Technologies in Clear Sky

For the next experiment, created three tables one for each technology GRAPES, CdTe, Si, for comparison all IV-MPPT Charger Regulator MPPT algorithms with commercial device Victron energy BlueSolar charge controller MPPT 100|30 in clear sky. For each MPPT algorithm at different PV technologies created, five graphs, **a)** Power - Time, **b)** Voltage - Time, **c)** Current - Time, **d)** Irradiance - Time, **e)** Duty Cycle - Time, for total 117 graphs. All measurement acquired at ~1000 W/m^2 and each measurement was taken for 10 minutes.

Photovoltaic GRAPES#7 (26/08/2021), 10 minutes each measurement	Victron Energy© BlueSolar Charge Controller MPTP 100|30	MPQAS1	MPQAS2	FOCV	FSCC	IC	HCPO	HC
E.Y. from the Sun for each Algorithm (Wh/m^2)	166.167	165.450	164.167	162.817	161.033	159.650	157.083	148.800
Algorithms Energy Yield (Wh/m^2)	1.275	1.646	1.556	1.426	1.378	1.325	1.276	0.832
Total GRAPES#7_Algorithms Efficiency n(%)	0.767	0.995	0.948	0.876	0.856	0.830	0.812	0.559
Comparison Commercial with Handmade MPPT		22.872	19.042	12.391	10.332	7.528	5.544	-37.203

Image 148. GRAPES#7 Comparison Table

From table of Image 148., observed that the best algorithms for GRAPES#7 photovoltaic, are the innovative algorithms MPQAS1 & 2 with 0.995% & 0.948% respectively total efficiency and FOCV with 0.876%. Also MPQAS1 has 22.872% bigger efficiency than the commercial device MPPT which has 0.767% total efficiency, MPQAS2 has 19.042% bigger efficiency and the FOCV has 12.391% bigger in turn.

Graphs of GRAPES#7, at all MPPT Algorithms, also and graphs of the commercial device:

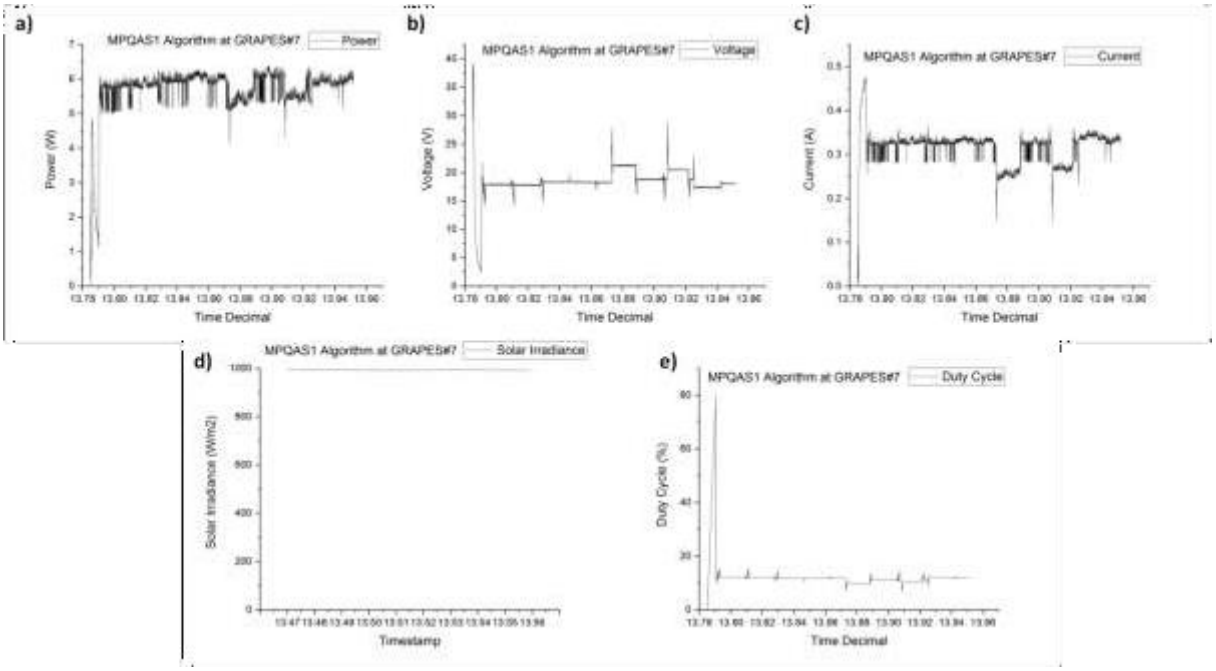


Image 149. MPQAS1 at GRAPES#7

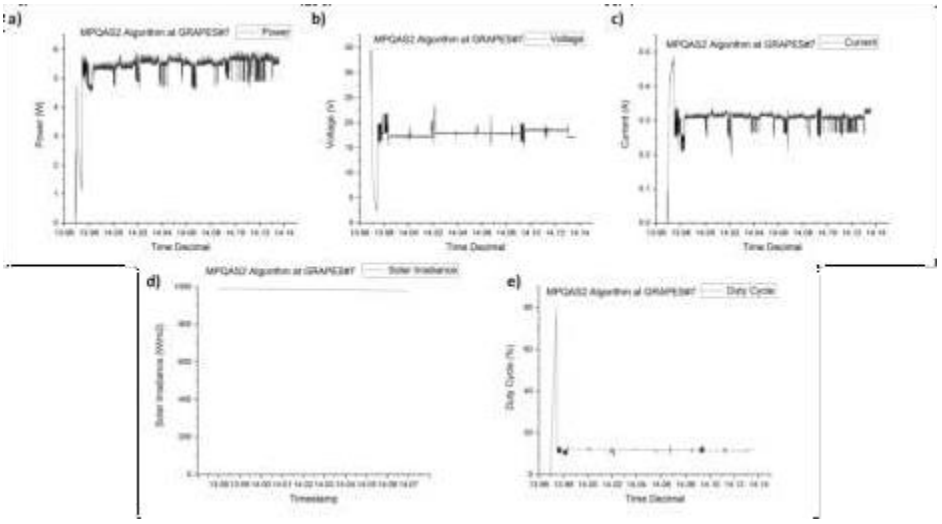


Image 150. MPQAS2 at GRAPES#7

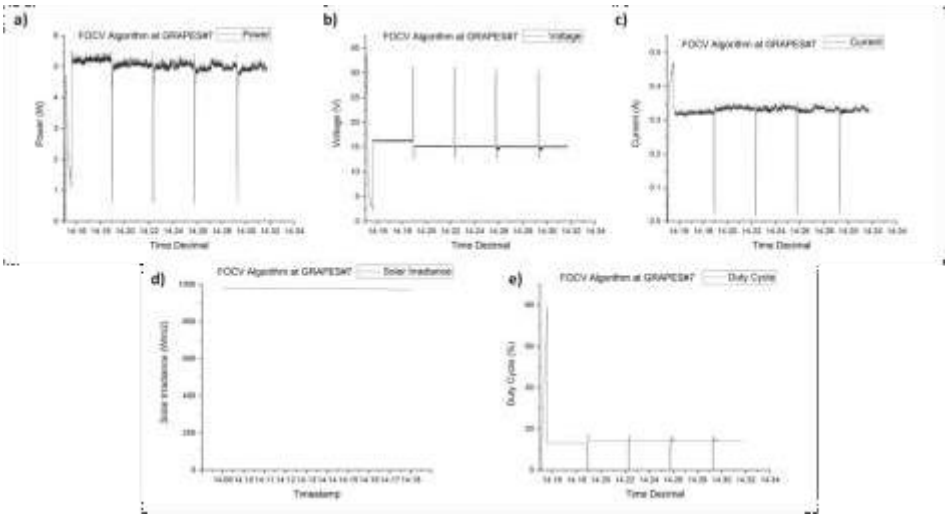


Image 151. FOCV at GRAPES#7

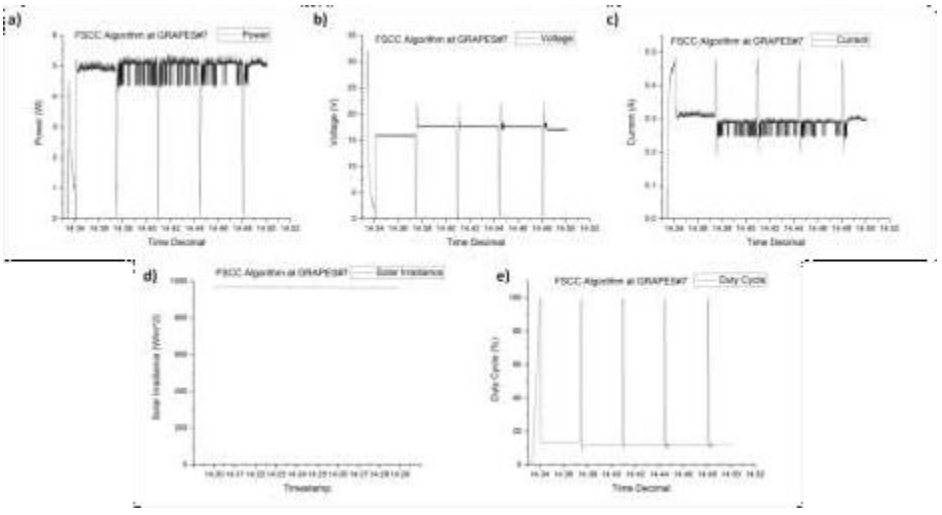


Image 152. FSCC at GRAPES#7

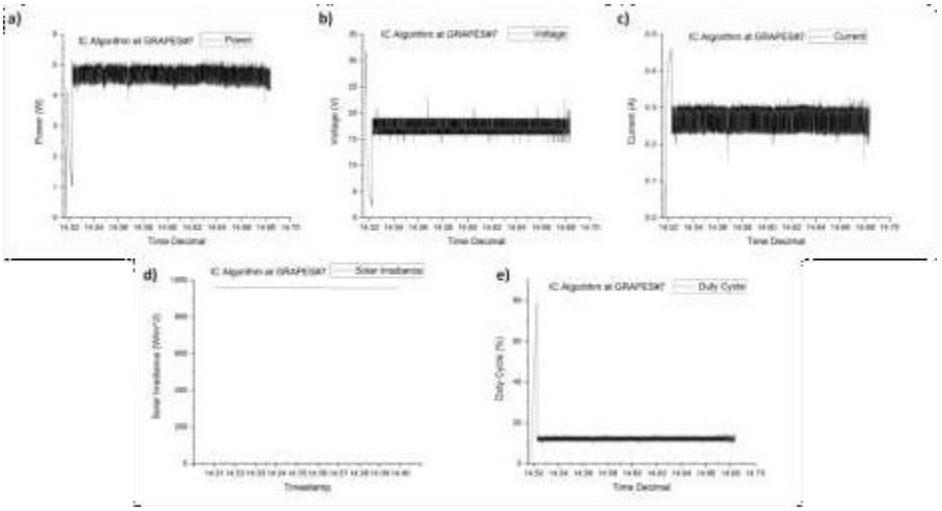


Image 153. IC at GRAPES#7

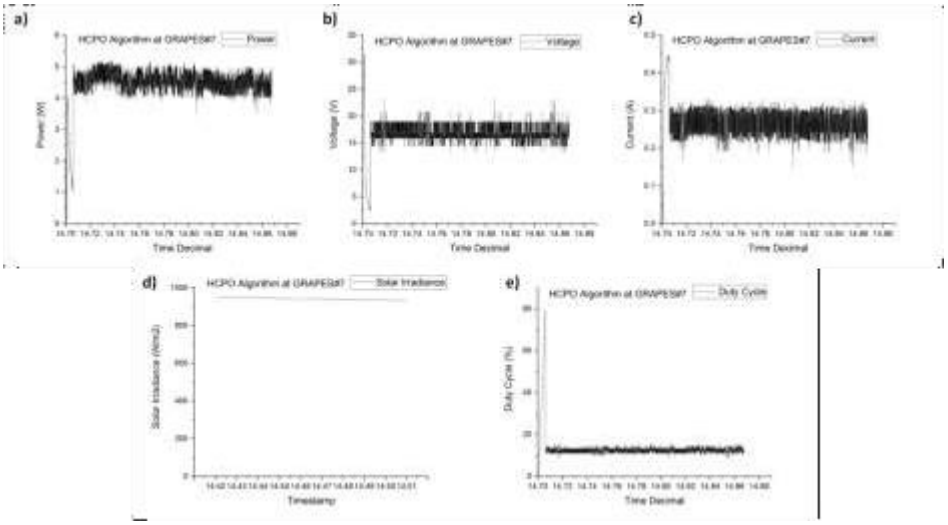


Image 154. HCPO at GRAPES#7

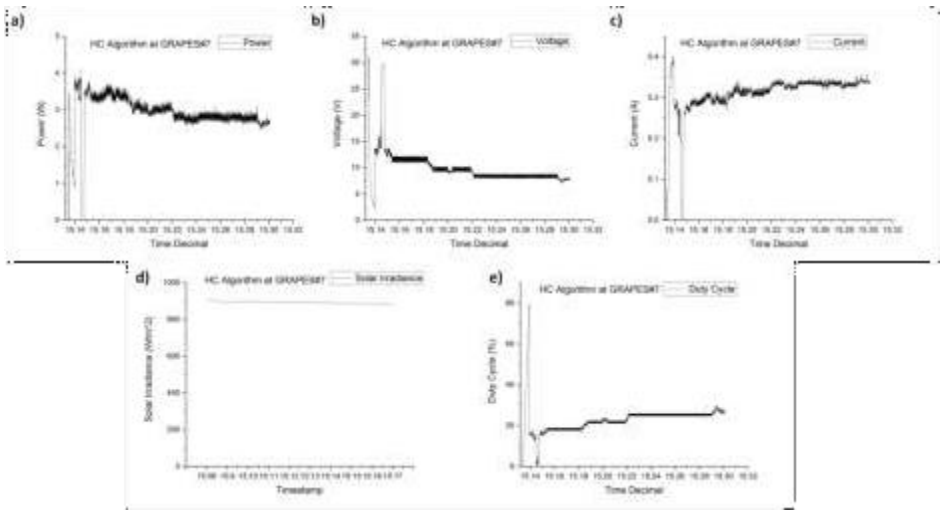


Image 155. HC at GRAPES#7

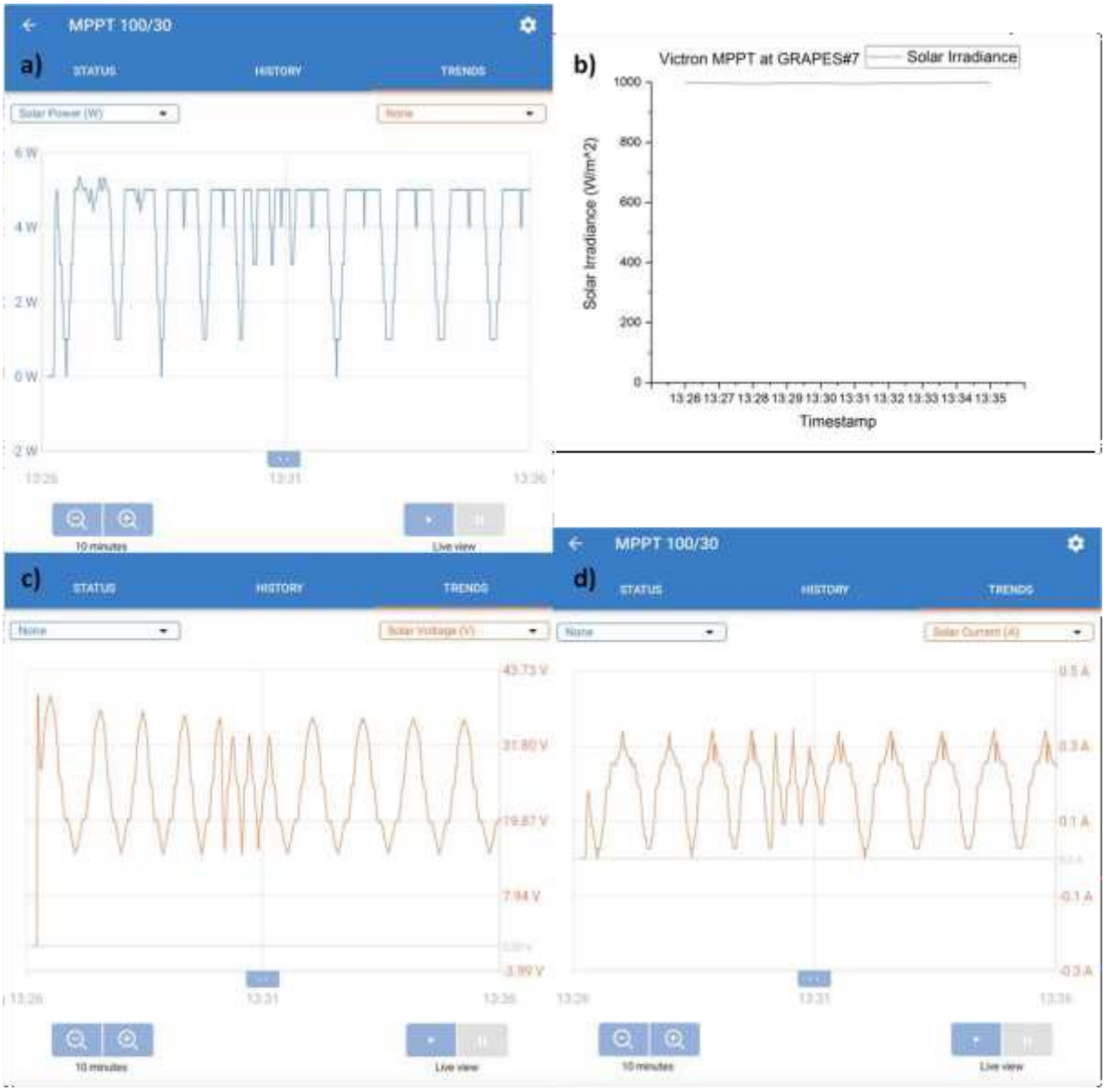


Image 156. Commercial Victron Energy MPPT Graphs at GRAPES#7, ***a)*** *Power - Time,* ***b)*** *Irradiance - Time,* ***c)*** *Voltage - Time,* ***d)*** *Current - Time*

Table and Graphs of all algorithms for the CdTe Technology.

Photovoltaic CdTe (25/08/2021), 10 minutes each measurement	Victron Energy© BlueSolar Charge Controller MPTP 100/30	MPQAS1	MPQAS2	FOCV	FSCC	IC	HCPO	HC
E.Y. from the Sun for each Algorithm (Wh/m^2)	170.617	170.650	170.483	168.917	166.550	164.450	161.833	158.183
Algorithms Energy Yield (Wh/m^2)	13.381	14.458	14.386	13.974	13.461	13.068	12.638	11.748
Total CdTe_Algorithms Efficiency η(%)	7.843	8.461	8.438	8.273	8.082	7.947	7.809	7.427
Comparison Commercial with Handmade MPPT		7.301	7.056	5.193	2.959	1.305	-0.429	-5.606

Image 157. CdTe Comparison Table

From table of Image 157., observed that the best algorithms for CdTe photovoltaic, are the innovative algorithms MPQAS1 & 2 with 8.461% & 8.438% respectively total efficiency

and FOCV with 8.273%. Also MPQAS1 has 7.301% bigger efficiency than the commercial device MPPT which has 7.843% total efficiency, MPQAS2 has 7.056% bigger efficiency and the FOCV has 5.193% bigger in turn.

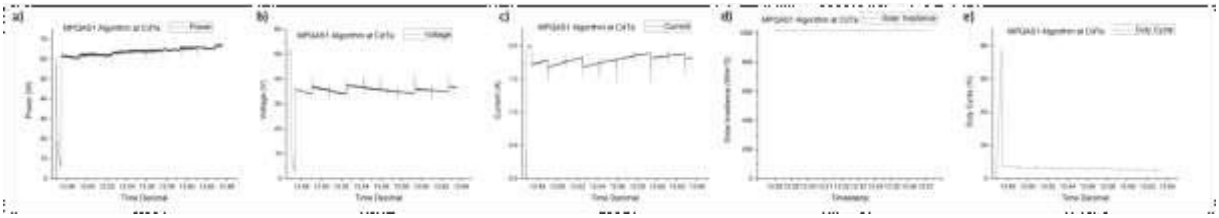


Image 158. MPQAS1 at CdTe

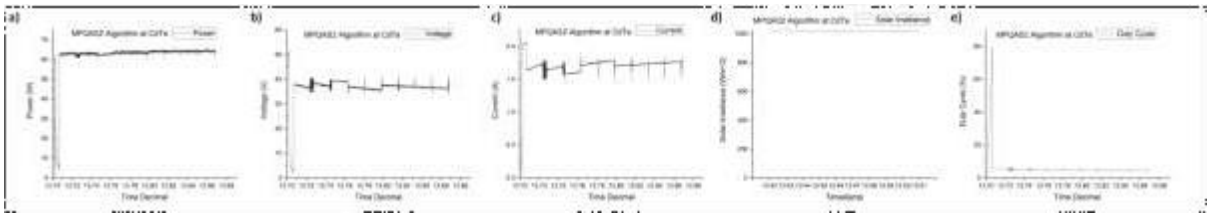


Image 159. MPQAS2 at CdTe

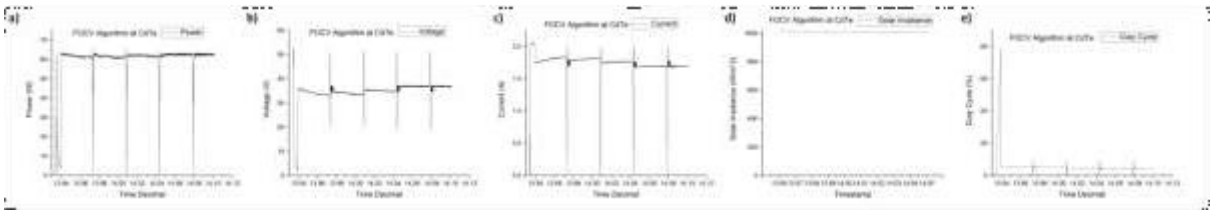


Image 160. FOCV at CdTe

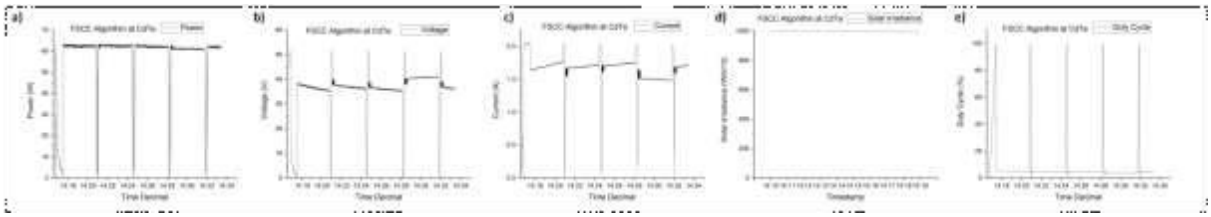


Image 161. FSCC at CdTe

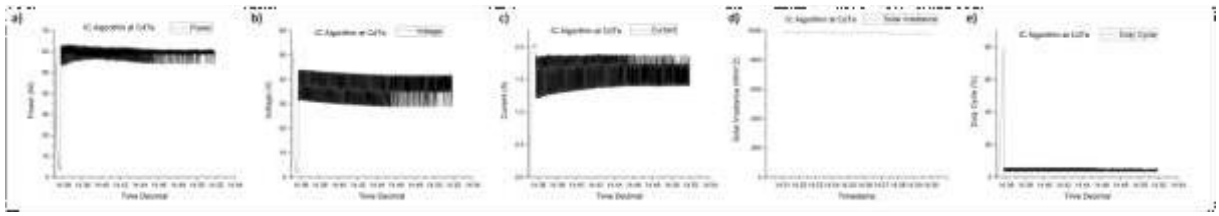


Image 162. IC at CdTe

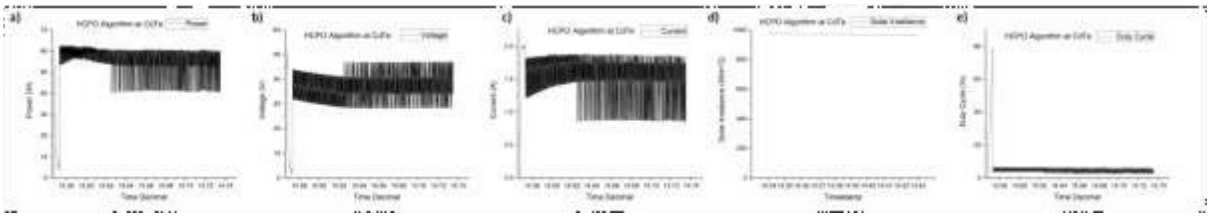


Image 163. HCPO at CdTe

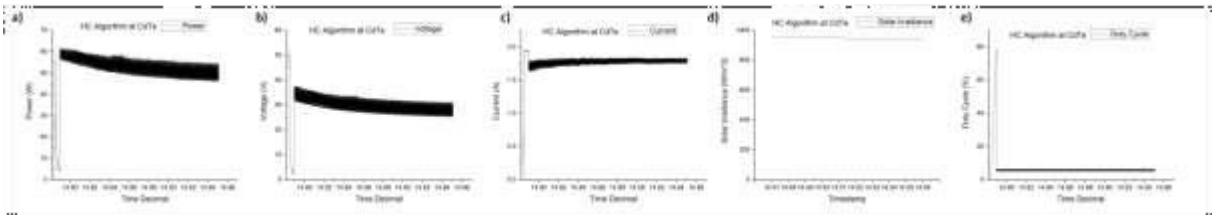


Image 164. HC at CdTe

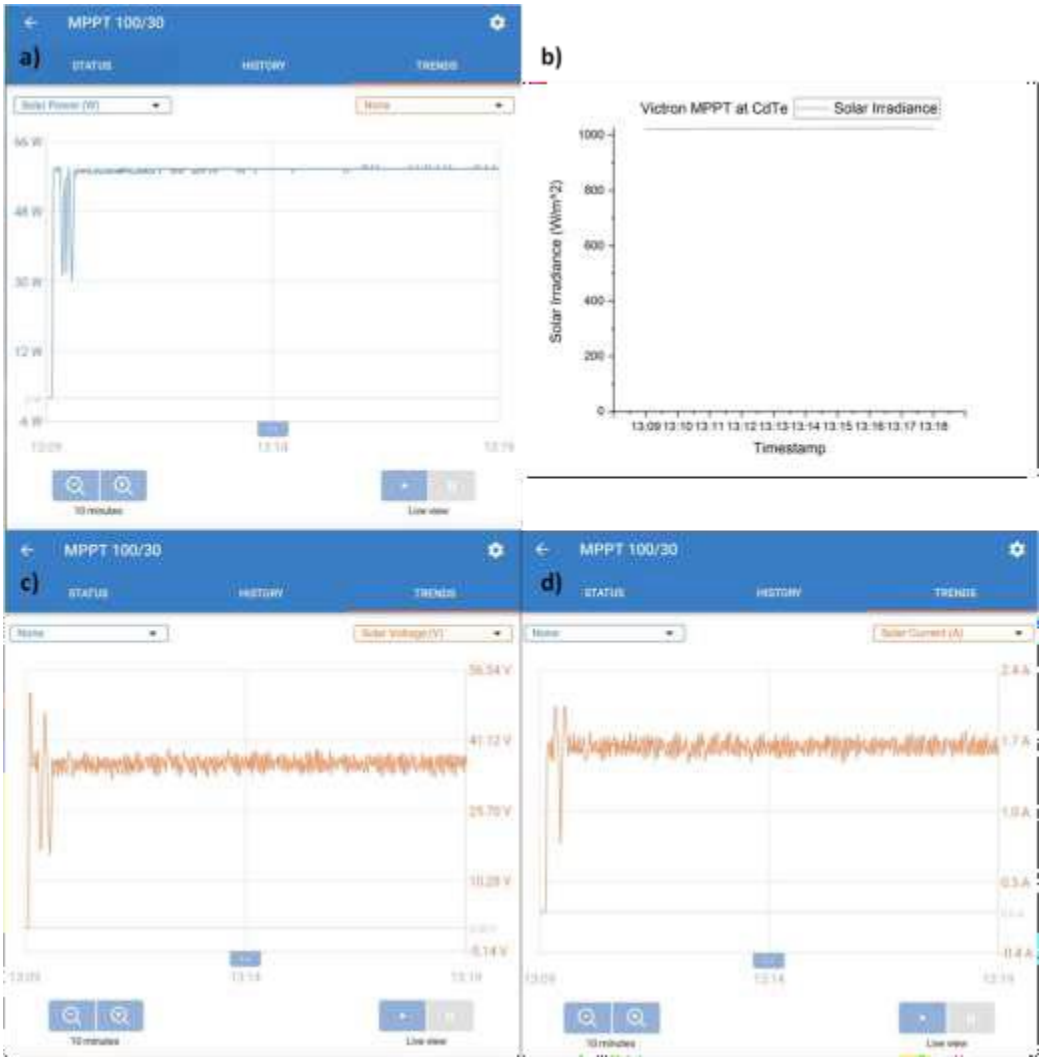


Image 165. Commercial Victron Energy MPPT Graphs at CdTe, ***a)*** *Power - Time,* ***b)*** *Irradiance - Time,* ***c)*** *Voltage - Time,* ***d)*** *Current - Time*

Table and Graphs of all algorithms for the Polycrystalline Si Technology.

Photovoltaic Polycrystalline Si (24/08/2021), 10 minutes each measurement	Victron Energy© BlueSolar Charge Controller MPTP 100|30	MPQAS1	MPQAS2	FOCV	FSCC	IC	HCPO	HC
E.Y. from the Sun for each Algorithm (Wh/m^2)	166.550	166.667	165.533	164.383	162.750	160.717	158.283	155.100
Algorithms Energy Yield (Wh/m^2)	15.905	16.727	16.699	16.507	15.993	15.812	15.527	14.482
Total Poly-Si_Algorithms Efficiency n(%)	9.550	10.036	10.088	10.042	9.827	9.838	9.810	9.337
Comparison Commercial with Handmade MPPT		4.846	5.331	4.896	2.816	2.931	2.647	-2.280

Image 166. Polycrystalline Si Comparison Table

From table of Image 166., observed that the best algorithms for Polycrystalline Si photovoltaic, are the innovative algorithms MPQAS1 & 2 with 10.036% & 10.088% respectively total efficiency and FOCV with 10.042%. Also MPQAS2 has 5.331% bigger efficiency than the commercial device MPPT which has 9.55% total efficiency, FOCV has 4.896% bigger efficiency and the MPQAS1 has 4.846% bigger in turn.

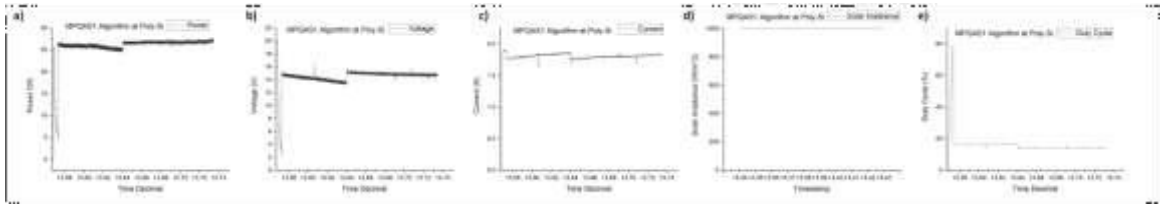


Image 167. MPQAS1 at Polycrystalline Si

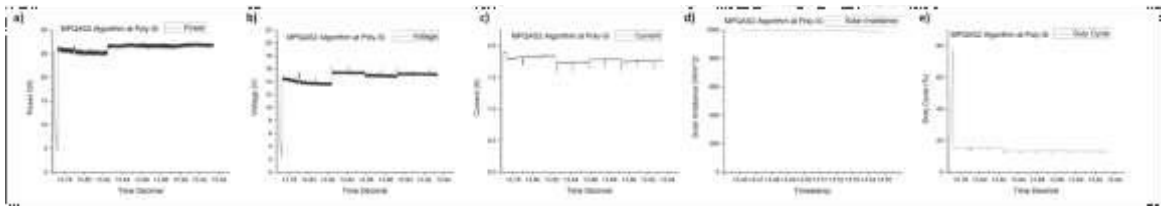


Image 168. MPQAS2 at Polycrystalline Si

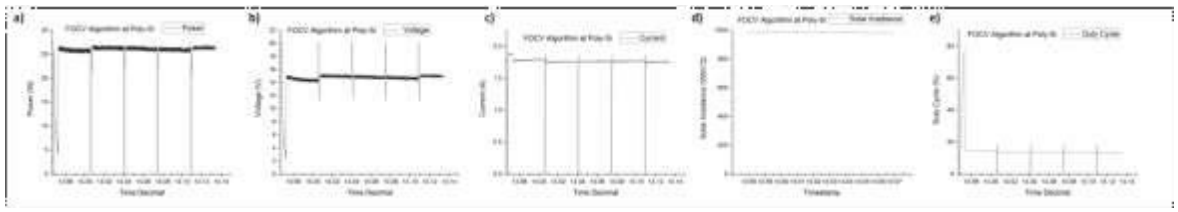


Image 169. FOCV at Polycrystalline Si

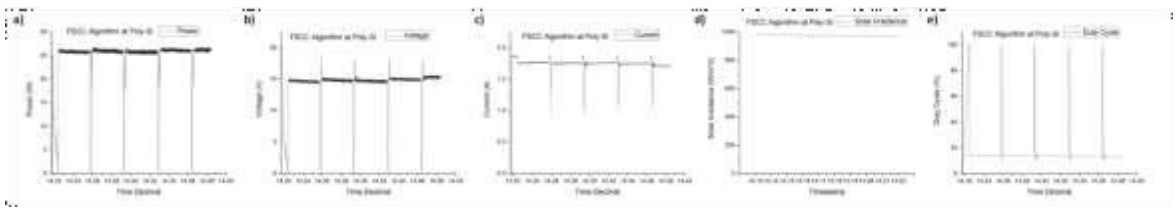


Image 170. FSCC at Polycrystalline Si

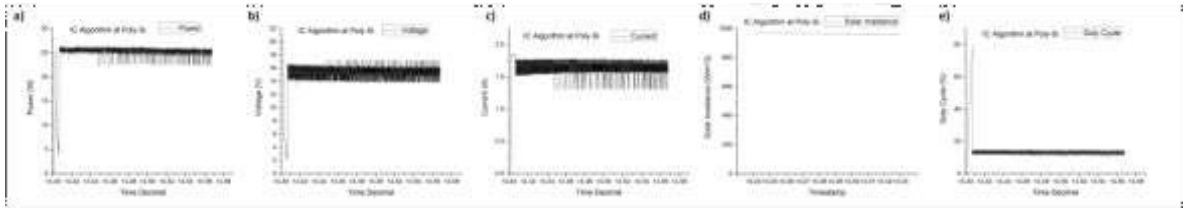


Image 171. IC at Polycrystalline Si

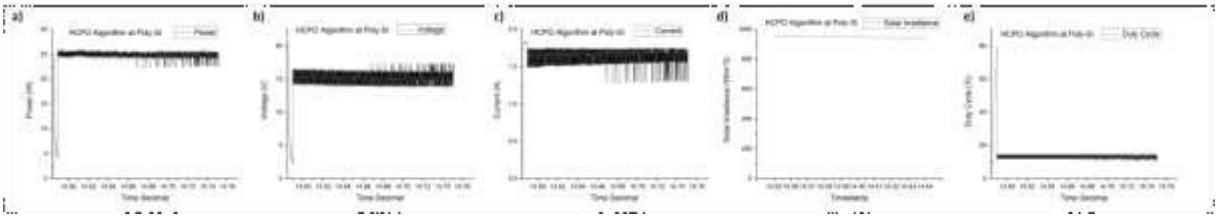


Image 172. HCPO at Polycrystalline Si

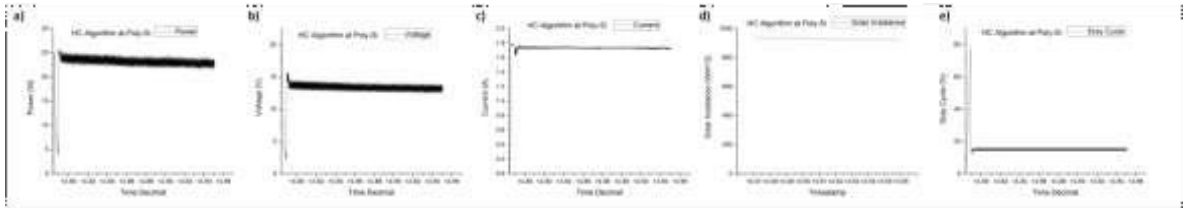


Image 173. HC at Polycrystalline Si

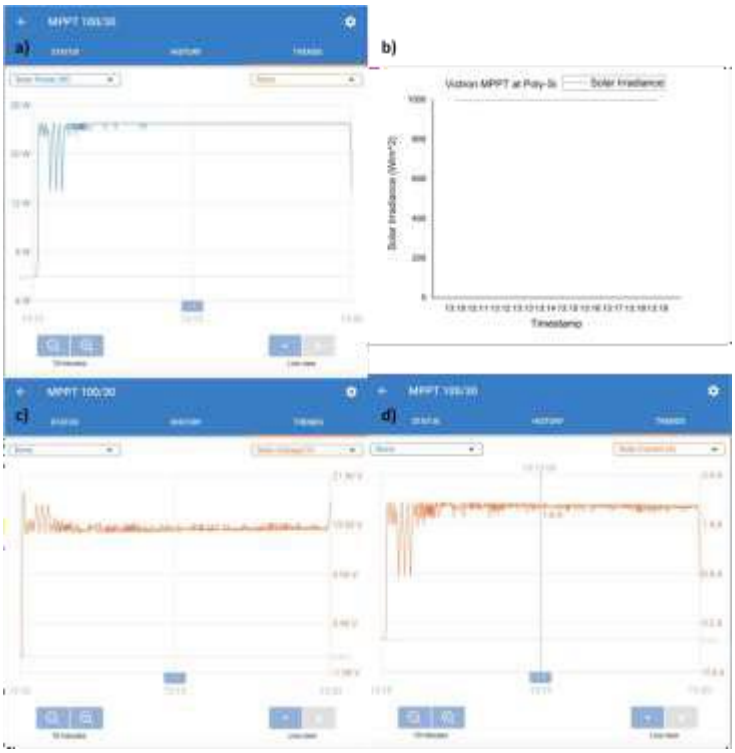


Image 174. Commercial Victron Energy MPPT Graphs at Poly-Si, ***a)*** *Power - Time,* ***b)*** *Irradiance - Time,* ***c)*** *Voltage - Time,* ***d)*** *Current - Time*

6.3.3 All MPPT Algorithms Comparison with a Commercial Device Algorithm at GRAPES PV Technology in Cloudy Sky

At this experiment, created a table for GRAPES technology for comparison all IV-MPPT Charger Regulator MPPT algorithms with commercial device Victron energy BlueSolar charge controller MPPT 100|30 in cloudy sky. For each MPPT algorithm created, five graphs, **a)** Power - Time, **b)** Voltage - Time, **c)** Current - Time, **d)** Irradiance - Time, **e)** Duty Cycle - Time, for total 53 graphs. All measurement was taken for 10 minutes.

Photovoltaic GRAPES#7 (20/07/2021), Cloudy Day, 10 minutes each measurement	Victron Energy© BlueSolar Charge Controller MPTP 100|30	MPQAS1	MPQAS2	MPQAS1 Extremely Cloudy	MPQAS2 Extremely Cloudy	FOCV	FSCC	IC	HCPO	HC
E.Y. from the Sun for each Algorithm (Wh/m^2)	165.667	167.633	166.750	12.302	17.350	166.017	165.533	165.533	153.650	164.182
Algorithms Energy Yield (Wh/m^2)	0.720	1.196	1.107	5.451	4.097	1.030	1.011	0.887	0.915	0.771
Total GRAPES#7_Algorithms Efficiency n(%)	0.435	0.713	0.664	0.302	0.306	0.620	0.611	0.536	0.595	0.470
Comparison Commercial with Handmade MPPT		39.078	34.512	13.833	11.687	29.937	28.832	18.889	26.993	7.473

Image 175. GRAPES#7 Comparison Table Cloudy sky

From table of Image 175., observed that the best algorithms for GRAPES#7 photovoltaic, are the innovative algorithms MPQAS1 & 2 with 0.713% & 0.664% respectively total efficiency and FOCV with 0.62%. Also MPQAS1 has 39.078% bigger efficiency than the commercial device MPPT which has 0.713% total efficiency, FOCV has 29.937% bigger efficiency and the MPQAS2 has 34.412% bigger in turn. A test became in extremely cloudy sky and shown that MPQAS2 algorithm is slightly better than MPQAS1 in this situation.

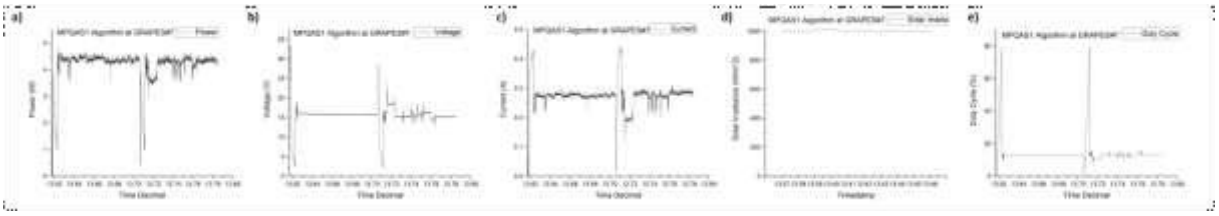


Image 176. MPQAS1 at GRAPES#7

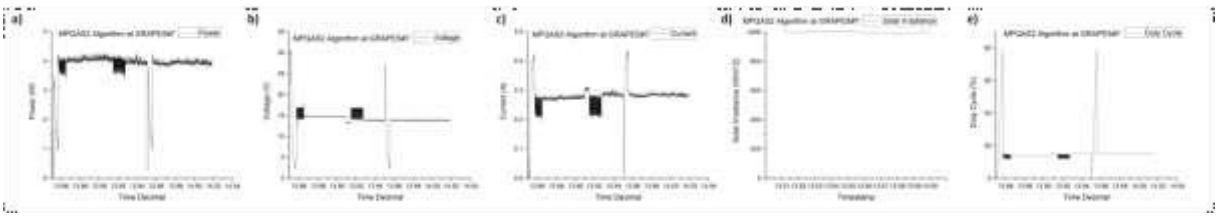


Image 177. MPQAS2 at GRAPES#7

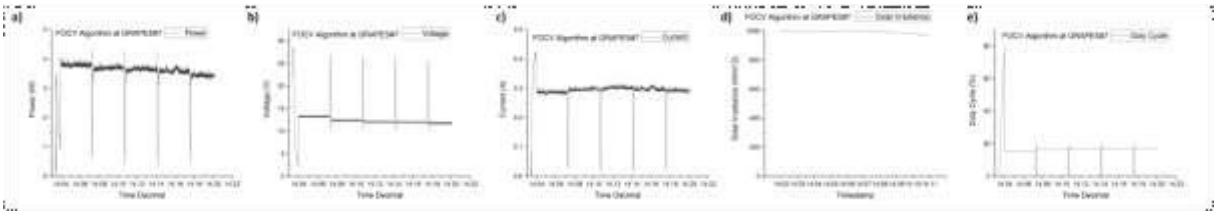


Image 178. FOCV at GRAPES#7

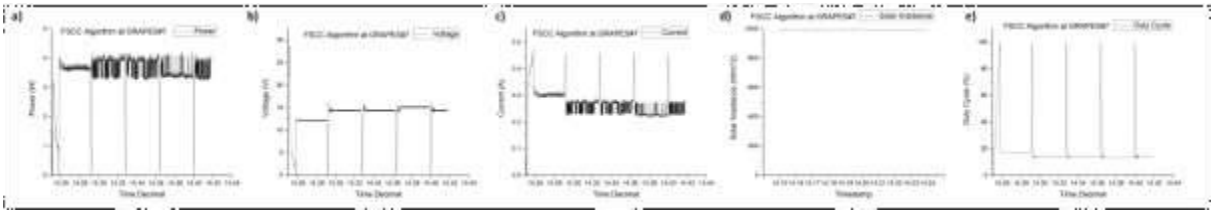


Image 179. FSCC at GRAPES#7

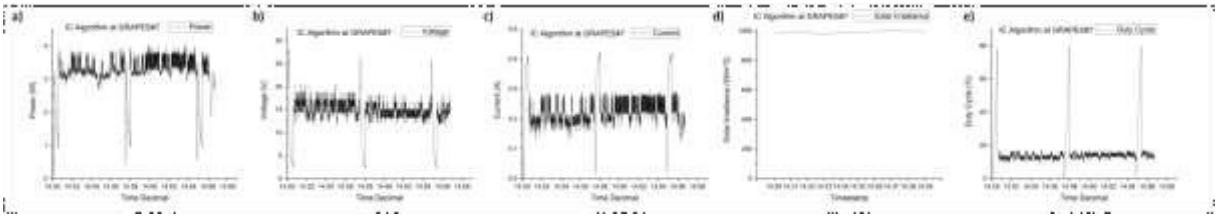


Image 180. IC at GRAPES#7

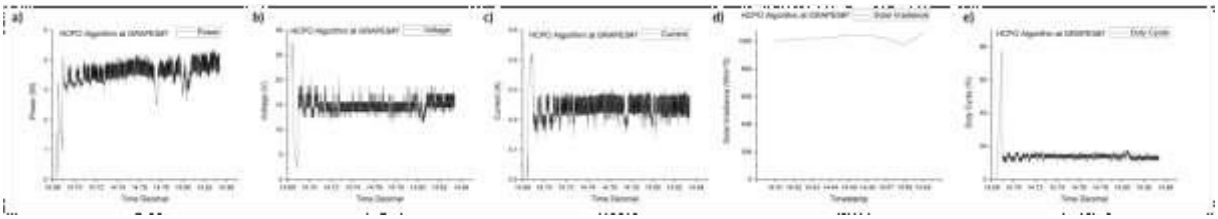


Image 181. HCPO at GRAPES#7

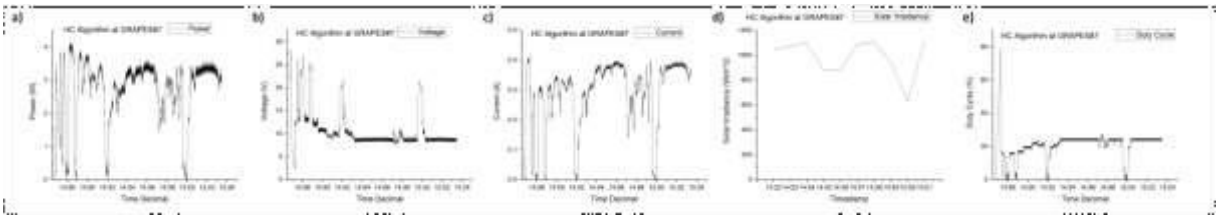


Image 182. HC at GRAPES#7



Image 183. Commercial Victron Energy MPPT Graphs at Poly-Si, ***a)*** *Power - Time,* ***b)*** *Irradiance - Time,* ***c)*** *Voltage - Time,* ***d)*** *Current - Time*

Continuous, with extremely cloud sky for the MPQAS1 and MPAQAS2 algorithms.

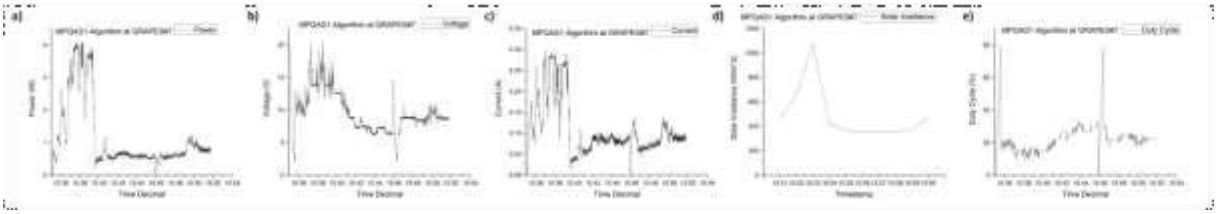


Image 184. Extremely Cloudy Sky, MPQAS1 at GRAPES#7

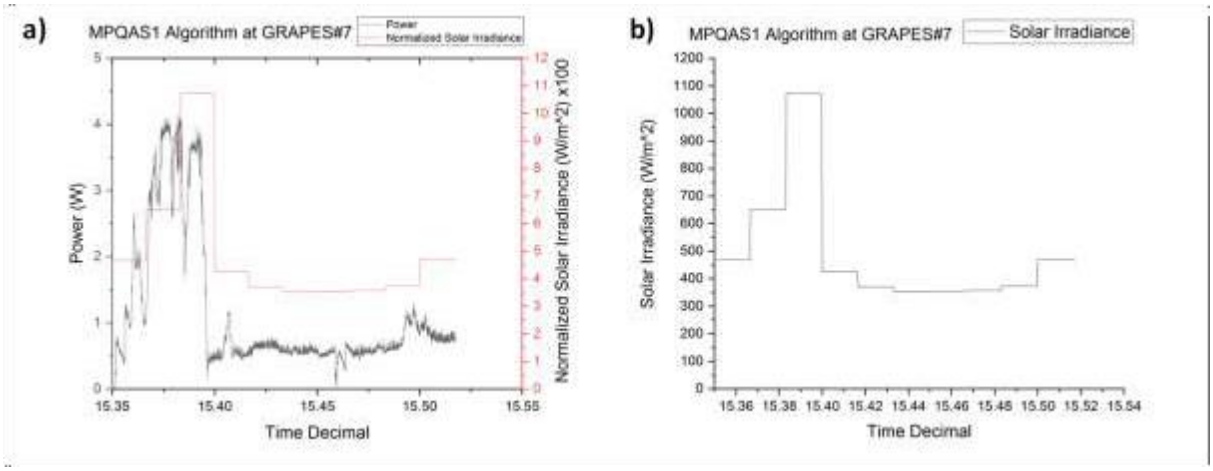


*Image 185. Extremely Cloudy Sky, MPQAS1 at GRAPES#7, **a)** Double Y Graph of Power and Normalized Solar Irradiance - Time, **b)** Solar Irradiance - Time Decimal Graph*

At Image 185. observed, that the MPQAS1 algorithms follows solar irradiance precisely. Follow graphs of MPQAS2.

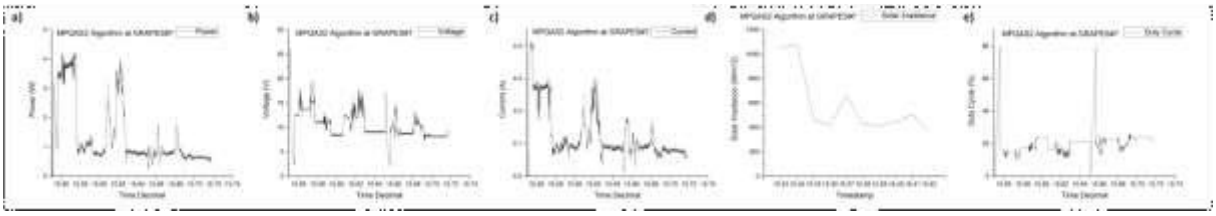


Image 186. Extremely Cloudy Sky, MPQAS2 at GRAPES#7

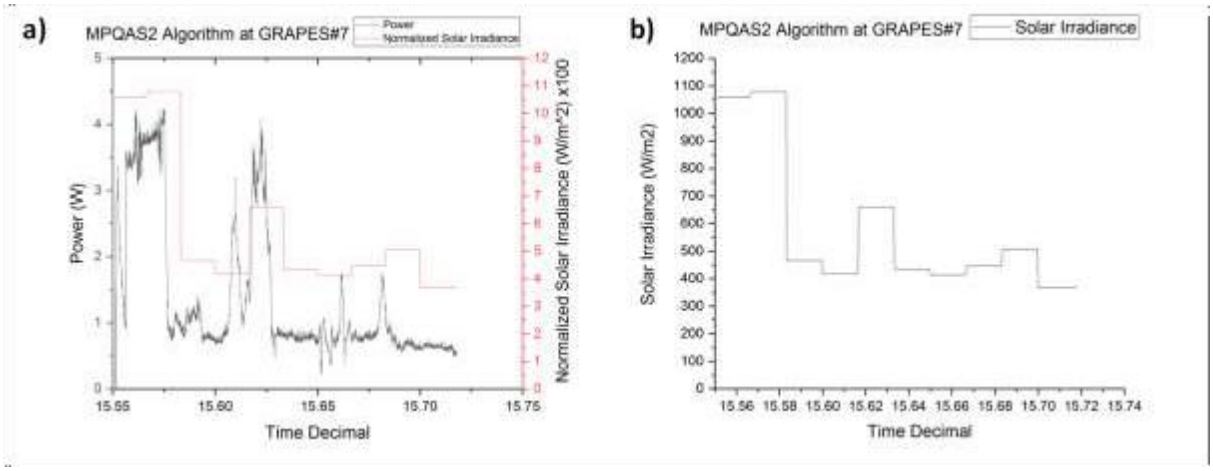


*Image 187. Extremely Cloudy Sky, MPQAS2 at GRAPES#7, **a)** Double Y Graph of Power and Normalized Solar Irradiance - Time, **b)** Solar Irradiance - Time Decimal Graph*

At Image 187. observed, that the MPQAS2 algorithms follows solar irradiance precisely too like MPQAS1. Changes in solar irradiation meaning instant changes in power.

6.4 Photovoltaics Behaviour Reading Algorithms Measurements and Experiments

This experiment has two parts, first the Pmax to Open Circuit Intervals (POCI Algorithm), to check the degradation of PV on sun exposure in real time and second the Pmax to Short Circuit Intervals (PSCI Algorithm), to check the degradation of PV on supply load. In two experiments, every 10 minutes changes on delays of intervals done, the delays in seconds are: 2, 10, 20, 30, 60, also every 5 minutes RES IV-Curve for re-calibration done.

6.4.1 Pmax Open Circuit Intervals Measurements

The POCI experiment starts at 13:15 and finished 14:44, observed that gradually losses power max (see Image 188.d.), due to sun exposure. The slope of Pmax - Time of the calculation of Image 188.d. is: Slope = -0.23915.

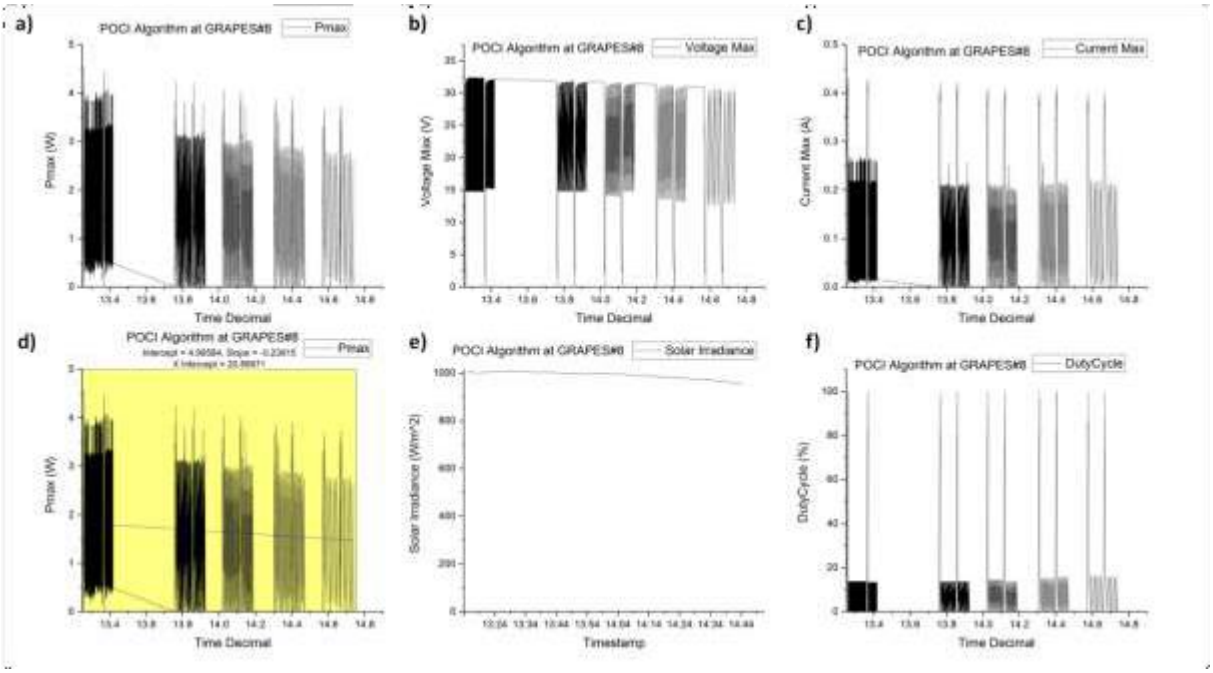


*Image 188. POCI Algorithm Graphs, **a)** Power Max - Time, **b)** Voltage Max - Time, **c)** Current Max - Time, **d)** Power Max degradation slope, **e)** Irradiance - Time, **f)** Duty Cycle - Time, at GRAPES#8 (26/07/2021)*

6.4.2 Pmax Short Circuit Intervals Measurements

After the POCI experiment, follows immediately the PSCI experiment, starts at 15:00 and finished at 16:13, observed that gradually losses power max (see Image 189.d.), due to supply load. The slope of Pmax - Time of the calculation of Image 189.d. is: Slope = -0.4096.

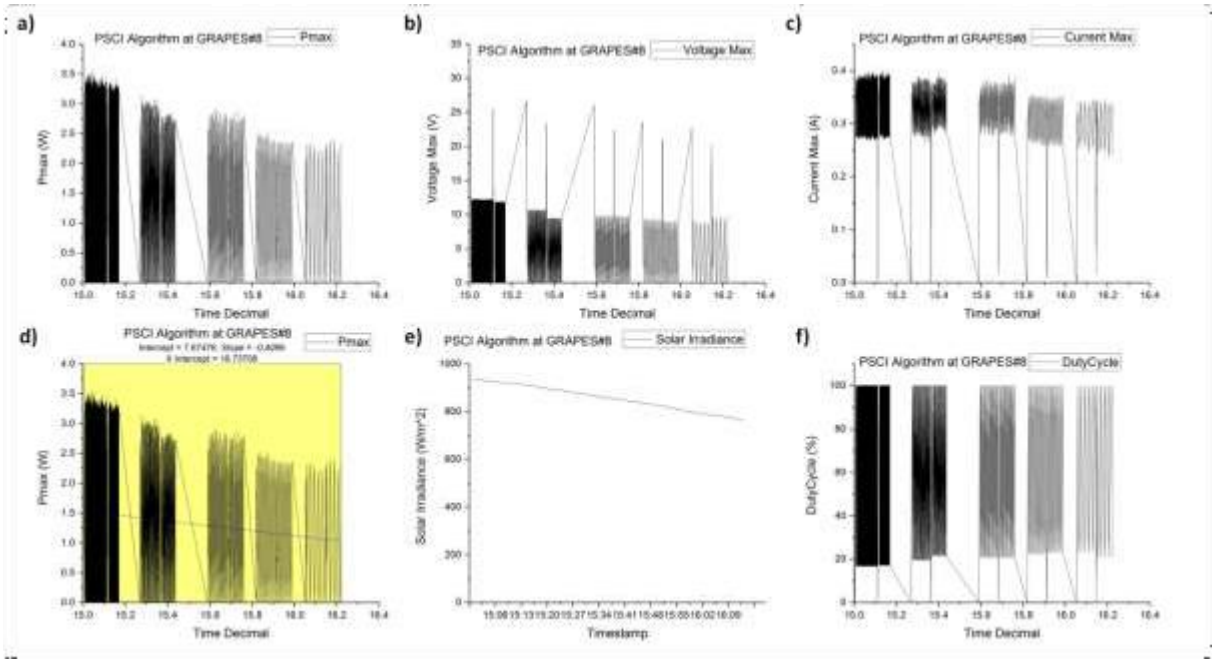


*Image 189. PSCI Algorithm Graphs, **a)** Power Max - Time, **b)** Voltage Max - Time, **c)** Current Max - Time, **d)** Power Max degradation slope, **e)** Irradiance - Time, **f)** Duty Cycle - Time, at GRAPES#8 (26/07/2021)*

From the comparison of the two experiments, observed that PSCI experiment, has 41.61% bigger slope than POCI experiment, this is happened because already exposed 1 hour and 45 minutes at the sun and about 1hour and 13 minutes is under short circuit at different delay intervals, also 1 hour for light soaking at the start, for a total exposure ~4 hours (12:15 to 16:13), also the solar irradiation starts to decrease with higher rate than the first experiment.

Discussion - Conclusions - Future Development

Summarizing, the future energy will originate from the renewable energy sources and specifically from the rising of the innovative photovoltaic technologies, such as GRAPES because of the tunable bandgap, it's stability and low fabrication method cost compared to conventional Si photovoltaic technology Czochralski method, also the tandem, and quantum dots concepts which surpass the Queisser limit.

So the fabrication purpose of innovative full programmable IV - MPPT Charger Regulator device is to run different IV, MPPT, PVBR algorithms to study efficient the behaviour of the innovative GRAPES Photovoltaics and other technologies such as CdTe , Si, etc., in real time outdoor conditions, also simultaneously charging the batteries.

Observed that the hysteresis effect is measure of degradation of GRAPES PVs, also the sun exposure and supply a load degrade it, if the GRAPES not exposured at the sun, they start regenerate their PCE due to activated meta stable trap states that relax in dark returning the device to its steady state.

Also observed that the RFES IV algorithm is less stressful on the GRAPES PVs and has the less hysteresis production than the other IV algorithms, in addition observed that as the average points raise the hysteresis decrease and we have smaller S-Shape IV Curves but the cost is on time acquisition.

At GRAPES PVs the current is proportional to solar irradiation and the voltage is almost proportional, that was the motivation for creation of innovative FOCV algorithm and measurements shown, that is the best algorithm for GRAPES and from the FOCV knowledge, created the innovative algorithms MPQAS1 and MPQAS2 which shown from the comparison experiments, that was the best algorithms for every PV technology on this device.

Future Development

In the future development of this master thesis, can upgraded the IV-MPPT Charger Regulator device, with new innovative algorithms such MPQAS3 or MPQAS4 with combination of FOCV and IC or HCPO algorithms for better performance, or even upgrade the hardware system with bigger cooling system or extra mosfets for more power drive, also new graphical interfaces like LabVIEW© or MATLAB© and last new research experiments can also be done.

Bibliography - References

1. Introduction

[1] tinyurl.com/4sxtumem (Accessed 01/09/2021)

[2] tinyurl.com/fvpvv9mp (Accessed 01/09/2021)

[3] tinyurl.com/yrv4y3h6 (Accessed 01/09/2021)

[4] tinyurl.com/z28h834b (Accessed 14/09/2021)

[5] tinyurl.com/2jdu36w6 (Accessed 02/09/2021)

[6] Hellenic Mediterranean University notes of course "Introduction of Renewable Energy", George Viskadouros, John Fragiadakis, Fotis Mauromatakis, (2015)

[7] tinyurl.com/wzy7xy4 (Accessed 02/09/2021)

[8] tinyurl.com/ymuwwfmt (Accessed 04/09/2021)

[9] tinyurl.com/ehhavvax (Accessed 04/09/2021)

[10] tinyurl.com/2n2cemxu (Accessed 04/09/2021)

[11] tinyurl.com/4r66xnaf (Accessed 05/09/2021)

[12] tinyurl.com/n4eut93e (Accessed 05/09/2021)

[13] tinyurl.com/afyted7w (Accessed 05/09/2021)

[14] tinyurl.com/3rr57hcu (Accessed 05/09/2021)

[15] tinyurl.com/2mvbetb7 (Accessed 05/09/2021)

[16] tinyurl.com/5ew4pxj4 (Accessed 05/09/2021)

[17] tinyurl.com/kf2f54u9 (Accessed 05/09/2021)

[18] WILLIAM SHOCKLEY AND HANS J. QUEISSER (1961), JOURNAL OF APPLIED PHYSICS

[19] Rühle, S. (2016),Elsevier Solar Energy,130,139–147. doi:10.1016/j.solener.2016.02.015

[20] Hellenic Mediterranean University, Inter-institutional Master in Science Nanotechnology for Energy Applications notes of course "Energy Devices", Marinos Tountas, Dimitris Tsikritzis, (2019)

[21] tinyurl.com/j3tmjrxd (Accessed 06/09/2021)

[22] tinyurl.com/k8k7kc83 (Accessed 07/09/2021)

[23] tinyurl.com/3522hmtp (Accessed 07/09/2021)

[24] tinyurl.com/5hxbnu4d (Accessed 07/09/2021)

2. Theory

[25] tinyurl.com/z8djj3jb (Accessed 08/09/2021)

[26] tinyurl.com/yb9f975h (Accessed 09/09/2021)

[27] tinyurl.com/eyhaywcn (Accessed 09/09/2021)

[28] Hellenic Mediterranean University, Inter-institutional Master in Science Nanotechnology for Energy Applications notes of course "Devices Processing Techniques and Characterization Methods" , Emmanuel Stratakis, Miron Krassas, Kyriaki Savva (2017)

[29] Hongwei Zhu 2018, Graphene: Fabrication, Characterizations, Properties and Applications, 978-0-12-812651-6 (ISBN).

[30] National University of Singapore, Centre of Advanced 2D Materials tinyurl.com/hfycfzbf (Accessed 10/09/2021)

[31] Weiss, N. O.,et al. , (2012), Advanced Materials, 24(43), 5782–5825. doi:10.1002/adma.201201482

[32] Md.SajibulAlamBhuyan et al. , International Nano Letters, (June 2016), Volume 6, Issue 2, pp 65–83

[33] tinyurl.com/4hdsux49 (Accessed 11/09/2021)

[34] Bellani, S., et al., Advanced Functional Materials, (2019), 1807659. doi:10.1002/adfm.201807659

[35] tinyurl.com/b747kb8s (Accessed 12/09/2021)

[36] He, Z., & Que, W. (2016). Molybdenum disulfide nanomaterials: Structures, properties, synthesis and recent progress on hydrogen evolution reaction. Applied Materials Today, 3, 23–56. doi:10.1016/j.apmt.2016.02.001

[37] tinyurl.com/2tj6d2xz (Accessed 12/09/2021)

3. Fabrication of the Electronic Device of IV-MPPT Charger Regulator

[38] tinyurl.com/bpb78taf (Accessed 13/09/2021)

[39] tinyurl.com/42a2d3u7(Accessed 13/09/2021)

[40] Hellenic Mediterranean University notes of course "Power Electronics", D.Pylarinos, (2017)

[41] tinyurl.com/4rbsvzhx (Accessed 13/09/2021)

[42] tinyurl.com/38mwjbtj (Accessed 17/09/2021)

[43] tinyurl.com/wjmvxj7c (Accessed 17/09/2021)

[44] tinyurl.com/ewcteuvy (Accessed 17/09/2021)

[45] tinyurl.com/35attf3a (Accessed 19/09/2021)

[46] tinyurl.com/55c59ar5 (Accessed 19/09/2021)

4. Algorithms of IV-MPPT Charger Regulator

[47] Billel Talbi. et all., Journal of Renewable and Sustainable Energy 9, 043503, (2017), doi: 10.1063/1.4999961

[48] Ahmed Ebrahim, et all., In book: Electric Power Conversion, (2019), doi:10.5772/intechopen.82302

[49] Saravana Selvan. et all., International Journal of Electrical and Computer Engineering (IJECE), Vol. 6, No. 2, (April 2016), pp. 567~582 ISSN: 2088-8708, DOI: 10.11591/ijece.v6i2.9204

[50] D. P. Hohm and M. E. Ropp, PROGRESS IN PHOTOVOLTAICS: RESEARCH AND APPLICATIONS Prog. Photovolt: Res. Appl. (2003), 11:47–62 (DOI: 10.1002/pip.459)

[51] Madhusmita MOHANTY. et all., Turkish Journal of Electrical Engineering & Computer Sciences, (2019) 27: 4640 – 4658 © TÜBİTAK, doi:10.3906/elk-1805-108

[52] tinyurl.com/5hejunvd (Accessed 28/09/2021)

[53] tinyurl.com/ahhvmk4y (Accessed 28/09/2021)

[54] tinyurl.com/8k37b58 (Accessed 28/09/2021)

[55] tinyurl.com/4r5v4cnh (Accessed 28/09/2021)

6. Experimental Measurements of IV-MPPT Charger Regulator

[56] Juan Bisquert, et all., (2021), ACS Physical Chemistry Au. , doi.org/10.1021/acsphyschemau.1c00009

[57] Tao Song, et all., (2021), Advanced Energy Materials, doi.org/10.1002/aenm.202100728

[58] tinyurl.com/bbj3dxmt (Accessed 03/10/2021)

[59] tinyurl.com/yd7c7ubp (Accessed 03/10/2021)

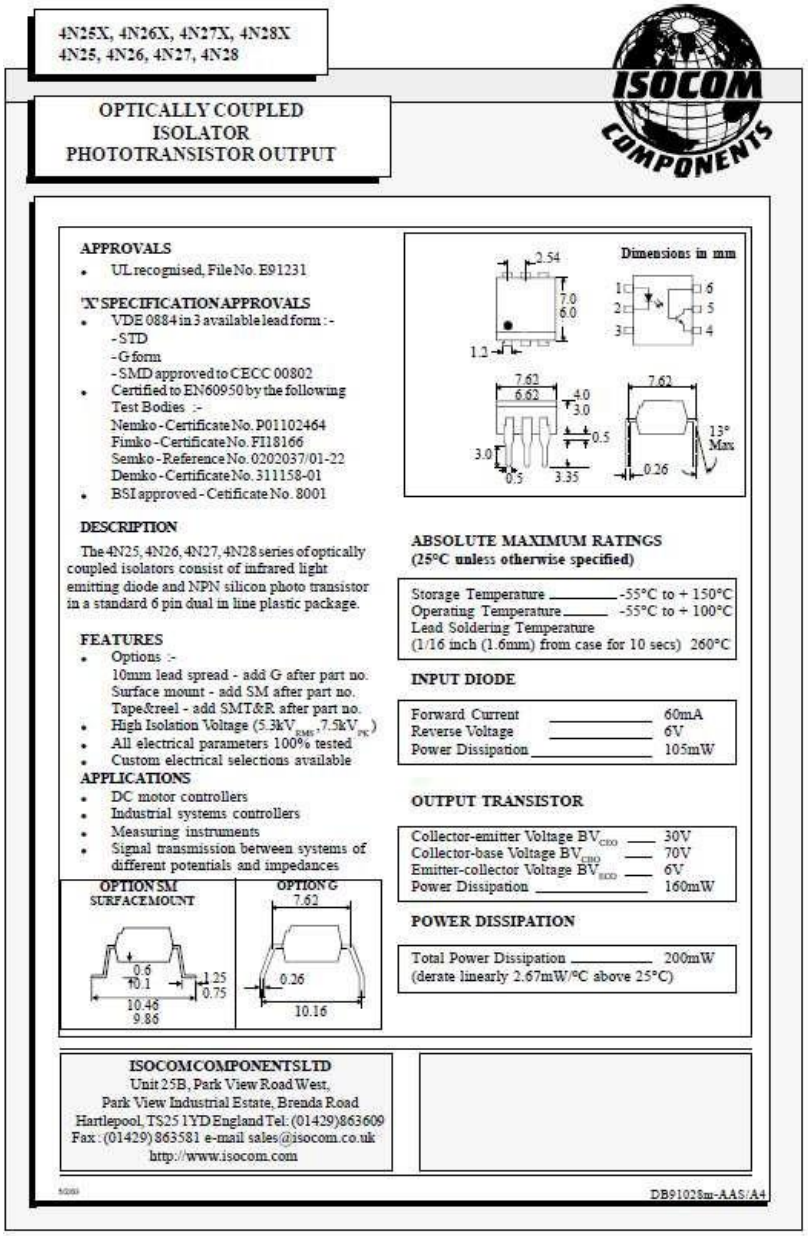
[60] Nie, W., Blancon, JC., Neukirch, A. et al. Light-activated photocurrent degradation and self-healing in perovskite solar cells. Nat Commun 7, 11574 (2016). https://doi.org/10.1038/ncomms11574

Supporting Information - Annex

ANNEX - APPLICATION CODE FOR IV-MPPT Charger Regulator Device

The IV-MPPT Charger Regulator device's application file: IV-MPPT_Charger_Regulator.ino, and the datalogger file in MicrosoftExcel with the name PLX-DAQ-v2.11, can be requested from the laboratory of Electronics of the Department of Electrical & Computer Engineering of the Hellenic Mediterranean University of Crete, or send a personal message to e-mail: john_kalogerakis_12@hotmail.com to have the application files sent to you.

Datasheets of device materials:



4N25X, 4N26X, 4N27X, 4N28X
4N25, 4N26, 4N27, 4N28

OPTICALLY COUPLED
ISOLATOR
PHOTOTRANSISTOR OUTPUT

ISOCOM COMPONENTS

APPROVALS
- UL recognised, File No. E91231

'X' SPECIFICATION APPROVALS
- VDE 0884 in 3 available lead form :-
  - STD
  - G form
  - SMD approved to CECC 00802
- Certified to EN60950 by the following Test Bodies :-
  Nemko - Certificate No. P01102464
  Fimko - Certificate No. FI18166
  Semko - Reference No. 0202037/01-22
  Demko - Certificate No. 311158-01
- BSI approved - Cetificate No. 8001

DESCRIPTION

The 4N25, 4N26, 4N27, 4N28 series of optically coupled isolators consist of infrared light emitting diode and NPN silicon photo transistor in a standard 6 pin dual in line plastic package.

FEATURES
- Options :-
  10mm lead spread - add G after part no.
  Surface mount - add SM after part no.
  Tape&reel - add SMT&R after part no.
- High Isolation Voltage (5.3kV$_{RMS}$, 7.5kV$_{PK}$)
- All electrical parameters 100% tested
- Custom electrical selections available

APPLICATIONS
- DC motor controllers
- Industrial systems controllers
- Measuring instruments
- Signal transmission between systems of different potentials and impedances

Dimensions in mm

ABSOLUTE MAXIMUM RATINGS
(25°C unless otherwise specified)

Storage Temperature	-55°C to + 150°C
Operating Temperature	-55°C to + 100°C
Lead Soldering Temperature (1/16 inch (1.6mm) from case for 10 secs)	260°C

INPUT DIODE

Forward Current	60mA
Reverse Voltage	6V
Power Dissipation	105mW

OUTPUT TRANSISTOR

Collector-emitter Voltage BV$_{CEO}$	30V
Collector-base Voltage BV$_{CBO}$	70V
Emitter-collector Voltage BV$_{ECO}$	6V
Power Dissipation	160mW

POWER DISSIPATION

Total Power Dissipation	200mW
(derate linearly 2.67mW/°C above 25°C)	

OPTION SM
SURFACE MOUNT

OPTION G

ISOCOM COMPONENTS LTD
Unit 25B, Park View Road West,
Park View Industrial Estate, Brenda Road
Hartlepool, TS25 1YD England Tel: (01429)863609
Fax : (01429) 863581 e-mail sales@isocom.co.uk
http://www.isocom.com

DB91028m-AAS/A4

Image 190. Datasheet of 4n25 Optocoupler



MICROCHIP

ATmega640/V-1280/V-1281/V-2560/V-2561/V

8-bit Microcontroller with 16/32/64KB In-System Programmable Flash

DATASHEET

Features

- High Performance, Low Power AVR® 8-Bit Microcontroller
- Advanced RISC Architecture
  - 135 Powerful Instructions – Most Single Clock Cycle Execution
  - 32 × 8 General Purpose Working Registers
  - Fully Static Operation
  - Up to 16 MIPS Throughput at 16MHz
  - On-Chip 2-cycle Multiplier
- High Endurance Non-volatile Memory Segments
  - 64K/128K/256KBytes of In-System Self-Programmable Flash
  - 4Kbytes EEPROM
  - 8Kbytes Internal SRAM
  - Write/Erase Cycles:10,000 Flash/100,000 EEPROM
  - Data retention: 20 years at 85°C/ 100 years at 25°C
  - Optional Boot Code Section with Independent Lock Bits
    - In-System Programming by On-chip Boot Program
    - True Read-While-Write Operation

Image 191. Datasheet of microcontroller Arduino®Mega2560



TDK

Power line chokes **B82725S2***

Current-compensated ring core double chokes

Rated voltage 250 V AC
Rated inductance 1.4 ... 7.8 mH
Rated current 6 ... 13 A, +60 °C, +70 °C

Construction

- Current-compensated ring core double choke
- Ferrite core with epoxy coating (UL 94 V-0)
- Plastic base plate (UL 94 V-0)
- Plastic spacer (UL 94 V-0, CTI 600)
- Coil fixed on base plate with tape
- Sector winding
- Clearance ≥ 2.5 mm, creepage distance ≥ 3 mm

Features

- High resonance frequency
- Approx. 0.5 ... 1% stray inductance for symmetrical interference suppression
- Suitable for wave soldering
- Design complies with EN 60938-2 (VDE 0565-2) and UL 1283
- B82725S2133N040: UL 1446 class 155(F) electrical insulation system
- RoHS-compatible

Applications

- Suppression of common-mode interferences
- Switch-mode power applications
- Frequency converters

Terminals

- Ends of winding wires
- Hot-dip tinned

Marking

- Product brand, electrical insulation system designation (only B82725S2133N040), ordering code, graphic symbol, rated current, rated voltage, rated inductance, date of manufacture (YYWWD.Internal ID code), production place identification code

Delivery mode

- Blister tray in cardboard box

Image 192. Datasheet of Inductor

JCET

JIANGSU CHANGJIANG ELECTRONICS TECHNOLOGY CO., LTD

TO-92 Plastic-Encap sulate Transistors

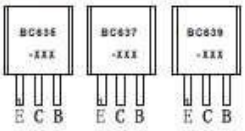
BC635 / BC637 / BC639 TRANSISTOR (NPN)



FEATURES

- High current transistors

MARKING

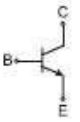


BC635,BC637,BC639=Device code

Solid dot=Green molding compound device, If none,the normal device

XXX=Code

Equivalent Circuit



ORDERING INFORMATION

Part Number	Package	Packing Method	Pack Quantity
BC635	TO-92	Bulk	1000pcs/Bag
BC635-TA	TO-92	Tape	2000pcs/Box
BC637	TO-92	Bulk	1000pcs/Bag
BC637-TA	TO-92	Tape	2000pcs/Box
BC639	TO-92	Bulk	1000pcs/Bag
BC639-TA	TO-92	Tape	2000pcs/Box

MAXIMUM RATINGS (T_A=25°C unless otherwise noted)

Symbol	Parameter		Value	Unit
V_{CBO}	Collector-Emitter Voltage	BC635	45	V
		BC637	60	V
		BC639	100	V
V_{CEO}	Collector-Emitter Voltage	BC635	45	V
		BC637	60	V
		BC639	80	V
V_{EBO}	Emitter-Base Voltage		5	V
I_C	Collector Current -Continuous		1	A
P_C	Collector Power Dissipation		0.83	W
T_J	Junction Temperature		150	°C
T_{stg}	Storage Temperature		-65-150	°C

Image 193. Datasheet of BC639

BC636...BC640

PNP Silicon Epitaxial Planar Transistor

Medium Power Transistors
for audio and video amplifiers



1. Emitter 2. Collector 3. Base
TO-92 Plastic Package

Absolute Maximum Ratings (T_a = 25 °C)

Parameter		Symbol	Value	Unit
Collector Base Voltage	BC636 BC638 BC640	$-V_{CBO}$	45 60 100	V
Collector Emitter Voltage	BC636 BC638 BC640	$-V_{CEO}$	45 60 80	V
Emitter Base Voltage		$-V_{EBO}$	5	V
Collector Current		$-I_C$	1	A
Peak Collector Current		$-I_{CM}$	1.5	A
Base Current		$-I_B$	100	mA
Peak Base Current		$-I_{BM}$	200	mA
Power Dissipation		P_{tot}	830	mW
Junction Temperature		T_j	150	°C
Storage Temperature Range		T_{stg}	- 65 to + 150	°C

Image 194. Datasheet of BC640

IXYS DSA50C100QB

Schottky Diode Gen 2

V_{RRM} = 100V
I_{FAV} = 2x 25A
V_F = 0.72V

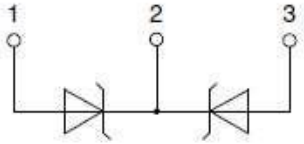
High Performance Schottky Diode
Low Loss and Soft Recovery
Common Cathode

Part number

DSA50C100QB



Backside: cathode



Features / Advantages:
- Very low Vf
- Extremely low switching losses
- Low Irm values
- Improved thermal behaviour
- High reliability circuit operation
- Low voltage peaks for reduced protection circuits
- Low noise switching

Applications:
- Rectifiers in switch mode power supplies (SMPS)
- Free wheeling diode in low voltage converters

Package: TO-3P
- Industry standard outline compatible with TO-247
- RoHS compliant
- Epoxy meets UL 94V-0

Image 195. Datasheet of Diode DSA50C100QB

International
IOR Rectifier

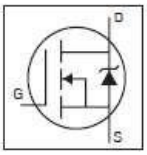
PD - 97369

IRLB4030PbF

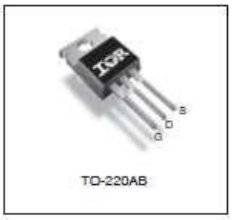
Applications
- DC Motor Drive
- High Efficiency Synchronous Rectification in SMPS
- Uninterruptible Power Supply
- High Speed Power Switching
- Hard Switched and High Frequency Circuits

Benefits
- Optimized for Logic Level Drive
- Very Low $R_{DS(ON)}$ at 4.5V V_{GS}
- Superior R*Q at 4.5V V_{GS}
- Improved Gate, Avalanche and Dynamic dV/dt Ruggedness
- Fully Characterized Capacitance and Avalanche SOA
- Enhanced body diode dV/dt and dI/dt Capability
- Lead-Free

HEXFET® Power MOSFET



V_{DSS}		100V
$R_{DS(on)}$	typ.	3.4mΩ
	max.	4.3mΩ
I_D		180A



TO-220AB

G	D	S
Gate	Drain	Source

Image 196. Datasheet of Mosfet IRLB4030Pbf



TEXAS INSTRUMENTS

LM117, LM317A, LM317-N

www.ti.com

SNVS774D – MAY 2004 – REVISED JANUARY 2016

LM117/LM317A/LM317-N Three-Terminal Adjustable Regulator

Check for Samples: LM117, LM317A, LM317-N

FEATURES

- Specified 1% Output Voltage Tolerance (LM317A)
- Specified max. 0.01%/V Line Regulation (LM317A)
- Specified max. 0.3% Load Regulation (LM117)
- Specified 1.5A Output Current
- Adjustable Output Down to 1.2V
- Current Limit Constant with Temperature
- P+ Product Enhancement tested
- 80 dB Ripple Rejection
- Output is Short-Circuit Protected

DESCRIPTION

The LM117 series of adjustable 3-terminal positive voltage regulators is capable of supplying in excess of 1.5A over a 1.2V to 37V output range. They are exceptionally easy to use and require only two external resistors to set the output voltage. Further, both line and load regulation are better than standard fixed regulators. Also, the LM117 is packaged in standard transistor packages which are easily mounted and handled.

In addition to higher performance than fixed regulators, the LM117 series offers full overload protection available only in IC's. Included on the chip are current limit, thermal overload protection and safe area protection. All overload protection circuitry remains fully functional even if the adjustment terminal is disconnected.

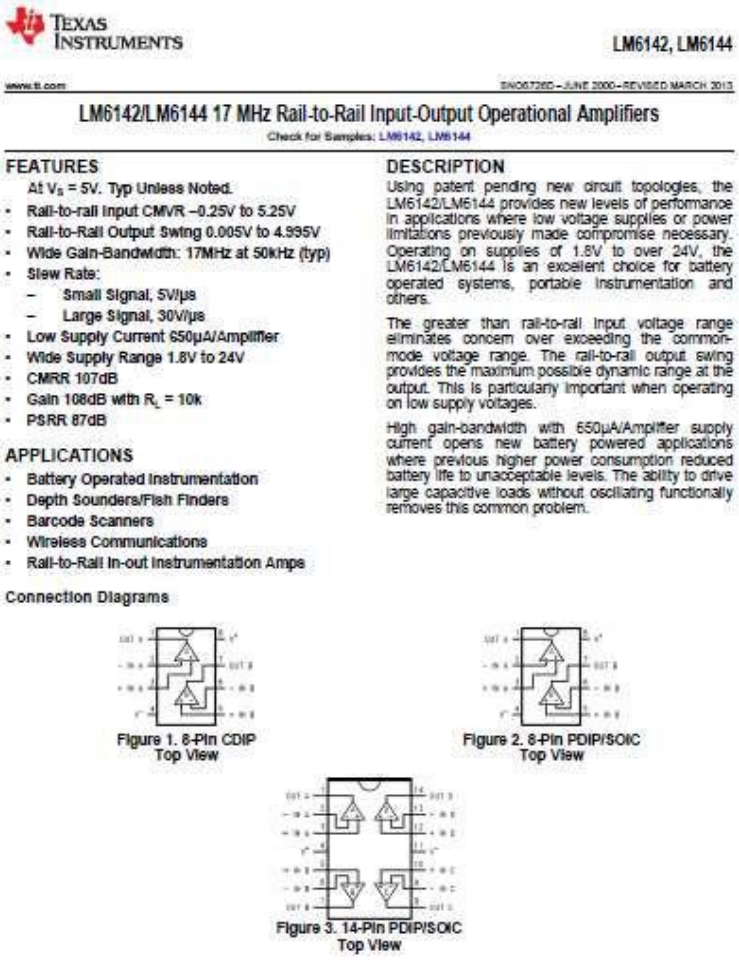
Normally, no capacitors are needed unless the device is situated more than 6 inches from the input filter capacitors in which case an input bypass is needed. An optional output capacitor can be added to improve transient response. The adjustment terminal can be bypassed to achieve very high ripple rejection ratios which are difficult to achieve with standard 3-terminal regulators.

Besides replacing fixed regulators, the LM117 is useful in a wide variety of other applications. Since the regulator is "floating" and sees only the input-to-output differential voltage, supplies of several hundred volts can be regulated as long as the maximum input to output differential is not exceeded, i.e., avoid short-circuiting the output.

Also, it makes an especially simple adjustable switching regulator, a programmable output regulator, or by connecting a fixed resistor between the adjustment pin and output, the LM117 can be used as a precision current regulator. Supplies with electronic shutdown can be achieved by clamping the adjustment terminal to ground which programs the output to 1.2V where most loads draw little current.

For applications requiring greater output current, see LM150 series (3A) and LM138 series (5A) data sheets. For the negative complement, see LM137 series data sheet.

Image 197. Datasheet of Adjustable Regulator LM317T



TEXAS INSTRUMENTS

LM6142, LM6144

www.ti.com

SNOS726D – JUNE 2000 – REVISED MARCH 2013

LM6142/LM6144 17 MHz Rail-to-Rail Input-Output Operational Amplifiers

Check for Samples: LM6142, LM6144

FEATURES

At V_S = 5V. Typ Unless Noted.

- Rail-to-rail Input CMVR −0.25V to 5.25V
- Rail-to-Rail Output Swing 0.005V to 4.995V
- Wide Gain-Bandwidth: 17MHz at 50kHz (typ)
- Slew Rate:
  - Small Signal, 5V/µs
  - Large Signal, 30V/µs
- Low Supply Current 650µA/Amplifier
- Wide Supply Range 1.8V to 24V
- CMRR 107dB
- Gain 108dB with R_L = 10k
- PSRR 87dB

APPLICATIONS

- Battery Operated Instrumentation
- Depth Sounders/Fish Finders
- Barcode Scanners
- Wireless Communications
- Rail-to-Rail In-out Instrumentation Amps

DESCRIPTION

Using patent pending new circuit topologies, the LM6142/LM6144 provides new levels of performance in applications where low voltage supplies or power limitations previously made compromise necessary. Operating on supplies of 1.8V to over 24V, the LM6142/LM6144 is an excellent choice for battery operated systems, portable instrumentation and others.

The greater than rail-to-rail input voltage range eliminates concern over exceeding the common-mode voltage range. The rail-to-rail output swing provides the maximum possible dynamic range at the output. This is particularly important when operating on low supply voltages.

High gain-bandwidth with 650µA/Amplifier supply current opens new battery powered applications where previous higher power consumption reduced battery life to unacceptable levels. The ability to drive large capacitive loads without oscillating functionally removes this common problem.

Connection Diagrams

Figure 1. 8-Pin CDIP
Top View

Figure 2. 8-Pin PDIP/SOIC
Top View

Figure 3. 14-Pin PDIP/SOIC
Top View

Image 198 Datasheet of OPAM LM6142

LM78XX (KA78XX, MC78XX) FIXED VOLTAGE REGULATOR (POSITIVE)

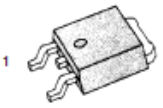
3-TERMINAL 1A POSITIVE VOLTAGE REGULATORS

The LM78XX series of three-terminal positive regulators are available in the TO-220/D-PAK package and with several fixed output voltages, making them useful in a wide range of applications. Each type employs internal current limiting, thermal shut-down and safe area protection, making it essentially indestructible. If adequate heat sinking is provided, they can deliver over 1A output current. Although designed primarily as fixed voltage regulators, these devices can be used with external components to obtain adjustable voltages and currents.

TO-220



D-PAK



1: Input 2: GND 3: Output

FEATURES

- Output Current up to 1A
- Output Voltages of 5, 6, 8, 9, 10, 11, 12, 15, 18, 24V
- Thermal Overload Protection
- Short Circuit Protection
- Output Transistor SOA Protection

ORDERING INFORMATION

Device	Output Voltage Tolerance	Packag	Operating Temperature
KA78XXCT	±4%	TO-220	0 ~ +125 °C
KA78XXAT	±2%		
KA78XXIT	±4%		-40 ~ +125 °C
KA78XXR		D-PAK	0 ~ +125 °C
KA78XXAR	±2%		
KA78XXIR	±4%		-40 ~ +125 °C

Image 199. Datasheet of Voltage Regulators LM7805, LM7809

VISHAY

www.vishay.com

WSHP2818

Vishay Dale

Power Metal Strip® Resistors, High Power (10 W), Low Value (down to 0.001 Ω), Surface Mount



FEATURES

- Improved thermal management incorporated into design
- All welded construction of the Power Metal Strip resistors are ideal for all types of current sensing, voltage division, and pulse applications
- Proprietary processing technique produces extremely low resistance values
- Sulfur resistance by construction that is unaffected by high sulfur environments
- Very low inductance (< 5 nH)
- Low thermal EMF (< 3 µV/°C)
- Solid metal nickel-chrome or manganese-copper alloy resistive element with low TCR (< 20 ppm/°C)
- AEC-Q200 qualified (1)
- PATENT(S): www.vishay.com/patents
- Material categorization: for definitions of compliance please see www.vishay.com/doc?99912

AUTOMOTIVE GRADE

Pb Pb-free

e3

RoHS COMPLIANT

HALOGEN FREE

GREEN (5-2008)

DESIGN SUPPORT TOOLS

click logo to get started

3D Models Available

Design Tools Available

Image 200. Datasheet of the Prototype Shunt Resistor